SIMPLIFIED LIMIT LOAD DETERMINATION FOR INTEGRITY ASSESSMENT

REZA ADIBI-ASL


CENTRE FOR NFLD. STUDIES
MEMORIAL UNIVERSITY
OF NEWFOUNDLAND

SIMPLIFIED LIMIT LOAD DETERMINATION FOR INTEGRITY ASSESSMENT

By

Reza Adibi-Asl ©

A Thesis submitted to the School of Graduate Studies
In partial fulfillment of the requirement for the degree of
Doctor of Philosophy

Faculty of Engineering and Applied Science

Memorial University

May, 2008

St. John's, NL, Canada

ABSTRACT

The codes and standards in the pressure vessels and piping areas of the energy, petrochemical and related industries are based on the identification of potential modes of failures and a strategy for their avoidance. Instantaneous failures, specifically limit state and fast fracture, in the components and structures, can lead to catastrophic events. Therefore, integrity assessment of components and structures is required.

Inelastic finite element method is widely used to conduct failure analysis. However, it can often be complicated, time consuming and expensive. As well, accurate results are dependent on the specification of adequate mesh density and an assurance of numerically stable solutions. Independent verification methods that are alternatives to inelastic finite element methods are often required for engineering designs. The methods discussed in this thesis, based on elastic modulus adjustment procedures (EMAP), provide rapid and stable solutions at a relatively lower cost.

The elastic modulus adjustment methods rely on the convergence of the specific moduli adjustment procedure. A criterion for assessing the degree of convergence of EMAP is developed, and a procedure for achieving improved convergence is studied in this thesis. Also, simplified methods are developed in order to estimate the limit load in components and structures using iterative linear elastic methods. One of these procedures is the concept of reference volume that can be used to identify the kinematically active volume and dead zones in the components or structures. The reference volume method is shown

to give a more accurate prediction of limit loads comparing to available traditional methods based on total volume. Furthermore, by invoking the concept of reference volume the systematic procedures are proposed to estimate the lower bound limit load solutions with high accuracy. This is very helpful for limit load analysis of the components/structures with stress razors such as notches and cracks.

The concept of equivalence of "static indeterminacy" that relates a multidimensional component configuration to a "reference two-bar structure" is introduced for rapid estimation of the limit loads in components or structures. The procedures and methods discussed in this thesis are applied to some practical components (including cracks and notches) in order to verify their effectiveness in analyzing different geometries. Based on the proposed methods, integrity assessment analysis of different crack configurations, including multiple cracks and three dimensional effects, are studied in this thesis.

ACKNOWLEDGEMENTS

The author wishes to express his sincere gratitude to his supervisor, Dr. R. Seshadri, for his always-helpful suggestions, discussions, support and guidance in all phases of this research work. This dissertation would not have been possible without his expertise and insights.

The author wishes to thank members of his committee, Dr. A. Swamidas and Dr. S. Adluri, for their helpful comments and advice. Also, the author would also like to thank the Engineering Faculty and Staff for providing excellent environment during the course of his studies.

The author would like to thank his parents, Jeiran and Abbas, and his parents-in-law, Fatemeh and Hossein, for their unconditional support.

Finally, the author sincerely thanks his wife, Leila, for her love, care and constant encouragement throughout the course of this Doctoral work.

TABLE OF CONTENTS

LIST OF TABLES

LIST OF FIGURES

LIST OF APPENDICES

LIST OF SYMBOLS AND ABBREVIATIONS

Symbols

a	crack length
D	dissipation energy
E	modulus of elasticity
E_0	original elastic modulus
E'	constant= E_0 for plane stress and $E_0/(1-\nu^2)$ for plane strain
E_t	tangential modulus
G	convergence parameter, and linear elastic energy release rate
G_2	convergence parameter based on multiplier m_2^0
G_1	convergence parameter based on multiplier m_1^0
H	height
J	J-integral
J_e	elastic J-integral
$J_{el\,p}$	elastic-plastic J-integral
J_p	fully plastic J-integral
K_I	mode I stress intensity factor
K_r	y-axis in failure assessment diagram (FAD)
L	length
L_r	x-axis in failure assessment diagram (FAD)
m	exact limit load multiplier
m^0	upper bound limit load multiplier
m_1^0	upper bound limit load multiplier based on total volume
m_2^0	upper bound limit load multiplier based on kinematically active volume

m''	lower bound multiplier introduced by Mura *et al.* (1962)
m_1''	lower bound multiplier based on multiplier m_1^0
m_2''	lower bound multiplier based on multiplier m_2^0
m_L	classical lower bound limit load multiplier
m_n	r-node limit load multiplier
m_U	classical upper bound limit load multiplier
m_α	multiplier Alpha
m_β	multiplier Beta
n	Ramberg-Osgood material model exponent
N	number of r-node locations
P	external load
P_d	design load
P_L	limit load
q	elastic modulus adjustment index
R	internal radius
R_e	elastic defect size parameter
$R_{e/p}$	elastic-plastic defect size parameter
R_p	fully plastic defect size parameter
$\bar{s}_{ij}^0$	statically admissible deviatoric stress field corresponding to the traction $m^0 T_i$
s_{ij}^0	statically admissible deviatoric stress field corresponding to the traction T_i
S_m	code allowable stress
S_T	surface of traction
S_u	surface of constraint
SI	von Mises equivalent stress in an element
t	thickness

T_i	traction
U	strain energy
V_D	dead zone volume
V_T	total volume
V_R	reference volume
W	width
W^*	strain energy density
β	parameter in m_β
β_R	reference parameter
γ	constant of proportionality
δ_{ij}	Kronecker delta
ε_{eq}	equivalent strain
ε_f	fracture strain
ε_{ref}	strain corresponding to reference stress
ϕ^0	a point function defined in conjunction with yield criterion
λ	bars length ratio in two-bar structure
Γ	path around the crack tip
μ^0	plastic flow parameter
ν	Poisson's ratio
θ	follow up angle on GLOSS diagram
η	element number
σ_0	reference value stress
σ_{eq}	equivalent stress
σ_M	maximum equivalent stress
σ_n	r-node stress
σ_{ref}	reference stress

σ_y	yield strength
ζ	iteration variable

Superscript

0	statically admissible

Subscripts

Bar	two-bar model
Comp	component
e	elastic
e/p	elastic-plastic
p	plastic

Abbreviation and Acronyms

2D	Two Dimensional
3D	Three Dimensional
API	American Petroleum Institute
APDL	ANSYS Parametric Design Language
ASME	American Society of Mechanical Engineers
BH	Bilinear Hardening
BS	British Standard
CT	Compact Tension
COD	Crack Opening Displacement
CDF	Crack Deriving Force
ECM	Elastic Compensation Method
EMAP	Elastic Modulus Adjustment Procedures
EPFM	Elastic Plastic Fracture Mechanics

EPP	Elastic Perfectly Plastic
EPRI	Electric Power Research Institute
ESED	Equivalent Strain Energy Density
FAD	Failure Assessment Diagram
FEA	Finite Element Analysis
GLOSS	Generalized Local Stress Strain
LEFM	Linear Elastic Fracture Mechanic
NSSC	Notch Stress Strain Conversion
PW	Plastic Work
PWC	Plastic Work Curvature
R-Node	Redistribution Node
RVM	Reference Volume Method
SIF	Stress Intensity Factor
SINTAP	Structural INTegrity Assessment Procedure
TED	Twice Elastic Displacement
TES	Twice Elastic Slope
TI	Tangent Intersection
VCEM	Virtual Crack Extension Method

CHAPTER 1

INTRODUCTION

1.1 INTRODUCTION

Structural and mechanical integrity assessment plays an important role in many industry efforts relating to fitness-for-service evaluation of components or structures containing defects. Stress, defect size and toughness are the three major parameters in designing a component/structure against fracture. The fitness of a component or structure for service can be evaluated, and the safety margins determined at operation conditions by having an understanding of these parameters. Many investigations have been carried out for such integrity assessment in the past twenty years. Some of the recent documents available are the R6-procedure (2001), API 579 (2000), SINTAP (1999), CEA-A16 guide (1999) and BS 7910 (1999). Inelastic finite element analysis (FEA) is widely used for estimating the limit load of a component/structure; however, it can often be complicated, time consuming and expensive. As a result, developing reasonably accurate robust

methods based on linear elastic solutions would be useful from a design point of view. There are some methods based on iterative elastic finite element analysis, i.e., elastic modulus adjustment procedures (EMAP). These are performed by specifying spatial variations in the elastic modulus, thereby generating numerous sets of statically admissible and kinematically admissible distributions leading to both lower and upper bounds on limit loads. However, these methods sometimes provide limit loads on the basis of partly converged distributions. Procedures that address accuracy of these methods are discussed in this thesis. Also, for limit load analysis several simplified methods including "reference volume" approach and "two-bar structure" method are developed in this thesis. These simplified methods can be used for fitness for service assessment of a component/structure.

1.2 THESIS ORGANIZATION

The overall organization of the Chapters in this thesis is shown in Fig. 1.1. The rationale for organizing the thesis in this manner is to bring out through Chapters 4-7 methods of limit load determination that are essential for structural integrity evaluation. Chapter 2 and 8 expand the applications pertaining to fitness for service evaluation of component/structure by emphasizing on fatigue and fracture (the required limit loads can be estimated using the methods given in Chapter 4-7).

In Chapter 2, a brief coverage of the integrity assessment issues of the components/structures under mechanical loading is presented. Different modes of failure

including failures that are caused by monotonic loading and cyclic loading are discussed, followed by integrity assessment methods proposed by different researchers, and codes and standards organizations.

The fundamentals and theoretical background of limit load analysis are discussed in Chapter 3. Various concepts of variational principles in limit load analysis and numerical methods for the estimation of limit load are discussed in detail. A unified approach is employed to drive agin some of the existing solutions.

EMAP based on iterative procedures depend on the elastic modulus adjustment algorithms employed. Procedures such as the elastic compensation method, used in the UK, have been shown to exhibit numerical instability and convergence problems. In Chapter 4, procedures that address these problems are incorporated into two themes: (1) EMAP algorithm based on the equivalent strain energy density (ESED) concept, and (2) the convergence parameter "G" that evaluates the degree of convergence using upper bound limit load parameters.

The next topic covered in Chapter 5 is the concept of kinematically active volume, Reference Volume, used to narrow the spread between upper and lower bound limit loads. Using the kinematically active volume, the limit load analysis leads to more accurate results. The limit load values are then compared with results obtained from inelastic finite element analysis for typical component configurations.

In Chapter 6, the lower bound limit load multiplier m_β, which is calculated from the stress fields acting over the entire volume in a component, is determined by evaluating a reference parameter β_R. However, the estimation of β_R may be difficult, especially for components or structures that experience local plastic collapse, i. e., cracks or notches. Here, a systematic procedure for estimating reference volume as well as identifying parameter β_R in defected components or structures is offered. The results obtained by proposed method are compared with results obtained from inelastic FEA.

The contribution introduced next in Chapter 7 is the concept of equivalence of "static indeterminacy", which is invoked to estimate the limit loads for mechanical components and structures. This method relates a multidimensional component configuration to a "reference two-bar structure." Simple scaling relationships are developed that enable the rapid determination of limit load multipliers. The reference two-bar structure method is applied to a number of configurations with or without cracks.

In Chapter 8, based on limit load estimation methods discussed in this thesis, a simple method for estimating the inelastic fracture energy release rate, J, for components or structures undergoing hardening material models, e.g. bilinear hardening and Ramberg-Osgood, is proposed. The integrity assessment of some typical crack configurations (including two-dimensional and three-dimensional crack configuration) are studied.

Finally, Chapter 9 consists of the conclusions based on the results and methods presented in this thesis, followed by some recommendations for future work.

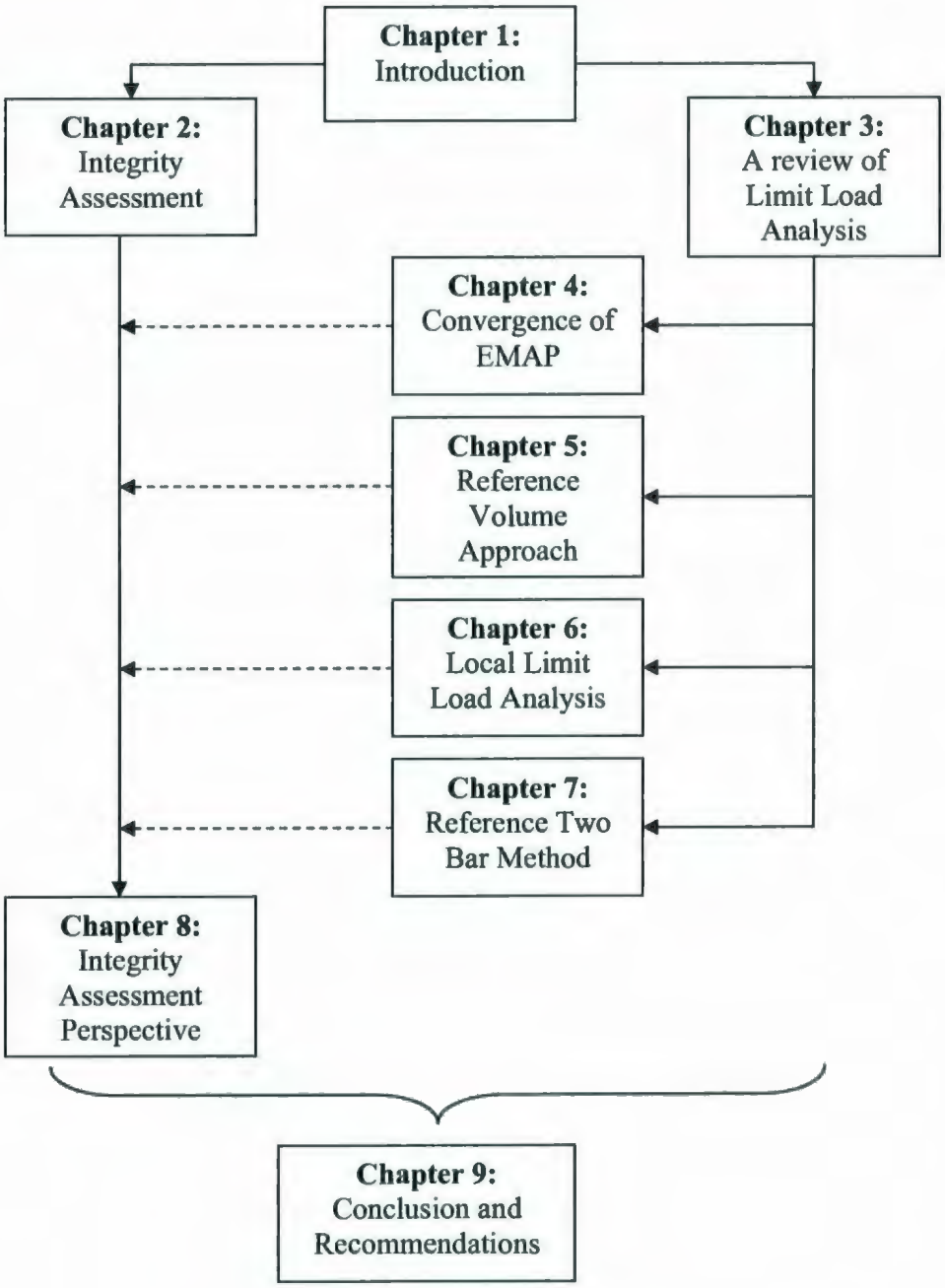

Figure 1.1: Thesis organization chart

CHAPTER 2

INTEGRITY ASSESSMENT

2.1 INTRODUCTION

Structural and mechanical integrity assessment plays an important role in many industry efforts relating to fitness-for-service evaluation of the components/structures containing defects. This means that a given defect can be left as it is, therefore avoiding unnecessary repairs. Also, integrity assessment provides helpful economic and safety benefits, which can be summarized as follows:

- Increasing human safety by assuring that a given component can safely continue to operate.

- Optimizing the maintenance strategy for an operating component and recommending possible ways to extend and improve the component life.

Structural integrity assessment in the energy sector is practiced at different levels of assessment. The lower level assessment provides conservative criteria that can be used with a minimum quantity of inspection data or information about the component. The middle level is proposed for use by facilities or field engineers, although some owner-operator organizations consider it suitable for a central engineering evaluation. The higher level assessments require complicated analysis by experts, where advanced computational procedures such as FEA are often carried out.

Many integrity assessment investigations have been carried out in the past twenty years. Some of the recent documents available are the R6-procedure (2001), API 579 (2000), SINTAP (1999), CEA-A16 guide (1999) and BS 7910 (1999). These codes and standards are mostly based on semi-empirical methods obtained from experimental data. However, to get more accurate results numerical simulation is required to enable an understanding of the influence of various parameters. In this Chapter, modes of failure that deal with static and fatigue failures are addressed for a component or a structure with defect(s).

2.2 REFERENCE STRESS

Earlier research on the reference stress method was based on estimating creep parameters in a complex component or structure under mechanical loading, by performing a single uniaxial experiment. The basic premise of reference stress method is the insensitivity of reference stress to the variation of creep parameters. This observation

has been the basis for several analytical methods of reference stress determination. For sake of the discussion, assume a beam with rectangular cross section in a second stage creep condition, for which the creep relationship can be expressed by the Norton equation as

$$\dot{\varepsilon}_c = B\sigma^n \tag{2.1}$$

where $\dot{\varepsilon}_c$ is the strain rate, B and n are material constants, and σ is the stress.

Plotting the variation of stress with respect to the vertical distance from the origin for different values of n, one gets curves similar to those shown in Fig. 2.1. All the curves intersect at a common point that is the location of reference stress, and the corresponding stress is the reference stress. Since the stress at this location is almost invariant, it can be considered a load controlled location, where equilibrium exists with externally applied loads and moments. Therefore, the reference stress point is located on a "limit type" of stress distribution.

Generally, the reference stress is directly proportional to the external tractions irrespective of the material constitutive relations. Consider a compact tension specimen subjected to a mechanical load. By increasing the load, the amount of primary stress in the component increases and plastic zone becomes larger until net section yielding occurs (plastic collapse condition). Figure 2.2 is a plot of equivalent stress versus equivalent strain for an element in a given finite element discretization scheme corresponding to the

maximum stress location. The relaxation loci RL_1, RL_2 and RL_3 correspond to the distribution of stress corresponding to points 1, 2 and 3, respectively. The trajectory of the relaxation locus, RL_2, is along 2-4-5-6. The initial portion of the locus (2-4) pertains to the redistribution of peak and secondary stresses.

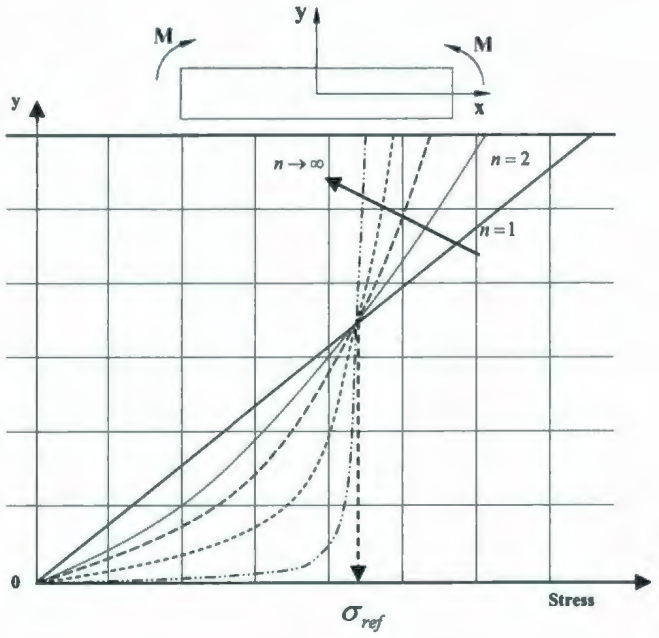

Figure 2.1: Creep reference stress definition

Referring to Fig. 2.2, the relaxation locus RL_1 corresponds to the plastic collapse process. If P_1, P_2 and P_3 are the external loads at points 1, 2 and 3 on linear elastic-line, the respective reference stress is related to the limit load by the relationship:

$$\sigma_{nk} = \frac{P_k \sigma_y}{P_L} \qquad (k = 1, 2, 3) \tag{2.2}$$

It follows that

$$\frac{P_1}{\sigma_{ref1}} = \frac{P_2}{\sigma_{ref2}} = \frac{P_3}{\sigma_{ref3}} \tag{2.3}$$

where σ_{ref1}, σ_{ref2}, and σ_{ref3} are reference stresses (primary stresses) corresponding to P_1, P_2 and P_3, respectively, and P_L is the limit load.

In the foregoing expression, the ratio σ_y / P_L is the geometry factor that can be calculated by analytical, numerical or experimental methods.

Ponter and Leckie (1970) have shown that this approximation constitutes an upper bound on the value of stress and is therefore on the safe side for design purposes. Reference stress method is not only used for creep analysis, but also it is useful for elastic-plastic fracture as shown by Ainsworth (1984).

For statically determinate components, the formation of a single plastic hinge will result in plastic collapse. The occurrence of a single reference stress location at plastic hinge cross-section is indicative of a load-controlled membrane mode of collapse. This

situation can be represented by a one bar model, Fig. 2.3, so that collapse occurs when $\sigma_{ref} = \sigma_y$. As presented in Fig. 2.3, the elastic and fully plastic stress distributions in the crack cross-section of compact tension specimen intersect at reference stress location.

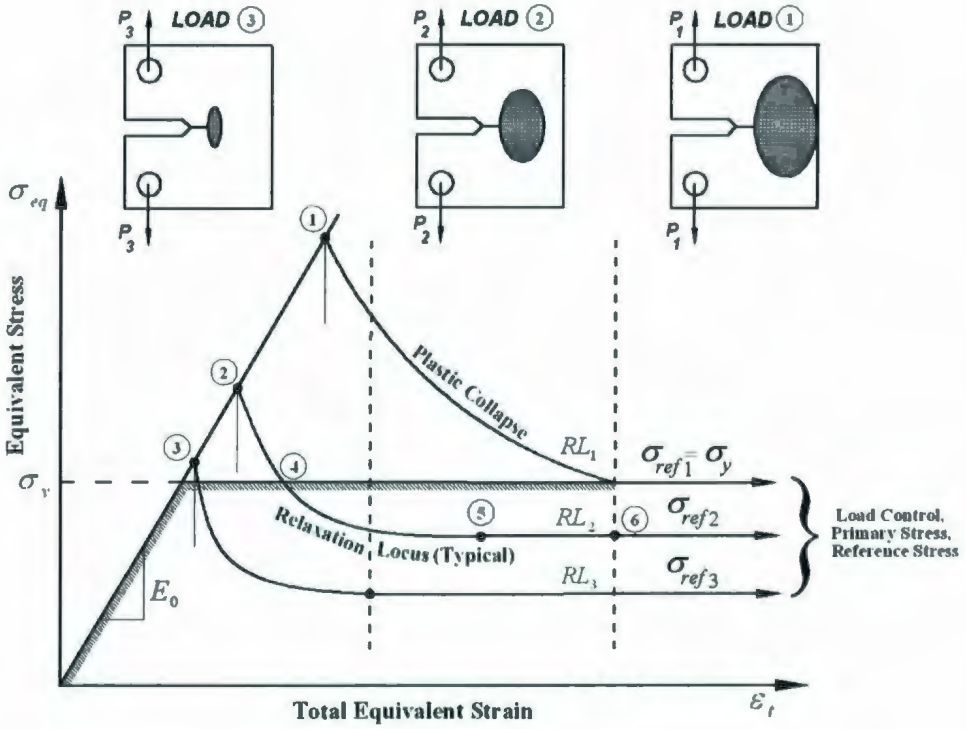

Figure 2.2: Relaxation locus for pressure components with a crack

Stresses in components consist of the combination of primary stress, secondary stress and peak stress. However, ideally, after stress redistribution, secondary stress along with peak stress disappears and only primary stress remains. This means that the relaxation locus will eventually reach the primary stress (reference stress) level. In highly localized stress in notched components, the primary stress is very small in comparison to

peak stress; therefore, by neglecting the primary stress the relaxation locus asymptotically reaches the zero stress level.

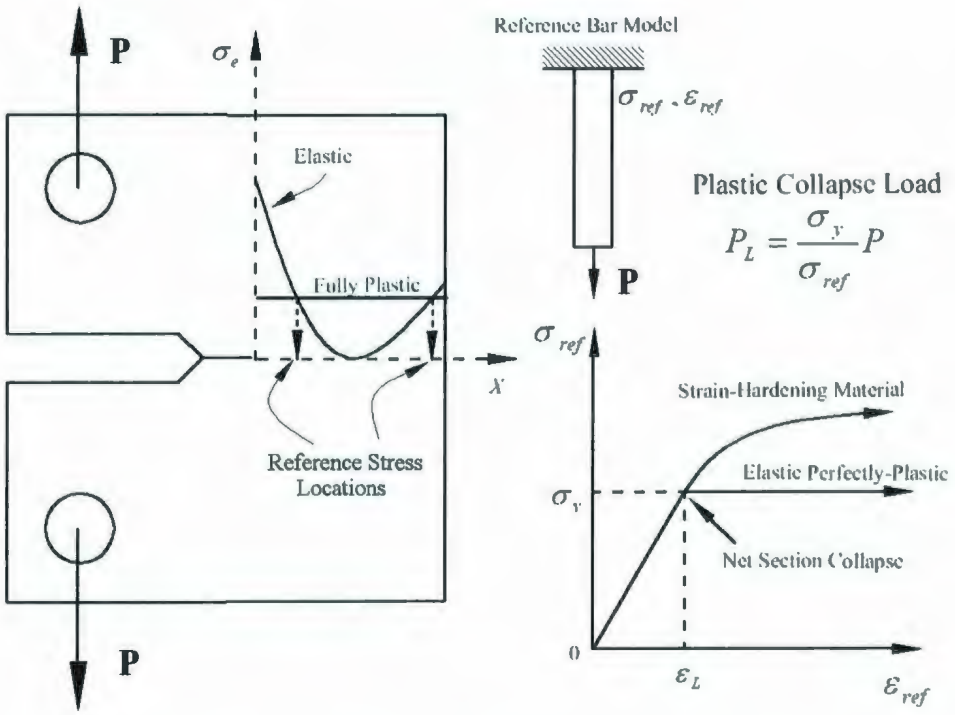

Figure 2.3: Compact tension (CT) specimen: reference stress and uniaxial stress-strain model

2.3 FRACTURE MECHANICS PARAMETERS

In order to assess a cracked component subjected to monotonic or cyclic loading, fracture mechanics parameters such as the stress intensity factor (SIF) and inelastic energy release rate (J-integral) need to be estimated. The closed form solutions of the

fracture mechanics problems are restricted to some simple crack configurations. Therefore, numerical methods (FEA) are widely used for this purpose.

Consider a two-dimensional crack with an arbitrary orientation as illustrated in Fig. 2.4. The expressions for SIFs in modes I and II (K_I and K_{II}) can be obtained in terms of the nodal stresses ahead of the crack tip (σ_{yy} and τ_{xy}), i.e. (Anderson, 2005)

$$K_I = \lim_{r\to 0}\left(\sigma_{yy}\sqrt{2\pi r}\right) \tag{2.4}$$

$$K_{II} = \lim_{r\to 0}\left(\tau_{xy}\sqrt{2\pi r}\right) \tag{2.5}$$

Similarly, expressions for K_I and K_{II} in terms of the relative displacement of points on opposite faces of the crack, along the line of the crack, Δu, and perpendicular to it, Δv, are

$$K_I = \lim_{r\to 0}\left(\frac{E}{8}\sqrt{\frac{2\pi}{r}}\Delta u\right) \tag{2.6}$$

$$K_{II} = \lim_{r\to 0}\left(\frac{E}{8}\sqrt{\frac{2\pi}{r}}\Delta v\right) \tag{2.7}$$

These stress components and relative displacements are defined with respect to the coordinate system attached to the crack tip, as shown in Fig. 2.4.

The effective stress intensity factor for two-dimensional mixed mode condition can be defined by following equation

$$K_{eff} = \sqrt{K_I^{\,2} + K_{II}^{\,2}} \tag{2.8}$$

Equation (2.8) can be extended for three dimensional mixed mode condition as

$$K_{eff} = \sqrt{K_I^{\,2} + K_{II}^{\,2} + K_{III}^{\,2}/(1-\nu)} \tag{2.9}$$

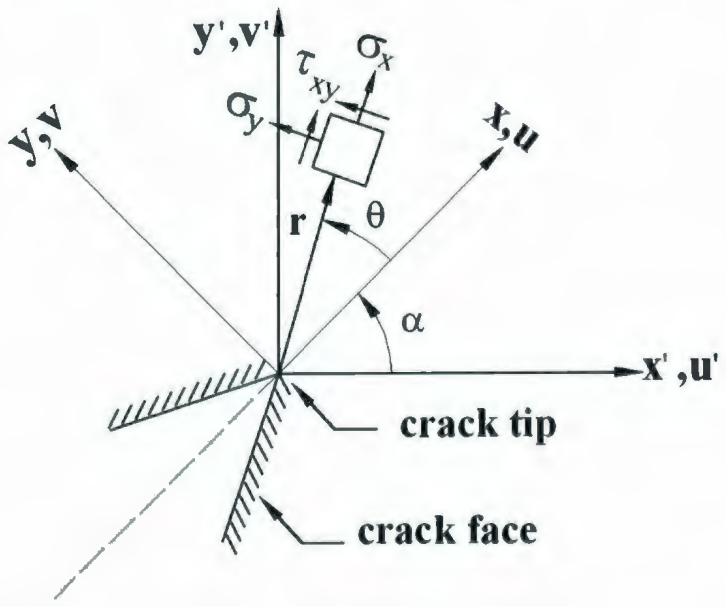

Figure 2.4: Stresses and coordinate systems in the vicinity of a crack

Failure occurs when SIF reaches the material toughness (K_{Ic}), which is obtained from the toughness test.

The LEFM-based SIF is valid only when the effect of plasticity is negligible; therefore, the J-integral has been introduced to characterize inelastic fracture mechanics. Rice (1968) showed that the J-integral, defined by Eq. (2.10), is independent of the path of integration around the crack tip*.

$$J = \oint_{\Gamma} (W^* \, dy - T_j \frac{\partial u_j}{\partial x} ds) \qquad (j = 1,2) \tag{2.10}$$

$$W^* = \int \sigma_{ij} \, d\varepsilon_{ij} \tag{2.11}$$

$$T_j = \sigma_{ij} \, n_i \tag{2.12}$$

where Γ is an arbitrary path encircling the crack tip (Fig. 2.5), W^* is strain energy density, x and y are local coordinate system along the line of the crack and perpendicular to it, respectively, T_j is traction vector, u_j is displacement vector, n_i is unit outer normal to path Γ, s is the length along the path Γ, and σ_{ij} and ε_{ij} are stress and strain tensor, respectively.

* For any closed contour, the value of J-integral is zero, from which it is concluded that the J-integral is path independent (Rice, 1968).

It should be noted that J-integral is equal to strain energy release rate for an elastic body that contains a crack.

$$J_e = G = \frac{K^2}{E} \tag{2.13}$$

Alternatively, J-integral can be rewritten in a matrix form,

$$J = \oint_\Gamma W\, ds - \oint_\Gamma \langle \sigma_n \quad \tau_n \rangle \begin{Bmatrix} \dfrac{\partial u_n}{\partial x} \\ \dfrac{\partial v_n}{\partial y} \end{Bmatrix} ds \tag{2.14}$$

where

$$W^* = \frac{1}{2E}\left(\sigma_{xx} + \sigma_{yy} + \sigma_{zz}\right)^2 + \frac{1+2\nu}{E}\left(\tau_{xy}^2 - \sigma_{xx}\sigma_{yy} - \sigma_{yy}\sigma_{zz} - \sigma_{zz}\sigma_{xx}\right)$$

$$\sigma_n = \sigma_{xx}\cos^2\alpha + \sigma_{yy}\sin^2\alpha + \tau_{xy}\sin\alpha\cos\alpha$$

$$\tau_n = \left(\sigma_{yy} - \sigma_{xx}\right)\sin\alpha\cos\alpha + \tau_{xy}\left(\cos^2\alpha - \sin^2\alpha\right)$$

$$u_n = u\cos\alpha + v\sin\alpha$$

$$v_n = -u\sin\alpha + v\cos\alpha$$

$\sigma_{zz} = \nu(\sigma_{xx} + \sigma_{yy})$ for plane strain and $\sigma_{zz} = 0$ for plane stress.

Equation (2.10) is the J-integral in two-dimensions; however, the concept has been extended to generalized three-dimensional configuration (Amestoy *et al.*, 1981; Kikuchi and Miyamoto, 1982; Barbero and Reddy, 1992). Also, Narasimhan and Rosakis (1988) studied the three-dimensional crack configuration, and found that the estimated J for three-dimensional problems are bounded between the J obtained from plane stress and plane strain conditions. Wu and Seshadri (1996) proposed a simplified method for estimating three-dimensional crack configurations, namely the 2½-D model. The equivalent stress intensity factor for 2½-D model was derived, and a correction factor was introduced that could be used in conjunction with existing experimental data.

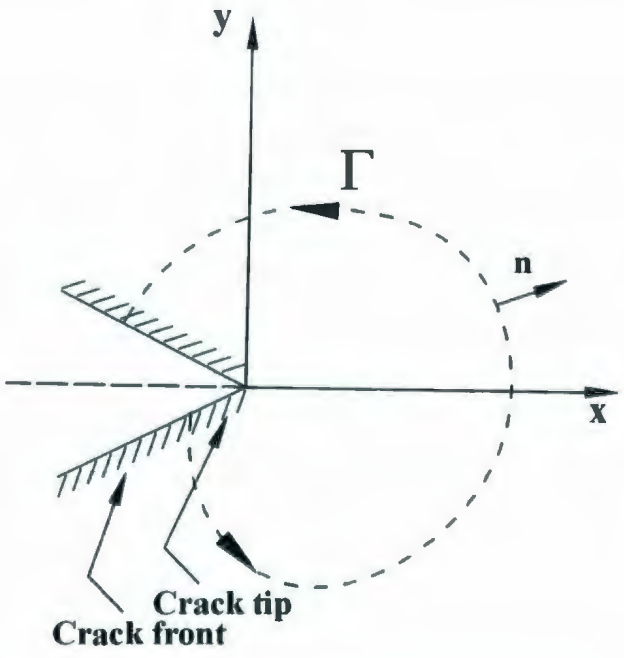

Figure 2.5: Arbitrary contour around the crack tip

2.4 INTEGRITY ASSESSMENT METHODOLOGY

2.4.1 Monotonic Loading

With reference to Harrison and Milne (1981), the possible failure mechanism paths can be illustrated schematically as shown in Fig. 2.6 when the load is applied monotonically on the components or structures containing defects. Generally, failure is usually due to net section collapse (ductile failure) or toughness dependent fracture (brittle failure), which it is dependent on the material properties, loading, boundary condition, and size and shape of the defect. The net section collapse becomes important in a high toughness material, in which the fracture mode of failure fades away as stress is insensitive to toughness; therefore, limit load would be a more appropriate quantity for predicting failure. Toughness dependent fracture may occur either in the elastic stage, Linear Elastic Fracture Mechanics (LEFM), or the plastic stage, Elastic-Plastic Fracture Mechanics (EPFM). LEFM is valid for brittle material that has low toughness. At higher toughness, as in ductile materials, the LEFM is no longer valid and nonlinear analysis (EPFM) is required for such a problem. In the LEFM range the plastic zone is small, and linear elastic energy release rate (G) and stress intensity factor (K) are considered as relevant crack tip parameters. In the EPFM range, due to the considerable plastic zone, the LEFM parameters are no longer valid; instead new parameters such as inelastic energy release rate (J) and crack opening displacement (COD) are used. Finally, if the material behavior, i. e., stress-strain curve is dependent on time, time dependent fracture parameter such as creep fracture parameter (C^*), should be estimated.

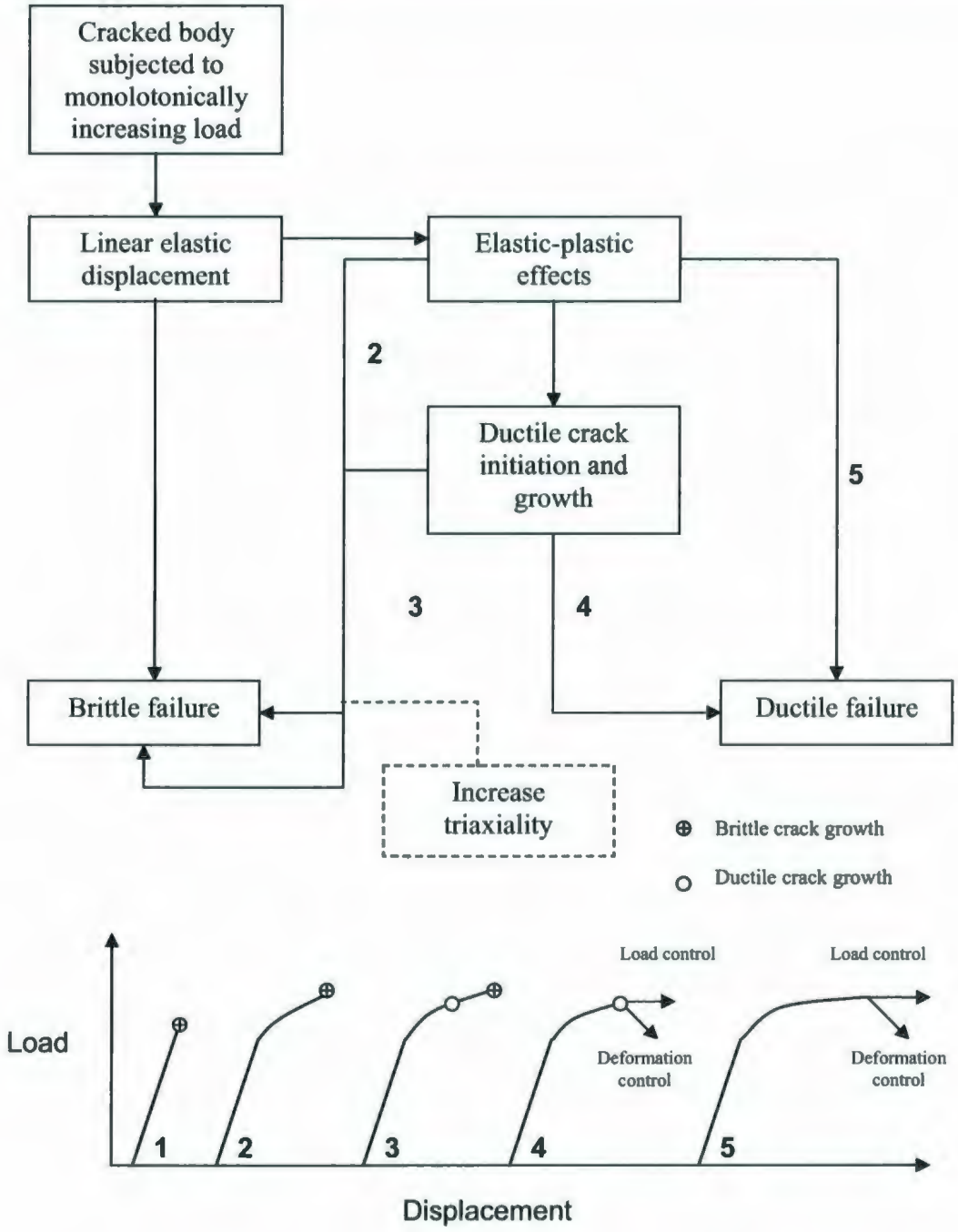

Figure 2.6: Different loading path to failure due to monotonic loading (adapted from Harrison and Milne, 1981)

For a failure assessment methodology, both failure mechanisms must be considered in order to estimate the safe operating parameters and remaining life of components or structures with defects.

Two main approaches for integrity assessment of a component or structure with defect are widely used as:

- Failure Assessment Diagram (FAD)
- Crack Driving Force (CDF)

The former approach, FAD, is based on a failure line, and is constructed by normalizing the crack tip loading by the material's fracture resistance. In contrast, in the CDF approach, determination of crack tip loading in the defected component or structure and its comparison with fracture resistance of the material are made in two different steps. The comprehensive study on structural integrity assessment is given in the 10-volume set book by Milne, Ritchie, and Karihaloo (2003).

The original concept of these approaches was first introduced by Dowling and Townley (1975), and Harrison *et al.* (1976) to describe the interaction between brittle fracture and net section collapse. In 1976, Central Electricity Generating Board (CEGB) developed fracture assessment methodology namely as R6 routine. The R6 routine initially was based on the original concept proposed by Dowling and Townley (1975), and Harrison *et al.* (1976). However, it has been revised several times in the past 30 years. In this section,

the formulation of modern assessment methodology, based on J-integral solution, is discussed; the procedure is also incorporated in the newest revision of R6 procedure (2001).

Failure Assessment Diagram (FAD)

A typical FAD is shown in Fig. 2.7. In this diagram, the fracture mechanics parameter, which is the ratio of calculated SIF to the fracture toughness (K_{IC}), is given on the vertical axis as:

$$K_r = \frac{K_I}{K_{IC}} \tag{2.15}$$

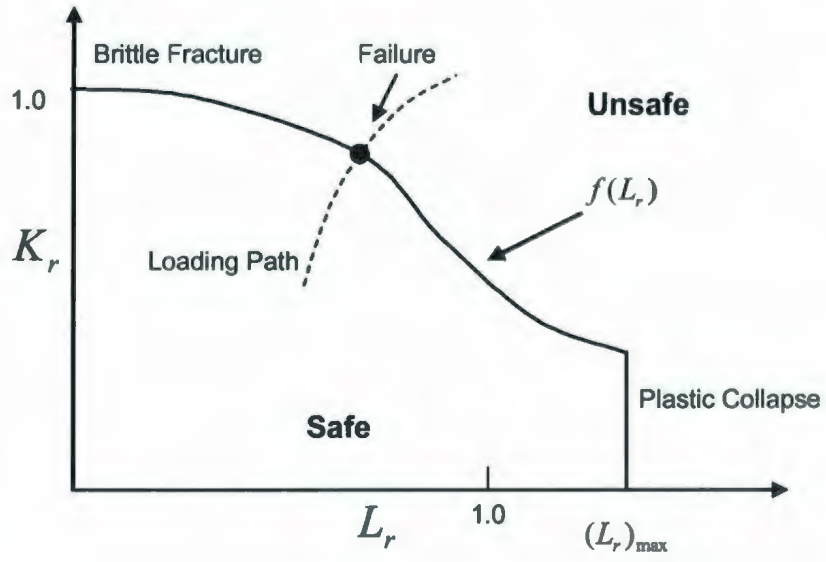

Figure 2.7: Failure assessment diagram (FAD) approach

The limit load parameter is defined by the ratio of the applied load (or corresponding reference stress σ_{ref}), to the limit load (or yield strength σ_y of a given component), i.e.,

$$L_r = \frac{P}{P_L} = \frac{\sigma_{ref}}{\sigma_y} \tag{2.16}$$

In Fig. 2.7, $L_r = 1$ corresponds to the plastic collapse load of the cracked component, and $L_r = (L_r)$ is referred to the limit load state (Zerbst *et al.*, 2000), which is defined as:

$$(L_r)_{\max} = \frac{\sigma_f}{\sigma_y} \tag{2.17}$$

where σ_f is the flow stress and is approximately defined as the average of yield strength and ultimate strength, i.e.,

$$\sigma_f = \frac{\sigma_y + \sigma_u}{2} \tag{2.18}$$

The function $f(L_r)$, Fig. 2.7, is the boundary of the safe and unsafe regions in FAD. Various expressions have been proposed for $f(L_r)$ based on different type of the problems and different level of required input data.

Using the FAD approach the component or structure with defect is considered to be safe if the following condition is satisfied

$$K_r \leq f(L_r) \tag{2.19}$$

Crack Driving Force (CDF)

The crack driving force or CDF approach is based on the variation of inelastic energy release rate (J) parameter with the limit load parameter. The commonly used curve based on this approach is schematically illustrated in Fig. 2.8. In this figure, the horizontal axis, L_r, is the ratio of applied load to the limit load, as defined in Eq. (2.16), the vertical axis (J) is the value of energy release rate, and J_{Ic} on the vertical axis is the critical J value (which is considered a material property). The appropriate value of J for design should ensure that $J_{design} \leq J_{Ic}$ (Webster and Ainsworth, 1994).

The FAD and CDF approaches are interchangeable. For instance, the estimated J can be calculated using the parameters in FAD approach, i.e.,

$$J_{e/p} = \frac{J_e}{[f(L_r)]^2} \tag{2.20}$$

Therefore, the FAD can be obtained as plotted schematically in Fig. 2.9.

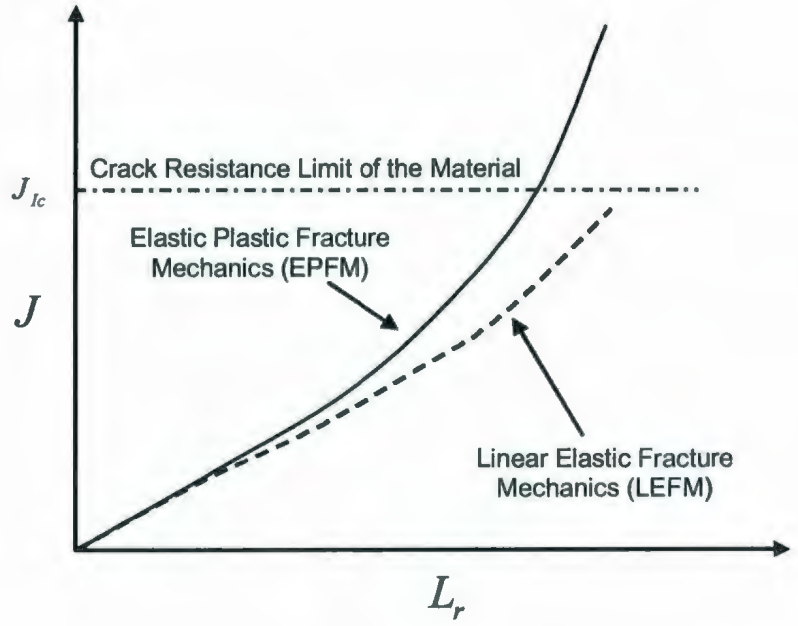

Figure 2.8: Crack driving force (CDF) approach

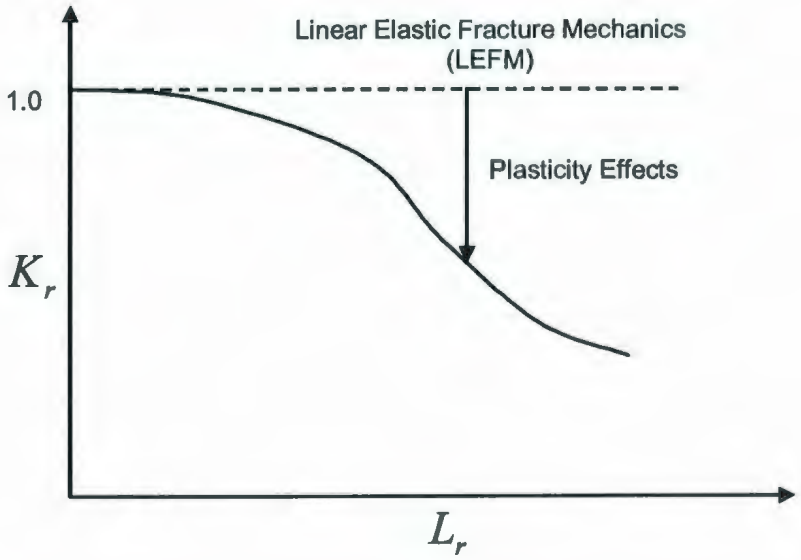

Figure 2.9: Alternative FAD using CDF approach (Anderson, 2005)

This procedure is being used by some codes such as the Structural Integrity Assessment Procedure for the European industry or SINTAP[1] (1999). The SINTAP (1999) procedure consists of seven different analysis levels (level 0 to level 6) such that each level of solution can be used based on the quality and completeness of the required input data (Zerbst *et al.*, 2000). The higher the level of solution is taken the more complex the procedure will be. The SINTAP (1999) procedure is studied in more detail by Ainsworth *et al.* (2001).

Having the knowledge of the elastic-plastic J-integral, the FAD and CDF curves can be created. Therefore, several methods have been proposed based on simplified approximations of failure avoidance curve $f(L_r)$ using the reference stress approach. These methods have been described in many publications; therefore, only a limited number can be discussed in this section.

Electric Power Research Institute (EPRI) method:

In this method, the elastic-plastic J-integral is estimated by adding the elastic part and plastic part of J (see Fig. 2.10), i.e.,

$$J_{e/p} = J_e + J_p \tag{2.21}$$

[1] The SINTAP procedure is the outcome of a research work from different countries in Europe (Belgium, France, Germany, Ireland, Netherlands, Spain, Sweden, U.K) sponsored by European Commission (in the period of 1996 to 1999). The main objective of this project was to unify the fracture mechanics based integrity assessment approaches available in Europe.

This method was originally developed by Shih and Hutchinson (1976), and later summarized in EPRI handbook in 1981. For a material following the Ramberg-Osgood stress-strain curve, the $J_{e/p}$ can be estimated as:

$$J_{e/p} = \frac{K^2(a_{eff})}{E'} + \alpha\sigma_0\varepsilon_0 hL\left(\frac{P}{P_0}\right)^{n+1} \tag{2.22}$$

In Eq. (2.22), P is applied load, P_0 is reference load, which is often identified with the limit load. The quantities n, α, σ_0 and ε_0 are material properties defined from the Ramberg-Osgood stress-strain curve. The parameter L is a characteristic dimension and can be freely chosen. The function h is dependent on geometry and material properties and has been tabulated using inelastic finite element results for various cracked configurations (EPRI handbook, 1981). The effective crack length, a_{eff}, can be defined as

$$a_{eff} = a + \frac{1}{a + (P/P_0)^2}\frac{1}{\beta\pi}\frac{n-1}{n+1}\left(\frac{K}{\sigma_0}\right)^2 \tag{2.23}$$

where parameter β is taken as 6 for plane strain and 2 for plane stress.

Although the EPRI method is based on the results from inelastic FEA, in EPRI handbook the function h is tabulated only for a few crack configurations, e.g., for a range of plate and cylindrical configurations.

The EPRI method is based on the CDF approach; however, the method has been also proposed in form of FAD approach by Bloom in 1980.

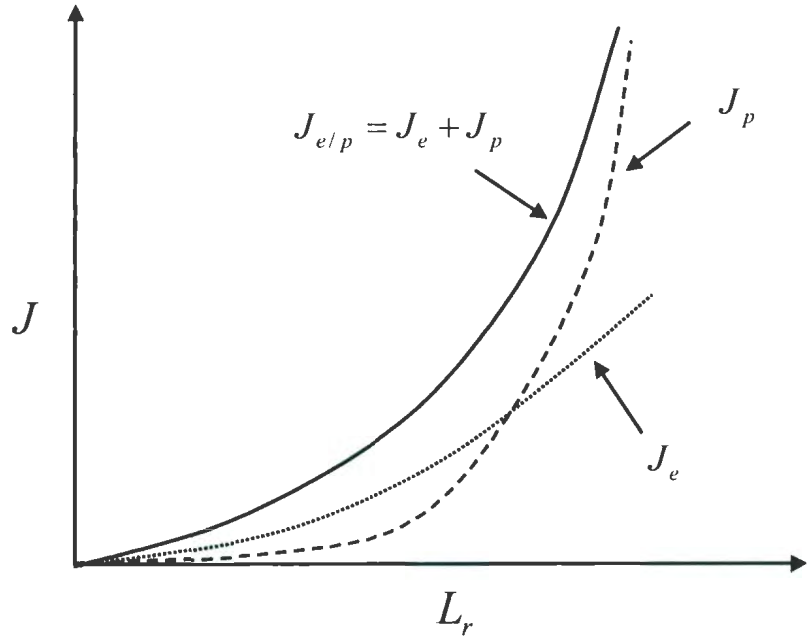

Figure 2.10: The EPRI method

R6 method:

One of the most commonly used approximations is given in R6 routine (2001). The early equation of the R6 routine (Rev.1) is based on the equation proposed by Dowling and Townley (1975), using the Dugdale model:

$$f(S_r) = S_r \times \left[\frac{8}{\pi^2}\ln\left(\frac{\pi}{2}S_r\right)\right]^{-1/2} \tag{2.24}$$

where $S_r = P/P_C$ (P is the applied load and P_C the nominal collapse load).

Equation (2.24) is based on elastic-perfectly material model; therefore, further revisions have been made in R6 routine to address a material with strain hardening.

In the option 2 of latest R6 routine (Rev.4, 2001), $f(L_r)$ estimated from stress strain data for the material of interest, and the plastic limit load by

$$f(L_r) = \frac{E\varepsilon_{ref}}{L_r\sigma_y} + \frac{L_r^{\,3}\sigma_y}{2E\varepsilon_{ref}} \tag{2.25}$$

where ε_{ref} is the reference strain corresponding to the reference stress (σ_{ref}) on the stress-strain curve.

Expression (2.25) requires that the stress-strain data be available. Therefore, option 1 in R6 routine, Rev. 4 (2001) has been proposed as a generic expression that can be used in the absence of stress-strain data as:

$$f(L_r) = [1 + 0.5(L_r)^2]^{-0.5}\,[0.3 + 0.7e^{-0.6L_r^{\,6}}] \tag{2.26}$$

Seshadri and Wu's method:

Alternatively, the estimation of J-integral based on reference stress, is also available. The elastic energy release rate can be expressed based on LEFM as

$$J_e = G = \frac{K_I^2}{E'} \tag{2.27}$$

where $K_I = Y\sigma_{ref}\sqrt{\pi a}$ is stress intensity factor, Y is the crack configuration factor and a is the crack length. σ_{ref} is reference stress, $E' = E_0$ for plane stress, and $E' = E_0/(1-\nu^2)$ for plane strain. Equation (2.27) can be rewritten in terms of reference stress and strain as

$$J_e = R_e\sigma_{ref}\varepsilon_{ref} = R_e E_0 \varepsilon_{ref}^2 \tag{2.28}$$

where ε_{ref} is reference strain, $\varepsilon_{ref} = \sigma_{ref}/E_0$, and R_e is a defect-size parameter for the elastic range can be calculated from

$$R_e = \frac{E_0 K_I^2}{E'\sigma_{ref}^2} \tag{2.29}$$

Extending the concept to the elastic-plastic and fully-plastic regimes, the related J can be written as

$$J_{e/p} = R_{e/p}\sigma_{ref}\varepsilon_{ref} \tag{2.30}$$

$$J_{r/p} = R_{r/p}\sigma_{y}\varepsilon_{ref} \tag{2.31}$$

where $R_{e/p}$ and $R_{r/p}$ are the defect size parameters for elastic-plastic and fully plastic state, respectively.

Comparing J_e and $J_{r/p}$, it can be seen that J_e is proportional to square of ε_{ref}, which represents parabola, and $J_{r/p}$ varies linearly with respect to ε_{ref}, as illustrated in Fig. 2.11. The relationship between R_e and $R_{r/p}$ can be obtained by intersection of the two curves J_e and $J_{r/p}$. If the two curves coincide at $\varepsilon_{ref} = \varepsilon^*_{ref}$ then

$$J_e(\varepsilon^*_{ref}) = J_{r/p}(\varepsilon^*_{ref}) \tag{2.32}$$

When the reference strain ε_{ref} (corresponding to reference stress σ_{ref}) equals to the strain ε^*_{ref} the collapse load is reached, and corresponding load will be P^*.

Seshadri and Wu (2001) applied the concept in Fig. 2.11 and derived J-integral estimation based on multiaxial constraint parameter that was introduced in GLOSS R-Node method (Seshadri and Fernando, 1992) as

$$\frac{J_{e/p}}{J_e(\varepsilon_y)} = \begin{cases} \left(\frac{\varepsilon_n}{\varepsilon_y}\right)^2 & 0 \le L_r \le 0.5 \\ 2\left(\frac{\varepsilon_n}{\varepsilon_y}\right)^3 & 0.5 < L_r < 1 \end{cases} \tag{2.33}$$

where $J_e(\varepsilon_y)$ is the elastic J-integral at collapse load, ε_n is the R-Node strain; in which when ε_n reaches to ε_y (R-Node strain at collapse), the corresponding applied load is the limit load of the component, P_L.

Since, the Eq. (2.33) is derived based on elastic analysis and R-Node locations are primary stress locations, the applied load is proportional to the stresses and strains in a given component, i.e.,

$$\frac{P}{P_L} = \frac{\sigma_n}{\sigma_y} = \frac{\varepsilon_n}{\varepsilon_y} \tag{2.34}$$

Therefore, the expression in Eq. (2.33) can be rewritten in terms of load parameter as:

$$\frac{J_{e/p}}{J_e(\varepsilon_y)} = \begin{cases} L_r^{\,2} & 0 \le L_r \le 0.5 \\ 2L_r^{\,3} & 0.5 < L_r < 1 \end{cases} \tag{2.35}$$

The design curve bounds for a component/structure with defect are presented in Fig. 2.12.

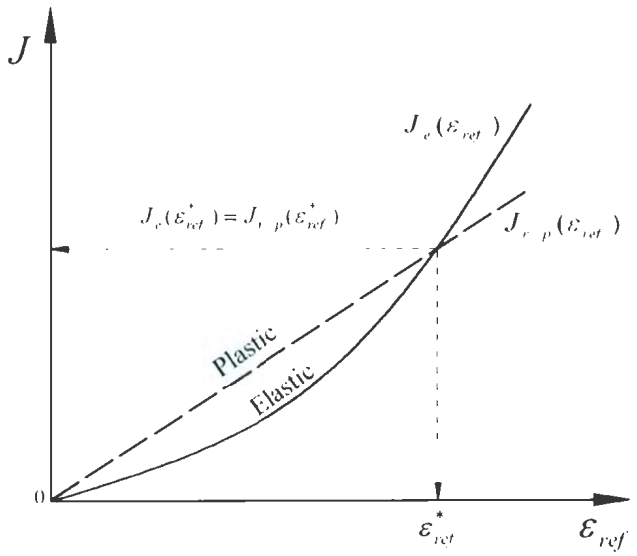

Figure 2.11: J_e and $J_{e/p}$ curves as a function of ε_{ref}

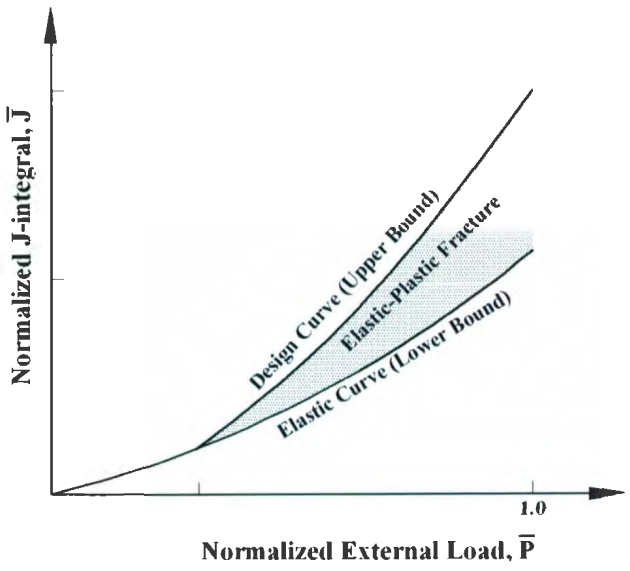

Figure 2.12: Design curves (Seshadri and Wu, 2001)

2.4.2 Cyclic Loading

Traditionally, fatigue analysis is separated into two parts, initiation and crack propagation. The initiation portion of fatigue life consists of crack nucleation caused by repeated plastic shear straining and a period of crystallographically oriented crack growth. Propagation consists of slow stable crack growth followed by rapid unstable crack growth to final fracture. Initiation may be analyzed using strain cycle fatigue concepts, and propagation by linear elastic fracture mechanics concepts.

Good estimates of the total life of notch components, subjected to variable amplitude load histories, can be obtained if both crack initiation, N_i, and crack propagation, N_p, are considered, i.e.

$$N_t = N_i + N_p \tag{2.36}$$

Crack initiation

As the quest for cost effective finite life designs continues, there is an increasing requirement to quantify the failure performance of components. However, the conventional methods of achieving this objective (e.g. prototype testing) are very expensive and time consuming.

A number of investigators (e.g. Topper and Gowda, 1970) have suggested alternative approaches based on local strain and obtained fatigue data from simple uniaxial unnotched specimen tests, where it is assumed that smooth and notched specimens with the same local strain range, $\Delta\varepsilon$, experience the same number of cycles to fatigue crack initiation, N_i. Smooth specimen fatigue life data, proposed by Manson-Coffin (Manson, 1965 and Coffin, 1969), may be expressed in the following form:

$$\frac{\Delta\varepsilon}{2} = \frac{\sigma'_f}{E}(2N_i)^b + \varepsilon'_f(2N_i)^c \tag{2.37}$$

However, the problem of fatigue crack initiation life prediction based on a local strain approach becomes one of estimating the local strain amplitude at the notch. Local strain amplitude can be determined by prototype component testing, or can be predicted using FEA or other numerical or analytical prediction methods. Prototype testing is very expensive and time consuming and, although finite element analysis is powerful, there are some difficulties when using the method for component design assessments. Therefore, various authors have proposed analytical relationships for predicting the local strain amplitude at the root of a notch. These relationships, known as notch stress-strain conversion (NSSC) rules, are used to determine the non-linear and history-dependent stress-strain behavior at the notch root in terms of the load history and the cyclic deformation properties of the metal. The commonly used conservative NSSC rule is the Neuber (1961) rule, which can be expressed as:

$$\Delta\sigma \times \Delta\varepsilon = K_t^2 \times \Delta\sigma_0 \times \Delta\varepsilon_0 \tag{2.38}$$

where $\Delta\sigma_0$ and $\Delta\varepsilon_0$ are the nominal stress and strain range respectively, $\Delta\sigma$ and $\Delta\varepsilon$ are the local maximum stress and strain range at the notch, and K_t is a stress concentration factor. Also, researches have suggested a modification of Neuber's hyperbola by considering the limit load in the stress-strain curve (see Dittmann, 1991 and Janković, 2001). The local strain approach associated with the NSSC rules is a useful and powerful method for estimating the fatigue crack initiation life of a notched component. The local strain range is found from the intersection of NSCC rules, i. e. Eq. (2.38), with the material cyclic stress-strain curve obtained from smooth specimen testing:

$$\frac{\Delta\varepsilon}{2} = \frac{\Delta\sigma}{2E} + \left(\frac{\Delta\sigma}{2K'}\right)^{1/n'} \tag{2.39}$$

By replacing the relevant local strain range in Eq. (2.37), the crack initiation life, N_i, can be obtained, as shown in Fig. 2.13.

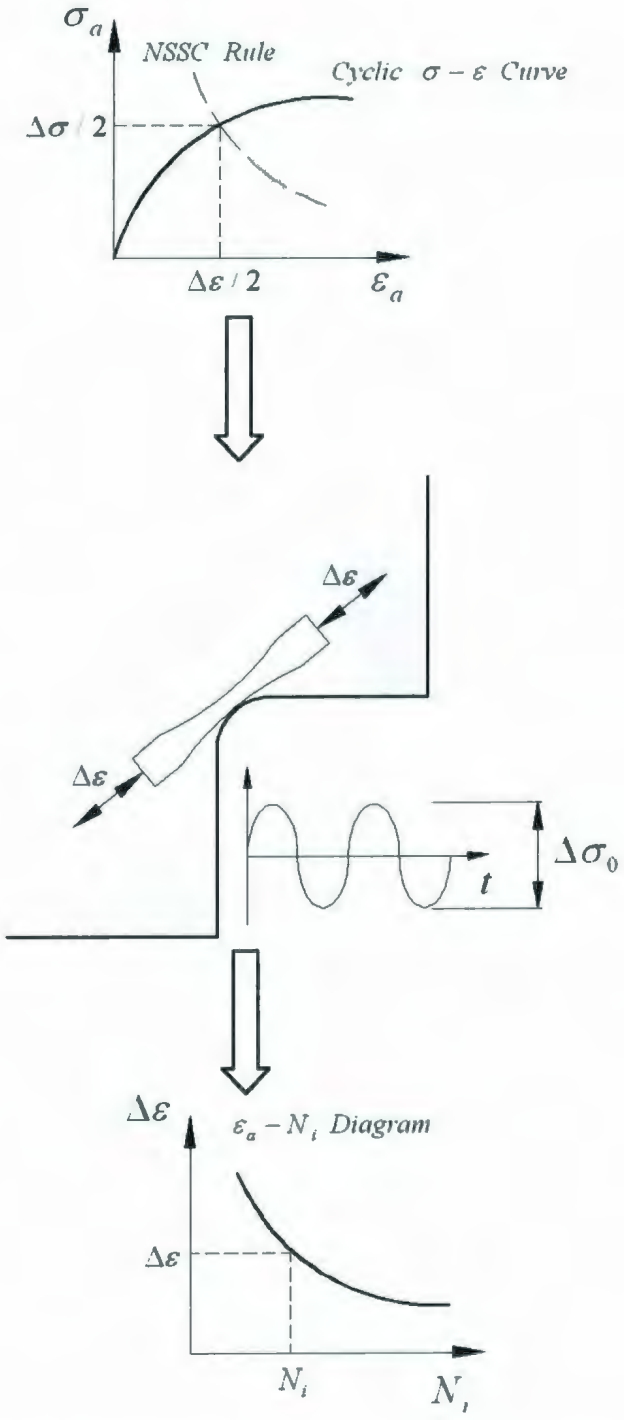

Figure 2.13: Fatigue crack initiation life prediction procedure

Crack propagation

The most widely accepted correlation between constant amplitude fatigue crack growth and the applied load is that suggested by Paris (1963). The rate of crack propagation per cycle, da/dN, is directly related to the mode I cyclic stress intensity, ΔK_I, for uniaxial specimen testing, in the following way

$$\frac{da}{dN} = C(\Delta K_I)^m \tag{2.40}$$

where $\Delta K = K_{max} - K_{min}$; and C and m is material constant.

Fatigue crack growth under mixed-mode loading has been studied since the 1960s (e.g. Iida and Kabayashi, 1969). Many parameters have been proposed to correlate crack growth rates under mixed-mode loading conditions. These include effective stress intensity factors, effective strain intensity factors, strain energy density factor and the J-integral (e.g. references Gdoutos, 2005 and Theocaris *et al.*, 1982). The parameters proposed for correlating the fatigue crack growth rate under mixed-mode loading include effective stress intensity factor, equivalent strain intensity factor and the J integral (e.g. references Tanaka, 1974, and Socie *et al.*, 1987). A detailed review of these theories, including advantages and limitations, has been presented by Bold *et al.* (1992).

It is worth noting that, although the effective SIF criterion is commonly used, the definition of a suitable model for determining effective stress intensities that accounts for load ratio, sequence and crack closure effects needs further work. However, a relationship of the form

$$\frac{da}{dN} = A(\Delta J)^B \tag{2.41}$$

which is analogous to the Paris law (e.g. Eq. (2.40)), has been suggested for crack propagation life predictions under mixed-mode loading conditions (Begley and Landes, 1972). Making analogy between cyclic loading and monotonic loading, the J-integral was introduced in Eq. (2.10) has been modified by Lamba (1975) as:

$$\Delta J = \oint_{\Gamma} (\Delta W^* \, dy - \Delta T_j \frac{\partial \Delta u_j}{\partial x} ds) \tag{2.42}$$

$$\Delta W^* = \int \Delta \sigma_{ij} \, d(\Delta \varepsilon_{ij}) \tag{2.43}$$

$$\Delta T_j = \Delta \sigma_{ij} \, n_i \tag{2.44}$$

The $\Delta\sigma_{ij}$, $\Delta\varepsilon_{ij}$, ΔT_j and Δu_j in Eqs. (2.42) to (2.44) are defined as:

$$\Delta\sigma_{ij} = \sigma_{ij}^{\max} - \sigma_{ij}^{\min}$$

$$\Delta\varepsilon_{ij} = \varepsilon_{ij}^{\max} - \varepsilon_{ij}^{\min}$$

$$\Delta T_j = T_j^{\max} - T_j^{\min}$$

$$\Delta u_j = u_j^{\max} - u_j^{\min}$$

For linear elastic materials, ΔJ reduces to its elastic value, i.e.,

$$\Delta J_e = \frac{\Delta K^2}{E}$$

The value of ΔJ below which no (measurable) amount of fatigue crack growth occurs is termed the threshold J-integral, J_{th}. The implication for design is important since, if in a cracked structure $\Delta J < J_{th}$, then crack propagation will not occur, which is a crucial requirement for components that experience a very large number of loading cycles in service. However, rapid crack advance leading to catastrophic failure occurs where

$$\Delta J = J_{Ic} \tag{2.45}$$

where J_{th} and J_{Ic} are material constants for a given thickness under specific environmental conditions.

The critical values of J_{th} and J_{Ic} are related to the threshold stress intensity factor, K_{th}, and the critical strain intensity factor (fracture toughness), K_{Ic}, as follows (Gdoutos, 2005):

$$J_{th} = \frac{1-\nu^2}{E} K_{th}^2 \tag{2.46}$$

$$J_{Ic} = \frac{1-\nu^2}{E} K_{Ic}^2 \tag{2.47}$$

If $\Delta J > J_{th}$, the fatigue crack propagation life, N_p, can be calculated by integrating the equation

$$N_p = \int_{a_0}^{a_c} \frac{da}{A(\Delta J)^B} \tag{2.48}$$

where A and B are material constants.

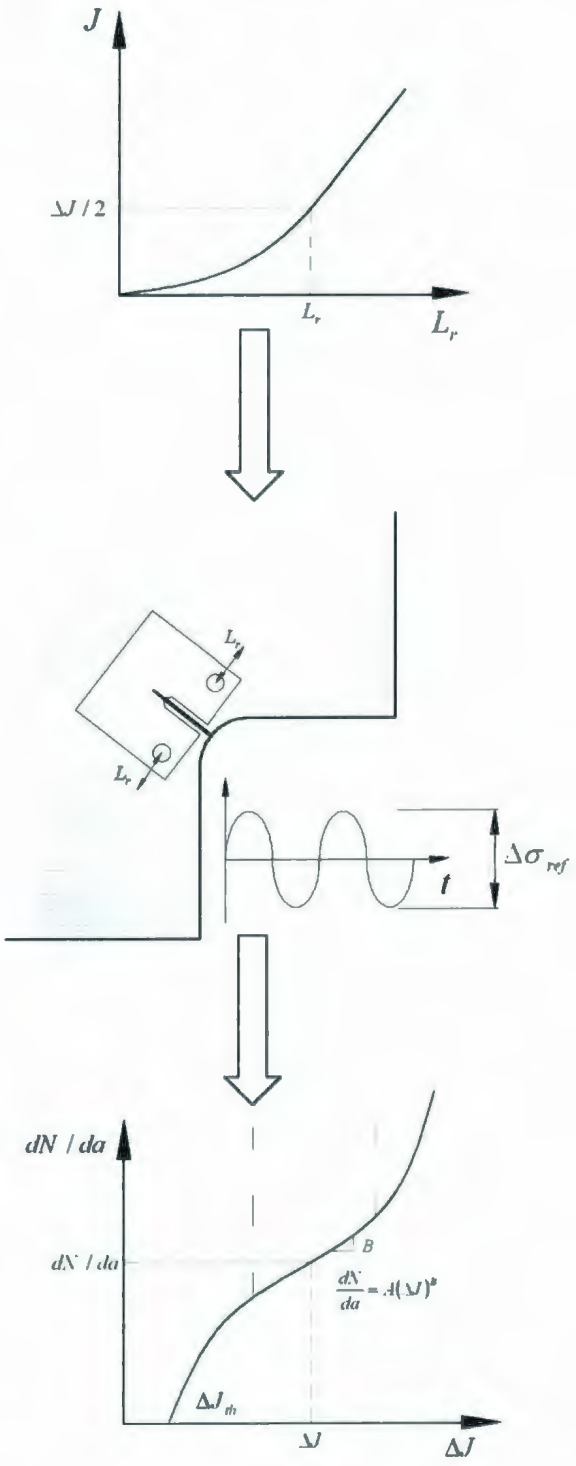

Figure 2.14: Fatigue crack propagation life prediction procedure based

CHAPTER 3

A REVIEW OF LIMIT LOAD ANALYSIS

3.1 INTRODUCTION

In this Chapter a comprehensive study of the available methods for limit load analysis is undertaken. Generally, the limit load can be estimated by one of the following methods:

- Analytical Techniques
- Numerical Procedures
- Experimental Analysis

Analytical techniques are limited to simple geometries and loading conditions. The alternative methods (numerical and experimental) are required for the more complicated problems. Experimental methods can be expensive and time consuming.

Therefore, the numerical approach is widely used for limit load analysis. Also, it is sometimes used in conjunction with other approaches like analytical methods.

3.2 ANALYTICAL TECHNIQUES

The analytical techniques for limit load analysis are used to determine the load carrying capacity of a component using mathematical formulations in the theory of plasticity. However, these methods are only feasible for some simple geometries and boundary conditions. These methods are sometimes combined with numerical methods; thus, a sharp division between the analytical techniques and the numerical procedures is not evident (Zyczkowski, 1981).

The following methods are generally considered as analytical approaches:

- Variational Methods
- Slip Lines Methods

3.2.1 Variational Principles in Theory of Plasticity

Consider a body under the following assumptions: the material is elastic-perfectly plastic, isotropic, incompressible and subjected to small deformations. The body is under traction T_i acting on the surface S_T. On the surface S_u, the velocity $\dot{u}_i = \overline{\dot{u}}_i$ is applied as shown in Fig. 3.1.

Based on the deformation theory of plasticity, the following expressions are valid for the stress, strain and displacement in the body,

1- Equilibrium Equation

$$\sigma_{ij,j} = 0 \tag{3.1}$$

2- Yield condition

$$s_{ij}s_{ij} - 2k^2 \leq 0 \tag{3.2}$$

3- Stress-strain rate relation

$$\dot{\varepsilon}_{ij} = \mu s_{ij} \tag{3.3}$$

4- Rate of strain-velocity relation

$$\dot{\varepsilon}_{ij} = \tfrac{1}{2}\left(\dot{u}_{i,j} + \dot{u}_{j,i}\right) \tag{3.4}$$

5- Incompressibility condition*

$$\dot{\varepsilon}_{ii} = 0 \tag{3.5}$$

* Incompressibility condition imposes that the volume is constant during plastic deformation

6- Boundary conditions

$$\sigma_{ij} n_j = T_i \qquad \text{on } S_T \tag{3.6}$$

$$\dot{u}_i = \bar{\dot{u}}_i \qquad \text{on } S_u \tag{3.7}$$

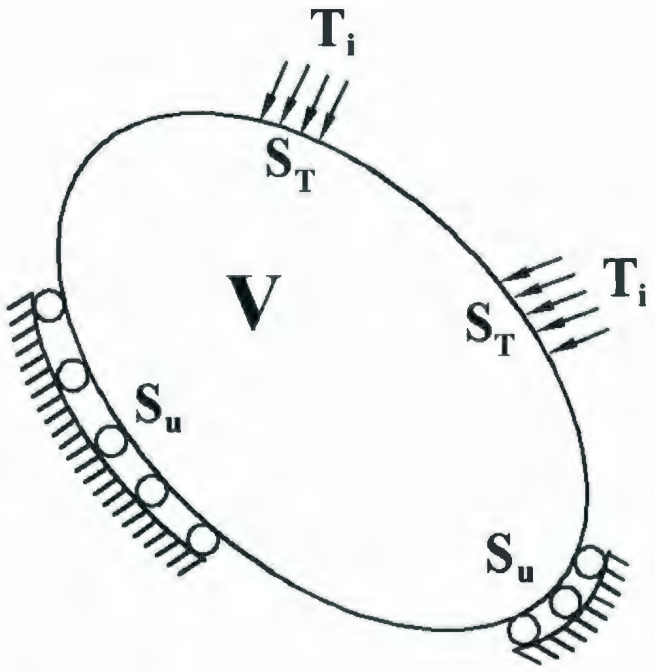

Figure 3.1: A body with elastic-perfectly plastic material

3.2.2 Variational Principles in Limit Load Analysis

One of the most important applications of variational method in the theory of plasticity is the limit load analysis. Consider a body made of elastic–perfectly plastic material that is in equilibrium with the surface traction T_i acting on the surface S_T. On the

surface S_u, the constraint $\dot{u}_i = 0$ is applied as shown in Fig. 3.2. It is assumed that the surface traction is applied as a proportional loading; that is, external tractions are assumed to be γT_i, where γ is a monotonically increasing parameter. For sufficiently small values of γ, the entire body will be in an elastic state. As γ is gradually increased, at a certain load multiplier $\gamma = m_e$ plastic flow initiates at a point or simultaneously more parts in the body reach the plastic state. The corresponding load ($T_i\big|_{elasic} = m_e T_i$) is called the elastic limit load and indicates the limit of applicability of the theory of elasticity. Then, by increasing the load parameter, plastic state spreads to several parts of the body. When the load mT_i is applied, where $\gamma = m$, the body will be in a state of impending plastic limit state. Here, m is the limit load multiplier and, in other words, the safety factor against collapse. The collapse load of a structure is then evaluated as:

$$T_i\big|_{collapse} = mT_i \tag{3.8}$$

In the plastic limit state the body fully or partially undergoes unrestricted plastic deformation under constant external load.

In the following section, the basis for different limit load multipliers based on the variational formulation in the limit load analysis are discussed.

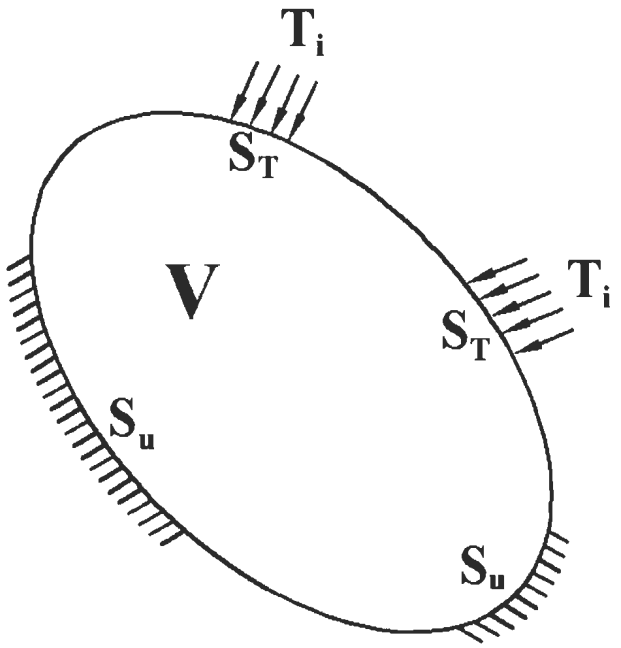

Figure 3.2: A body with elastic-perfectly plastic material-fixed boundary conditions

3.2.3 Classical Lower and Upper Bound Limit Load Multipliers

The main objective of the limit load analysis is to estimate the limit load multiplier at the impending plastic limit state of a body. However, for complicated problems it may very difficult to find the exact limit load. Therefore, based on the extremum principles of limit load analysis, the lower bound theorem or the upper bound theorem is employed to estimate the limit load directly without considering the entire loading history.

Classical lower bound theorem

The lower bound limit load can be calculated by invoking the lower bound limit load theorem that states that if a statically admissible stress distribution throughout a given body can be found in which the stress nowhere exceeds yield under given loading and everywhere in equilibrium internally and balances certain external loads the applied load is a lower bound on the limit (Calladine, 2000).

A stress field σ_{ij}^{0} is called statically admissible if it satisfies the following:

$$\sigma_{ij,j}^{0} = 0 \tag{3.9}$$

$$s_{ij}s_{ij} - 2k^2 \leq 0 \tag{3.10}$$

$$\sigma_{ij}^{0} n_j = m_L T_i \qquad \text{on } S_T \tag{3.11}$$

In the above expressions m_L is the classical statically admissible limit load multiplier, and n_j is a normal vector on the surface. Based on the lower bound limit theorem of limit analysis, any statically admissible limit load multiplier is less than or equal to the exact limit load multiplier (the proof is given next),

$$m_L \leq m \tag{3.12}$$

Proof: Since small deformation is assumed, the virtual work principal can be used. For a body shown in Fig. 3.2, the principle of virtual work can be written for actual limit state stress field (σ_{ij}) caused by the external load of mT_i and an arbitrary statically admissible stress field (σ_{ij}^0) with external load of $m_L T_i$ as

$$m \int_{S_T} T_i \dot{u}_i \, dS = \int_V \sigma_{ij} \dot{\varepsilon}_{ij} \, dV \tag{I}$$

$$m_L \int_{S_T} T_i \dot{u}_i \, dS = \int_V \sigma_{ij}^0 \dot{\varepsilon}_{ij} \, dV \tag{II}$$

The left hand sides of the Eqs. (I) and (II) represent the work done by the surface or external forces, and the right hand sides are the plastic work dissipated to create an increment of plastic strain.

Subtracting equation (II) from (I) results in following expression

$$(m - m_L) \int_{S_T} T_i \dot{u}_i \, dS = \int_V (\sigma_{ij} - \sigma_{ij}^0) \dot{\varepsilon}_{ij} \, dV \tag{III}$$

According to the maximum work principle and the normality rule, the expression in the right hand side of Eq. (III) must be greater or equal to zero (see Fig. 3.3). Thus

$$(m - m_L) \int_{S_T} T_i \dot{u}_i \, dS \geq 0 \tag{IV}$$

The integral in expression (IV) represents the work done by external forces that cannot be negative. Therefore, $m_L \leq m$ and the stated principle has been proved.

Classical upper bound theorem

The classical upper bound limit load theorem states that if for a given load set the rate at which the external forces do work is equal to or exceeds the rate of internal dissipation, then the applied load set will be equal to or more than the plastic collapse load (Calladine, 2000). A set of velocity components $\dot{u}_i^*$ will be called kinemattically admissible if it satisfies the following conditions

$$\dot{\varepsilon}_{ij}^* = \tfrac{1}{2}\left(\dot{u}_{i,j}^* + \dot{u}_{j,i}^*\right) \tag{3.13}$$

$$\dot{\varepsilon}_{ii}^* = 0 \tag{3.14}$$

$$\dot{u}_i^* = 0 \qquad \text{on } S_u \tag{3.15}$$

$$\int_{S_T} T_i \dot{u}_i^* \, dV > 0 \tag{3.16}$$

Here σ_{ij}^* denotes the stress field associated with the kinematically admissible strain rate field $\dot{\varepsilon}_{ij}^*$ and satisfies the yield condition $f(\sigma_{ij}^*, k) = 0$ at each point in the body.

The classical upper bound multiplier, m_U, can be obtained in the following manner, using the Schwarz's* inequality:

$$s_{ij}\dot{\varepsilon}^*_{ij} \le \sqrt{s_{ij}s_{ij}}\sqrt{\dot{\varepsilon}^*_{ij}\dot{\varepsilon}^*_{ij}} \tag{3.17}$$

At plastic state $s_{ij}s_{ij} = 2k^2$; therefore, Eq. (3.17) can be rewritten as

$$s_{ij}\dot{\varepsilon}^*_{ij} \le \sqrt{2}k\sqrt{\dot{\varepsilon}^*_{ij}\dot{\varepsilon}^*_{ij}} \tag{3.18}$$

Integrating the above inequality

$$m_U \int_{S_T} T_i \dot{u}^*_i dS \le \sqrt{2}k \int_V \sqrt{\dot{\varepsilon}^*_{ij}\dot{\varepsilon}^*_{ij}}\, dV \tag{3.19}$$

Therefore, the classical upper bound limit load multiplier is found as

$$m_U = \sqrt{2}k \frac{\int_V \sqrt{\dot{\varepsilon}^*_{ij}\dot{\varepsilon}^*_{ij}}\, dV}{\int_{S_T} T_i \dot{u}^*_i dS} \tag{3.20}$$

---

* Schwarz inequality, also known as the Cauchy–Schwarz inequality is given as

$$(x,y) \le \|x\|\|y\|$$

The (x,y) is the inner product of x and y, i.e.,

$$(x,y) = \int xy dz$$

And $\|x\|$ and $\|y\|$ are the norms of x and y, respectively.

$$\|x\| = \sqrt{\int x^2 dz}\,;\ \|y\| = \sqrt{\int y^2 dz}$$

Based on the upper bound theorem of limit load analysis, any kinematically admissible limit load multiplier is greater or equal to the exact limit load multiplier

$$m_U \geq m \tag{3.21}$$

The proof of the above statement is given next.

Proof: The classical upper bound limit load theorem can be written in form of following inequality

$$m_U \int_{S_T} T_i \dot{u}_i^* dS \geq \int_V \sigma_{ij}^* \dot{\varepsilon}_{ij}^* dV \qquad \text{(I)}$$

Now, consider the actual stress filed σ_{ij} in a body that is under the plastic limit load $T_i\big|_{collapse} = mT_i$. Then, using any arbitrary kinematically admissible strain rate and velocity field and applying the principle of virtual velocities results in

$$m \int_{S_T} T_i \dot{u}_i^* dS = \int_V \sigma_{ij} \dot{\varepsilon}_{ij}^* dV \qquad \text{(II)}$$

Subtracting Eq. (II) from Eq.(I) yields

$$(m_U - m) \int_{S_T} T_i \dot{u}_i^* dS \geq \int_V (\sigma_{ij}^* - \sigma_{ij}) \dot{\varepsilon}_{ij}^* dV \qquad \text{(III)}$$

Considering the convexity of yield surface and normality rule (Fig. 3.4), we can write

$$(\sigma_{ij}^* - \sigma_{ij}) \dot{\varepsilon}_{ij}^* \geq 0 \qquad \text{(IV)}$$

Therefore, Eq. (III) results in following expression

$$(m_U - m) \int_{S_T} T_i \dot{u}_i^* dS \geq 0 \qquad \text{(V)}$$

The integral in expression (V) represents the work done by external forces that cannot be negative; therefore, $m_U \geq m$.

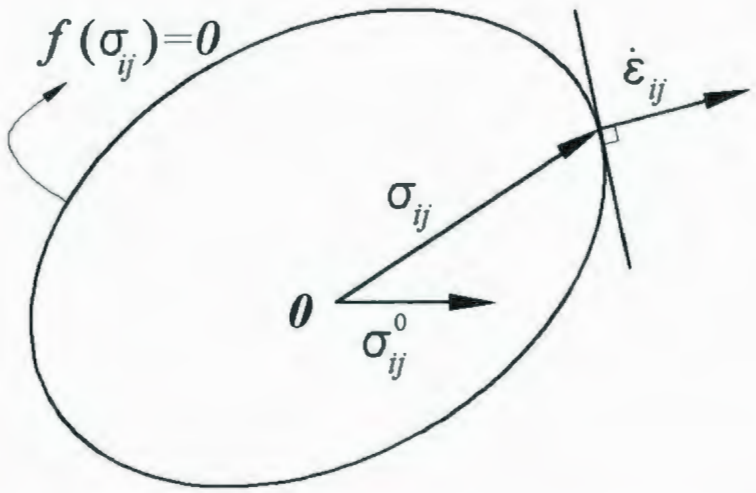

Figure 3.3: Yield surface and normality rule, statically admissible stress field

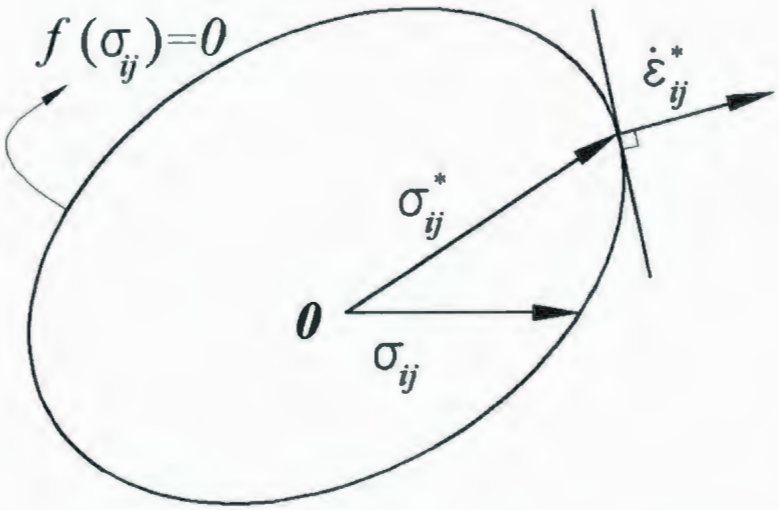

Figure 3.4: Yield surface and normality rule, kinematically admissible strain field

3.2.4 New Lower and Upper Bound Limit Load Multipliers

In the theory of elasticity, the method of Treffz is a powerful tool to estimate the lower bound and upper bound value of a functional which is the potential energy of a given system in equilibrium. Mura and Lee (1963) extended this idea to the theory of plasticity, and introduced a functional so that the extremum values of the functional are lower bound and upper bound values of the actual limit load. Also, Mura *et al.* (1964) extended this method to orthotropic solids. Lee *et al.* (1967) generalized the method for anisotropic and non-homogeneous materials, and Sacchi and Save (1968) proposed some approximate procedures for three-dimensional rigid-perfectly plastic continuum which follow from Mura and Lee (1963) variational method.

Mura and Lee (1963) showed that the state of impending plastic flow is provided by the stationary condition of the following functional

$$F[\dot{u}_i, s_{ij}, \sigma_m, R_i, \mu, m, \varphi] = \int_V s_{ij} \frac{1}{2}(\dot{u}_{i,j} + \dot{u}_{j,i}) dV + \int_V \sigma_m \delta_{ij} \dot{u}_{i,j} dV - \int_{S_u} R_i \dot{u}_i dS - m\left(\int_{S_T} T_i \dot{u}_i dS - 1 \right) - \int_V \mu \{ f(s_{ij}) + \varphi^2 \} dV \tag{3.22}$$

subjected to the constraint condition

$$\mu \geq 0 \tag{3.23}$$

They also showed that the safety factor (limit load multiplier) is the stationary value of the same functional. In Eq. (3.22) the function $f(s_{ij})$ is the yield criterion, and the arguments of F are the independent variables: velocity $\dot{u}_i$, deviatoric stress s_{ij}, the hydrostatic σ_m, the reaction R_i on $S_{\dot{u}}$, T_i is surface traction, m is the limit load multiplier, μ is the positive scalar factor in the linear relation between the strain rate and deviatoric stress and φ is the point function . For an elastic-perfectly plastic material, the following expression is valid

$$\begin{cases} if\ \varphi \neq 0 \rightarrow \mu = 0\ and\ \frac{1}{2}s_{ij}s_{ij} - k^2 < 0 & (elastic) \\ if\ \varphi = 0 \rightarrow \mu \neq 0\ and\ \frac{1}{2}s_{ij}s_{ij} - k^2 = 0 & (plastic) \end{cases} \tag{3.24}$$

Taking the first variation of Eq. (3.22), the following natural conditions can be obtained:

$$\frac{1}{2}(\dot{u}_{i,j} + \dot{u}_{j,i}) = \mu \frac{\partial f}{\partial s_{ij}} \qquad \text{in } V \tag{3.25}$$

where $\mu \geq 0$

$$(s_{ij} + \sigma_m \delta_{ij})_{,j} = 0 \qquad \text{in } V \tag{3.26}$$

$$(s_{ij} + \sigma_m \delta_{ij}) n_j = m T_i \quad \text{on } S_T \tag{3.27}$$

$$(s_{ij} + \sigma_m \delta_{ij}) n_j = R_i \qquad \text{on } S_u \tag{3.28}$$

$$f(s_{ij}) + \varphi^2 = 0 \qquad \text{in } V \tag{3.29}$$

$$\mu \varphi = 0 \qquad \text{in } V \tag{3.30}$$

$$\delta_{ij} \dot{u}_{i,j} = 0 \qquad \text{in } V \tag{3.31}$$

$$\dot{u}_i = 0 \qquad \text{on } S_u \tag{3.32}$$

$$\int_{S_T} T_i \dot{u}_i dS = 1 \tag{3.33}$$

It should be noted that the variables σ_m, R_i, m and μ are considered as the Lagrangian multipliers associated with the required conditions for plastic flow, all of which are of physical significance.

Consider now the arbitrary arguments:

$$\left|\begin{array}{l} \dot{u}_i^0 = \dot{u}_i + \delta\dot{u}_i \\ s_{ij}^0 = s_{ij} + \delta s_{ij} \\ \sigma_m^0 = \sigma_m + \delta\sigma_m \\ R_i^0 = R_i + \delta R_i \\ m^0 = m + \delta m \\ \mu^0 = \mu + \delta\mu \\ \varphi^0 = \varphi + \delta\varphi \end{array}\right. \tag{3.34}$$

where $\dot{u}_i$, s_{ij}, etc., denote the stationary set of arguments of the Eq. (3.22) and $\delta\dot{u}_i$, δs_{ij} etc., are the corresponding variations. Substituting the arguments of Eq. (3.22) with Eq. (3.34), giving regard to the stationary conditions Eqs. (3.25) to (3.33), and noting that the right-hand side of Eq. (3.22) in this case is equal to m, the functional F takes the form

$$\begin{aligned} F\left[\dot{u}_i^0, s_{ij}^0, \sigma_m^0, R_i^0, \mu^0, m^0, \varphi^0\right] = m &+ \int_V \delta s_{ij} \tfrac{1}{2}(\delta\dot{u}_{i,j} + \delta\dot{u}_{j,i})\,dV + \int_V \delta\sigma_m^0 . \delta_{ij} . \delta\dot{u}_{i,j}\,dV \\ &- \int_{S_u} \delta R_i . \delta\dot{u}_i\,dS - \delta m \int_{S_T} T_i \delta\dot{u}_i\,dS - \int_V \mu \left\{\tfrac{1}{2}\delta s_{ij}\delta s_{ij} + (\delta\varphi)^2\right\} dV \\ &- \int_V \delta\mu \left\{f(s_{ij}^0) + (\varphi^0)^2\right\} dV \end{aligned} \tag{3.35}$$

Lower bound theorem

Mura *et al.* (1965) proposed the lower bound limit load multiplier m' as

$$m' = \frac{m^0}{1 + \frac{1}{2k^2}\max\left\{f(s_{ij}^0) + (\varphi^0)^2\right\}} \le m \tag{3.36}$$

in which the set s_{ij}^0, σ_m^0, m^0, μ^0, and φ^0 satisfy the requirement of statically admissible stress field, i. e.,

$$(s_{ij}^0 + \sigma_m^0 \delta_{ij})_{,j} = 0 \qquad \text{in } V \tag{3.37}$$

$$(s_{ij}^0 + \sigma_m^0 \delta_{ij}) n_j = m^0 T_i \qquad \text{on } S_T \tag{3.38}$$

$$\int_V \mu^0 \left\{f(s_{ij}^0) + (\varphi^0)^2\right\} dV = 0 \tag{3.39}$$

$$\mu^0 \ge 0 \tag{3.40}$$

The quantity $\max\left\{f(s_{ij}^0) + (\varphi^0)^2\right\}$ is the maximum value of $\left\{f(s_{ij}^0) + (\varphi^0)^2\right\}$ inside the domain V.

Proof: The theorem is proven as follows: Eq. (3.35) can be reduced to

$$F = m - \int_V \mu \left\{ \tfrac{1}{2} \delta s_{ij} \delta s_{ij} + (\delta\varphi)^2 \right\} dV - \int_V \delta\mu \left\{ f(s_{ij}^0) + (\varphi^0)^2 \right\} dV \tag{I}$$

By integrating the second and third terms by parts in view of Eqs. (3.26) to (3.28), (3.37) and (3.38) and

$$(s_{ij}^0 + \sigma_m^0 \delta_{ij}) n_j = R_i^0 \tag{II}$$

Also integrating Eq. (3.22) with the arbitrary set of arguments $\dot{u}_i^0$, s_{ij}^0, σ_m^0, m^0, μ^0, and φ^0 and making use of Eqs. (3.37), (3.38) and (II) leads to

$$F = m^0 - \int_V \mu^0 \left\{ f(s_{ij}^0) + (\varphi^0)^2 \right\} dV \tag{III}$$

In view of Eq. (3.39), Eqs. (II) and (III) yield

$$m^0 \le m - \int_V \delta\mu \left\{ f(s_{ij}^0) + (\varphi^0)^2 \right\} dV \tag{IV}$$

Since $\mu^0 = \mu + \delta\mu$ Eq. (3.39) gives

$$- \int_V \delta\mu \left\{ f(s_{ij}^0) + (\varphi^0)^2 \right\} dV = \int_V \mu \left\{ f(s_{ij}^0) + (\varphi^0)^2 \right\} dV \tag{V}$$

(Cont'd...)

Substituting Eq. (V) into Eq. (IV) and taking the maximum value of the integrand, which is always positive because of Eqs. (3.39) and (3.40), leads to

$$m^0 \le m + \max\left\{f(s_{ij}^0) + (\varphi^0)^2\right\} \int_V \mu \, dV \tag{VI}$$

On the account of Eqs. (3.25) to (3.33), the following holds

$$\begin{aligned} m = m \int_{S_T} T_i \dot{u}_i dS &= \int_S \left(s_{ij} + \delta_{ij}\sigma_m\right) n_j \dot{u}_i dS = \int_S s_{ij} n_j \dot{u}_i dS + \int_S \delta_{ij}\sigma_m \, n_j v_i dS \\ &= \int_V s_{ij} \dot{u}_{i,j} dV + \int_V \left(s_{ij} + \sigma_m \delta_{ij}\right)_{,j} \dot{u}_i dV = \int_V s_{ij} \frac{1}{2}\left(\dot{u}_{i,j} + \dot{u}_{j,i}\right) dV \\ &= \int_V s_{ij} \mu \, s_{ij} dV = 2k^2 \int_V \mu \, dV \end{aligned}$$

Therefore,

$$\int_V \mu \, dV = \frac{m}{2k^2} \tag{VII}$$

The proof is completed by combining Eqs. (VI) and (VII).

Equation (3.38) includes the classical definition of the lower bound, by taking the special case of Eq. (3.39) as

$$f(s_{ij}^0) + (\varphi^0)^2 = 0 \tag{VIII}$$

In this case $\max[f(s_{ij}^0) + (\varphi^0)^2]$ vanishes, and Eq. (3.36) reduces to $m_L \le m$.

Thus, the new lower bound expressed by Eq. (3.36) holds for a broader stress field than the classical statically admissible stress field by taking the integral mean of the yield criterion.

Upper bound theorem

The upper bound limit load multiplier m^* has been introduced by Mura *et al.* (1965) as

$$m^* = \left(\int_V 2k\mu^* dV \right) \max\left\{ \tfrac{1}{2} s_{ij}^* s_{ij}^* \right\} \geq m \tag{3.41}$$

if the quantities $\dot{u}_i^*$, s_{ij}^* and μ^* satisfy

$$\dot{u}_i^* = 0 \qquad \text{on } S_V \tag{3.42}$$

$$\delta_{ij}\dot{u}_{i,j}^* = 0 \qquad \text{on } V \tag{3.43}$$

$$\int_{S_T} T_i \dot{u}_i^* dS = 1 \tag{3.44}$$

$$\mu^0 \frac{\delta f}{\delta s_{ij}^*} = \mu^* s_{ij}^* = \tfrac{1}{2}(\dot{u}_{i,j}^* + \dot{u}_{j,i}^*) = \dot{\varepsilon}_{ij}^* \tag{3.45}$$

$$\int_V \mu^* f(s_{ij}^*) dV = 0 \tag{3.46}$$

$$\mu^* \geq 0 \tag{3.47}$$

The notation $\max\left\{\frac{1}{2}s_{ij}^{*}s_{ij}^{*}\right\}$ means the maximum value of $\left\{\frac{1}{2}s_{ij}^{*}s_{ij}^{*}\right\}$ and $\dot{\varepsilon}_{ij}^{*}$ denotes the strain rate associated with $\dot{u}_i^*$.

Proof: The theorem can be proven as follow. Multiplying both sides of Eq. (3.45) by s_{ij} and applying Schwarz's inequality

$$\mu^{*}[s_{ij}^{*}s_{ij}^{*}]^{1/2}[s_{ij}^{*}s_{ij}^{*}]^{1/2} \geq s_{ij}\,\tfrac{1}{2}(\dot{u}_{i,j}^{*}+\dot{u}_{j,i}^{*}) \tag{I}$$

Also from Eqs. (3.24) and (3.29),

$$\tfrac{1}{2}s_{ij}s_{ij}-k^2 \leq 0 \rightarrow \sqrt{2}k \geq [s_{ij}^{*}s_{ij}^{*}]^{1/2} \tag{II}$$

Substituting (II) into Eq. (I), integrating both of Eq. (I) in V and taking the maximum values of $[s_{ij}^{*}s_{ij}^{*}]^{1/2}$ lead to

$$\left(\int_V 2\mu^{*}k dV\right)\max\left\{\tfrac{1}{2}s_{ij}^{*}s_{ij}^{*}\right\}^{1/2} \geq \int_V s_{ij}\,\tfrac{1}{2}(\dot{u}_{i,j}^{*}+\dot{u}_{j,i}^{*})dV \tag{III}$$

On the other hand

$$\int_V s_{ij}\,\tfrac{1}{2}(\dot{u}_{i,j}^{*}+\dot{u}_{j,i}^{*})dV = \int_V (s_{ij}+\delta_{ij}\sigma_m)v_{i,j}^{*}dV = \int_S (s_{ij}+\delta_{ij}\sigma_m)n_j\dot{u}_i^{*}dS = m \tag{IV}$$

Because of Eqs. (3.26), (3.27) and (3.42) to (3.44). Adding Eqs. (III) and (IV) completes the proof. Equation (3.41) includes the classical upper bound limit load definition, by applying special form of Eq. (3.46) as

$$f(s_{ij}^{*}) = 0 \tag{V}$$

(Cont'd ...)

In this case $\max(\frac{1}{2}s_{ij}^{*}s_{ij}^{*})^{\frac{1}{2}} = k$, and Eq. (3.41) reduces to

$$m^{*} = \int_{V} 2k^{2}\mu^{*}dV \geq m \tag{VI}$$

Multiplying both sides of the Eq. (3.45) by s_{ij}^{*} conjunction with Schwarz inequality results in

$$\mu^{*}s_{ij}^{*}s_{ij}^{*} = \tfrac{1}{2}s_{ij}^{*}(\dot{u}_{i,j}^{*} + \dot{u}_{j,i}^{*}) \leq \sqrt{s_{ij}s_{ij}}\sqrt{\tfrac{1}{2}(\dot{u}_{i,j}^{*} + \dot{u}_{j,i}^{*})\tfrac{1}{2}(\dot{u}_{i,j}^{*} + \dot{u}_{j,i}^{*})} \tag{VII}$$

Therefore, using the equality sign

$$\mu^{*} = \sqrt{\frac{\frac{1}{2}(\dot{u}_{i,j}^{*} + \dot{u}_{j,i}^{*})\frac{1}{2}(\dot{u}_{i,j}^{*} + \dot{u}_{j,i}^{*})}{s_{ij}^{*}s_{ij}^{*}}} = \sqrt{\frac{\frac{1}{2}(\dot{u}_{i,j}^{*} + \dot{u}_{j,i}^{*})\frac{1}{2}(\dot{u}_{i,j}^{*} + \dot{u}_{j,i}^{*})}{2k^{2}}} \tag{VIII}$$

Substituting Eq. (VIII) into Eq. (VI), and making use of Eq. (3.45), the classical upper bound limit load can be obtained as

$$\int_{V} 2k^{2}\sqrt{\frac{\frac{1}{2}(\dot{u}_{i,j}^{*} + \dot{u}_{j,i}^{*})\frac{1}{2}(\dot{u}_{i,j}^{*} + \dot{u}_{j,i}^{*})}{2k^{2}}}dV \geq m \tag{IX}$$

$$m_{U} = \sqrt{2}k\int_{V}\sqrt{\dot{\varepsilon}_{ij}^{*}\dot{\varepsilon}_{ij}^{*}}dV \geq m \tag{X}$$

The new upper bound is introduced in Eq. (3.41) holds the broader stress field than classical upper bound limit load formulation (Mura *et al.*, 1965).

3.2.5 Slip Line Method

Slip line method is widely used in metal forming and soil mechanics to estimate limit load in a component or structure in plane strain condition. The inception of slip line method in metal plasticity dates back to the works of Hencky (1923), Prandtl (1923), and Carthcodory and Schmidt (1923). However, detailed studies have been later done by Hill (1950), and Prager and Hodge (1951).

The aim of slip line method is to define a coordinate system that lies on a potential failure surfaces in a given component (Davis and Selvadurai, 2002). Indeed, using this coordinate system, the system of equations become very simple. In a two-dimensional systems the potential failure surfaces become lines (slip lines), and combinations of these lines form a network that covers the failing regions. The axis of the new coordinate system, say α and β, need to be defined in such a way that at each point they align on the potential failure surfaces. In other words, the direction of the new axis is on the direction of maximum shear stress when plastic flow occurs.

As illustrated in Fig. 3.5, the definition of the α and β can be understood by using Mohr diagram. In this figure, α-line and β-line are located at two maximum shear stress failure lines (potential failure surface). Therefore, these two lines are orthogonal. Also, when plastic flow occur the magnitude of shear stresses on these lines are equal (assuming non-hardening material model).

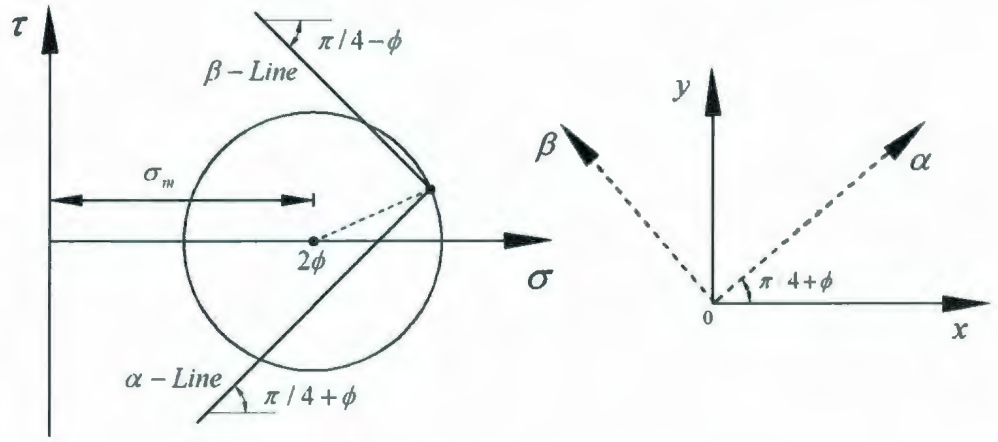

Figure 3.5: Definition of slip line on Mohr diagram

3.3 NUMERICAL PROCEDURES

Limit load analysis using analytical techniques is restricted to simple problems. However, it can lead to good estimation of limit load or even the exact solution. Therefore, numerical approach has been developed to solve more complicated problem.

In numerical methods the following points should be considered:

- The problem should be analyzed in a discrete form.
- Suitable discretization[1] depends on the problem under consideration (i.e., fine discretization around the stress raisers).

[1] Discretization means to convert a given continues model into smaller parts (discrete counterparts). This process is usually carried out to make the problem suitable for numerical simulation , i.e. finite element method.

In what follows, some of the most important and commonly used numerical methods are discussed.

3.3.1 Programming Methods

Programming methods have been used since 1940 in many different fields including economics, strategic planning, structural engineering and cryptography (Gill *et al.*, 1991). However, the application of programming methods in limit analysis dates back to the work by Charnes and Greenberg in 1951. The programming methods were initially developed to compute limit load for trusses, beams, and frames (Dorn and Gavarini, 1957, and Charnes *et al.*, 1959), and later developed for plate structures (Koopman and Lance, 1965, and Hodge and Belytschko, 1968) and shell structures (Biron and Hodge, 1967, and Dinno and Gill, 1974). The limit load analysis using programming method is based on minimizing or maximizing a function subjected to certain constraints, which can be expressed in terms of equality or inequality.

Generally, programming methods can be divided into two main approaches:

- Linear programming
- Non-linear programming

The linear programming approach is based on replacing the non-linear yield condition by a piecewise linear function (linearization of yield surface).

The non-linear programming approach, which is more accurate but more difficult (Zyczkowski, 1981), was first published by Hodge (1964) for limit analysis of beams and arches. This approach applies a non-linear yield function and higher order approximations to the stress and velocity fields.

The finite element method is widely used in limit analysis using programming methods. Discretization of the continuum using finite element leads to a standard optimization problem where the objective function is maximizing/minimizing of lower/upper bound limit load multiplier subjected to set of equality and inequality constraints. The application of finite element method in programming method is briefly discussed in the following section.

Lower bound solution

The lower bound theorem of limit load analysis states that the lower bound limit load multiplier is less than or equal to the exact limit load, i. e.,

$$m_{Lower} \leq m \tag{3.48}$$

This inequality can be written as (see Fig. 3.6)

$$m = \max[m_{Lower}] \tag{3.49}$$

Therefore, the programming method is an optimization problem of the form:

$$\text{Maximized: } m_{Lower}$$

$$\text{Subjected to: } \begin{cases} g(x) = 0 \\ f(x) \le 0 \end{cases} \tag{3.50}$$

Upper bound solution

Referring to the definition of the upper theorem of limit analysis, the upper bound limit load multiplier m_{Upper} is greater than or equal to the exact limit load solution m, i. e.

$$m \le m_{Upper} \tag{3.51}$$

Therefore, the limit analysis problem can be considered as minimizing problem as (see Fig. 3.7)

$$m = \min[m_{Upper}] \tag{3.52}$$

Therefore, the optimization problem can be written in following format

$$\text{Minimized: } m_{Upper}$$

$$\text{Subjected to: } \begin{cases} g(x) = 0 \\ f(x) \leq 0 \end{cases} \tag{3.53}$$

The programming problem then requires that the upper bound limit load multiplier m_{Upper} becomes minimized with respect to the rate of nodal displacement (using the definition of classical upper bound theory). Due to the complexity of programming methods in nature, these methods have only been used for two-dimensional components and some simple three dimensional configurations. More recently, Lyamin and Sloan (2002 a, b) developed the work of Zouain *et al.* (1993) to perform upper bound and lower bound limit load analysis in three dimensional structures. However, they applied a simple element type (hexagonal element) in the finite element discretization. Still these methods seem to be not easily implemented into available commercial finite element packages. Also, because of the huge number of constraint equations and the degrees of freedom, these methods require large computer memory and a considerable computational time. More work is required to overcome some of the difficulties and complexity when using programming methods.

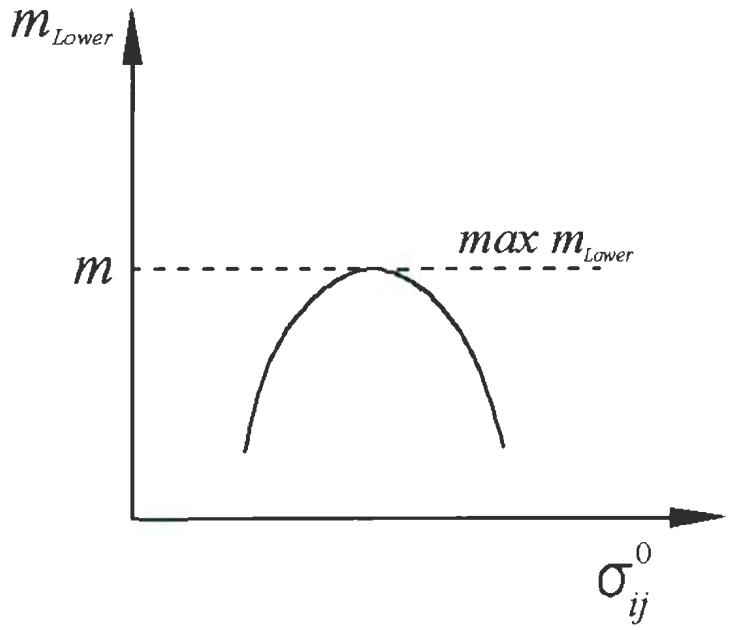

Figure 3.6: Concept of lower bound solution

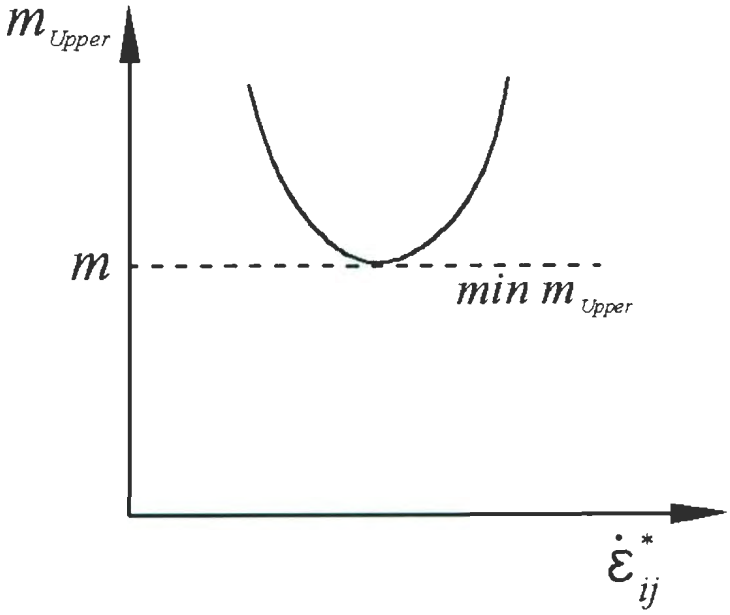

Figure 3.7: Concept of upper bound solution

3.3.2 Elastic Modulus Adjustment Procedure (EMAP)

Jones and Dhalla (1981) were one of the earliest users of elastic modulus adjustment procedures (EMAP) in their research work. Highly stressed regions of the component or structure were systematically softened by a reduction of their modulus of elasticity in an attempt to simulate local inelastic action.

Marriott (1988) developed an iterative procedure for estimating lower-bound limit loads on the basis of linear elastic FEA by generating statically admissible stress fields and using them in conjunction with established theorems of limit analysis. In this method, an arbitrary load that guarantees the yielding in the component is applied and an initial elastic analysis is performed. All the elements in which corresponding stress intensities exceed the code allowable stresses are selected and elastic modulus of these elements are modified using the following expression

$$E_R = E_0 \frac{S_m}{SI} \tag{3.54}$$

where, E_0 is initial elastic modulus, S_m is the allowable stress given by the codes and SI is element stress intensity. The procedure continues in an iterative manner until the maximum stress in the component does not change with the further iteration or all the elements have the equivalent stress below the S_m. Finally, using the following expression the limit load can be estimated:

$$P_L = P\frac{\sigma_y}{\sigma_{\max}} \tag{3.55}$$

where σ_y is yield strength and $\sigma_{\max}$ is the maximum equivalent stress in the component.

Seshadri and Fernando (1992) made use of the elastic modulus adjustment procedure to determine lower bound limit loads by adopting reference stress concepts in creep design (Kraus, 1980). Their technique, called the Redistribution Node (R-Node) Method, is based on two linear elastic FEA in which the load control location (R-Nodes) are determined and using stresses in these location, the limit load of the component will be achieved. The procedure can be performed in following manner:

- The first analysis is carried out with homogeneous material properties, i. e. E_0,v .
- The second linear elastic FEA is performed by systematically, but artificially, reducing the elastic moduli of the elements that exceed the yield strength.

$$(E_s)_j = \left[\frac{\sigma_y}{(\sigma_e)_j}\right] E_0 \tag{3.56}$$

where the subscript "*j*" is the element number.

- Using the results of these two linear elastic analysis, as presented in Fig. 3.8, the follow up angle (θ) can be determined on the Generalized Localized Stress Strain curve (GLOSS) as

$$\theta = tag^{-1}\left(\frac{\sigma_A - \sigma_B}{\varepsilon_B - \varepsilon_A}\right) \tag{3.57}$$

- The location where θ=90 are the R-Node locations, where stresses in these locations are proportional to external load for elastic-perfectly plastic material model. This means that, when R-Node locations reach to yield strength of the component, the corresponding external load is limit load, and estimated as

$$P_L = \left[\frac{\sigma_y}{\overline{\sigma}_n}\right] P \tag{3.58}$$

where $\overline{\sigma}_n$ is the average R-Node stress location, and can be obtained as

$$\overline{\sigma}_n = \frac{\sum_{j-1}^{N} \sigma_{nj}}{N} \tag{3.59}$$

where N is the number of R-Node locations in the component.

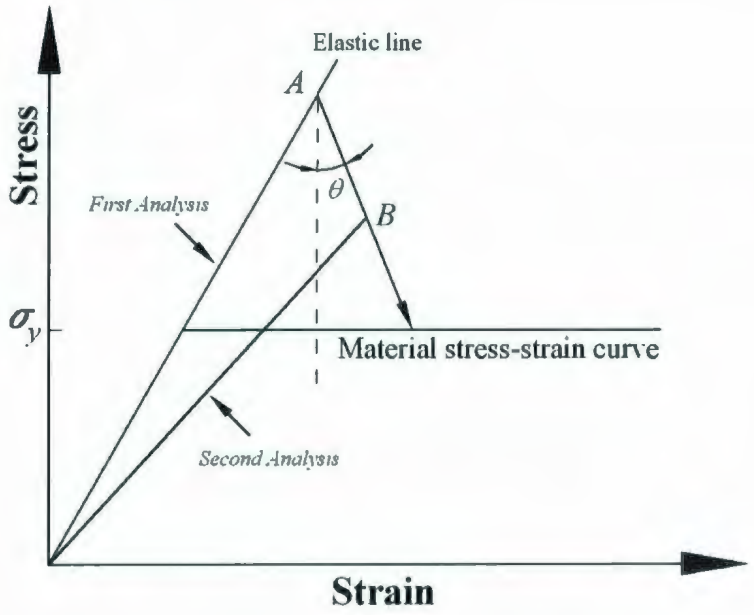

Figure 3.8: GLOSS diagram (Seshadri and Fernando, 1992)

The application of the R-Node method has also been extended to stress classification by Seshadri and Marriott (1993), fatigue design by Seshadri and Kizhatil (1993), residual stress estimation and shakedown evaluation by Seshadri (1994), fracture mechanics by Seshadri and Kizhatil (1995), minimum weight design by Mangalaramanan and Seshadri (1997), fracture mechanics by Seshadri and Wu (2001), inelastic local strains determination by Seshadri and Babu (2000), limit load estimation in multiple loading by Fanous *et al.* (2005) and some other applications which have been addressed in a monograph by Seshadri (1998).

Mackenzie and Boyle (1993) utilized the elastic modulus adjustment procedure suggested by Marriott (1988) and Seshadri (1991), named as the elastic compensation method (ECM), and obtained for every iterations lower- and upper-bound limit loads by

invoking the classical theorems of limit analysis. The procedure of ECM for estimating lower bound limit load can be summarized as follow:

- An elastic finite element is carried out using homogenous material property, i.e. E_0, with arbitrary load set, e.g. the design load (P_d).

- The previous solution is considered as iteration zero in series of subsequent linear elastic solution. Now, all the elements modified by following expression

$$E_{i+1} = \left[\frac{\sigma_n}{(\sigma_e)_{i-1}}\right] E_i \tag{3.60}$$

  where the subscript "*i*" is iteration variable, σ_n is nominal stress and σ_{i-1} is maximum (unaverage) nodal equivalent stress of the element from previous iteration.

- This procedure is continued until suitable convergence is achieved, and maximum equivalent stress in the component at each subsequent iteration with respect to the iteration number is plotted.

- At each iteration the lower bound limit load can be determined as

$$P_{Li} = P_{di} \frac{\sigma_y}{\sigma_{\max i}} \tag{3.61}$$

- The best estimation of lower bound limit load is the iteration with minimum value of maximum stress, i.e. R^{th} iteration, in which the corresponding maximum stress is σ_R. Therefore, the lower bound limit load (P_L) can be estimated as

$$P_L = \max(P_{Li}) \tag{3.62}$$

or

$$P_L = P_d \frac{\sigma_y}{\sigma_R} \tag{3.63}$$

Also, the procedure for estimating upper bound limit load based on ECM is as follows:

- Similar to the previous process, the elastic modulus of each element is modified using Eq. (3.60).

- Applying the classical theory, the upper bound limit load at each iteration can be estimated as

$$P_{Li}^{U} = \frac{D_i}{U_i} P_d \tag{3.64}$$

where P_d is the design load, D is the energy dissipation, and U is the strain energy.

- The best estimation of upper bound limit load given by this method is the lowest value of the estimated upper bound limit load among all the iterations, i.e.,

$$P_L^U = \min(P_{Li}^U) \tag{3.65}$$

The ECM procedure has been used to estimate the lower and upper bound limit loads for different pressurized components, which are available in Mackenzie *et al.* (1994) and Boyle *et al.* (1997). The method has been also applied for shakedown analysis by Hamilton *et al.* (1996), and Nadarajah *et al.* (1996).

A detailed development of the formal basis for the elastic modulus adjustment and related procedures has been provided by Ponter and Carter (1997), Ponter *et al.* (2000), and Ponter and Chen (2000). The generalized approach has similarities to the EMAP and can be better described as "linear matching methods" where a sequence of linear solutions is matched to the nonlinear problem.

A comprehensive review of the elastic iterative methods for limit load and shakedown analysis determination has been done by Mackenzie *et al.* (2000). The elastic iterative methods have been verified and studied independently by Plancq and Berton (1998) for limit analysis of branch pipe tee connection under different loading conditions, Mohammad *et al.* (1999) for limit and shakedown analysis of some typical pressurized configuration under combined pressure and thermal gradient loading condition, Hardy *et al.* (2001) for estimating limit and shakedown loads in internal and external flanges, and Yang *et al.* (2005) for limit load determination of nozzle-to-cylinder junctions.

General Formulation of EMAP

The aim of EMAP is to generate statically admissible stress distributions and kinematically admissible strain distributions by modifying the local elastic moduli in order to obtain the inelastic-like stress redistributions. Numerous sets of statically admissible and kinematically admissible distributions make it possible to calculate both lower and upper bounds limit loads. An arbitrary load set (P) with the original elastic modulus (E_0) is applied in the first iteration of elastic FEA. Subsequently, the elastic modulus of each element is modified in each successive iteration by following equation:

$$E^{i+1} = \left(\frac{\sigma_{ref}^{i}}{\sigma_{eq}^{i}} \right)^{q} E^{i} \tag{3.66}$$

where q is the elastic modulus adjustment parameter, σ_{ref} is a reference stress, σ_{eq} is the equivalent stress and the superscript "i" is the iteration number ($i = 1$ for the initial elastic analysis). This formula describes how the elastic modulus at a location with the equivalent stress σ_{eq} (e.g., the von Mises equivalent stress) is updated from the i^{th} to the $(i+1)^{th}$ elastic iteration. This procedure is continuous until suitable convergence of a subsequent iteration is achieved. (A flow chart of this procedure is presented in Fig. 3.9). Based on the theorem of nesting surfaces (Calladine and Drucker, 1962), Seshadri and Mangalaramanan (1997) suggested following expression for reference stress.

$$\sigma_{ref}^{i} = \left[\frac{\int_{V_T} \sigma_{eq}^{2} \, dV}{V_T} \right]_{i}^{1/2} \tag{3.67}$$

The general EMAP has been applied in variety of problems for instance: tubesheet design by Reinhardt, and Mangalaramanan (2001), limit load estimation in layered structures by Pan and Seshadri (2002), limit analysis in anisotropic material by Pan and Seshadri (2002), and limit load analysis in metal forming by Adibi-Asl and Seshadri (2006).

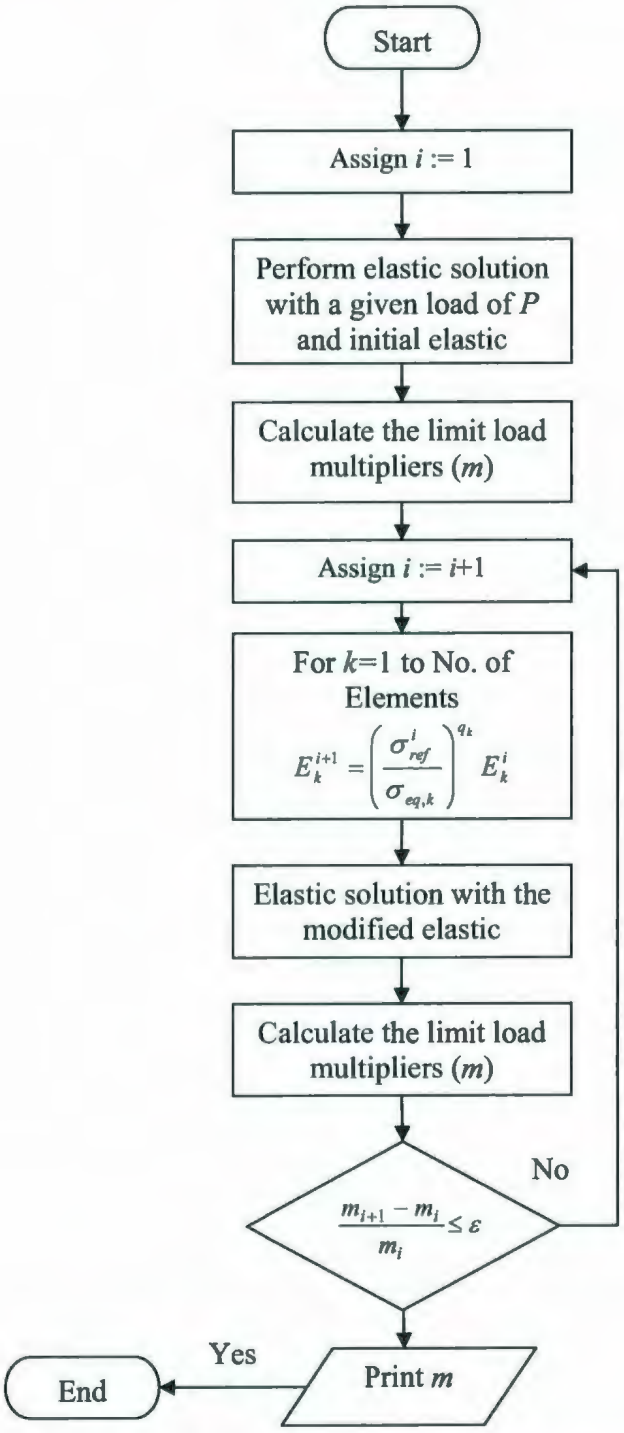

Figure 3.9: Flowchart of Elastic Modulus Adjustment Procedure (EMAP)

3.4 EXPERIMENTAL METHODS

Experimental techniques that determinate limit load are based on actual behavior of a component (i.e., real material like strain hardening, and large deformation). This means that the assumptions of ideal conditions (which are involved in analytical method) are not valid anymore. This condition also exists when inelastic FEA with strain hardening or large deformations are being considered. Several researchers have proposed different criteria of limit load estimation for these classes of problems. Most of the proposed methods are based on graphical criteria implemented on load-deflection or load-strain curve, which are generally considered as load-deformation curve.

3.4.1 Twice Elastic Slope (TES)

With regard to Fig. 3.10, limit load is defined by drawing a straight line from the origin with twice the slope of the initial elastic slope in load-deformation curve ($\tan\psi = 2\tan\varphi$). The intersection of this drawn line with the load-deformation curve is considered as limit load location. The TES method is recommended by ASME Boiler and Pressure Vessels Code Section III Div 1 (1998) and Section VIII Div 2 (1998). However, Kirkwood and Moffat (1994) and Moffat *et al.* (2001) showed that the TES method could not predict the unique value of limit load for some pressurized components. Also, Robertson *et al.* (2005) pointed out this method could not be applied to a component that the failure due to instability was reached before the limit state.

3.4.2 Tangent Intersection (TI)

As illustrated in Fig. 3.10, TI method is based on intersection of initial elastic line and plastic tangent line. In the CEN TC54 draft standard (1999), this method is recommended for limit load analysis using load-displacement curve.

Moffat *et al.* (2001) found that although the TI method predicts a unique value of limit load, it is sensitive to where the tangent is drawn to the plastic portion of the curve, and it is the designer's ability to select the correct plastic slope.

3.4.3 Twice Elastic Deformation (TED)

In TED method the location of elastic and inelastic behavior of a component is determined on load-deformation curve (say u_0 on deformation axis). Then a vertical line of $2u_0$ is drawn (Fig. 3.10), and intersection of this line and load-deformation curve is considered as limit load (Gerdeen, 1979).

In addition to the above-mentioned methods, there are similar methods for limit load solution that are not discussed in details in this thesis. The one percent strain (1%) method (Townley *et al.*, 1971), two percent (2%) strain offset method (American Society for Mechanical Engineers, 1971), the proportional limit method (American Society for Mechanical Engineers, 1971), plastic work or PW method (Gerdeen, 1979), and plastic

work curvature or PWC method (Li and Mackenzie, 2005) are all as methods that apply the load-deformation curve for estimating limit load in a given component.

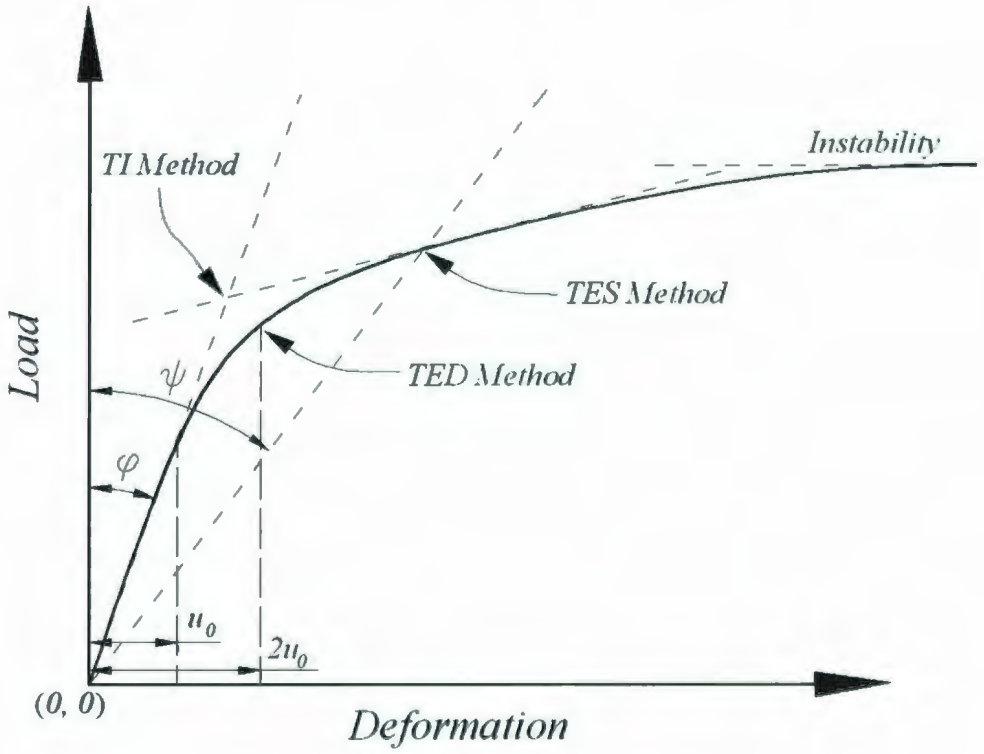

Figure 3.10: Various definition of limit load

3.5 LIMIT LOAD THEOREMS IN DISCRETE FORMULATION

Consider a component or structure made of elastic–perfectly plastic material that is in equilibrium with the surface traction T_i applied on the surface S_T. The component is discretized into smaller elements with regular shape. The shape of the elements can be triangles or rectangles for two dimensional problems, and tetrahedral or hexahedral in three dimensions. On the surface S_u, the constraint $u_i = 0$ is applied as shown in

Fig. 3.11. When the load of mT_i is applied the structure will be in a state of impending plastic collapse, where m is the exact limit load multiplier (i. e., $T_i\big|_{collapse} = mT_i$).

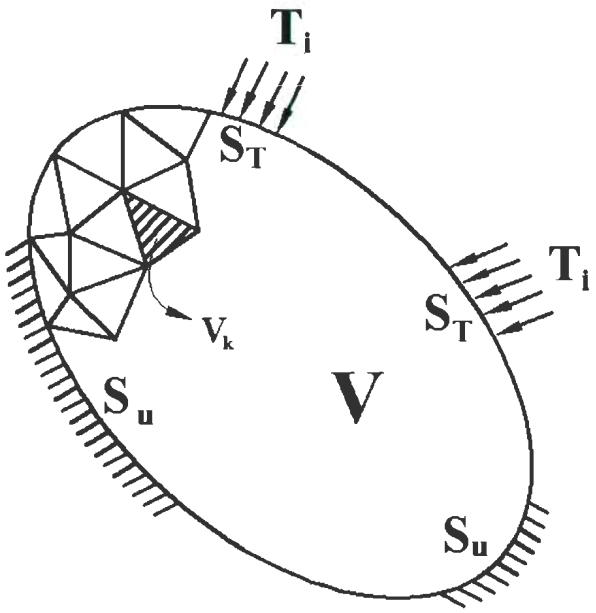

Figure 3.11: A body with elastic-perfectly plastic material-discrete model

In this section different multipliers in relation to upper and lower bound solutions are discussed. By using the iterative elastic procedure, relevant quantities of each element are used to calculate the limit load multipliers.

3.5.1 Upper Bound Multipliers

Classical Upper Bound Multiplier, m_U

According to the classical upper bound limit load theorem, if for a given load set the rate of internal dissipation of energy in a body is equal to the rate at which the external forces do work in any postulated mechanism of deformation, then the applied load set will be equal to or greater than the plastic collapse load (Calladine, 2000). The classical upper-bound multiplier, m_U, can be obtained from the following equation

$$\int_{S_T} T_i u_i \, dS \leq \int_{V_T} D \, dV \tag{3.68}$$

where T_i is the traction acting on the surface S_T, u_i is the compatible displacement, D is the increment of plastic dissipation energy per unit volume and V_T is the total volume.

Since as linear elastic analysis is used, it is possible to substitute strains and displacements with their corresponding rates.

For the von Mises yield criterion, the plastic dissipation energy is given as

$$D = \sigma_y \int_{V_T} \sqrt{\frac{2}{3}\left(\varepsilon_1^2 + \varepsilon_2^2 + \varepsilon_3^2\right)} \, dV \tag{3.69}$$

where ε_i (i=1, 2, 3) are the three principal strains.

In case of the Tresca perfectly plastic material, the plastic dissipation energy (D) can be expressed as:

$$D = \sigma_y \int_{V_T} \varepsilon_{\max} \, dV \tag{3.70}$$

where $\varepsilon_{\max}$ is the maximum principal strain.

Using the divergence theorem, we have:

$$\int_{S_T} T_i \, u_i \, dS = \int_{V_T} \sigma_{ij} \, \varepsilon_{ij} \, dV \tag{3.71}$$

Substituting Eqs. (3.69) and (3.71) into Eq. (3.68), and making use of the equality sign, the upper-bound multiplier m_U for the von Mises yield criterion can be obtained as

$$m_U = \frac{\int_{V_T} \sigma_y \, \varepsilon_{eq} \, dV}{\int_{V_T} \sigma_{ij} \, \varepsilon_{ij} \, dV} \Leftrightarrow \frac{\sigma_y \sum_{k=1}^{N} (\varepsilon_{eq} \, \Delta V)_k}{\sum_{k=1}^{N} (\sigma_{eq} \, \varepsilon_{eq} \, \Delta V)_k} \tag{3.72}$$

where ε_{eq} is the equivalent strain that can be directly evaluated for any linear elastic FEA results.

The classical upper bound limit load estimation can be also described by plotting total strain energy and total energy dissipation against load increment. As presented in Fig. 3.12, the strain energy is proportional to square of external load while the energy dissipation varies linearly respect to applied load; however, in a specific location they intersect each other. The corresponding load that the two energies have an equal value is considered as upper bound limit load.

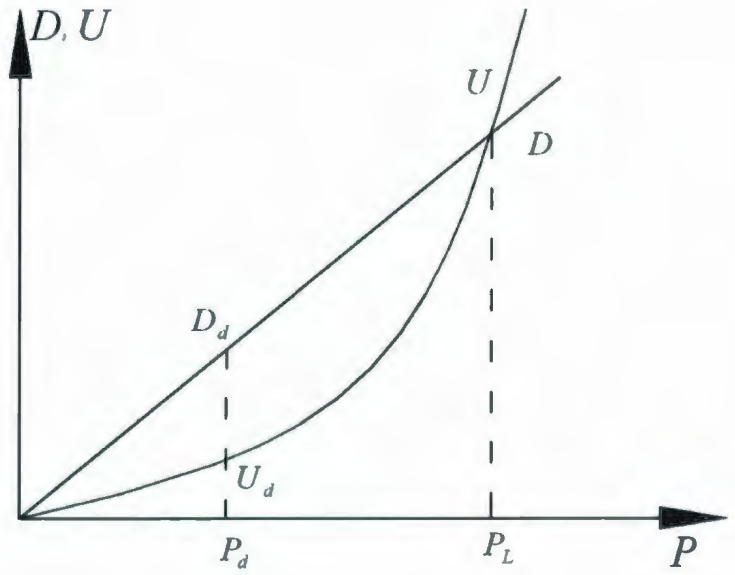

Figure 3.12: Variation of strain energy and dissipated energy against applied external load

Multiplier m_1^0

In classical limit analysis, the statically admissible stress field (equilibrium set) cannot lie outside the yield surface, and the stress associated with a kinematically

admissible strain rate field in calculating the plastic dissipation should lie on the yield surface. Mura *et al.* (1965) proposed an approach to eliminate such a requirement, and replaced it by the concept of "integral mean of yield" in the context of a variational formulation. The integral mean of yield criterion can be expressed as

$$\int_{V_T} \mu^0 \left[f(\bar{s}_{ij}^0) + (\varphi^0)^2 \right] dV = 0 \tag{3.73}$$

The superscript "0" corresponds to statically admissible state, and $\bar{s}_{ij}^0$ is the deviatoric stress corresponding to impending limit state: whereby, $\bar{s}_{ij}^0 = m^0 s_{ij}^0$. The deviatoric stresses s_{ij}^0 equilibrates the applied set of load ($s_{ij}^0 = \sigma_{ij}^0 - \frac{1}{3}\sigma_{kk}^0 \delta_{ij}$, where δ_{ij} is the Kronecker delta). φ^0 is a point function that takes on a value zero if s_{ij}^0 is at yield and remains positive below yield. The von-Mises yield criterion can be expressed as

$$f(\bar{s}_{ij}) = \frac{3}{2} \bar{s}_{ij}^0 \bar{s}_{ij}^0 - \sigma_y^2 \tag{3.74}$$

The associated flow rule can be expressed as

$$\dot{\varepsilon}_{ij} = \mu \left(\frac{\partial f}{\partial s_{ij}} \right) \tag{3.75}$$

Assuming an unspecified, but constant flow parameter μ^0 in Eq. (3.73), the upper bound limit load multiplier proposed by Mura *et al.* (1965) becomes ($\varphi^0 = 0$)

$$m_1^0 = \frac{\sigma_y \sqrt{V_T}}{\sqrt{\int_{V_T} (\sigma_{eq})^2 dV}} \Leftrightarrow \frac{\sigma_y \sqrt{V_T}}{\sqrt{\sum_{k-1}^{N} (\sigma_{eq}^2 \Delta V)_k}} \tag{3.76}$$

The m_1^0 limit load multiplier shown to be greater than the classical lower bound (m_L) and classical upper bound (m_U) limit load multiplier (Reinhardt and Seshadri, 2003).

Proof: In here proof of Eq. (3.76) can be obtained as follows:

The general formulation of von Mises yield criteria can be written as

$$f(s_{ij}) = \frac{3}{2} s_{ij}^0 s_{ij}^0 - \sigma_y^2 \tag{I}$$

At limit load state ($\bar{s}_{ij}^0 = m^0 s_{ij}^0$) Eq. (I) can be rewritten as

$$f(\bar{s}_{ij}) = \frac{3}{2} (m^0)^2 s_{ij}^0 s_{ij}^0 - \sigma_y^2 \tag{II}$$

Substituting Eq. (II) into Eq. (3.73) yields into following equation

$$\int_{V_T} \mu^0 \left[\frac{3}{2} (m^0)^2 s_{ij}^0 s_{ij}^0 - \sigma_y^2 + (\varphi^0)^2 \right] dV = 0 \tag{III}$$

Also,

$$\begin{aligned} s_{ij}^0 s_{ij}^0 &= \left[\sigma_{ij}^0 - \frac{1}{3} \sigma_{kk}^0 \delta_{ij} \right] \left[\sigma_{ij}^0 - \frac{1}{3} \sigma_{mm}^0 \delta_{ij} \right] \\ &= \sigma_{ij}^0 \sigma_{ij}^0 - \frac{1}{3} \sigma_{kk}^0 \sigma_{ij}^0 \delta_{ij} - \frac{1}{3} \sigma_{mm}^0 \sigma_{ij}^0 \delta_{ij} + \frac{1}{9} \sigma_{kk}^0 \sigma_{mm}^0 \delta_{ij} \delta_{ij} \\ &= \sigma_{ij}^0 \sigma_{ij}^0 - \frac{2}{3} \sigma_{kk}^0 \sigma_{jj}^0 + \frac{1}{3} \sigma_{kk}^0 \sigma_{mm}^0 \\ &= \sigma_{ij}^0 \sigma_{ij}^0 - \frac{1}{3} \sigma_{kk}^0 \sigma_{mm}^0 = \sigma_{eq}^2 - \frac{1}{3} \sigma_{eq}^2 = \frac{2}{3} \sigma_{eq}^2 \end{aligned} \tag{IV}$$

$$\int_{V_T} \mu^0 \left[\frac{3}{2} (m^0)^2 \times \frac{2}{3} \sigma_{eq}^2 - \sigma_y^2 + (\varphi^0)^2 \right] dV = 0 \tag{V}$$

Making use of the conditions in Eq. (3.24) along with Eq. (V), the expression for m_1^0 limit load multiplier in Eq. (3.76) is proved.

Proof: The proof of $m_1^0 \geq m_L$ can be shown by dividing numerator and denominator of Eq. (3.76) by the maximum stress, $\sigma_{\max}$, in a body as

$$m_1^0 = \frac{\frac{\sigma_y}{\sigma_{\max}}\sqrt{V_T}}{\sqrt{\int_{V_T}(\frac{\sigma_{eq}}{\sigma_{\max}})^2 dV}} \qquad \text{(I)}$$

Referring to definition of classical lower bound ($m_L = \sigma_y / \sigma_{\max}$), Eq. (I) can be written as

$$m_1^0 = m_L \sqrt{\frac{\int_{V_T} 1^2 dV}{\int_{V_T}(\frac{\sigma_{eq}}{\sigma_{\max}})^2 dV}} \qquad \text{(II)}$$

Keeping in mind that $\sigma_{\max} \geq \sigma_{eq}$ (or in other definition $\sigma_{\max} = \max(\sigma_{eq})$); thus

$$\int_{V_T}(\frac{\sigma_{eq}}{\sigma_{\max}})^2 dV \leq \int_{V_T} 1^2 dV \qquad \text{(III)}$$

In other words the expression under the root in Eq. (II) is equal or greater than unity; therefore it can be concluded that $m_1^0 \geq m_L$.

Proof: The proof of $m_1^0 \geq m_U$ can be shown by applying Schwarz's inequality as

$$(x, y) \leq \|x\|\|y\| \Rightarrow (\sigma_{eq}, 1) \leq \|\sigma_{eq}\|\|1\| \tag{I}$$

Therefore,

$$\int_{V_T} \sigma_{eq} \times 1 \times dV \leq \sqrt{\int_{V_T} \sigma_{eq}^2 dV} \sqrt{\int_{V_T} 1^2 dV} \tag{II}$$

The second term in the right hand side of Eq. (II) is equal to the square root of total volume (V_T); thus,

$$\sqrt{V_T} \geq \frac{\int_{V_T} \sigma_{eq} dV}{\sqrt{\int_{V_T} \sigma_{eq}^2 dV}} \tag{III}$$

Substituting expression (III) into Eq. (3.76) the following expression can be obtained

$$m_1^0 \geq \frac{\sigma_y \int_{V_T} \sigma_{eq} dV}{\int_{V_T} \sigma_{eq}^2 dV} \tag{IV}$$

Using $\sigma_{eq} = E\varepsilon_{eq}$, Eq. (IV) can be rewritten as

$$m_1^0 \geq \frac{\sigma_y \int_{V_T} E\varepsilon_{eq} dV}{\int_{V_T} E\varepsilon_{eq}\sigma_{eq} dV} = \frac{\sigma_y \int_{V_T} \varepsilon_{eq} dV}{\int_{V_T} \varepsilon_{eq}\sigma_{eq} dV} \tag{V}$$

The right hand side of Eq. (V) is the definition of classical upper bound limit load that introduced in Eq. (3.72). So, the proof is completed in here.

Multiplier m_2^0

Equation (3.76) implies that the calculation of m_1^0 is based on the total volume V_T. If plastic collapse occurs over a localized region of the structure, m_1^0 will be significantly overestimated. To overcome this problem, Pan and Seshadri (2001) have proposed a new formulation for evaluating m^0, namely m_2^0. On the basis of deformation theory of plasticity, the flow rule can be expressed as

$$e_{ij} = \mu s_{ij} \tag{3.77}$$

where e_{ij} and s_{ij} are the deviatoric strain and stress, respectively. Therefore, μ can be defined as

$$\mu = \frac{3\bar{\varepsilon}}{2\bar{\sigma}} \tag{3.78}$$

where $\bar{\sigma} = \sqrt{3/2 s_{ij} s_{ij}}$ is the effective stress and $\bar{\varepsilon} = \sqrt{2/3 e_{ij} e_{ij}}$ is the effective strain.

Substituting Eq. (3.78) into the integral mean of yield criterion, the m_2^0 limit load multiplier can be obtained as

$$m_2^0 = \sigma_y \frac{\sqrt{\int_{V_T}\left(\frac{\varepsilon_{eq}}{\sigma_{eq}}\right)dV}}{\sqrt{\int_{V_T}\sigma_{eq}\varepsilon_{eq}\,dV}} \Leftrightarrow \sigma_y \frac{\sqrt{\sum_{k=1}^{N}\left(\frac{\varepsilon_{eq}}{\sigma_{eq}}\Delta V\right)_k}}{\sqrt{\sum_{k=1}^{N}\left(\sigma_{eq}\varepsilon_{eq}\Delta V\right)_k}} \tag{3.79}$$

Proof: The proof of $m_2^0 \geq m_L$ can be achieved by applying $\sigma_{eq} = E\varepsilon_{eq}$ into Eq. (3.79), therefore;

$$m_2^0 = \sigma_y \frac{\sqrt{\int_{V_T}\frac{1}{E}dV}}{\sqrt{\int_{V_T}\frac{\sigma_{eq}^2}{E}dV}} \tag{I}$$

Dividing numerator and denominator of Eq. (I) by the maximum stress, $\sigma_{\max}$, in a component or structure, and using the definition of classical lower bound ($m_L = \sigma_y / \sigma_{\max}$), the Eq. (I) can be written as

$$m_2^0 = \frac{\sigma_y}{\sigma_{\max}} \sqrt{\frac{\frac{1}{E}dV}{\int_{V_T}\frac{1}{E}\underbrace{\left(\frac{\sigma_{eq}}{\sigma_y}\right)^2}_{\leq 1}dV}} = m_L \overbrace{\sqrt{\frac{\int_{V_T}E\,dV}{\int_{V_T}\frac{1}{E}dV}}}^{\geq 1} \tag{II}$$

Therefore, $m_2^0 \geq m_L$.

Proof: The proof of $m_2^0 \geq m_U$ can be shown by applying Schwarz's inequality as

$$(x,y) \leq \|x\|\|y\| \Rightarrow \left(\sqrt{\frac{\varepsilon_{eq}}{\sigma_{eq}}} \times \sigma_{eq}, \sqrt{\frac{\varepsilon_{eq}}{\sigma_{eq}}} \times 1\right) \leq \left\|\sqrt{\frac{\varepsilon_{eq}}{\sigma_{eq}}} \times \sigma_{eq}\right\| \left\|\sqrt{\frac{\varepsilon_{eq}}{\sigma_{eq}}} \times 1\right\| \tag{I}$$

Therefore,

$$\int_{V_T} \frac{\varepsilon_{eq}}{\sigma_{eq}} \times \sigma_{eq} \times 1 \times dV \leq \sqrt{\int_{V_T} \frac{\varepsilon_{eq}}{\sigma_{eq}} \times \sigma_{eq}^2 \times dV} \times \sqrt{\int_{V_T} \frac{\varepsilon_{eq}}{\sigma_{eq}} \times 1^2 \times dV} \tag{II}$$

Equation (II) can be rewritten as

$$\sqrt{\int_{V_T} \frac{\varepsilon_{eq}}{\sigma_{eq}} dV} \geq \frac{\int_{V_T} \varepsilon_{eq} dV}{\sqrt{\int_{V_T} \sigma_{eq} \varepsilon_{eq} dV}} \tag{III}$$

Substituting expression (III) into Eq. (3.79) the following expression can be obtained

$$m_2^0 \geq \frac{\sigma_y \int_{V_T} \varepsilon_{eq} dV}{\int_{V_T} \sigma_{eq} \varepsilon_{eq} dV} = \frac{\int_{V_T} \sigma_y \varepsilon_{eq} dV}{\int_{V_T} \sigma_{eq} \varepsilon_{eq} dV} \tag{V}$$

The left hand side of Eq. (V) is upper bound classical limit load that, Eq. (3.72). Therefore,

$$m_2^0 \geq m_U \tag{VI}$$

3.5.2 Lower Bound Multipliers

Classical Lower Bound Multiplier, m_L

The classical lower bound can be calculated by invoking the lower bound limit load theorem, which states, if a statically admissible stress field in which the stress no where exceeds yield for a given component under given loading, the loading is a lower bound on the limit (Calladine, 2000). The EMAP satisfies the first requirement of the lower bound theorem in that it is statically admissible. As the iteration solutions are linear elastic, there is a linear relation between the stress magnitude and applied load. A lower bound load can therefore be established by estimating the load required to give a maximum equivalent stress equal to the nominal yield strength, σ_y.

Therefore, the classical lower bound multiplier (m_L) is given by

$$m_L = \frac{\sigma_y}{(\sigma_{eq})_{\max}} \tag{3.80}$$

Lower Bound Limit Load Multiplier Based on R-Node

The concept of redistribution node (R-Node) has been extensively used to understand better the definition of reference stress, primary stress and limit loads. The R-Node locations are statically determinate in that they are induced in order to preserve

equilibrium with externally applied loads (load control). Generally, R-Node location can be defined by intersecting the elastic redistribution with plastic one at limit load state (see Fig. 3.13).

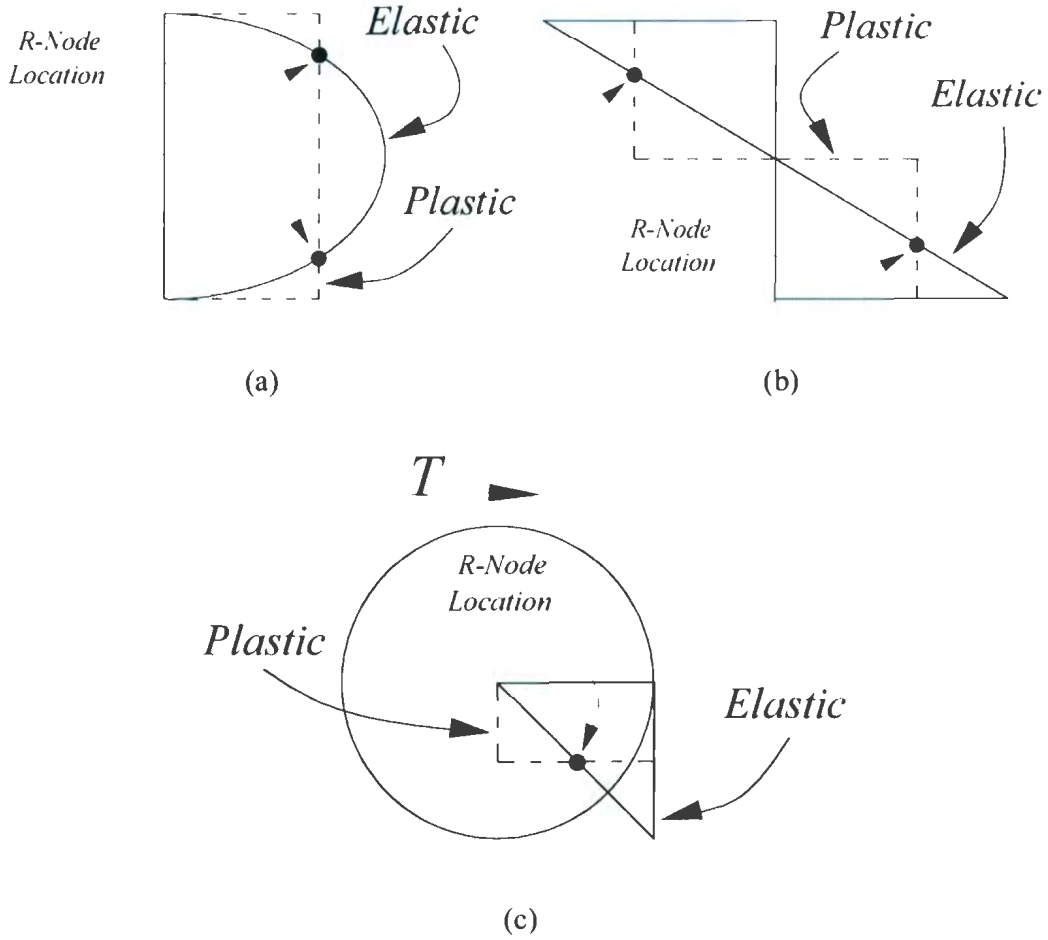

Figure 3.13: R-Node concept: (a) direct shear, (b) bending, (c) shear due to torsion

For an elastic-perfectly plastic material model, when stress at R-Node location approaches yield strength of the material, the corresponding applied load is considered as limit load, this situation can be represented by a one-bar model as presented in Fig. 3.14. Therefore, the limit load multiplier can be written as:

$$m_n = \frac{\sigma_y}{(\sigma_e)_{R-Node}} \tag{3.81}$$

For a component in which collapse mechanism forms with multiple hinges, more than one R-Node location will be available in the component. For example, if a plastic collapse mechanism corresponding to two hinges develops for an indeterminate beam, then there would be a pair of R-Nodes at the hinge locations since bending is dominant. The combined R-Node effective stress can be expressed as the arithmetic average of the pseudo-elastic R-Node stresses; i.e.,

$$\overline{\sigma}_n = \frac{\sigma_{n1} + \sigma_{n2}}{2} \tag{3.82}$$

Generalizing the foregoing expressions for N plastic hinges

$$\overline{\sigma}_n = \frac{\sum_{k=1}^{N} \sigma_{nj}}{N} \tag{3.83}$$

where σ_{nj}'s are the R-Node stresses and N is the number of R-Node locations in the component. Then, the limit load multipliers is given by

$$m_n = \frac{\sigma_y}{\overline{\sigma}_n} \tag{3.84}$$

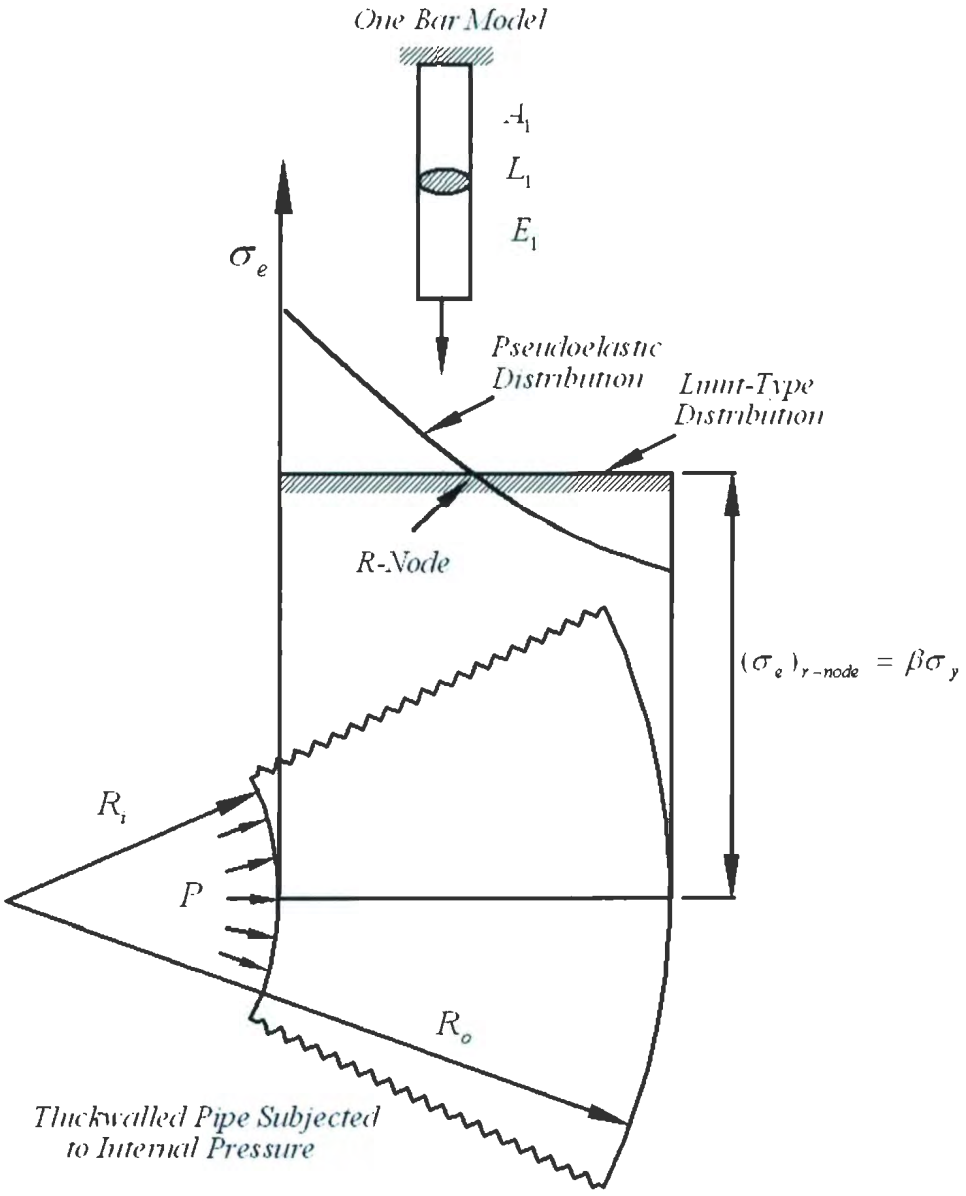

Figure 3.14: R-node bar model

Multiplier m_α

This multiplier depends on m_L and m^0 multipliers, and can be obtained as (Reinhardt and Seshadri, 2003):

$$m_\alpha = 2m^0 \frac{2\left(\frac{m^0}{m_L}\right)^2 + \sqrt{\frac{m^0}{m_L}\left(\frac{m^0}{m_L}-1\right)^2\left(1+\sqrt{2}-\frac{m^0}{m_L}\right)\left(\frac{m^0}{m_L}-1+\sqrt{2}\right)}}{\left(\left(\frac{m^0}{m_L}\right)^2+2-\sqrt{5}\right)\left(\left(\frac{m^0}{m_L}\right)^2+2+\sqrt{5}\right)} \tag{3.85}$$

The condition for the lower-boundedness of m_α is discussed by Reinhardt and Seshadri (2003). Dividing both sides of Eq. (3.85) by the exact multiplier, we get

$$R_\alpha = 2R_0 \frac{2R_L^2 + \sqrt{R_L(R_L-1)^2(1+\sqrt{2}-R_L)(R_L-1+\sqrt{2})}}{(R_L^2+2-\sqrt{5})(R_L^2+2+\sqrt{5})} \tag{3.86}$$

where $R_\alpha = m_\alpha / m$, $R_L = m^0 / m_L$ and $R_0 = m^0 / m$.

$R_\alpha = 1$ is the boundary between the upper bound ($R_\alpha > 1$) and lower bound ($R_\alpha < 1$), as shown in Fig. 3.15. The expression under the root in Eq. (3.86) encompasses four factors, which define the sign of the whole expression under the root (see Table 3.1)

Table 3.1: Sign analysis of the expression under the root in Eq. (3.86)

	0		$\sqrt{2}-1$		1		$\sqrt{2}+1$	
R_L	(-)	(+)		(+)		(+)		(+)
$(R_L-1)^2$	(+)		(+)		(+)		(+)	
$(1+\sqrt{2}-R_L)$	(+)		(+)		(+)		(+)	(-)
$(R_L-1+\sqrt{2})$	(-)		(-)		(+)		(+)	(+)
Total	(+)	(-)		(+)		(+)		(-)

As it can be seen from Table 3.1, the m_α limit load multiplier becomes imaginary for the following conditions:

$$\begin{vmatrix} 0 < R_L < \sqrt{2}-1 \\ \quad or \\ R_L > \sqrt{2}+1 \end{vmatrix}$$

Since $R_L = m^0 / m_L \geq 0$, the first expression above never occurs; therefore, the only case that causes m_α to be imaginary is $R_L > \sqrt{2}+1 \approx 2.414$, as is the case for components with notches and cracks due to presence of peak stresses.

The $m_0 / m_L (= (\sigma_e)_{\max} / \sigma_{ref})$ can be a measure of the theoretical stress-concentration factor at the notch. Therefore, $m_0 / m_L \geq 1+\sqrt{2}$ represents the threshold for pronounced notch effects. The region bounded by $m^0(\max)$, $1 \leq m^0 / m_L \leq 1+\sqrt{2}$ and $1 \leq m^0 / m \leq 1+\sqrt{2}$ is designated as the "m_α triangle".

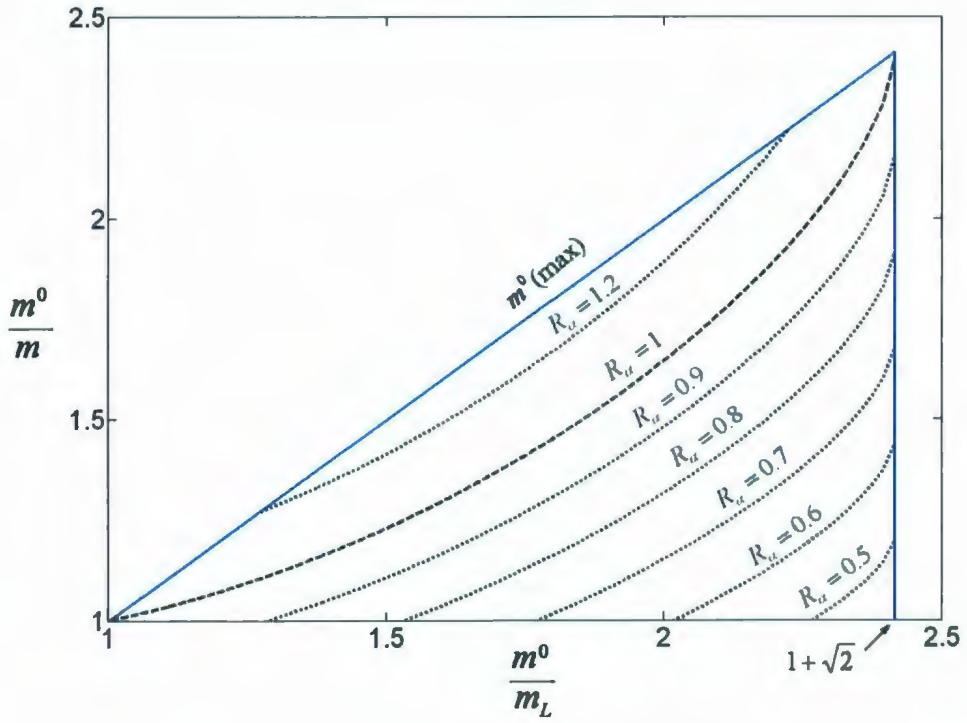

Figure 3.15: Regions of lower and upper bounds of m_α

Proof: The proof of Eq. (3.85) is given here.

Mura's lower bound limit load multiplier, $m' = f(m^0, m_L)$, defined by Eq. (3.36) can be rewritten making use of Eq. (3.80) as

$$m' = \frac{2m^0}{1+\left(\frac{m^0}{m_L}\right)^2} \tag{I}$$

Differentiating $m' = f(m^0, m_L)$ respect to iteration variable, ζ, follows the expression

$$\frac{dm'}{d\zeta} = \left(\frac{\partial m'}{\partial m^0}\right)_{\zeta=\zeta_i} \frac{dm^0}{d\zeta} + \left(\frac{\partial m'}{\partial \frac{1}{m_L}}\right)_{\zeta=\zeta_i} \frac{d\frac{1}{m_L}}{d\zeta} \tag{II}$$

In terms of finite difference, Eq. (II) can be expressed as:

$$\Delta m' = \left.\frac{\partial m'}{\partial m^0}\right|_{\zeta=\zeta_i} \Delta m^0 + \left.\frac{\partial m'}{\partial \frac{1}{m_L}}\right|_{\zeta=\zeta_i} \Delta\left(\frac{1}{m_L}\right) \tag{III}$$

where

$$\begin{cases} \Delta m' = m' - m_\alpha \\ \Delta m^0 = m^0 - m_\alpha \\ \Delta m_L = m_L - m_\alpha \end{cases}$$

The limit load multiplier m_α is assumed to be the estimated actual limit load (Seshadri and Mangalaramanan, 1997).

(Cont'd ...)

Therefore,

$$m' - m_\alpha = 2\frac{1-\left(\frac{m^0}{m_L}\right)^2}{\left(1+\left(\frac{m^0}{m_L}\right)^2\right)^2}\left(m^0 - m_\alpha\right) - 4\frac{(m^0)^3}{m_L\left(1+\left(\frac{m^0}{m_L}\right)^2\right)^2}\left(\frac{1}{m_L} - \frac{1}{m_\alpha}\right) \qquad \text{(IV)}$$

Equation (IV) is a polynomial of second degree in m_α, which can be shown in general formulation as

$$Am_\alpha^2 + Bm_\alpha + C = 0 \qquad \text{(V)}$$

where

$$A = \left(\frac{m^0}{m_L}\right)^4 + 4\left(\frac{m^0}{m_L}\right)^2 - 1$$

$$B = -8m^0\left(\frac{m^0}{m_L}\right)^2$$

$$C = 4(m^0)^2\left(\frac{m^0}{m_L}\right)$$

The parameters A, B and C can be calculated from the results of linear elastic FEA.

$$m_\alpha = \frac{-B \pm \sqrt{B^2 - 4AC}}{2A} \qquad \text{(VI)}$$

Keeping in mind that the limit lower multiplies are positive, Eq. (VI) results in Eq. (3.85). When the expression under the root in Eq. (VI) becomes negative (i. e., $B^2 - 4AC < 0$) the solution of m_α vanishes.

Multiplier *m''*

Mura *et al.* (1965) developed an extended lower bound theorem, in an attempt to develop an alternative approach to classical limit analysis. Based on "integral mean of yield criterion", Eq. (3.73), the Mura's lower bound multiplier is stated as an inequality, which can be expressed as

$$m^0 \leq m + \int_{V_T} \mu \left[f(\bar{s}_{ij}^0) + (\phi^0)^2 \right] dV \tag{3.87}$$

Equation (3.87) can be rewritten as

$$m^0 \leq m + \int_{V_T} \mu \, f^0 dV \tag{3.88}$$

A multiplier m'' can be obtained from Eq. (3.88) as (Seshadri and Indermohan, 2004)

$$m'' = \frac{m^0}{1+G} \tag{3.89}$$

The parameter G evaluated acts as a convergence parameter, and is indicative of any deviation of statically admissible stress distributions from the limit state. That is, $G \to 0$ as $\zeta \to \infty$ would correspond to the converged exact solution. G is calculated from following expression:

$$G = \sqrt{\frac{\int_{V_T}\left[\left(m^0\frac{\sigma_{eq}}{\sigma_y}\right)^2 - 1\right]^2 dV}{4V_T}} \Leftrightarrow \sqrt{\frac{\sum_{k=1}^{N}\left[\left(m^0\frac{\sigma_{eq}}{\sigma_y}\right)^2 - 1\right]_k^2 \Delta V_k}{4V_T}} \tag{3.90}$$

Multiplier m_β

Seshadri and Indermohan (2004) showed that m'' based on m_1^0 need not be a lower bound. Therefore, they modified m'' by introducing a parameter β and obtained the m_β multiplier as

$$m_\beta = \frac{m_1^0}{1+\beta G} \tag{3.91}$$

Plotting multiplier m_β for different values of β with respect to the iteration variable ζ, similar behavior will be achieved as presented in Fig. 3.16. As can be obtained from Fig. 3.16, m_β is sensitive to the value of β. The best estimation of the exact solution is achieved when $\beta = \beta_R$ (where β_R is reference parameter and is as yet undefined), which also guarantee that $m_\beta \le m$.

The reference parameter β_R would be the lowest possible value of β that would generate $m_\beta(\zeta)$ which satisfies following requirements:

$$
\begin{aligned}
&\text{(I)} && m^0 \geq m \geq m_\beta && \text{for } \zeta \geq 0 \\
&\text{(II)} && \frac{dm_\beta}{d\zeta} \geq 0 && \text{for } \zeta \geq 0 \\
&\text{(III)} && \frac{dm^0}{d\zeta} \leq 0 && \text{for } \zeta \geq 0 \\
&\text{(IV)} && m^0 = m_\beta = m && \text{at } \zeta \rightarrow \zeta_L
\end{aligned}
\tag{3.92}
$$

The last condition, (IV), represents the converged limit state, for which all the multipliers reach the exact solution. However, estimation of β_R is relevant, especially for components or structures that experience local plastic collapse, i. e., component with cracks or notches.

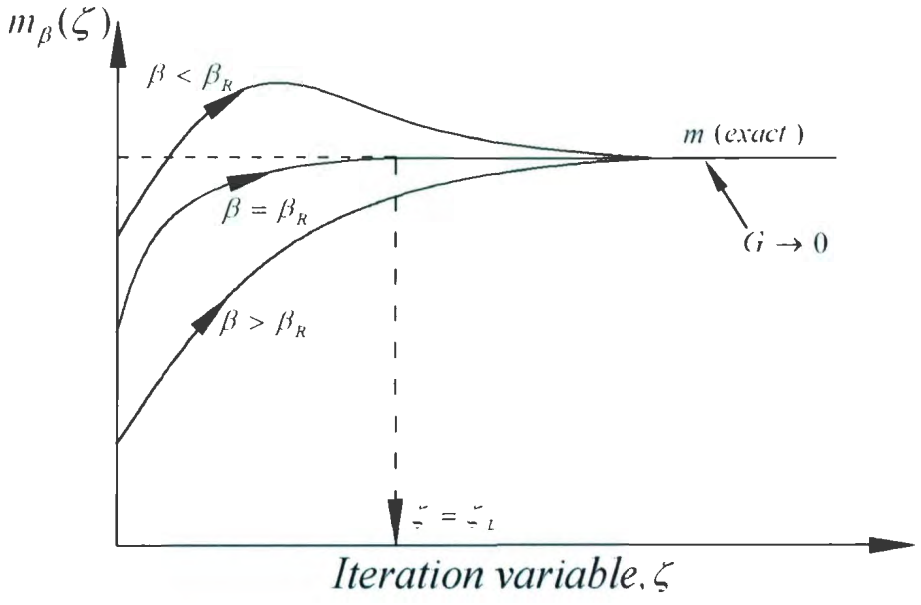

Figure 3.16: Variation of m_β with iteration variable for different value of β

3.6 TWO BAR STRUCTURE

3.6.1 Basic Expressions

A simple configuration, a two-bar system, is used to explain the various limit load multipliers and illustrate the elastic modulus adjustment procedure (EMAP). As shown in Fig. 3.17, the two-bar system is under the tensile load P; therefore, the bars are subjected to uniaxial loading. The bar stresses and strains are determined by invoking equilibrium, strain-displacement and the stress-strain relationship.

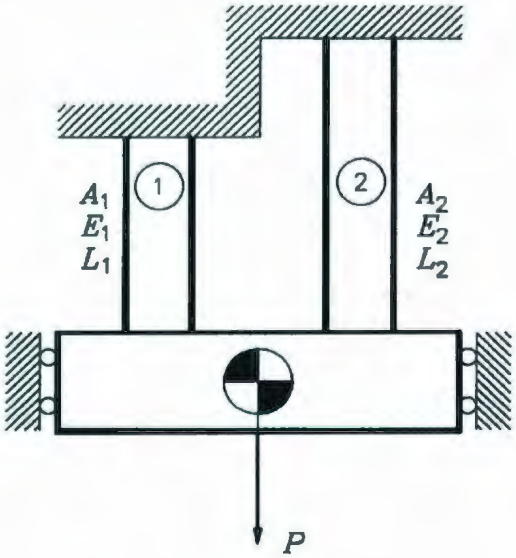

Figure 3.17: Two-bar model

From the equilibrium equation, the relationship between internal load in the bars (P_1 and P_2 in bars 1 and 2, respectively) and the external load (P) can be written as

$$P = P_1 + P_2 \tag{3.93}$$

Also, using compatibility conditions, the relationship between the displacements of the bars is as

$$\delta = \delta_1 = \delta_2 \tag{3.94}$$

where δ_1 and δ_2 are displacements in bars 1 and 2, respectively.

Solving Eqs. (3.93) and (3.94), the relation between internal load and the displacement is

$$\begin{cases} \delta_1 = \dfrac{P_1 L_1}{A_1 E_1} \\ \delta_2 = \dfrac{P_2 L_2}{A_2 E_2} \end{cases} \tag{3.95}$$

Equation (3.95) can be written as

$$\begin{cases} P_1 = \dfrac{A_1 E_1}{L_1}\delta \\ P_2 = \dfrac{A_2 E_2}{L_2}\delta \end{cases} \tag{3.96}$$

Therefore, the corresponding stresses in the bars are as follow:

$$\begin{cases} \sigma_1 = \dfrac{E_1}{L_1}\delta \\ \sigma_2 = \dfrac{E_2}{L_2}\delta \end{cases} \tag{3.97}$$

Applying Eqs. (3.94) and (3.95) into Eq.(3.93), we have

$$P = \frac{A_1 E_1}{L_1}\delta + \frac{A_2 E_2}{L_2}\delta \tag{3.98}$$

Also, Eq. (3.98) can be rewritten in following form

$$\delta = \frac{P}{\dfrac{A_1 E_1}{L_1} + \dfrac{A_2 E_2}{L_2}} \tag{3.99}$$

Combining Eqs. (3.96), (3.98) and (3.99), the stress in each bar can be expressed as follows:

$$\begin{cases} \sigma_1 = \dfrac{\dfrac{E_1}{L_1}}{\dfrac{A_1 E_1}{L_1} + \dfrac{A_2 E_2}{L_2}} P \\ \sigma_2 = \dfrac{\dfrac{E_2}{L_2}}{\dfrac{A_1 E_1}{L_1} + \dfrac{A_2 E_2}{L_2}} P \end{cases} \tag{3.100}$$

If the material and geometric parameters are so chosen, such that σ_1 is greater than σ_2, then bar 1 is considered as the local bar.

3.6.2 Exact Limit Load Solution

Initial yielding occurs when the bar with maximum stress, say bar 1, reaches the yield strength of material. By increasing the load, the bar 2 reaches to the yield, the two-bar system reaches to its limit state. Therefore, the required load corresponding to limit state will be

$$P_L = \sigma_y(A_1 + A_2) \tag{3.101}$$

The corresponding limit load multiplier can be expressed as

$$m = \frac{P_L}{P} = \frac{\sigma_y(A_1 + A_2)}{P} \tag{3.102}$$

3.6.3 Programming Method

Lower bound solution

The yield criterion in the bars can be written as

$$f(\sigma) = \sigma - \sigma_y \tag{3.103}$$

Therefore, the lower bound limit load multiplier using programming method, can be obtained by maximizing limit load subjected to following conditions:

$$\begin{cases} -\sigma_y \le \sigma_1 \le +\sigma_y \\ -\sigma_y \le \sigma_2 \le +\sigma_y \end{cases} \Rightarrow \begin{cases} -\sigma_y \le \dfrac{P_1}{A_1} \le +\sigma_y \\ -\sigma_y \le \dfrac{P_2}{A_2} \le +\sigma_y \end{cases} \tag{3.104}$$

Substituting Eq. (3.93) into Eq. (3.104) results in following expression:

$$\begin{cases} -\sigma_y \le \dfrac{P_1}{A_1} \le +\sigma_y \\ -\sigma_y \le \dfrac{P - P_1}{A_2} \le +\sigma_y \end{cases} \tag{3.105}$$

Also, Eq. (3.105) can be rewritten as

$$\begin{cases} -1 \le \dfrac{P_1}{A_1 \sigma_y} \le +1 \\ -1 \le \dfrac{A_1}{A_2}\dfrac{P}{A_1 \sigma_y} - \dfrac{A_1}{A_2}\dfrac{P_1}{A_1 \sigma_y} \le +1 \end{cases} \tag{3.106}$$

As illustrated in Fig. (3.17), a graphical solution can be obtained for this problem. Equation (3.106) represents a domain where equality signs are the boundaries of this domain. The maximum value of limit load in this domain is

$$\frac{P_L}{A_1\sigma_y} = 1 + \frac{A_1}{A_2} \tag{3.107}$$

Therefore, the limit load multiplier can be obtained as

$$m = \frac{P_L}{P} = \frac{\sigma_y(A_1 + A_2)}{P} \tag{3.108}$$

Equation (3.108) is the same as Eq. (3.102).

Upper bound solution

Applying the upper bound theorem, the energy dissipation balance can be expressed as

$$P\dot{\delta} = P_1\dot{\delta}_1 + P_2\dot{\delta}_2 \tag{3.109}$$

Equation (3.109) can be rewritten in terms of strains as

$$P\dot{\delta} = P_1L_1|\dot{\varepsilon}_1| + P_2L_2|\dot{\varepsilon}_2| \tag{3.110}$$

The limit load can be estimated by minimizing external load in Eq. (3.110) subjected to compatibility equation as

$$\dot{\delta} = \dot{\delta}_1 = \dot{\delta}_2 = \dot{\varepsilon}_1 L_1 = \dot{\varepsilon}_2 L_2 \tag{3.111}$$

Therefore,

$$PL_1\dot{\varepsilon}_1 = P_1 L_1 |\dot{\varepsilon}_1| + P_2 L_2 |\dot{\varepsilon}_2| \tag{3.112}$$

At limit state, the two bars concurrently reach the yield strength

$$PL_1\dot{\varepsilon}_1 = \sigma_y A_1 L_1 |\dot{\varepsilon}_1| + \sigma_y A_2 L_2 |\dot{\varepsilon}_2| \tag{3.113}$$

Making use of Eq. (3.111), Eq. (3.113) can be expressed as:

$$P = \sigma_y (A_1 + A_2) \frac{|\dot{\varepsilon}_1|}{\dot{\varepsilon}_1} \tag{3.114}$$

Equation (3.114) is plotted in Fig. (3.19), and can be rewritten as:

$$\frac{P}{\sigma_y (A_1 + A_2)} = \begin{cases} +1 & if\ \dot{\varepsilon}_1 > 0 \\ -1 & if\ \dot{\varepsilon}_1 < 0 \end{cases} \tag{3.115}$$

The graphical upper bound approach is illustrated in Fig. 3.18.

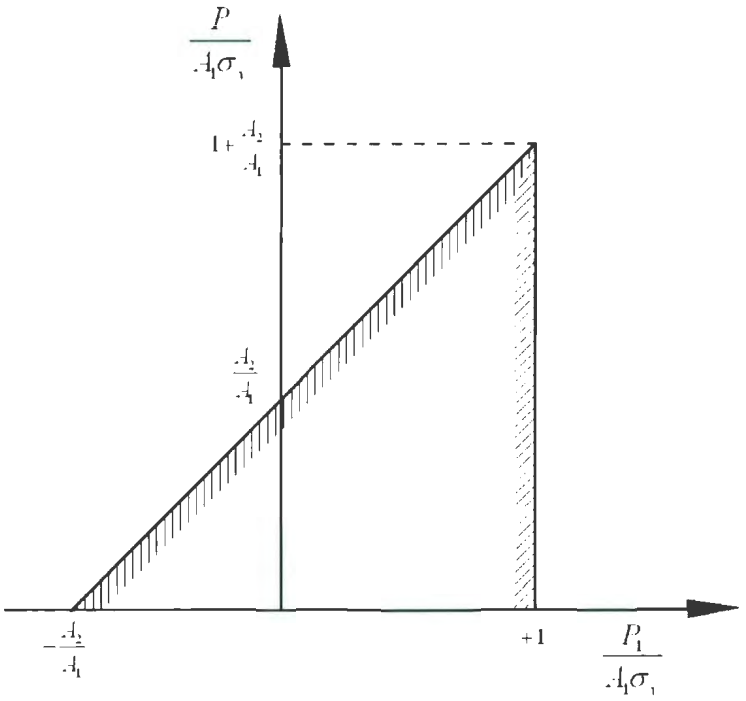

Figure 3.17: Programming method, lower bound solution

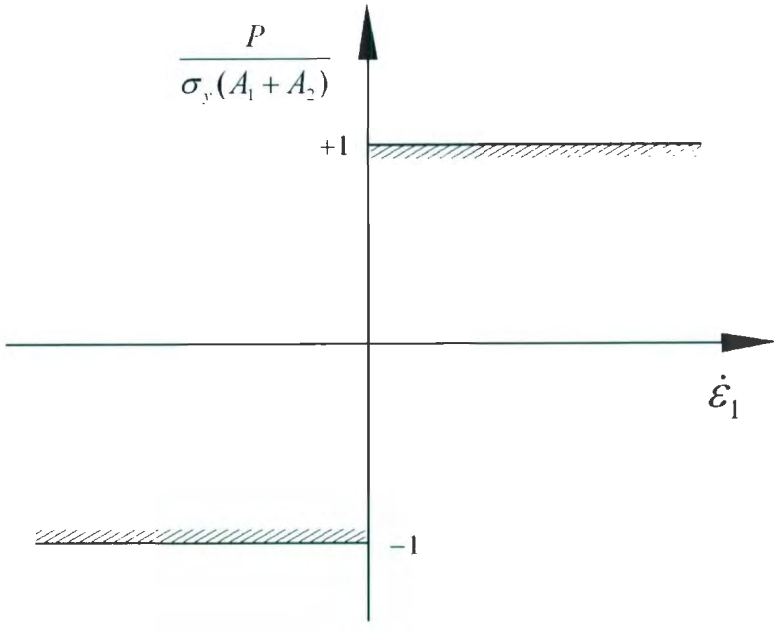

Figure 3.18: Programming method, upper bound solution

Assuming the limit load is non-negative, the limit load multiplier will be the same as the exact solution in Eq. (3.102). The lower bound and upper bound results and the programming method yield to the same value of limit load. Therefore, they are considered as dual problems (Martin, 1975). It is worth noting that applying the programming methods to the complex problems are very difficult.

3.6.4 Upper Bound and Lower Bound Limit Load Multipliers

The classical upper bound limit load is obtained by equating the rate of work by external loads to the corresponding plastic dissipation energy. Applying Eq. (3.72) for the two bar model, the classical upper bound limit load multiplier can be obtained as i. e.,

$$m_U = \frac{\sigma_y(\sigma_1 A_1 L_1 E_2 + \sigma_2 A_2 L_2 E_1)}{\sigma_1^2 A_1 L_1 E_2 + \sigma_2^2 A_2 L_2 E_1} \tag{3.116}$$

Applying Eq. (3.76) to the two-bar structure, the upper bound multiplier m_1^0 can be written as

$$m_1^0 = \frac{\sigma_y \sqrt{A_1 L_1 + A_2 L_2}}{\sqrt{\sigma_1^2 (A_1 L_1) + \sigma_2^2 (A_2 L_2)}} \tag{3.117}$$

Applying Eq. (3.79), the limit load multiplier m_2^0 for the two-bar structure can be expressed as

$$m_2^0 = \frac{\sigma_y \sqrt{A_1 L_1 E_2 + A_2 L_2 E_1}}{\sqrt{\sigma_1^2 (A_1 L_1 E_2) + \sigma_2^2 (A_2 L_2 E_1)}} \tag{3.118}$$

As discussed earlier, in the classical method of determining lower bound limit load, the maximum equivalent stress value is all that is needed from a statically admissible stress field, i. e.,

$$P_L = \left(\frac{\sigma_y}{\sigma_{\max}} \right) P \tag{3.119}$$

Assuming $\sigma_1 > \sigma_2$ then $\sigma_{\max} = \sigma_1$, and the classical lower bound multiplier can be determined as

$$m_L = \frac{\sigma_y}{\sigma_1} \tag{3.120}$$

The limit load multiplier m'' can be estimated using Eq. (3.89). The parameter G in Eq. (3.90) can be expressed for two-bar model as

$$G = \sqrt{\frac{[(m^0 \sigma_1 / \sigma_y) - 1]^2 A_1 L_1 + [(m^0 \sigma_2 / \sigma_y) - 1]^2 A_2 L_2}{4(A_1 L_1 + A_2 L_2)}} \tag{3.121}$$

As discussed earlier, limit load multiplier m_α depends on m_L and m^0/m_L; therefore, for the two-bar structure, making use of Eqs. (3.117) and (3.120), the limit load multiplier m_α can be obtained. Also, making use Eqs. (3.36) and (3.120), the lower bound limit load multiplier m' for two-bar model can be obtained.

Rewriting Eq. (3.93) in terms of stresses, following expression can be obtained:

$$\sigma_n A = \sigma_1 A_1 + \sigma_2 A_2 \tag{3.122}$$

where A is the summation of the bars cross sections, i. e., $A = A_1 + A_2$.

$$\sigma_n = \sigma_1 \mu_1 + \sigma_2 \mu_2 \tag{3.123}$$

where $\mu_1 = \dfrac{A_1}{A_1 + A_2}$ and $\mu_2 = \dfrac{A_2}{A_1 + A_2}$

Substituting Eq. (3.100) into Eq. (3.123),

$$\sigma_n = \frac{P}{\dfrac{A_1 E_1}{L_1} + \dfrac{A_2 E_2}{L_2}} \left(\mu_1 \frac{E_1}{L_1} + \mu_2 \frac{E_2}{L_2} \right) \tag{3.124}$$

The limit load is proportional to the external load, i.e.,

$$P_L = \left(\frac{\sigma_y}{\sigma_n}\right) P \tag{3.125}$$

Making use of Eqs. (3.124) and (3.125), the limit load can be obtained as

$$P_L = \left[\frac{\dfrac{A_1 E_1}{L_1} + \dfrac{A_2 E_2}{L_2}}{\mu_1 \dfrac{E_1}{L_1} + \mu_2 \dfrac{E_2}{L_2}}\right] \sigma_y \tag{3.126}$$

Plastic collapse is not dependent on statically indeterminate parameters, i. e., E_1, E_2, L_1 and L_2. Therefore, two cases are considered next.

Case 1: $E_1 / L_1 = E_2 / L_2$

Substituting into Eq. (3.126), we got

$$P_L = \left[\frac{A_1 + A_2}{\mu_1 + \mu_2}\right] \sigma_y \tag{3.127}$$

Here, $P_L = (A_1 + A_2)\sigma_y$ provided that $\mu_1 + \mu_2 = 1$. From Eqs. (3.124) and (3.125)

$$\frac{\sigma_1}{\sigma_2} = \frac{E_1 L_2}{E_2 L_1} = 1 \tag{3.128}$$

i.e., $\sigma_1 = \sigma_2$. This case would have to be regarded as trivial since the two-bar model would fail to generate unequal pseudo-elastic stresses.

Case 2: $A_1 = A_2 = A_0$

This case leads to $\mu_1 = \mu_2 = 1/2$. Substituting into Eq. (3.126)

$$P_L = 2A_0\sigma_y \tag{3.129}$$

and

$$\sigma_n = \frac{P}{2A_0} = \frac{P_1 + P_2}{2A_0} = \frac{\sigma_1 + \sigma_2}{2} \tag{3.130}$$

This means that the combined effective stress can be expressed as the arithmetic average of the pseudo-elastic stresses.

Finally, the limit load multiplier using R-Node concept can be obtained as

$$m_n = \frac{P_L}{P} = \frac{\sigma_y}{\sigma_n} = \frac{\sigma_y}{\left(\frac{\sigma_1 + \sigma_2}{2}\right)} \tag{3.131}$$

3.6.5 EMAP for the Two Bar Structure

By assuming the material properties are the same for the bars, the stresses in the two bars introduced in Eq. (3.100) can be rewritten in as iterative form as

$$\begin{cases} \sigma_1^i = \dfrac{E_1^i L_2}{A_1 E_1^i L_2 + A_2 E_2^i L_1} P \\ \sigma_2^i = \dfrac{E_2^i L_1}{A_1 E_1^i L_2 + A_2 E_2^i L_1} P \end{cases} \tag{3.132}$$

In the first iteration ($i = 1$), which is the first elastic solution without any elastic modulus modification, the following expression is valid :

$$E_1^{i=1} = E_2^{i=1} = E_0 \tag{3.133}$$

Therefore, submitting Eq. (3.133) into Eq. (3.132), the values of stresses $\sigma_1^{i=1}$ and $\sigma_2^{i=1}$ can be calculated.

In the second iteration ($i = 2$), the elastic modulus of the bars are modified using following expression

$$\begin{cases} E_1^{i=2} = \left(\dfrac{\sigma_{ref}}{\sigma_1^{i=1}}\right)^q E_1^{\,i=1} \\ E_2^{i=2} = \left(\dfrac{\sigma_{ref}}{\sigma_2^{i=1}}\right)^q E_2^{\,i=1} \end{cases} \tag{3.134}$$

The reference stress for the two-bar system can be evaluated using Eq. (3.67) as

$$\sigma_{ref}^{i} = \left[\frac{\sigma_1^2 A_1 L_1 + \sigma_2^2 A_2 L_2}{A_1 L_1 + A_2 L_2}\right]_i^{1/2} \tag{3.135}$$

Similar to the first iteration, $\sigma_1^{i=2}$ and $\sigma_2^{i=2}$ can be calculated by applying Eq. (3.134) into Eq. (3.132).

At the m^{th} iteration ($i = m$), the following expression is valid between elastic modulus of two subsequent iterations

$$\begin{cases} E_1^{i=m} = \left(\dfrac{\sigma_{ref}^{i=m-1}}{\sigma_1^{i=m-1}}\right)^q E_1^{\,i=m-1} \\ E_2^{i=m} = \left(\dfrac{\sigma_{ref}^{i=m-1}}{\sigma_2^{i=m-1}}\right)^q E_2^{\,i=m-1} \end{cases} \tag{3.136}$$

Consequently, $\sigma_1^{i=m}$ and $\sigma_2^{i=m}$ can be calculated using Eq. (3.136). The procedure is repeated until suitable convergence is achieved.

3.6.6 Numerical Example

Consider a two-bar system subjected to external load of P=15 kN with material properties and geometry configurations given in Table 1.

Table 3.2: Geometry and material properties for two-bar system

Parameters	Bar 1	Bar2
A (Area)	40 mm^2	60 mm^2
L (Length)	80 mm	150 mm
E (Elastic modulus)	200 GPa	200 GPa
σ_y (Yield strength)	250 MPa	250 MPa

Applying Eq. (3.100), the stresses in the bars can be calculated as

σ_1=208.33 MPa

σ_2=111.11 MPa

The limit load solution is acquired using the exact solution in Eq. (3.101) as

$P_L = \sigma_y(A_1 + A_2)$=25 kN

Therefore, the corresponding exact limit load multiplier can be obtained as

$$m_{exact} = \frac{P_L}{P} = 1.6667$$

Different upper bounds and lower bounds form linear elastic analysis are compared in Table. 3.3.

Table 3.3: Upper bound and Lower bound limit load multipliers (initial elastic analysis)

m_1^0	m_2^0	m_{Exact}	m_α	m''	m_L	m'
1.7464	1.7464	1.6667	1.4521	1.3098	1.2000	1.1202

The variation of upper bound and lower bound limit load multipliers with successive iterations for the two-bar system is plotted in Figs. (3.20) and (3.21) for different values of elastic modulus adjustment index, q. From Figs. (3.20) and (3.21), it can be seen that the limit load multipliers converge to the exact limit load. This indicates that by applying a proper value for parameter q, the convergence to the exact solution will be faster.

Also, variation of parameter G with linear elastic iteration is shown in Fig. 3.22. As it can be seen in Fig. 3.22, at the converged state G=0; therefore, this parameter can be used as the criterion to assess the convergence of solution obtained from EMAP.

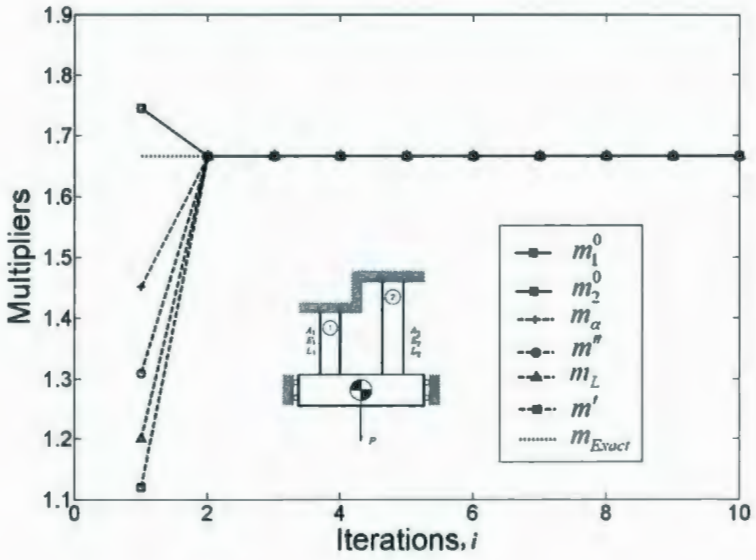

Figure 3.20: Variation of limit load multipliers with iterations, q=1

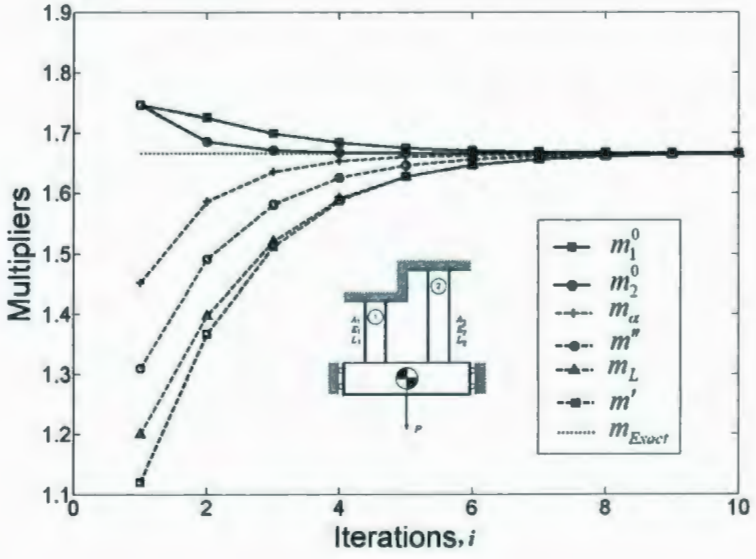

Figure 3.21: Variation of limit load multipliers with iterations, q=0.5

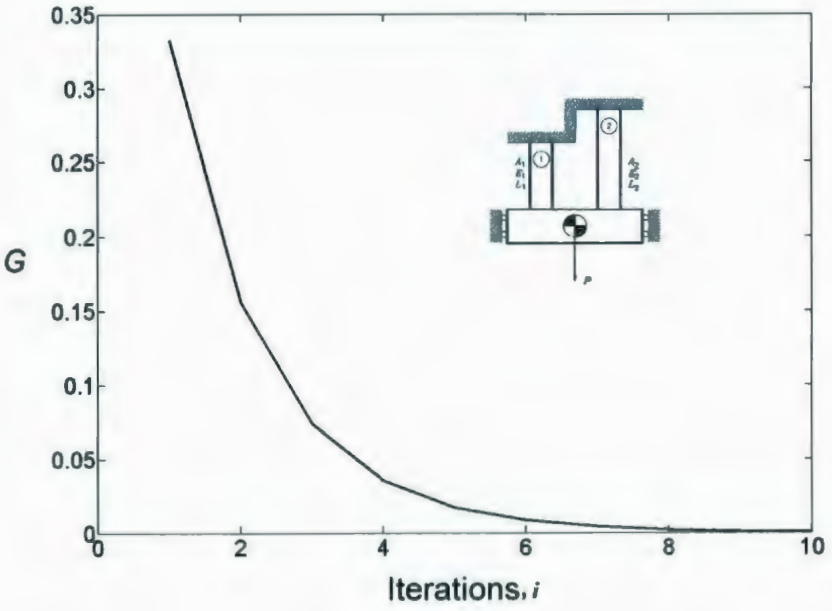

Figure 3.22: Variation of parameter G with linear elastic iterations, q=0.5

CHAPTER 4

CONVERGENCE OF EMAP

4.1 INTRODUCTION

Elastic modulus adjustment procedures (EMAP) have been employed to determine limit loads of pressure components. On the basis of linear elastic Finite Element Analysis (FEA) with non-hardening elastic properties, i.e., by specifying spatial variations in the elastic modulus, numerous sets of statically admissible and kinematically admissible distributions can be generated, and both lower and upper bounds on limit loads can be obtained. Some methods such as the classical, R-Node and the m_α methods provide limit loads on the basis of partly-converged distributions, whereas the accuracy of linear matching procedures rely on fully converged distributions.

By plotting upper and lower bound limit load multipliers obtained from EMAP versus linear elastic iteration for a given component, Seshadri and Mangalaramanan

(1997) reported different trends when using constant q in Eq. (3.76). Therefore, they classified components and structures into three different categories: Class I, II and III. Class I category are the components or structures that are characterized by monotonic convergent behavior in lower and upper bound limit load multipliers when using EMAP. Thick walled cylinder and indeterminate beam are example of this class of problem. In Class II problems, the magnitude of maximum stress in a body is not consistently decreasing during successive elastic iterations; therefore, the limit load multiplier that is dependent on the maximum stress (i.e., classical lower bound limit load multiplier, m_L) has the problem of converging to the exact limit load solution. This behavior has been observed in thin structures without a re-entrant corner such as spherical pressure vessel with a cylindrical nozzle and a compact tension specimen. In the Class III problems, the non-convergence can be seen in both upper and lower bound limit load multipliers. A rectangular plate with nonsymmetric boundary conditions is an example of this class of problems. Accordingly, for Classes II and III behavior, Seshadri and Mangalaramanan (1997) suggested to use $0 < q < 1$ (for instance 0.5 or 0.25) to obtain the behavior similar to Class I, resulting in a more stable prediction of the limit load multipliers. Although using the small value of q results in a stable solution, it considerably increases the number of linear elastic iterations required to reach the convergence state. In this Chapter, a criterion for establishing the degree of convergence of EMAP is developed, and a simple procedure for achieving improved convergence is described. The procedure is applied to some practical pressure component configurations.

4.2 THEORY

For the sake of discussion, consider a pressure component that is subjected to a mechanical load. In EMAP for limit analysis, the objective is to make all elements in the FEA involved in plastic collapse at the same level of stress, σ_{ref}. As illustrated in Fig. 4.1, in order to bring point A (which represents the equivalent stress and strain in first iteration) to the reference stress level, q would be dependent on the local constraint. Several constraints can be categorized by using the elastic modulus adjustment parameter, q, using general EMAP expression as

$$E^{i+1} = \left(\frac{\sigma_{ref}^{i}}{\sigma_{eq}^{i}} \right)^{q} E^{i} \tag{4.1}$$

Depending on the geometry and loading conditions, the value of q could be specified as an initial guess. For example, q equal to 1 and 2 are suitable for plane strain and plane stress, respectively. To avoid this guess work, we assess the value of q by equating the two shaded region in Fig. 4.2. The idea comes from Molski and Glinka (1981) (known as the ESED concept), the procedure for obtaining q expression is discussed here. By equating the two shaded areas in Fig. 4.2, we have:

$$\frac{1}{2}\sigma_{eq}\,\varepsilon_{eq} = \frac{1}{2}\sigma_{ref}\,\varepsilon_{0} + \sigma_{ref}\left(\varepsilon_{ref} - \varepsilon_{0}\right) \tag{4.2}$$

Therefore,

$$\varepsilon_{ref} = \frac{\sigma_{eq}\,\varepsilon_{eq} - \sigma_{ref}\,\varepsilon_0}{2\,\sigma_{ref}} + \varepsilon_0 \tag{4.3}$$

Substituting $\varepsilon_{eq} = \frac{\sigma_{eq}}{E_i}$ and $\varepsilon_0 = \frac{\sigma_{ref}}{E_i}$ into Eq. (4.3), ε_{ref} can be obtained as:

$$\varepsilon_{ref} = \frac{\sigma_{eq}^2 + \sigma_{ref}^2}{2\,\sigma_{ref}\,E_i} \tag{4.4}$$

From Fig. 4.2, ε_{ref} can be written as

$$\varepsilon_{ref} = \frac{\sigma_{ref}}{E_{i+1}} \tag{4.5}$$

From Eqs. (4.4) and (4.5), the relation between E_{i+1} and E_i can be obtained as:

$$E_{i+1} = \frac{2\,\sigma_{ref}^2}{\sigma_{eq}^2 + \sigma_{ref}^2} E_i \tag{4.6}$$

Comparing Eqs. (4.1) and (4.6), the following expression can be obtained

$$\left(\frac{\sigma_{ref}}{\sigma_{eq}}\right)^{q} = \frac{2\sigma_{ref}^{2}}{\sigma_{eq}^{2}+\sigma_{ref}^{2}} \tag{4.7}$$

The final equation can be expressed as:

$$q = \frac{\ln\left(\dfrac{2\sigma_{ref}^{2}}{\sigma_{eq}^{2}+\sigma_{ref}^{2}}\right)}{\ln\left(\dfrac{\sigma_{ref}}{\sigma_{eq}}\right)} \tag{4.8}$$

By using the last expression there is no need to predefine q, which for each element in different iterations will be calculated from the respective elastic FEA solution.

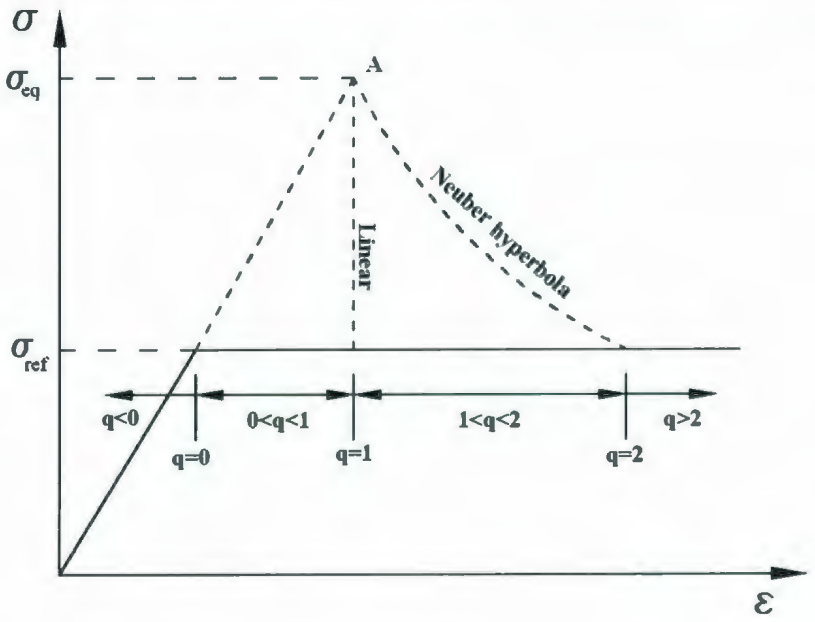

Figure 4.1: Stress redistribution regions

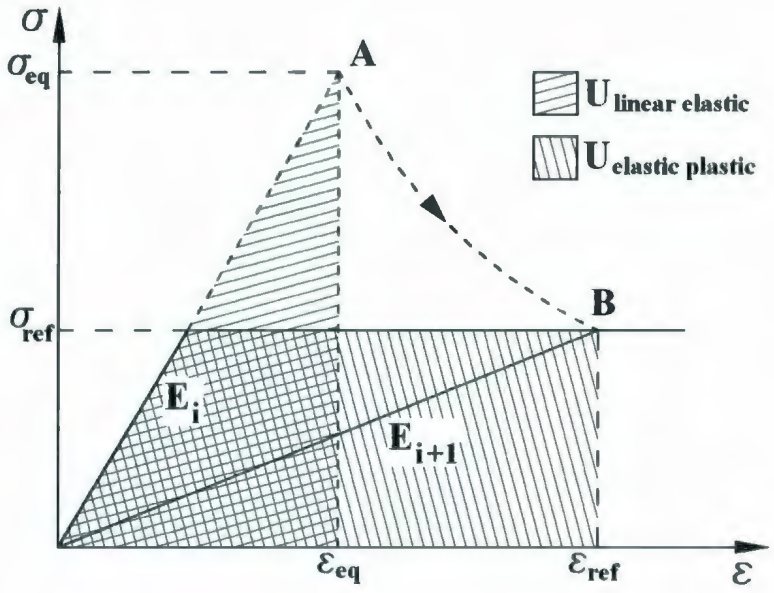

Figure 4.2: Graphical representation of ESED concept

4.3. NUMERICAL EXAMPLES

4.3.1 Indeterminate Beam (Plane Stress)

An indeterminate beam with one end simply supported and the other clamped is modeled (Fig. 4.3). The beam length is L=508 mm (20 in), the width is W=25.4 mm (1 in). A uniform distributed load 0.1724 MPa (25 psi) is applied with plane stress condition. The material is assumed to be elastic-perfectly plastic. The modulus of elasticity is 206,850 MPa (30E6 psi), and the yield strength is 206.85 MPa (30E3 psi). The variation of the limit load multipliers, predicted by different values of q, with iterations are presented in Figs. 4.4-4.7. Likewise, the variation in the value of G parameters G_2^0 is presented in Fig. 4.8 (where G_U, G_1^0 and G_2^0 are based on m_U, m_1^0 and m_2^0,

respectively). It can be seen that a non-zero of parameter G indicates partially converged state. Comparing to the results obtained using constant q, variable q demonstrates improved convergence and prediction of limit load. Relatively low value of q (Fig. 4-6) causes stable results; however, the convergence is very slow. On the other hand, choosing q between 1 and 2 (Fig. 4.4 and Fig. 4-5,) helps fast convergence but increase the amount of numerical difficulties before convergence. Therefore, variable q approach not only avoids the numerical difficulties when using EMAP but also helps achieving fast convergence.

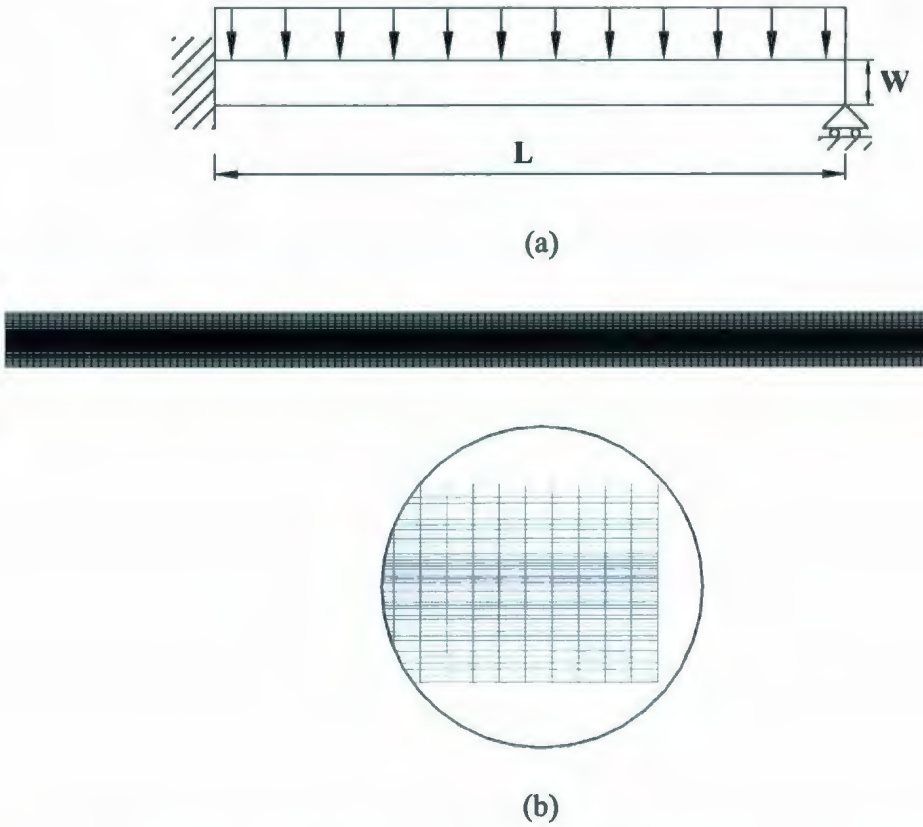

Figure 4.3: Indeterminate beam: (a) Geometry and dimensions, (b) Finite element mesh

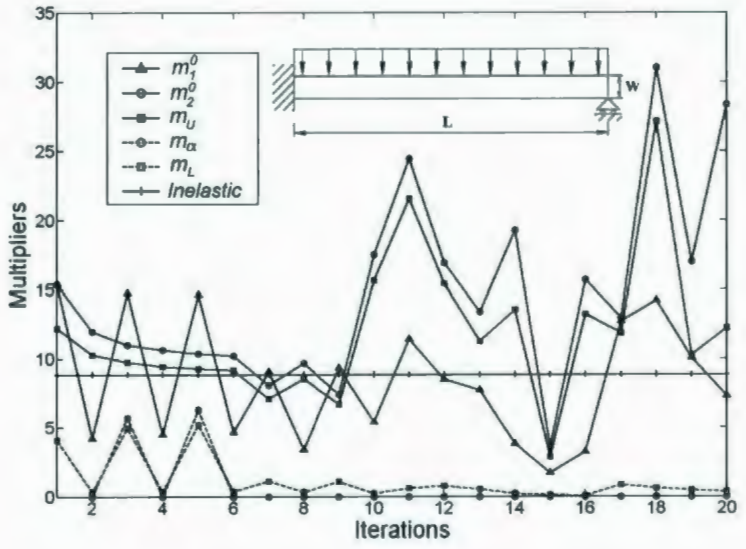

Figure 4.4: Variation of limit load multipliers for indeterminate beam, q=2 for all elements

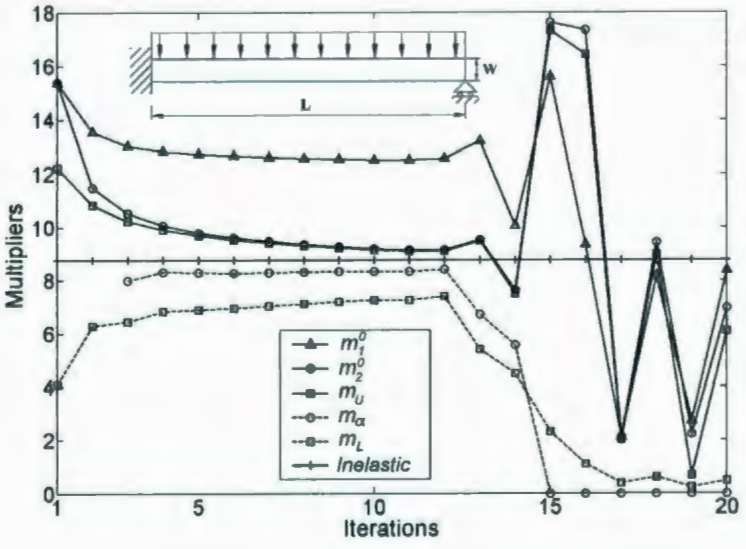

Figure 4.5: Variation of limit load multipliers for indeterminate beam, q=1 for all elements

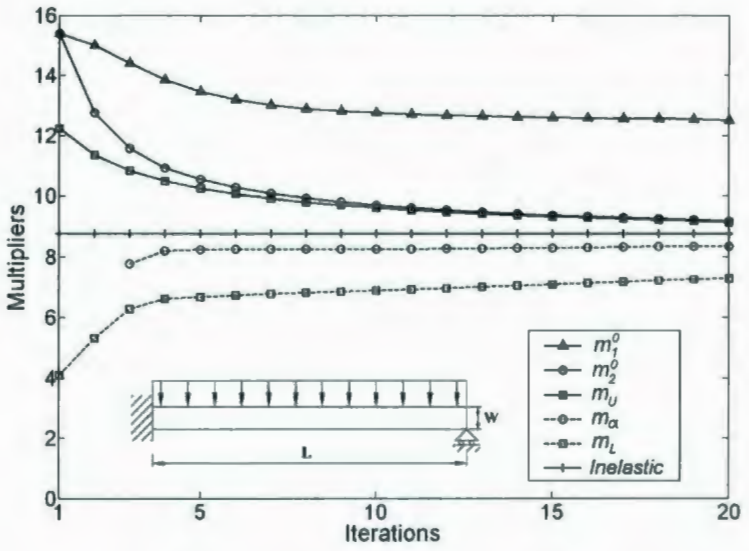

Figure 4.6: Variation of limit load multipliers for indeterminate beam, q=0.5 for all elements

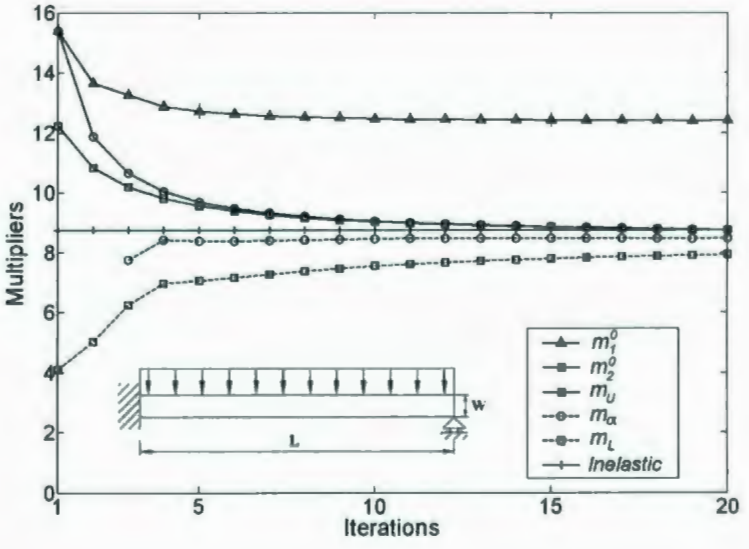

Figure 4.7: Variation of limit load multipliers for indeterminate beam, q=variable (present study)

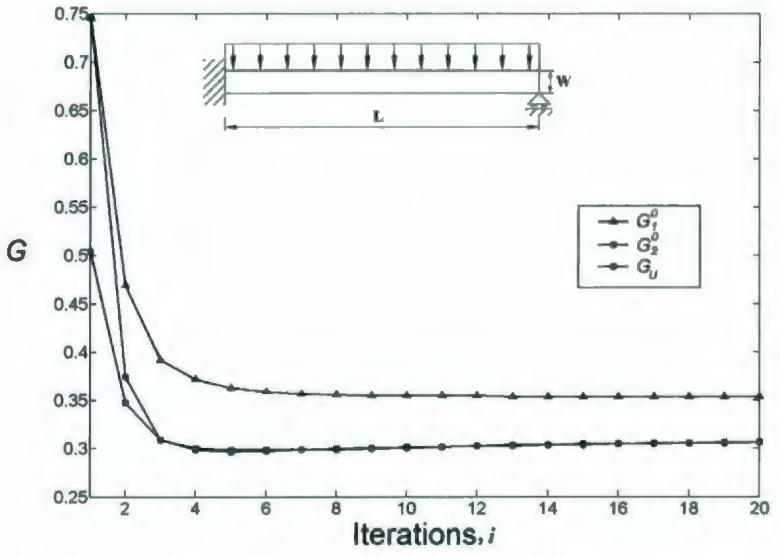

Figure 4.8: Variation of different values of parameter G for indeterminate beam (variable q)

4.3.2 Compact Tension (CT) Specimen

A compact tension specimen shown in Fig. 4.9 (a) with a width W=100 mm, height H=125 mm, thickness t=3 mm and crack length a=46 mm is subjected to a tensile load P =10 KN. The material properties are: elastic modulus E=211 GPa and yield strength σ_y=250 MPa, with a Poisson's ratio of ν=0.3. Due to symmetry in geometry and loading, only a half of the plate is modeled with plane stress condition. The plate is modeled using eight noded isoparametric quadrilateral elements, with singular elements around the crack-tip. A typical finite element mesh is presented in Fig. 4.9 (b). Symmetry

boundary condition is used ahead if the crack tip and in order to avoid rigid body motion the node at the crack tip is fixed.

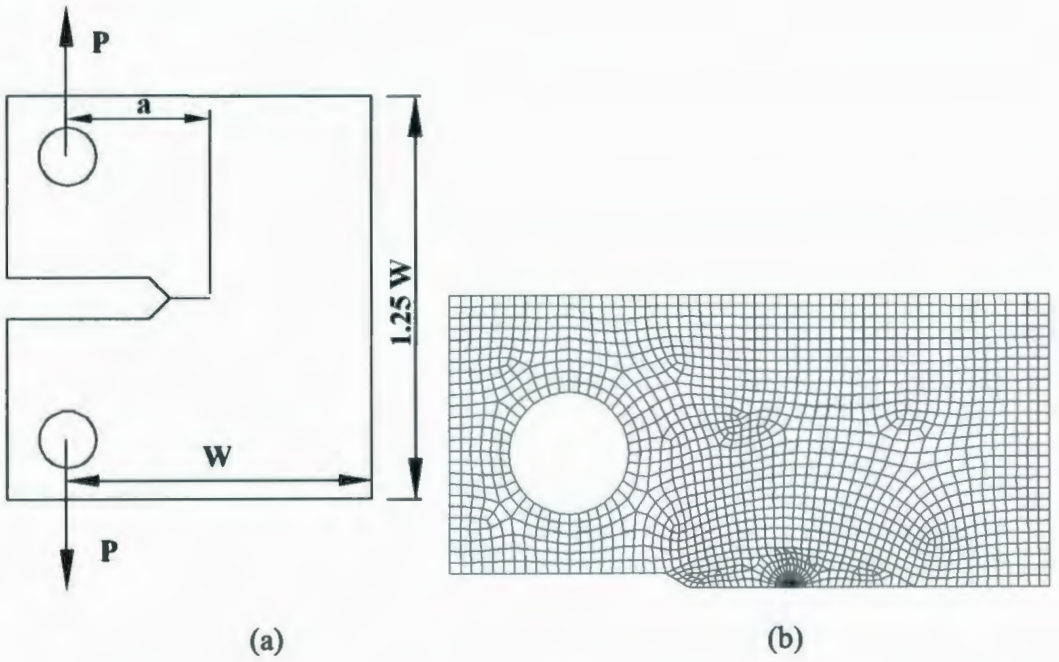

Figure 4.9: Compact tension (CT) specimen: (a) Geometry and dimensions, (b) Finite element mesh

The variation of limit load multipliers during successive iterations predicated by different values of q are plotted in Figs. 4.10-4.12. The difference between m_1^0 and m_2^0 is due to local plastic regions in the body. The variation in the value of G_2^0 (estimated G based on the upper limit load multiplier m_2^0) is shown in Fig. 4.13. As can be inferred from Fig. 4.13, the value of G_2^0 decreases during the successive iterations, reaching a converged state.

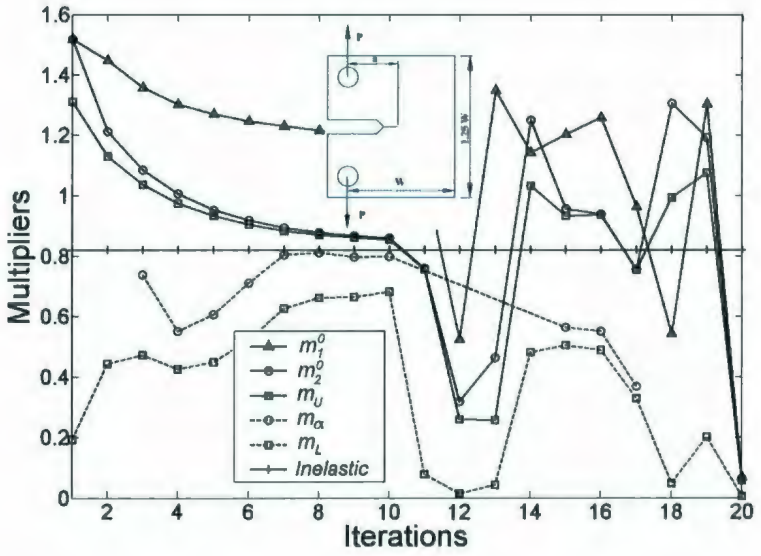

Figure 4.10: Variation of limit load multipliers with iterations, q=1

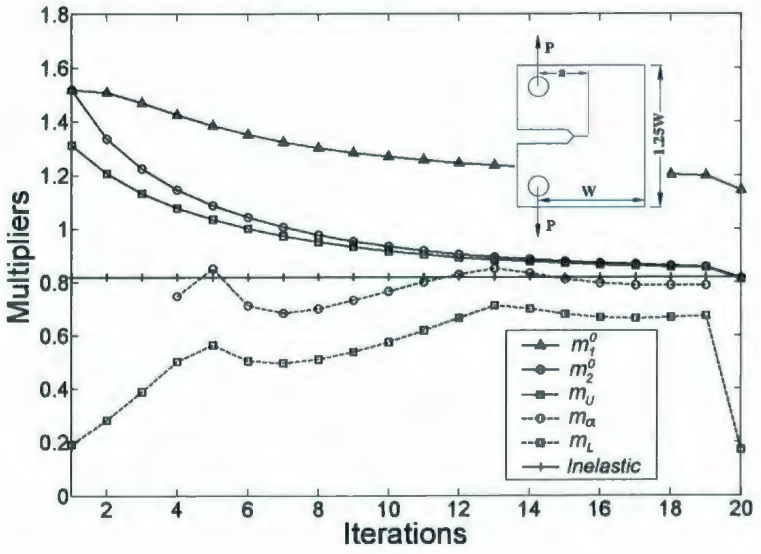

Figure 4.11: Variation of limit load multipliers with iterations, q=0.5

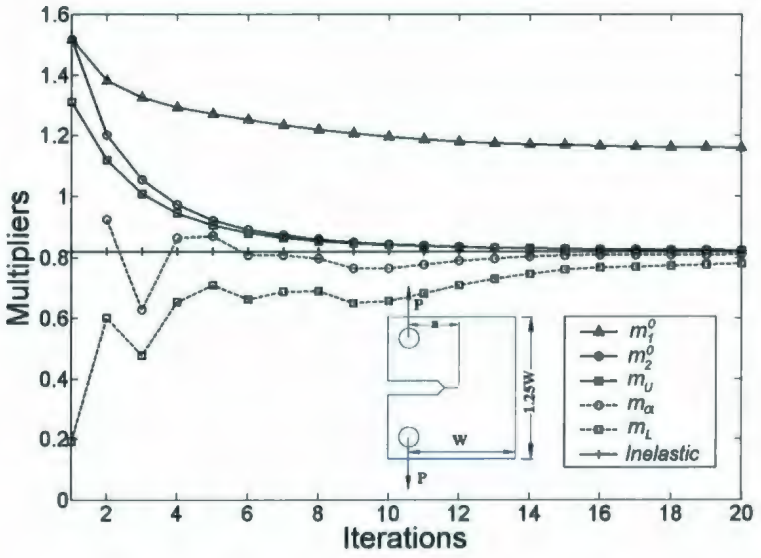

Figure: 4.12: Variation of limit load multipliers with iterations, q= variable

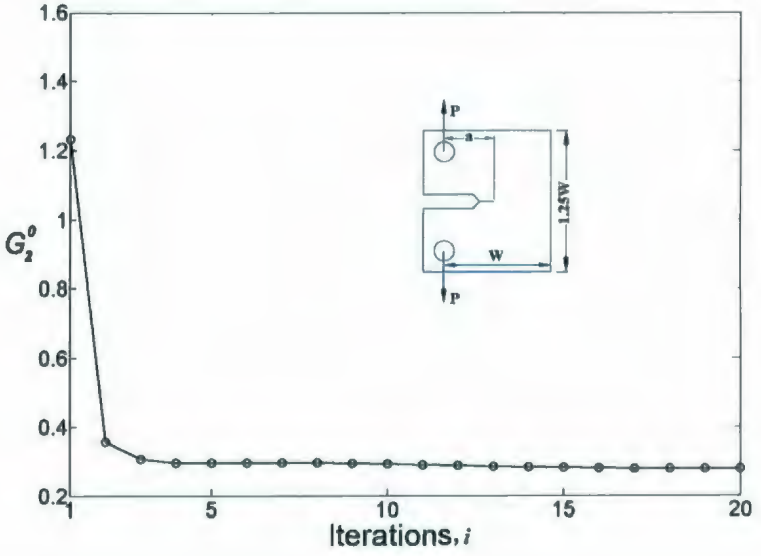

Figure: 4.13: Variation of G_2^0 with iteration, q= variable

4.3.3 Thick Walled Cylinder (Plane Strain)

The thick walled cylinder (Fig. 4.14) with inside radius of R –60 mm and thickness t =120 mm is modeled. An internal pressure of 50 MPa is applied. The material is assumed to be elastic-perfectly plastic. Due to symmetry only a quarter of the cylinder is modeled and symmetry boundary conditions are applied on the edges. The modulus of elasticity is specified as 200 GPa and the yield strength is assumed to be 300 MPa. The variation of limit load multipliers with iterations using the improved convergence scheme is shown in Fig. 4.15. Likewise, the variation in the value of G_2^0 is presented in Fig. 4.16. It can be seen that the solution converge within four iteration, i.e., G_2^0 is zero.

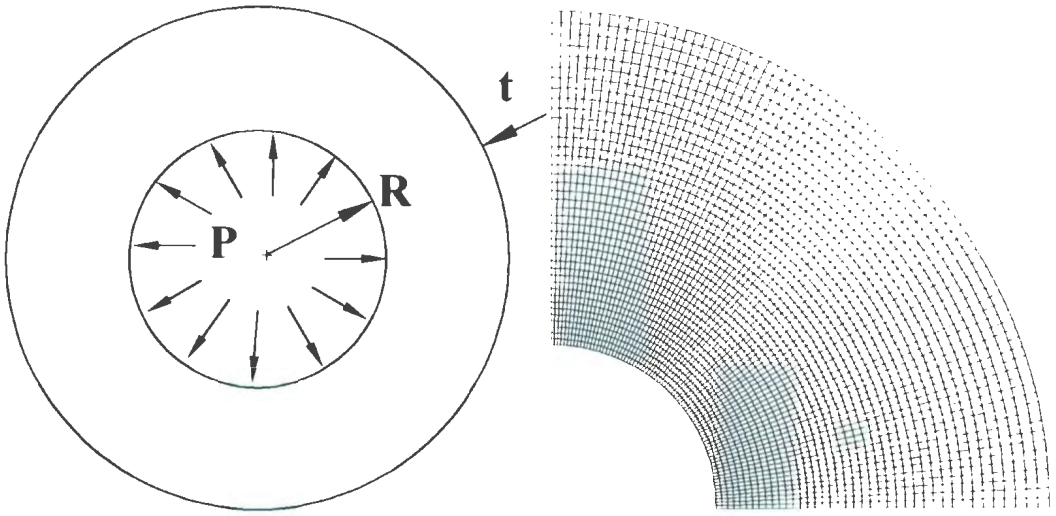

(a) (b)

Figure 4.14: Thick walled cylinder: (a) Geometry and dimensions, (b) Finite element mesh (a quarter model)

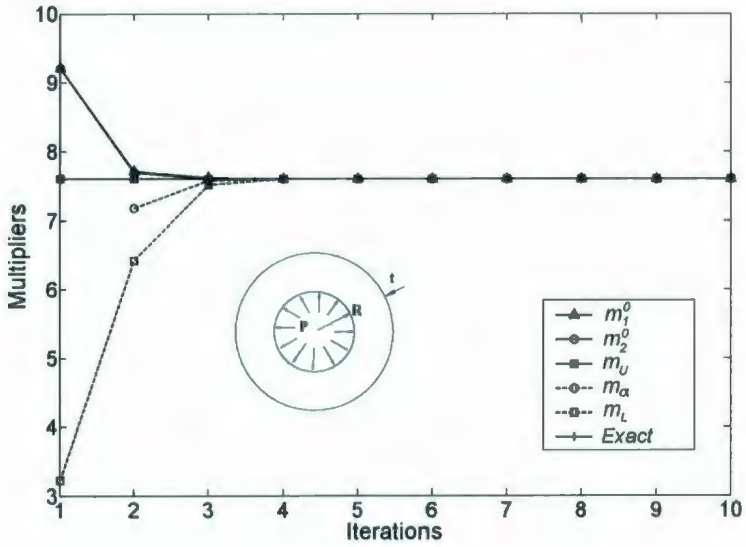

Figure 4.15: Variation of limit load multipliers for thick walled cylinder (variable q)

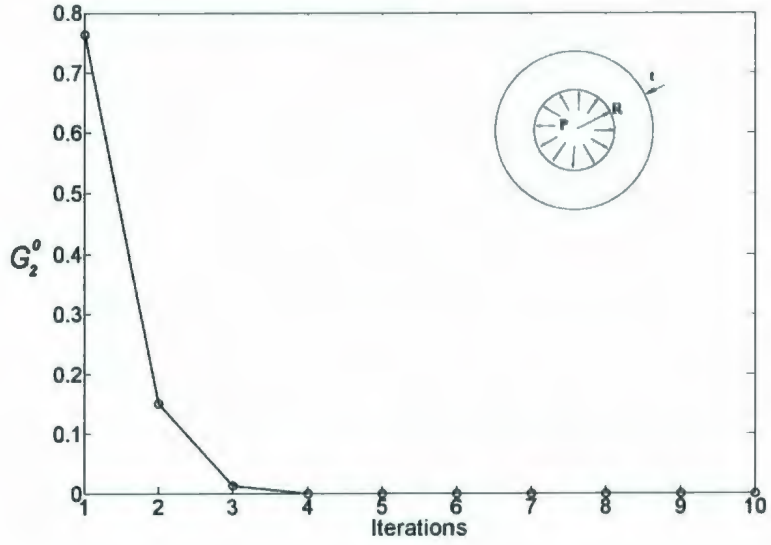

Figure 4.16: Variation of G_2^0 for thick walled cylinder (variable q)

4.3.4 Welded-In Flat Head (Axisymmetric)

A welded-in flat head configuration (Fig. 4.17) with the cylinder radius R=200 mm, thickness t_c=21.5 mm, flat head thickness t_h=43 mm, overall length L=243 mm, and with weld groove of r_f=10 mm is considered. The material is same as for the thick walled cylinder. An internal pressure of 10 MPa is applied. The variation of limit load multipliers with iterations predicted by this method is the presented in Fig. 4.18, and variations of G_2^0 by linear elastic iteration is presented in Fig. 4.19.

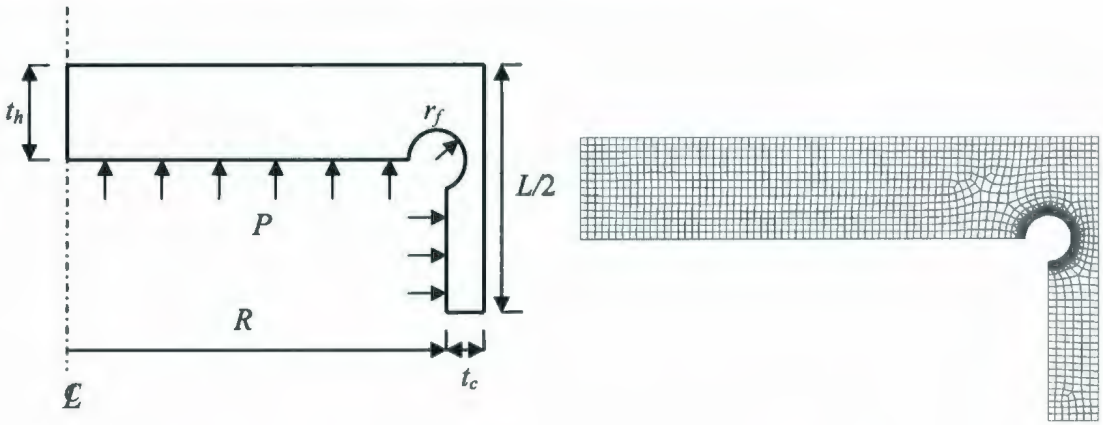

Figure 4.17: Welded-In flat head: (a) Geometry and dimensions, (b) Finite element mesh

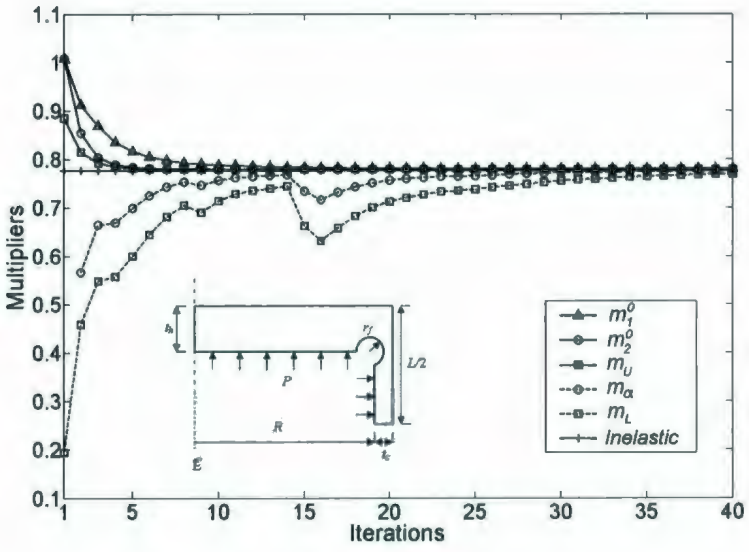

Figure 4.18: Variation of limit load multipliers for welded-in flat head (variable q)

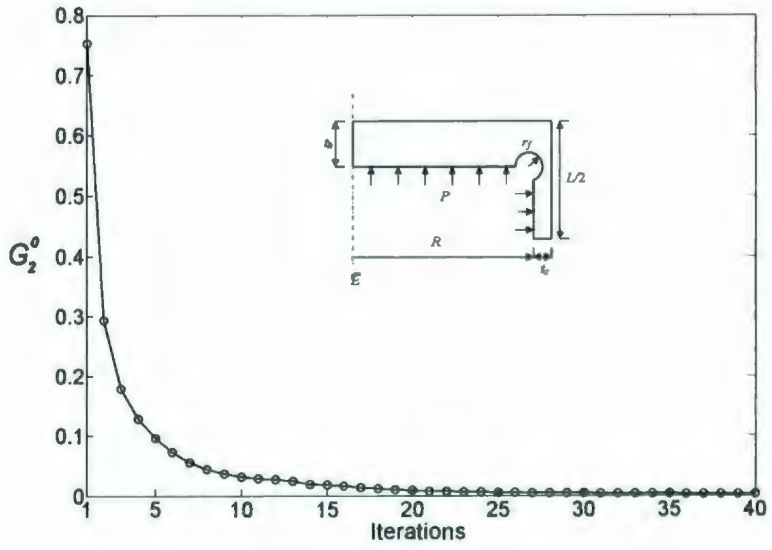

Figure 4.19: Variation of G_2^0 for welded-in flat head (variable q)

4.3.5 Plate with Multiple Cracks

A plate with multiple cracks (Fig. 4.20) has one horizontal crack (length $2a$=20 mm) at the center and four cracks inclined at 45° (length $2b$=21.2 mm) symmetrically located on both sides of the horizontal and vertical lines of symmetry. The crack tips are spread vertically with c=20 mm and with horizontally d=40 mm. The plate has a width W=100 mm and height H=200 mm, and is loaded by a tensile stress of σ=100 MPa. The material properties are the same as that for the compact tension specimen. Due to symmetry only one-quarter of the plate is modeled.

The multipliers predicted by various methods (Direct EMAP) versus iterations are plotted in Fig. 4.21. Similarly, the variation in the value of G_2^0 is presented in Fig. 4.22. Figure 4.21 suggests that most of the multipliers converge to the inelastic FEA value at the last iteration. Although the parameter G_2^0 is not zero at the last iteration, referring to Fig. 4.22, it tends to stabilize in the last iterations. This implies that for assessing the convergence of a solution the results need to stabilize during last iterations.

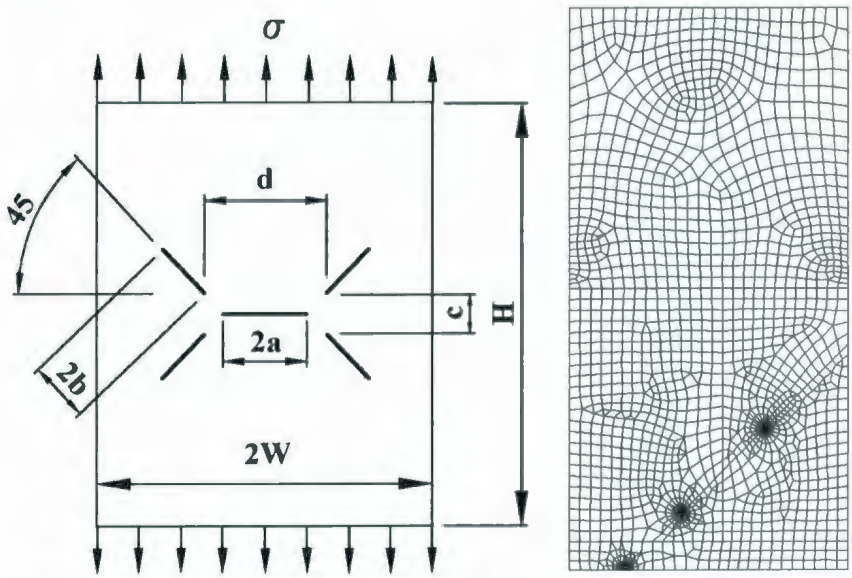

(a) (b)

Figure 4.20: Plate with multiple cracks: (a) Geometry and dimensions (b) Finite element mesh (a quarter model, top right)

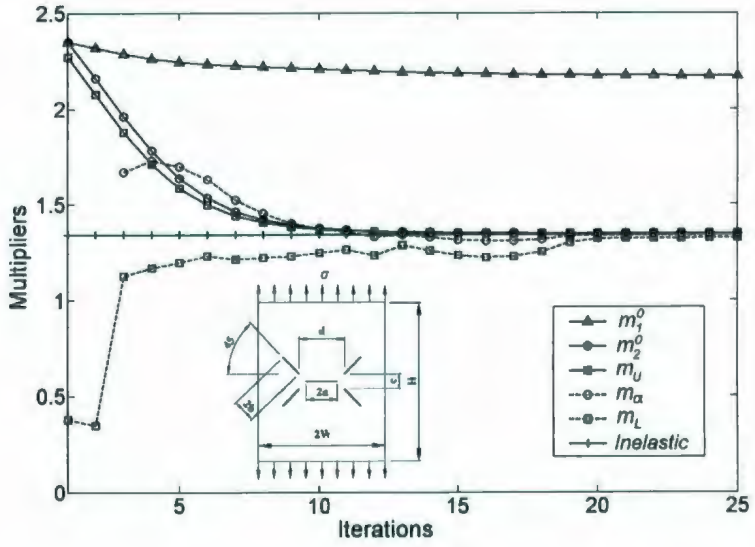

Figure 4.21: Variation of limit load multipliers for plate with multiple cracks (variable q)

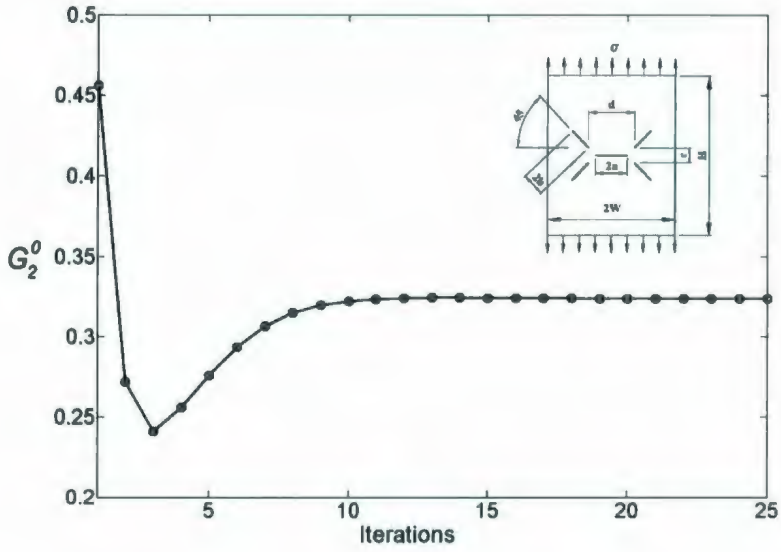

Figure 4.22: Variation of G_2^0 for plate with multiple cracks (variable q)

4.3.5 Axial Semi-Elliptical (Inner) Surface Cracked Pipe

A cylinder with two inner axial semi-elliptical surface cracks located in the same plane (Fig. 4.23) subjected to internal pressure of 150 MPa is considered in here. The inner radius of the cylinder is R/t=2, the crack depth is a/t=0.4 and the half crack length is c/t=0.5. The material is same as for the thick walled cylinder. The three dimensional FEA using 20-node iso-parametric brick element is used to model a 1/8 of the cylinder (due to the axisymmetric condition). Also, to simulate the crack tip the singular element is applied. The variation of limit load multipliers respect to all iterations predicted by this method is the presented in Fig. 4.24. The variations of G_2^0 by EMAP is presented in Fig. 4.25. With regards to Fig. 4.25, the parameter G_2^0 tends to reach to zero during the successive iterations (convergence).

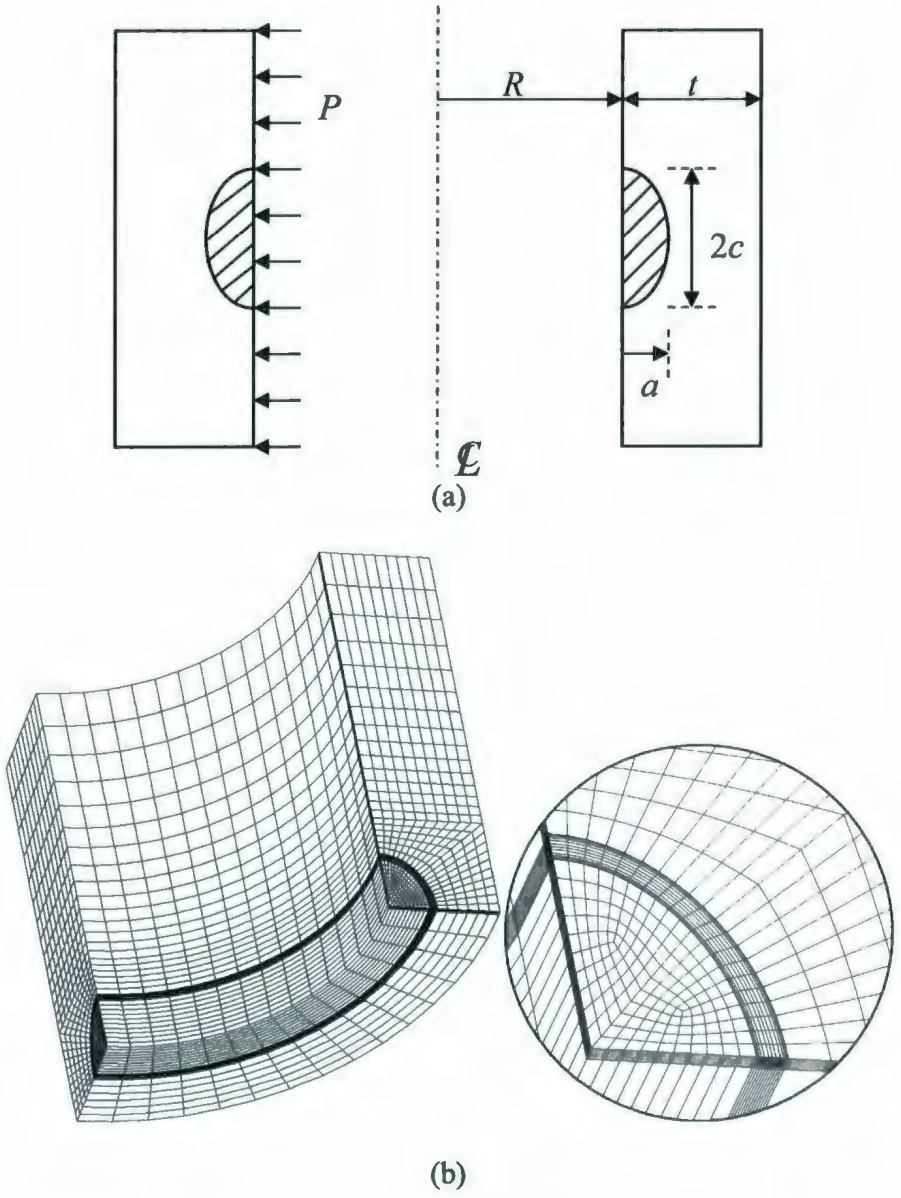

Figure 4.23: Axial semi-elliptical (inner) surface cracked pipe: (a) Geometry and dimensions, (b) Finite element mesh (one eighth of the component is modeled)

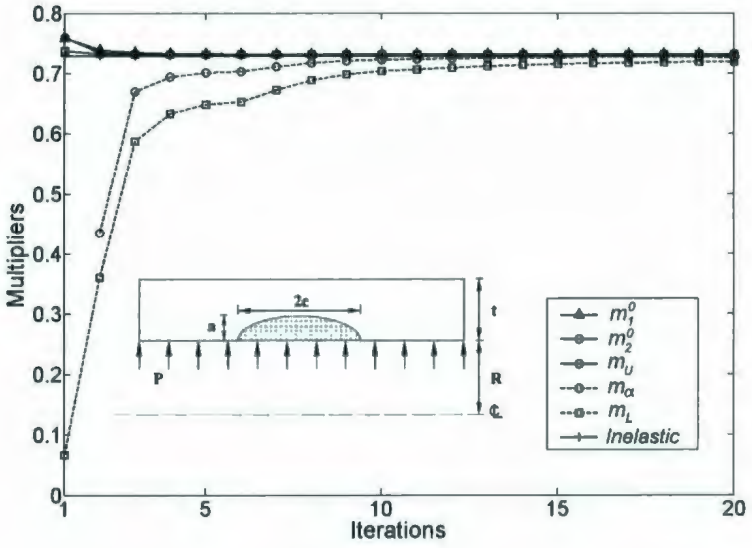

Figure 4.24: Variation of limit load multipliers for axial semi-elliptical surface cracked pipe (variable q)

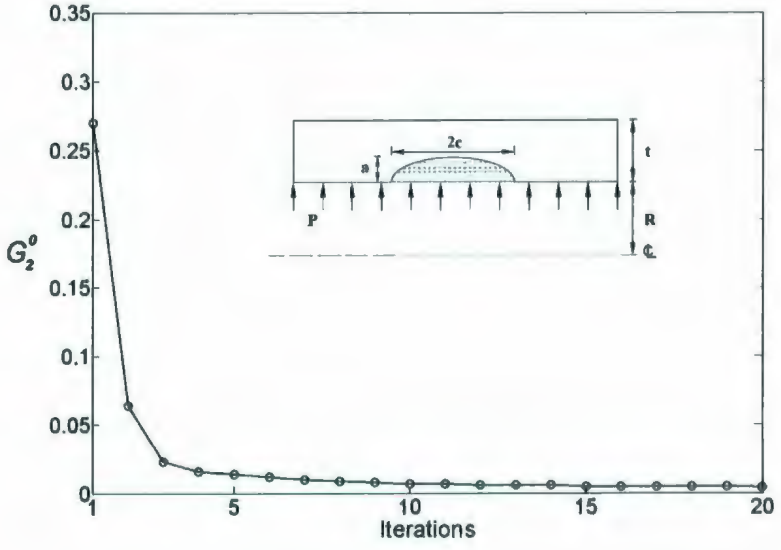

Figure 4.25: Variation of G_2^0 for axial semi-elliptical surface cracked pipe (variable q)

4.4 CLOSURE

The elastic modulus adjustment procedure has been applied to several well-known component configurations under different loading conditions and the results are compared with exact (if applicable) or nonlinear FEA. An enhancement to the conventional EMAP procedure is carried out by the introduction of a simple expression that varies the elastic modulus adjustment parameter, q. Comparison of the results from present work (variable q approach) with constant q demonstrates improved convergence and prediction of limit load. Incorporation of the proposed method is straightforward and offers an attractive alternate to the elastic-plastic analysis due to the achievement of better convergence. Varying the q has also permitted simulation of the "near incompressible" state by increased iterations without encountering numerical difficulty. This method also represents a theoretical approach that prevents arbitrary assumptions about the value for q as is conventionally done in EMAP. The parameter G evaluated acts as a convergence criterion, and is indicative of the deviation of any statically admissible stress distributions from the limit state. Lower the value of G the better is the estimate of the limit load, i.e., $G = 0$ would correspond to the converged solution. This method should enhance and provide some closure to the implementation of EMAP based on linear codes of the commercially available finite element software relating to the analysis of plasticity models.

CHAPTER 5

REFERENCE VOLUME APPROACH

5.1 INTRODUCTION

It is well known that at limit load state of a component/structure, there are some regions that do not participate in inelastic action (dead volume) and may remain rigid or elastic. On the other hand, the remaining volumes are directly active in plastic action (reference volume) are the only regions that carry the external loads at the limit state. As schematically presented in Fig. 5.1, plasticity spread at the collapse mechanism of an indeterminate beam that is built-in on one end, and simply supported at the other and subjected to a uniformly distributed load is a good example. The shaded regions in Fig. 5.1 represent the reference volume where the two hinges at collapse located at these regions. The main objective of this Chapter is to estimate the limit load and the corresponding volume that participates in inelastic action (reference volume) using

EMAP. In this Chapter, variable q approach discussed in Chapter 4 is used in all the numerical examples.

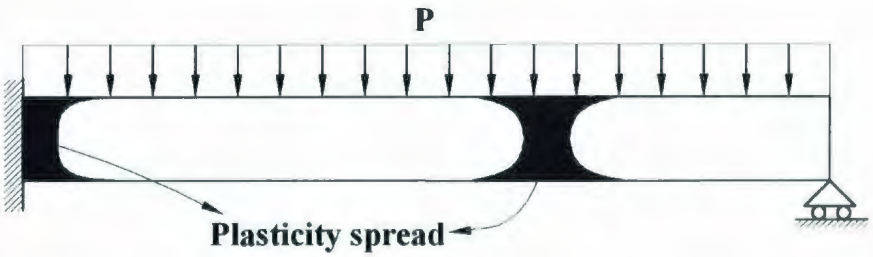

Figure 5.1: Schematically plasticity spread at collapse for an indeterminate beam

5.2 THEORY

In the "Reference Volume Approach", it is assumed that the plastic collapse occurs over a localized region of the mechanical component or structure. Clearly, m_1^0 will be significantly overestimated if it is based on total volume, V_T. The concept of reference volume has been introduced to identify the "kinematically active" region of the component or structure that participates in plastic action.

Consider a component subjected to arbitrary loading condition, Fig. 5.2. The component is divided into two regions: (1) reference volume (V_R), which is kinematically active volume; and (2) the dead zone (V_D). It means that some parts of the component take part in plastic action, and the plastic flow does not occur in the remaining part. If V_T is the total volume thus,

$$V_T = V_R + V_D \tag{5.1}$$

where V_R is the reference volume, and V_D is the volume of the dead zone in the component.

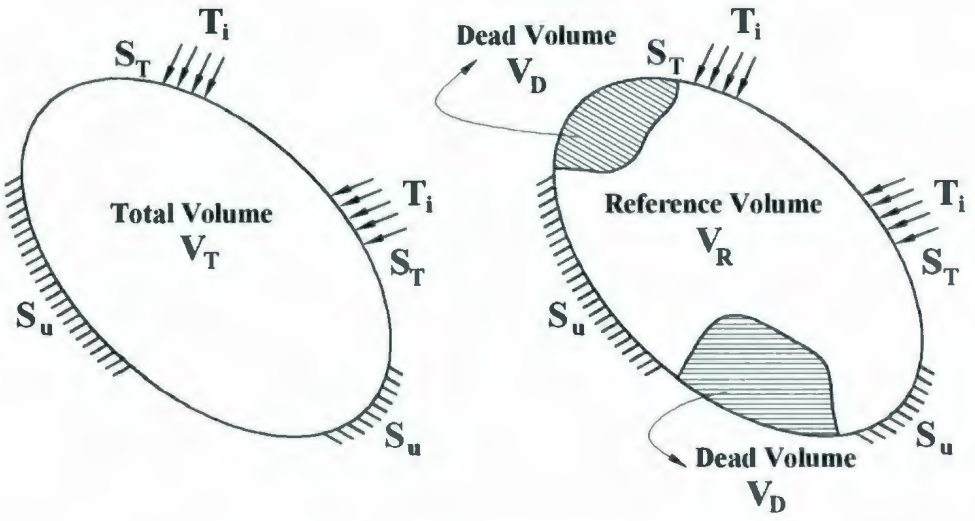

Figure 5.2: Total, reference and dead volumes

Therefore, the multiplier m_2^0, Eq. (3.79), can be written in terms of the reference volume and the dead zone volume as

$$m_2^0 = \sigma_y \frac{\sqrt{\int_{V_R} \frac{\varepsilon_{eq}}{\sigma_{eq}} dV + \int_{V_D} \frac{\varepsilon_{eq}}{\sigma_{eq}} dV}}{\sqrt{\int_{V_R} \sigma_{eq}\varepsilon_{eq}\, dV + \int_{V_D} \sigma_{eq}\varepsilon_{eq}\, dV}} \tag{5.2}$$

If we assume that the dead zone has no plastic flow occurring, then Eq. (5.2) can be simplified as

$$m_2^0 = \frac{\sigma_y \sqrt{\int_{V_R} \frac{\varepsilon_{eq}}{\sigma_{eq}} dV}}{\sqrt{\int_{V_R} \sigma_{eq} \varepsilon_{eq} \, dV}} \tag{5.3}$$

The magnitude of the upper bound multiplier, m_2^0, would therefore depend on the sub-volume, V_η, where

$$V_\eta = \sum_{k=1}^{\eta} \Delta V_k \tag{5.4}$$

In order to identify the reference volume V_R and multiplier $m_2^0(V_R)$, two procedures are suggested as follows:

Procedure 1: The stress distribution within the elements obtained from finite element analysis is sorted in descending order, i. e., $\sigma_{eq}^{(1)} > \sigma_{eq}^{(2)} > \sigma_{eq}^{(3)} > \ldots > \sigma_{eq}^{(N)}$. Corresponding to the stresses $\sigma_{eq}^{(1)}$, $\sigma_{eq}^{(2)}$, $\sigma_{eq}^{(3)}$,...., $\sigma_{eq}^{(N)}$ are the volumes $\Delta V^{(1)}$, $\Delta V^{(2)}$, $\Delta V^{(3)}$,...., $\Delta V^{(N)}$, respectively. Here, V_η is the sub-volume that is the volume summations started from the element with the highest equivalent stress to η^{th} element.

For the maximum stress element of volume $\Delta V^{(1)}$, m_2^0 increase with "i". On the other hand, m_2^0 evaluated on the basis of the total volume would decrease with increasing in iteration variable "i".Therefore, for some volume V_R (where $\Delta V_1 < V_R < V_T$ corresponding to $\eta = \eta^*$), the multiplier m_2^0 would be invariant, i. e., $(m_2^0)_I = (m_2^0)_{II}$. The schematic of variation of $m_2^0(\overline{V}_\eta)$ with the iteration variable (i) is shown in Fig. 5.3, where $\overline{V}_\eta = V_\eta / V_T$.

Procedure 2: Similar to the procedure 1, the stress sequence of the elements obtained from FEA is sorted in descending order. Next, the variation of multiplier m_2^0 with each subsequent iterations, $m_2^0(i)$, will plotted against the volume ratio, $\overline{V}_\eta$, as illustrated schematically in Fig. 5.4. The subsequent iterations will eventually intersect at a specific location, $\overline{V}_\eta = \overline{V}_{\eta^*}$, showing that the multiplier m_2^0 would be invariant, i. e., $(m_2^0)_I = (m_2^0)_{II}$.

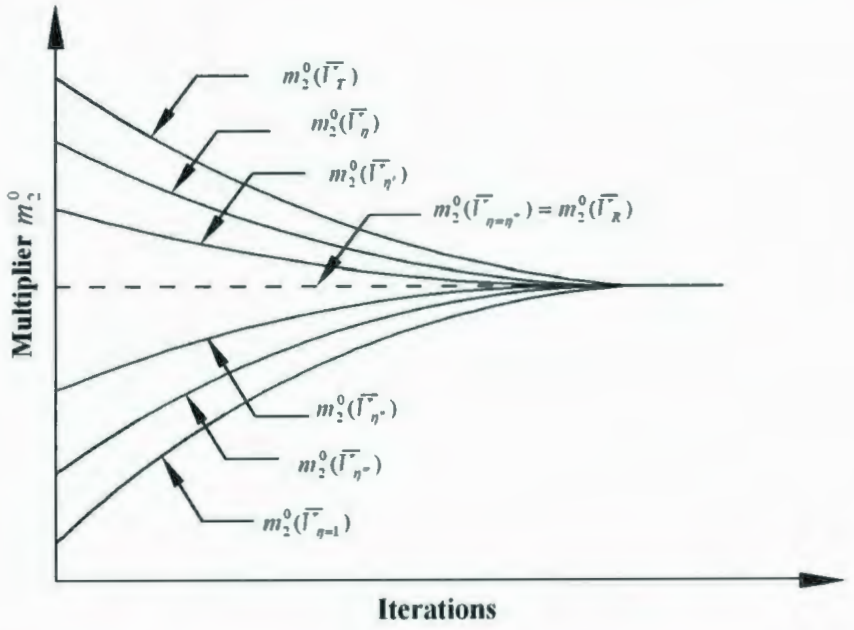

Figure 5.3: Variation of m_2^0 with elastic iterations

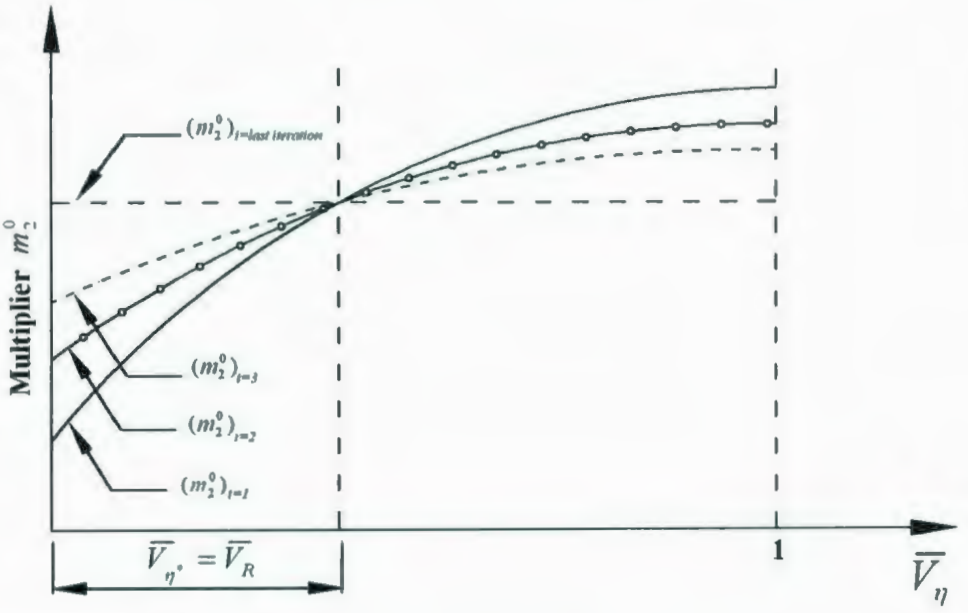

Figure 5.4: Variation of m_2^0 with volume ratio

5.3 NUMERICAL EXAMPLES

5.3.1 Thick-walled cylinder

One of the corollaries discussed by Kachanov (1971) in limit load analysis is that adding material to a component or structure cannot reduce the limit load. This statement is clarified by Kachanov (1971) using a simple example involving a thick walled cylinder and a square prism with a circular hole that are subjected to a uniform internal pressure at the inner bore (see Fig. 5.5).

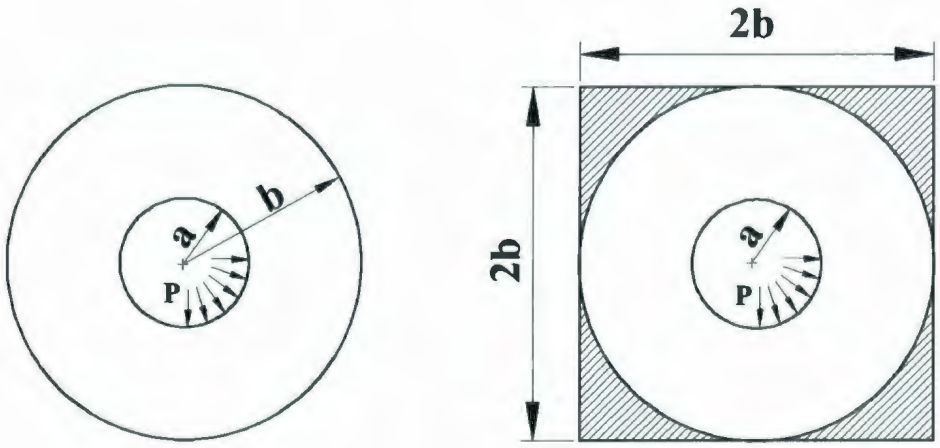

Figure 5.5: Cylinder and square prism with a circular hole

The stresses in the shaded area are assumed to be zero; therefore, these regions do not participate in inelastic action (dead volume). The relationship between the limit load multipliers of the cylinder and square can be written as (Kachanov, 1971):

$$m_{Squre} \geq m_{Circle} \tag{5.5}$$

To demonstrate the concept, consider the square prism shown in Fig. 5.5 with a=60 mm, b=180 mm that is subjected to an internal pressure of P=100 MPa. The material properties are: elastic modulus E= 200 GPa, yield strength σ_y=250 MPa and Poisson's ratio of ν =0.3. Due to symmetry of geometry and loading only a quarter of the square is modeled using 8-noded isoparametric quadrilateral elements. The contour of the plastic region using inelastic FEA is shown in Fig. 5.6. It can be seen from Fig. 5.6, that the reference volume is almost equal to the volume of the cylinder, for the same internal radius and external radius of b=180 mm. Therefore, the reference volume for this particular problem is

$$\overline{V}_R = \frac{\pi(b^2 - a^2)}{4b^2 - \pi a^2} = 0.764 \tag{5.6}$$

The limit load multiplier is given by:

$$m = \frac{2}{\sqrt{3}} \cdot \frac{\sigma_y}{P} \ln(b/a) = 3.171 \tag{5.7}$$

Using the Reference Volume Approach, it is possible to find the active volume, and the related multipliers, as described before in procedure 1 and procedure 2. Fig. 5.7

represents procedure 1, in which variation of m_2^0 respect to $\overline{V}_\eta$ for different iterations is plotted. It can be seen from the figure that almost all the curves (except the first linear elastic solution) intersect at a point ($\overline{V}_\eta$=0.725), which represents the reference volume. The variation of $m_2^0(\overline{V}_\eta)$ with elastic iterations is presented in Fig. 5.8. It can be seen from the figure, that at $\overline{V}_\eta$=0.725, the value of m_2^0 is almost constant during successive iterations and is a good estimate of the limit load.

Comparing the results, all three methods (analytical, inelastic FEA and Reference Volume Approach) give almost the same values for the limit load and reference volume. Also, in the same manner the other corollaries were discussed by Kachanov (1971), e. g., "removal of material cannot increase the limit load", can be verified by the proposed method.

Figure 5.6: Plasticity distribution at limit load sate for square prism with a hole (a quarter model)

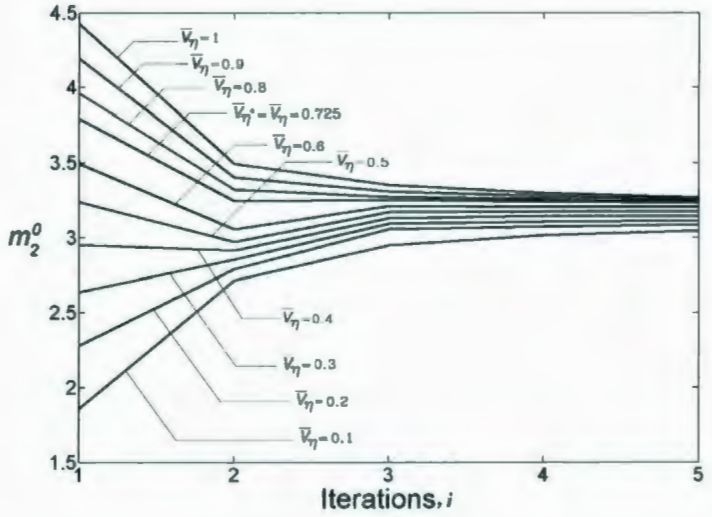

Figure 5.7: Variation of m_2^0 versus $\overline{V}_\eta$ for thick-walled cylinder, Reference Volume Approach (Procedure 1)

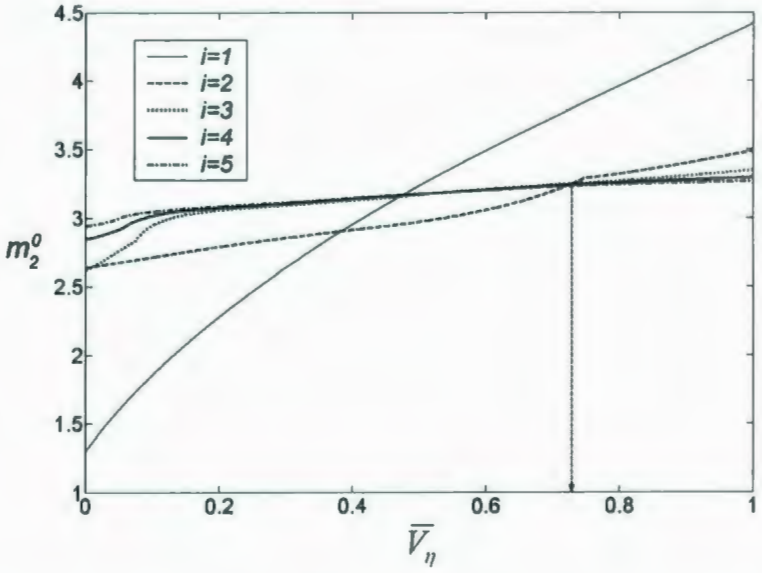

Figure 5.8: Variation of m_2^0 with elastic iterations for thick-walled cylinder, Reference Volume Approach (Procedure 2)

5.3.2 Indeterminate Beam

Using the Reference Volume Approach, it is possible to find the active volume, and the related multipliers, as described before in procedures 1 and 2. An indeterminate beam subjected to distributed uniform load is modeled. Using Reference Volume Approach procedure 1, the variation of $m_2^0(\eta)$ with elastic iterations is presented in Fig. 5.9. As can be seen from the figure, at $\overline{V}_\eta$ =0.281 the value of m_2^0 is almost constant during the successive iterations leading to a good estimate of the exact solution. Using Reference Volume Approach procedure 2, the variation of m_2^0 with respect to $\overline{V}_\eta$ for different iterations is plotted in Fig. 5.10. The volume ratio of $\overline{V}_\eta$ =0.281 represents the active volume of the component, and the corresponding limit load multiplier, m_2^0, which is a good approximation of the limit load multiplier can be obtained.

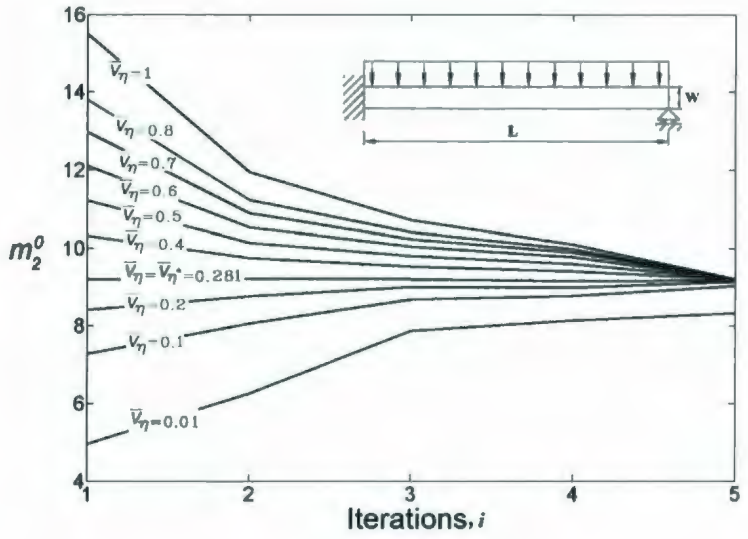

Figure 5.9: Variation of m_2^0 with elastic iterations for indeterminate beam, Reference Volume Approach (Procedure 1)

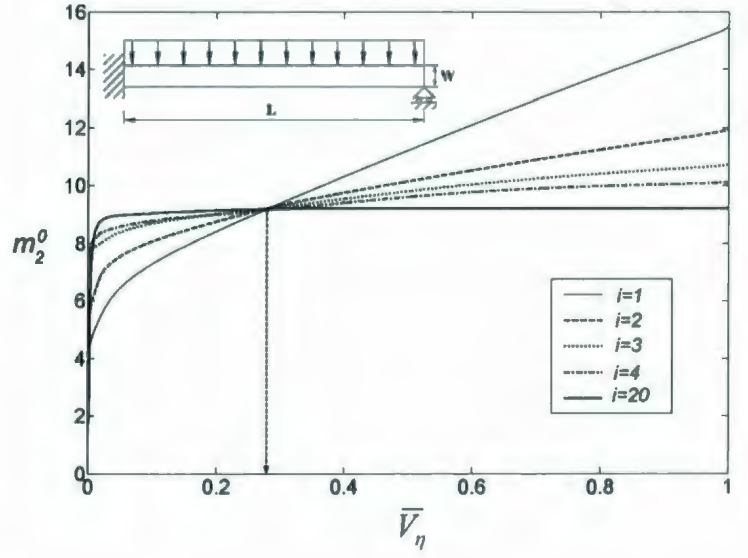

Figure 5.10: Variation of m_2^0 versus $\overline{V}_\eta$ for indeterminate beam, Reference Volume Approach (Procedure2)

5.3.3 Compact Tension (CT) Specimen

The variation of $m_2^0(\eta)$ with elastic iterations is presented in Fig. 5.11. It can be seen from the figure, that at $\overline{V}_\eta$=0.12, the value of m_2^0 is almost constant during successive iterations and is a good estimate of the limit load. Figure 5.12 represents procedure 2, in which variation of m_2^0 respect to $\overline{V}_\eta$ for different iterations is plotted. It can be seen from the figure that all the curves intersect at a point ($\overline{V}_\eta$=0.12) which represents the reference volume.

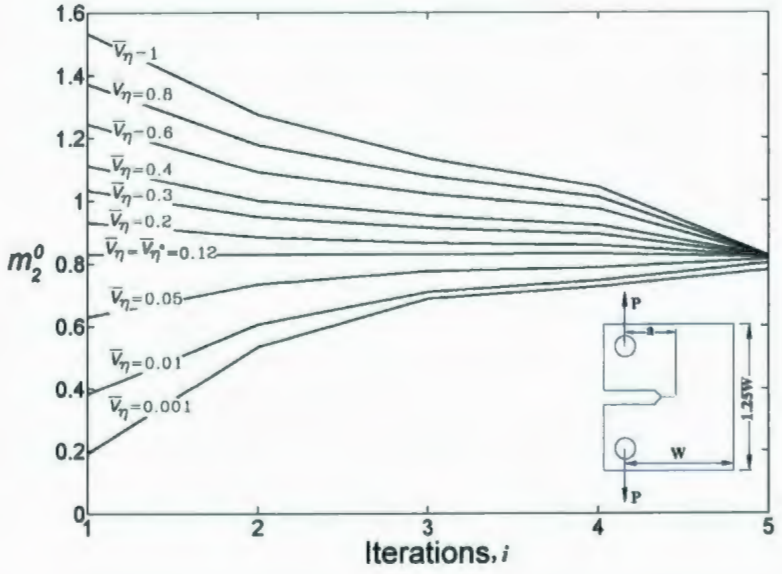

Figure 5.11: Variation of m_2^0 with elastic iterations for compact tension (CT) specimen, Reference Volume Approach (Procedure 1)

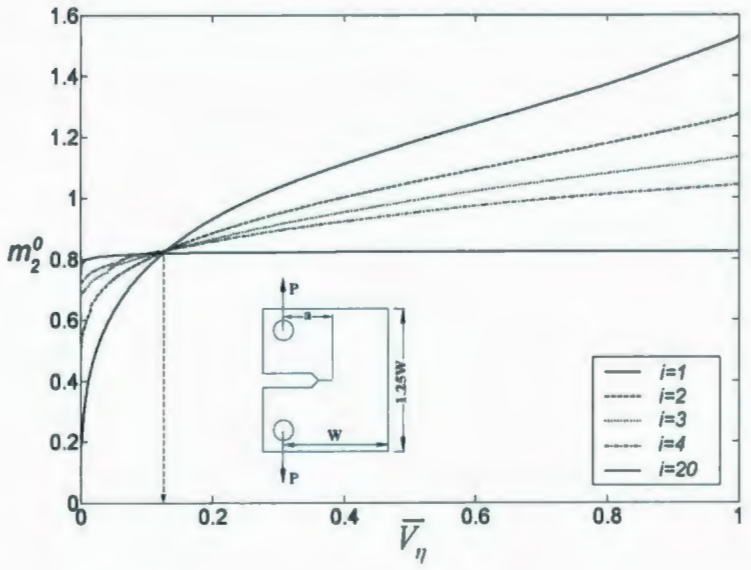

Figure 5.12: Variation of m_2^0 versus $\overline{V}_\eta$ for compact tension (CT) specimen, Reference Volume Approach (Procedure 2)

5.3.4 Plate with Multiple Cracks

A plate with multiple cracks is modeled next. The variation of $m_2^0(\eta)$ with elastic iterations is presented in Fig. 5.13 procedure 1). As can be seen from the figure, at $\overline{V}_\eta$=0.06 the value of m_2^0 is almost constant during the successive iterations leading to a good estimate of the limit load. Using procedure 2, the variation of m_2^0 with respect to $\overline{V}_\eta$ for different iterations is plotted in Fig. 5.14. All curves intersect at $\overline{V}_\eta$=0.06 which represents the active volume of the component. Again, by calculating the upper bound multiplier, m_2^0, a good approximation of the limit load multiplier can be obtained.

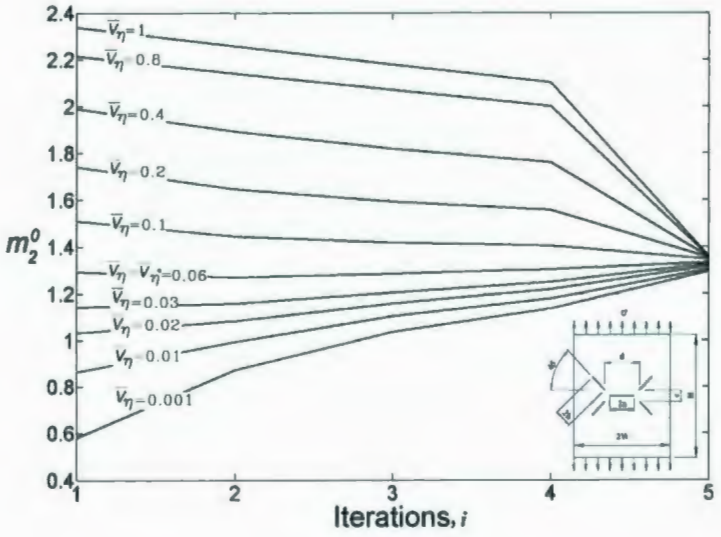

Figure 5.13: Variation of m_2^0 with elastic iterations for plate with multiple cracks, Reference Volume Approach (Procedure 1)

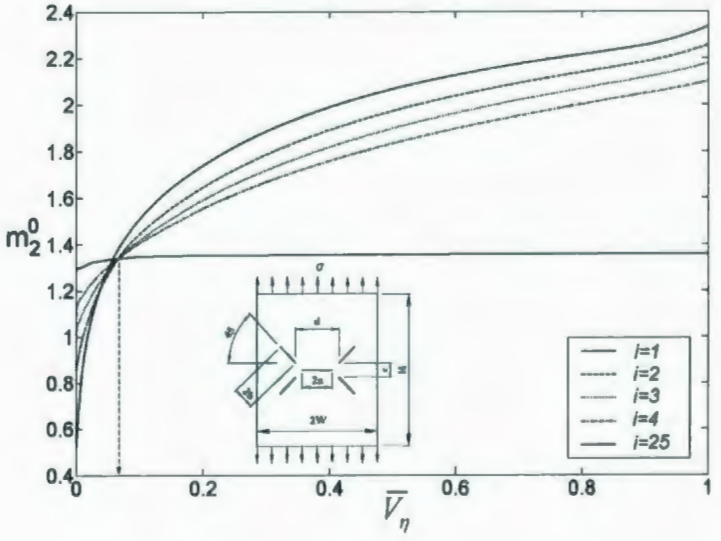

Figure 5.14: Variation of m_2^0 versus $\overline{V}_\eta$ for plate with multiple cracks, Reference Volume Approach (Procedure 2)

5.3.5 Axial Semi-elliptical (Inner) Surface Cracks (3D)

A cylinder with two inner axial semi-elliptical surface cracks located in the same plane subjected to an internal pressure of 150 MPa is considered here. The variation of $m_2^0(\eta)$ with elastic iterations is presented in Fig. 5.15 by applying the procedure 1. As can be seen from the figure, at $\overline{V}_\eta$ =0.93 the value of m_2^0 is almost constant during the successive iterations leading to a good estimate of the limit load. Using the procedure 2, the variation of m_2^0 with respect to $\overline{V}_\eta$ for different iterations number is plotted in Fig. 5.16. All curves (except the first linear elastic solution) intersect at a specific point ($\overline{V}_\eta$=0.93), representative of the active volume of the component. Again, by calculating the upper bound multiplier, m_2^0, a good approximation of the limit load multiplier is obtained. The intersection point for different numbers of iterations is crisp for iterations beyond the first.

Table 5.1 is a comparison of relative computational times for various component analyses (all the times are in seconds). It can be seen that the direct EMAP and Reference Volume Methods represent savings in time. The main advantage of the direct EMAP and the Reference Volume Method is that they are independent verification methods.

Table 5.1: Comparison of Computational Time (Seconds)

Component	Direct EMAP (s)	Reference Volume Method (s)	Inelastic FEA* (s)
Compact Tension Specimen (2D)	10 iterations: 45	24	44
Multiple Cracks (2D)	10 iterations: 47	23	65
Axial Semi-Elliptical Surface Cracks (3D)	10 iterations: 8375	4186	51453

* Using automatic time stepping

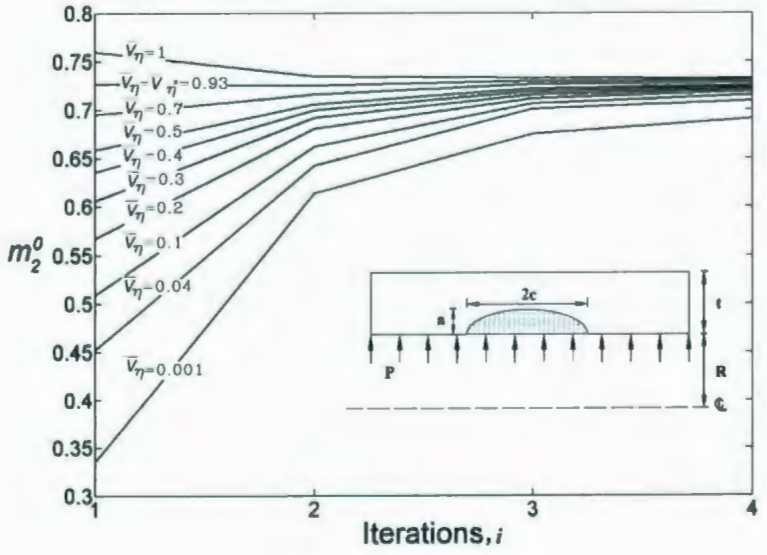

Figure 5.15: Variation of m_2^0 with elastic iterations for two axial semi elliptical surface cracks, Reference Volume Approach (Procedure 1)

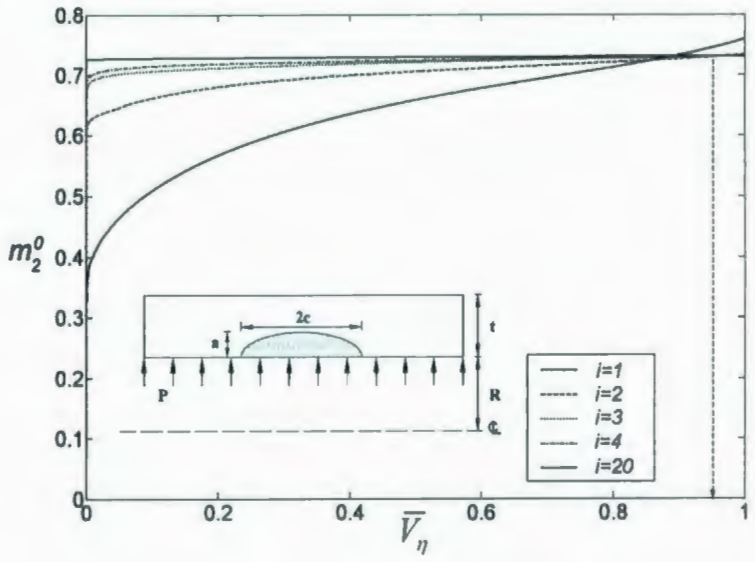

Figure 5.16: Variation of m_2^0 versus $\overline{V}_\eta$ for two axial semi elliptical surface cracks, Reference Volume Approach (Procedure 2)

5.4 OPTIMUM LIMIT LOAD DESIGN

The ideal condition in the limit state is when the full plastification occurs in a given component (Zyczkowski, 1981), which may be unachievable in reality. Therefore, the first step in optimal design is to distinguish the reference volumes and dead volumes in the component or structure. By removing the dead volumes or specifying the material of the higher strength in reference volume regions, an optimal solution may be achieved.

Many investigations have been carried out in optimal design in plasticity that utilize the cost of material, cost of machining and plastic forming (Szczepinski and

Szlagowski, 1990). Drucker and Shield (1957) proposed a criterion based on the classical upper bound limit load theory to identify a minimum volume of a body made of homogeneous material that is able to carry the prescribed load. The optimal criterion suggested by Drucker and Shield (1957) has been applied by different researchers on different components or structures such as beams, frames, plates, shells and disks (more details are given in Save and Prager, 1985). However, Szczepinski and Szlagowski (1990) concluded that for a complex geometries finding the optimal solution that meets exactly the criteria suggested by Drucker and Shield (1957) is very difficult or sometimes impossible. Therefore, attempts have been made to find the optimal design based on other methods for instance mathematical programming (Foulkes, 1955; Cyras, 1983; Zavelani, 1973), boundary perturbation method (Bochenek *et al.*, 1983 and 1994; Egner, 2000) and inelastic finite element analysis (Dems and Mróz, 1978; Capsoni and Corradi, 1997). Applying the mathematical programming or boundary perturbation methods for complex geometry and boundary conditions is very difficult from a mathematical standpoint view. Inelastic finite element analysis is broadly used for limit design; however, it can often be complicated, time consuming and expensive. As a result, the development of reasonably accurate and independent robust methods based on linear elastic solutions can be useful from a design point of view.

In this section, a study of optimum design of several practical configurations using the Reference Volume Approach and inelastic FEA is carried out. The limit loads and reference volumes are predicted by various methods for elastic-perfectly plastic materials obeying von-Mises criterion.

Projections on plates, bars and tubes are often used as a means of transmitting axial load between two components, e.g. T-shapes at bars, bolted joints, shouldered plates/shafts/ tubes , connecting collars , lifting lugs, turbine blade roots and many other geometric shapes with similar features. For remote loading conditions, the collapse mechanism is usually due to net section collapse at the weaker bar/plate/tube. However, when the load or the reaction of the loading is applied at the shoulders or such "loaded projections", the mechanism of failure may vary from shear failure in the head to net section collapse at the shank for different combinations of geometries configurations. Therefore, optimum design of such components at limit load state has been an attractive method for many researchers.

Consider an axisymmetric element subjected to a tensile force acting downwards (Fig. 5.17), where the maximum value of the tensile load causes stresses equal to the yield strength of the component in the bar. The geometry of the component is described by the shank length, L, the shank diameter, $2a$, the head radius, b, and angle of inclination of the shoulder surface, θ.

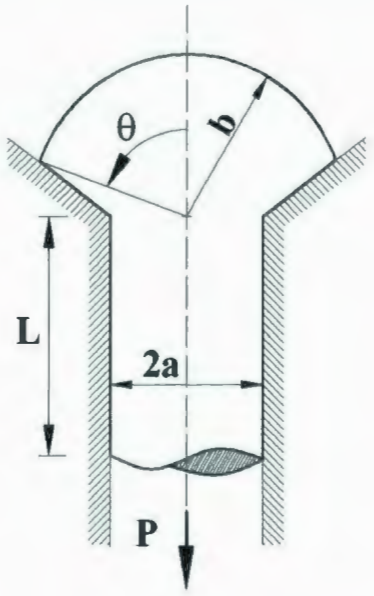

Figure 5.17: Axisymmetric shank and head component

The purpose of this example is to study the behavior of the component for different values of the external head radius, b, at the limit load state. The component is modeled with the shank bar radius of $2a$=160 mm, length of L=400 mm and $\theta=\pi/2$ with the material properties of E=70.3 GPa, σ_y=89.6 MPa and ν =0.3. Due to the symmetry in geometry and loading, only half of the component is modeled. The limit load multipliers based on classical lower bound and upper bound are given by Szczepinski (1972), i. e.,

$$\text{Lower bound multiplier}: m_L = \frac{2\sigma_y}{P}\ln(b/a) \tag{5.8}$$

$$\text{Upper bound multiplier}: m_U = \frac{2\sigma_y}{\sqrt{3}\,aP}\sqrt{b^2 - a^2} \tag{5.9}$$

Applying the Reference Volume Approach and inelastic FEA, the variation of the limit load multiplier with normalized reference volume for different *b/a* ratios are presented in Figs. 5.18 and 5.19, respectively. Referring to these two figures, when $b/a<1.423$ the limit load and reference volume increases due to increase in the magnitude of *b/a*. In contrast, for $b/a>1.423$ the limit load becomes constant (net section collapse in the bar) and the reference volume decreases for an increasing of *b/a*. At point $b/a=1.423$, the collapse mechanism changes from collapse due to the head shear to net section collapse in the bar. This point can be considered as the optimum design condition where the reference volume reaches to its maximum value, and the safety factor has its highest magnitude. To better understand these two collapse mechanisms, the plastic distributions at limit load state for different range of *b/a* using inelastic FEA are presented in Fig. 5.20. The value of the optimum values of *b/a* and corresponding limit load multipliers estimated from inelastic FEA and analytical procedurea are reported by Szczepinski and Szlagowski (1990) (in which the limit load solution based on upper bound method is derived based on Tresca; however, to enable consistency in all results, the upper bound limit load is obtained based on the von-Mises criterion and by using the procedure proposed by Szczepinski and Szlagowski (1990): see Table 5.2.

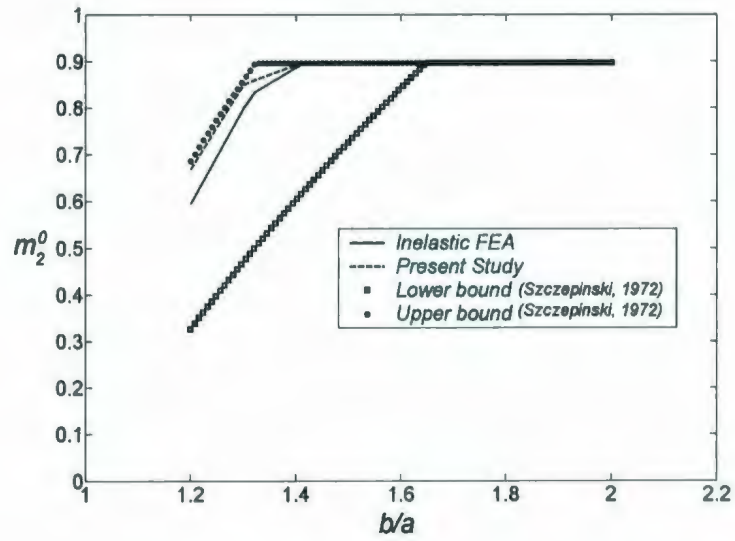

Figure 5.18: Variation of limit load multipliers versus *b/a* ratio, $\theta=\pi/2$

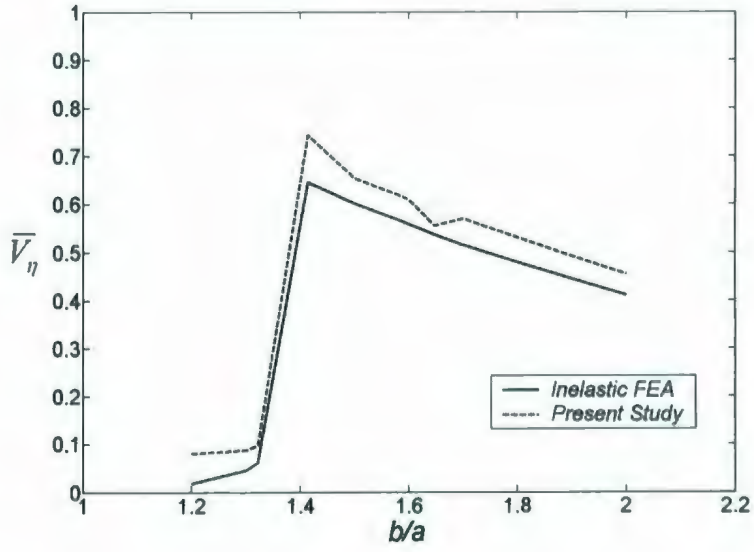

Figure 5.19: Variation of reference volume versus *b/a* ratio, $\theta=\pi/2$

Figure 5.20: Plastic distributions at limit load state for different values of b/a, $\theta=\pi/2$

Table 5.2: Comparison of optimum (b/a), $\theta=\pi/2$

	Inelastic FEA	Szczepinski and Szlagowski, (1990)	Present study
$(b/a)_{opt}$	1.423	lower bound method : $e^{0.5} \approx 1.648$ upper bound method : $\sqrt{7}/2 \approx 1.322$	1.423

As a typical example for b/a=1.6 the variation of limit load multipliers during successive iterations for direct EMAP is plotted in Fig. 5.21. Using the Reference Volume Approach, it is possible to find the active volume, and the related multipliers, as described

before in procedure 1 and procedure 2. The variation of $m_2^0(\eta)$ with elastic iterations is presented in Fig. 5.22. As it can be seen from the figure, at $\overline{V}_\eta$ =0.615 the value of m_2^0 is almost constant during successive iterations, and is a good estimate of the exact solution. Fig. 5.23 represents procedure 2, in which variation of m_2^0 with respect to $\overline{V}_\eta$ for different iterations is plotted. It can be seen from the figure that all the curves intersect at a point $\overline{V}_\eta$ =0.615, which represents the reference volume.

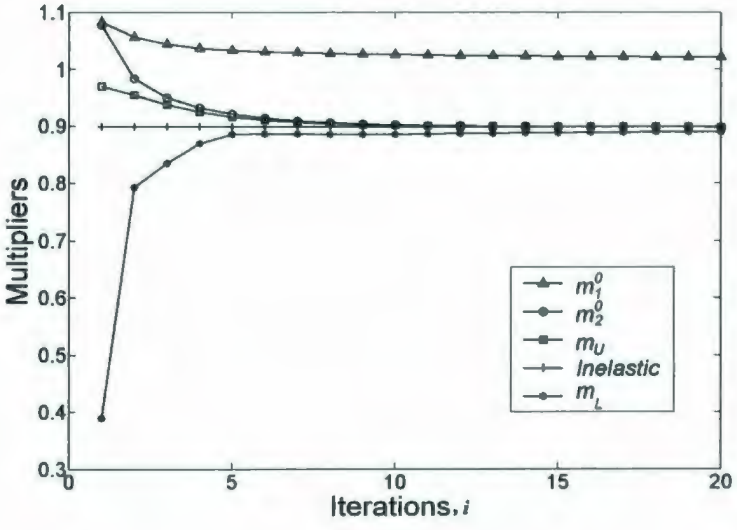

Figure 5.21: Variation of limit load multipliers for b/a=1.6, θ=π/2

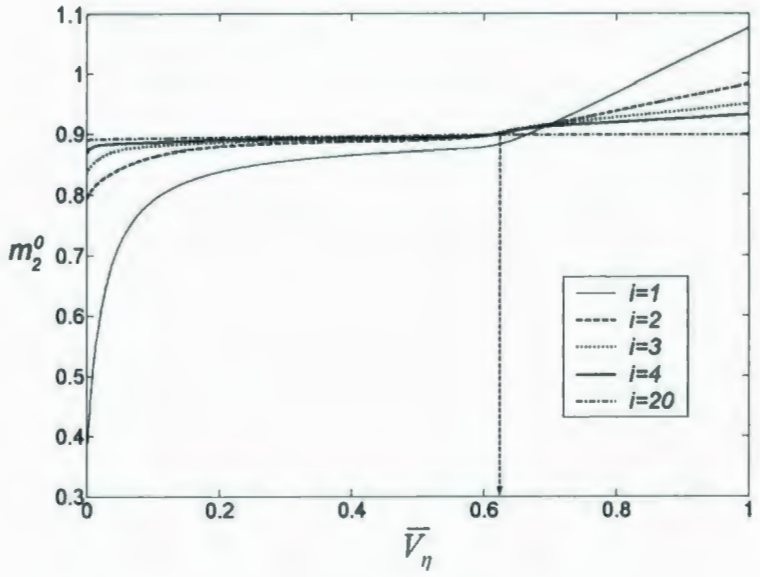

Figure 5.22: Variation of m_2^0 with elastic iterations for b/a=1.6, Reference Volume Approach (Procedure 1)

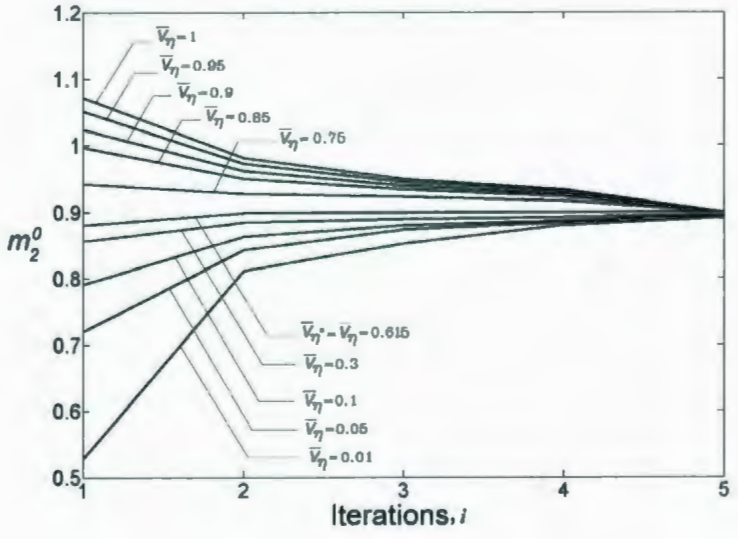

Figure 5.23: Variation of m_2^0 versus $\overline{V}_\eta$ for b/a=1.6, Reference Volume Approach (Procedure 2)

The proposed procedures may also be used for plastic optimum design of conical heads. Figures 5.24 and 5.25 show the variation of the limit load multiplier and reference volume ratio versus *b/a* using Reference Volume Method, and inelastic FEA, for a skew angle of $\theta=\pi/3$.The same material properties have been used as for the semispherical head, Fig. 5.20. The plastic distributions at the limit load state for different values of *b/a* using inelastic FEA are presented in Fig. 5.26.

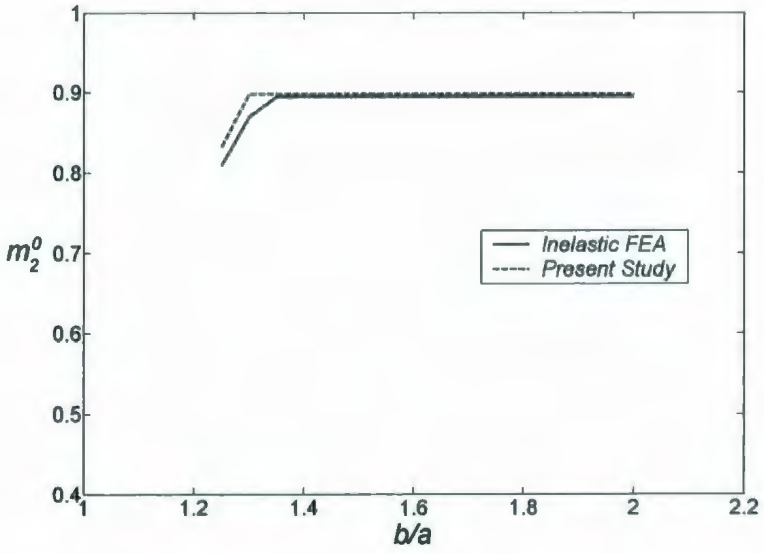

Figure 5.24: Variation of limit load multipliers versus *b/a* ratio, $\theta=\pi/3$

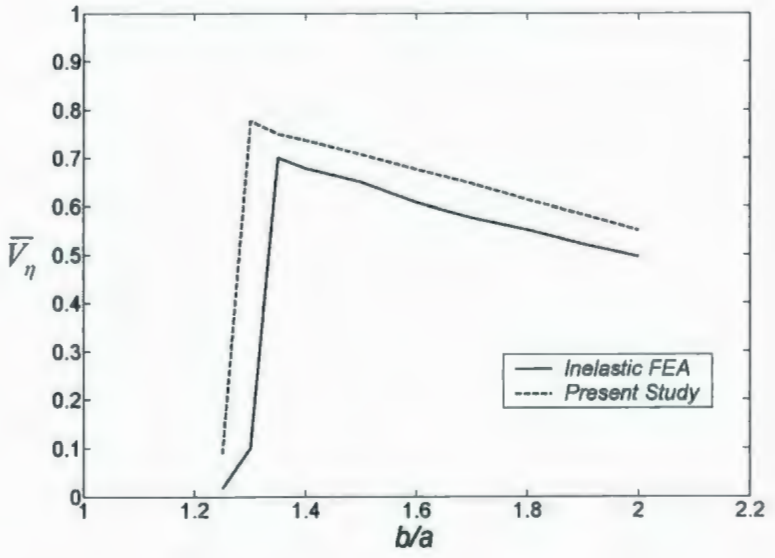

Figure 5.25: Variation of reference volume versus b/a ratio, $\theta=\pi/3$

Figure 5.26: Plastic distributions at limit load state for different values of b/a, $\theta=\pi/3$

5.5 CLOSURE

The Reference Volume Method, which enables the identification of "kinematically active" regions in a component, is a useful method for estimating the improved limit loads. In comparison with the conventional inelastic FEA, good agreement is observed from the results. Moreover, the Reference Volume Approach can be applied to study the optimum design at limit load state.

CHAPTER 6

LOCAL LIMIT LOAD ANALYSIS

6.1 INTRODUCTION

The statically admissible stress distributions obtained from EMAP may not sometimes converge to a limit type of distribution even after several iterations. In this Chapter, a method is proposed based on the determination of the m_β multiplier (Seshadri, and Indermohan, 2004) in conjunction with the choice of an appropriate reference volume, which would enable convergence to the exact limit solution of a given component or structure.

6.2 THEORY

In Chapter 5, reference volume concept was introduced to identify kinematically active and dead zones in the component or structure. Using the kinematically active volume, limit load analysis would be more accurate.

The multiplier m_β, which is calculated from entire stress distribution in a component, is determined by evaluating a reference parameter β_R. However, estimation of β_R sometimes may be difficult, especially, for components or structures experience local plastic collapse, i. e., where cracks or notches exist.

In the Reference Volume Approach, we assume that the plastic collapse occurs over a localized region of the mechanical component or structure. Clearly, m_1^0 and corresponding m'' (m_1'') will be significantly overestimated (Fig. 6.1) if it is based on total volume, V_T. However, m_2'', calculated based on m_2^0, underestimates the exact solution due to inactive region in the component (dead zone).

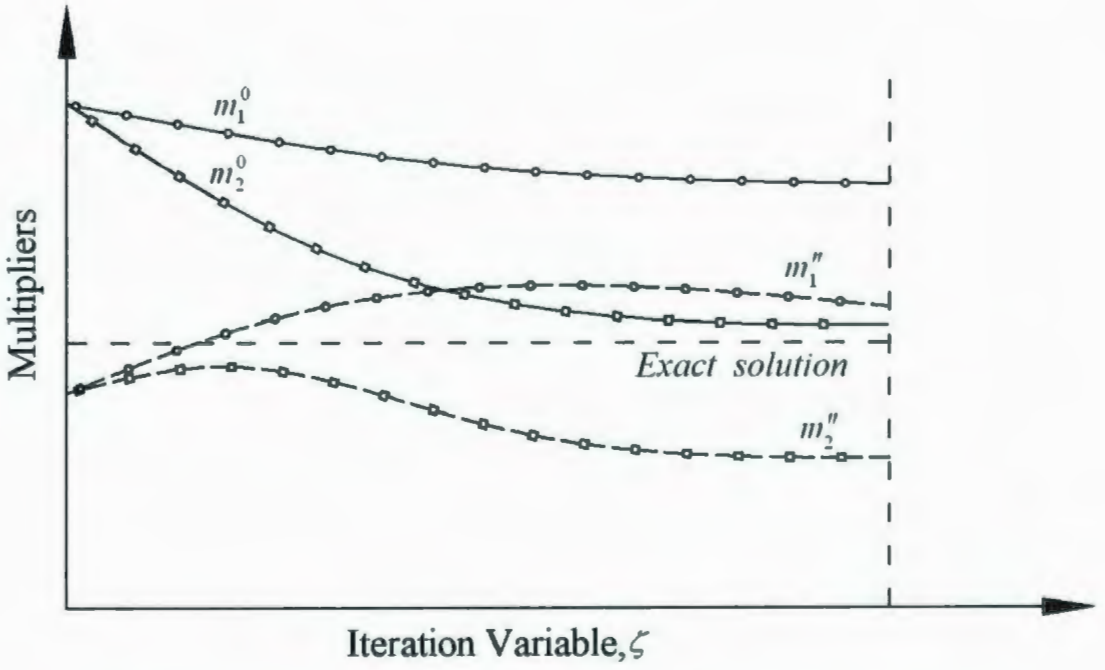

Figure 6.1: Variation of m^0 and m'' multipliers respect to elastic iterations

Therefore, the multiplier m_2^0, Eq. (3.79), can be written in terms of the reference volume and the dead zone volume as follows:

$$m_2^0(V_T) = \sigma_y \frac{\sqrt{\int_{V_R} \frac{\varepsilon_{eq}}{\sigma_{eq}} dV + \int_{V_D} \frac{\varepsilon_{eq}}{\sigma_{eq}} dV}}{\sqrt{\int_{V_R} \sigma_{eq}\varepsilon_{eq}\, dV + \int_{V_D} \sigma_{eq}\varepsilon_{eq}\, dV}} \tag{6.1}$$

If we assume that the dead zone is kinematically inactive then Eq. (6.1) can be simplified as

$$m_2^0(V_R) = \frac{\sigma_y \sqrt{\int_{V_R} \frac{\varepsilon_{eq}}{\sigma_{eq}} dV}}{\sqrt{\int_{V_R} \sigma_{eq}\varepsilon_{eq}\, dV}} \tag{6.2}$$

It is implied here that $m_2^0(V_T) = m_2^0(V_R)$

The magnitude of the upper bound multiplier, m_2^0, would therefore depend on the sub-volume, V_η, where

$$V_\eta = \sum_{k=1}^{\eta} \Delta V_k \tag{6.3}$$

In order to identify the reference volume V_R and multiplier $m''(V_R)$ the following procedure is used:

(1) The stress distribution within a discretized component obtained from a finite element analysis is sorted in descending order, i. e., $\sigma_{eq}^{(1)} > \sigma_{eq}^{(2)} > .... > \sigma_{eq}^{(\eta)} > .... > \sigma_{eq}^{(N)}$. Corresponding to the stresses $\sigma_{eq}^{(1)}$, $\sigma_{eq}^{(2)}$,..., $\sigma_{eq}^{(\eta)}$,...., $\sigma_{eq}^{(N)}$ are the volumes $\Delta V^{(1)}$, $\Delta V^{(2)}$, ..., $\Delta V^{(\eta)}$,...., $\Delta V^{(N)}$, respectively. Here, V_η is the sub-volume that is the volume summations started from the element with the highest equivalent stress to the η^{th} element.

(2) The variation of m_2'' and G_2^0 is plotted against the volume ratio, $\overline{V}_\eta$ (a typical trend is illustrated in Fig. 6.2 and Fig. 6.3, respectively). $\overline{V}_\eta$ is the ratio of normalized sub-volume to the total volume (V_T), and is the volume summation starting from the element with the highest equivalent stress to η^{th} element. Equation (3.79) is expressed in terms of sub-volumes that are suitable for FEA results, i. e.,

$$m_2^0(\overline{V}_\eta) = \sigma_y \left[\frac{\sum_{k=1}^{\eta} \left(\frac{\varepsilon_{eq,k}}{\sigma_{eq,k}} \right) \Delta \overline{V}_k}{\sum_{k=1}^{\eta} \sigma_{eq,k} \ \varepsilon_{eq,k} \Delta \overline{V}_k} \right]^{1/2} \tag{6.4}$$

Subsequently, the multiplier m_2'' introduced in Eq. (3.89), can be expressed in terms of sub-volume and based on m_2^0 as

$$m_2''(\overline{V}_\eta) = \frac{m_2^0(\overline{V}_\eta)}{1 + G_2^0(\overline{V}_\eta)} \tag{6.5}$$

and

$$G_2^0(\overline{V}_\eta) = \frac{1}{2}\sqrt{\sum_{k=1}^{\eta}\left[\left(m_2^0(\overline{V}_\eta)\frac{\sigma_{eq,k}}{\sigma_y}\right)^2 - 1\right]^2 \Delta\overline{V}_k} \tag{6.6}$$

(3) As presented in Fig. 6.2, the curves can be divided into two regions. Region I represents the part of the component which is kinematically active, whereas region II represents part of a component or structure that is kinematically inactive (the dead zone). In region I, the multiplier m_2'' increases until it reaches a maximum value; however, m_2^0 is variable. In region II, m_2'' decreases while m_2^0 is almost constant.

(4) The transition between regions I and II where m_2'' is maximum, (such that $m_2^0(V_R)/m_2^0(V_T) \approx 1$), is identified as the reference volume $\overline{V}_R$.

(5) The exact limit load lies between $m_2^0(V_R)$ and $m_2''(V_R)$; therefore, the estimated m_2'' at the reference volume, $m_2''(V_R)$, would be the highest lower bound value of limit load that guarantees a margin of safety in a component or a structure against plastic collapse.

The parameter β_R can be evaluated by solving the equation

$$m_2''(\overline{V}_R) = \frac{m_2^0(\overline{V}_T)}{1+\beta_R G_2^0(\overline{V}_T)} \tag{6.7}$$

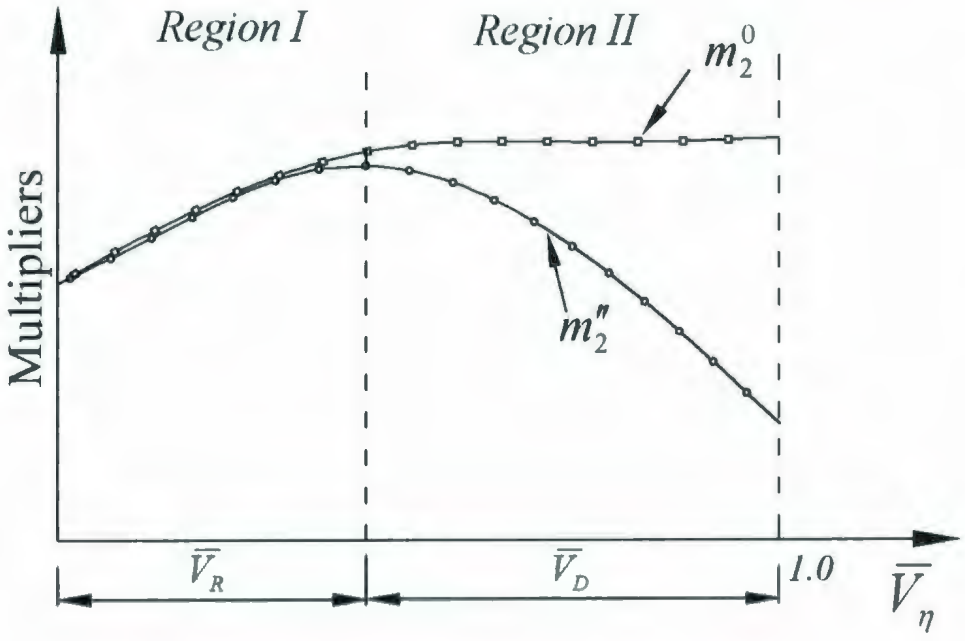

Figure 6.2: Variation of m_2'' and m_2^0 respect to $\overline{V}_\eta$

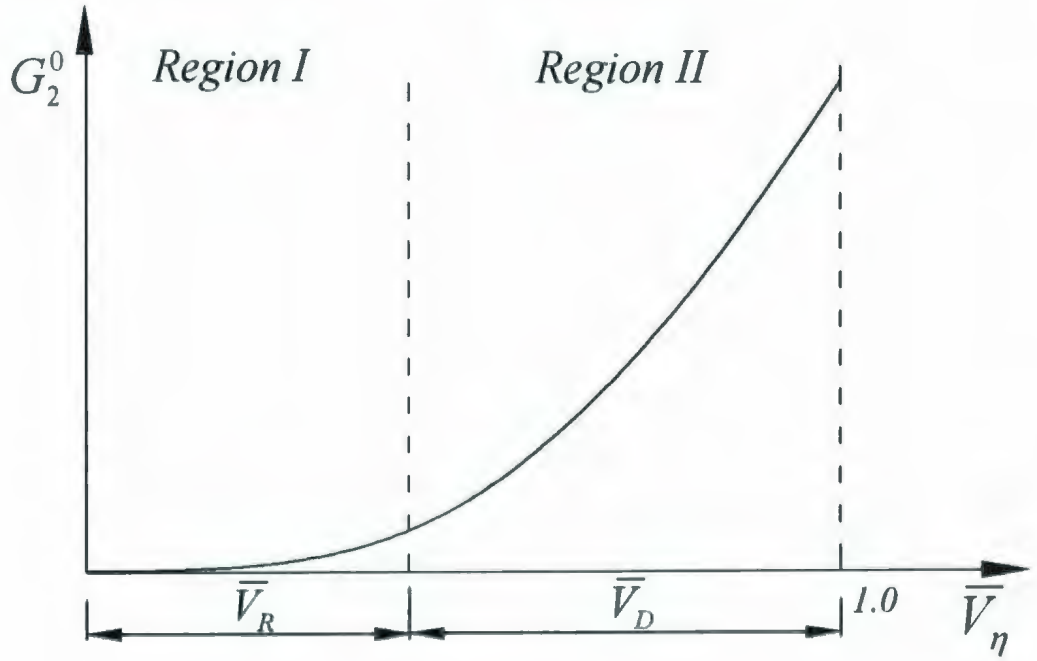

Figure 6.3: Variation of G_2^0 respect to $\overline{V}_\eta$

6.3 NUMERICAL EXAMPLES

In this section, the method for determining m_2^n described in the previous section is applied to several practical geometric configurations. The material is assumed to be elastic-perfectly plastic in all cases. The various problems are modeled using the commercial finite element program ANSYS (university research version). While modeling the cracked components using FEA, it was necessary to use singular elements around the crack-tip to simulate the singularity of the strain field at the crack-tip. The variable q approach discussed in Chapter 4 is used in all the numerical examples in this Chapter.

6.3.1 Thick Walled Cylinder (Plane Strain)

A long thick walled cylinder with an inside radius of R=60 mm, thickness t=120 mm and an internal pressure of 50 MPa is modeled. The modulus of elasticity is specified as 200 GPa, with a Poisson's ratio of ν=*0.3*. The yield strength is assumed to be 300 MPa. The different multipliers converge to the exact solution within five iterations. The variation of limit load multipliers and G_2^0 with $\overline{V}_\eta$ are shown in Figs. 6.4 and 6.5, respectively. It can be seen that the solution converges at the last iteration (5th iteration), i.e., G_2^0 is zero. Therefore, there is no dead zone volume in the component and all the regions participate in plastic action, $\overline{V}_R$=1.

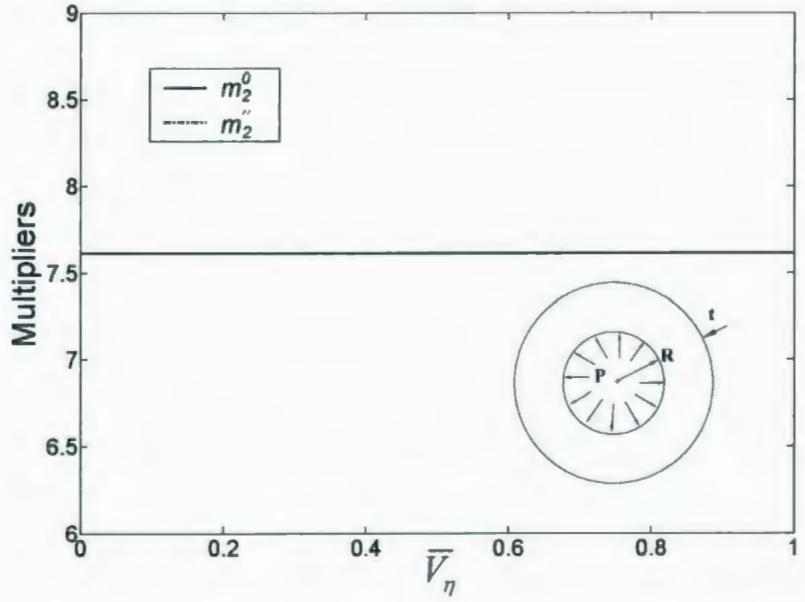

Figure 6.4: Variation of multipliers versus $\overline{V}_\eta$ (Iteration No. 5), Thick walled cylinder

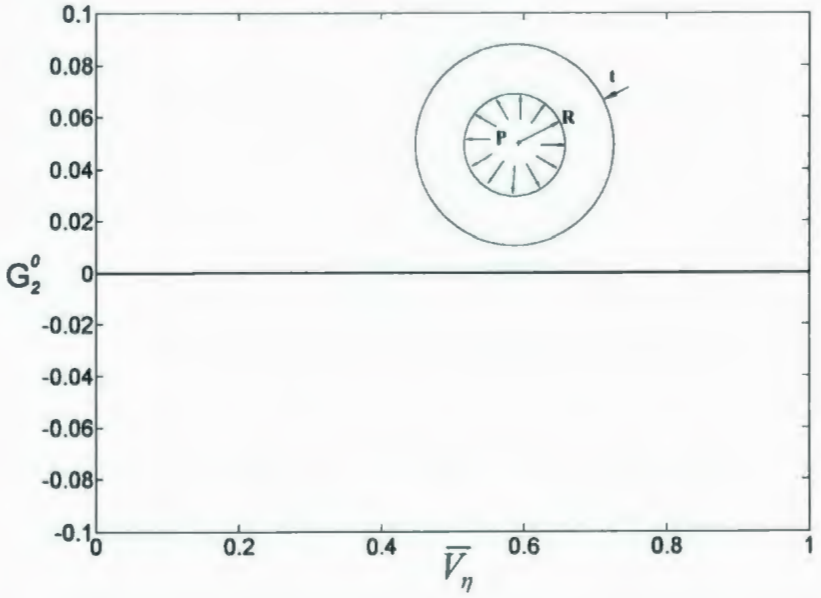

Figure 6.5: Variation of G_2^0 versus $\overline{V}_\eta$ (Iteration No. 5), Thick walled cylinder

6.3.2 Flat Thin Head

A flat thin head (Fig. 6.6) is modeled using an axisymmetric element and is subjected to an internal pressure of P=0.69 MPa with the same material properties as that for the thick cylinder. The overall length L=254 mm, the flat head thickness t_h=25.4 mm, cylinder thickness t_c=101.6 mm, inner radius of R=254 mm and the fillet radius of r_f= 25.4 mm are used. Figure 6.7 shows the variation of limit load multipliers along with inelastic FEA solution. The reference volume is estimated as $\bar{V}_\eta$=0.169 (Figs. 6.7 and 6.8). Therefore, the required value of the lower bound multiplier is estimated as $m_2''(V_R)$=17.450.

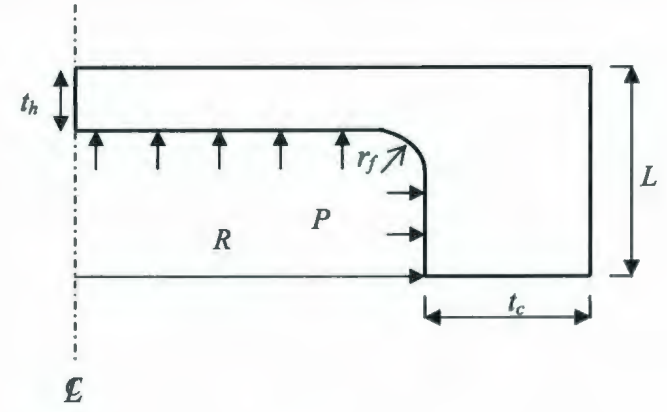

(a)

(b)

Figure 6.6: Flat thin head: (a) Geometry and dimensions,

(b) Finite element mesh

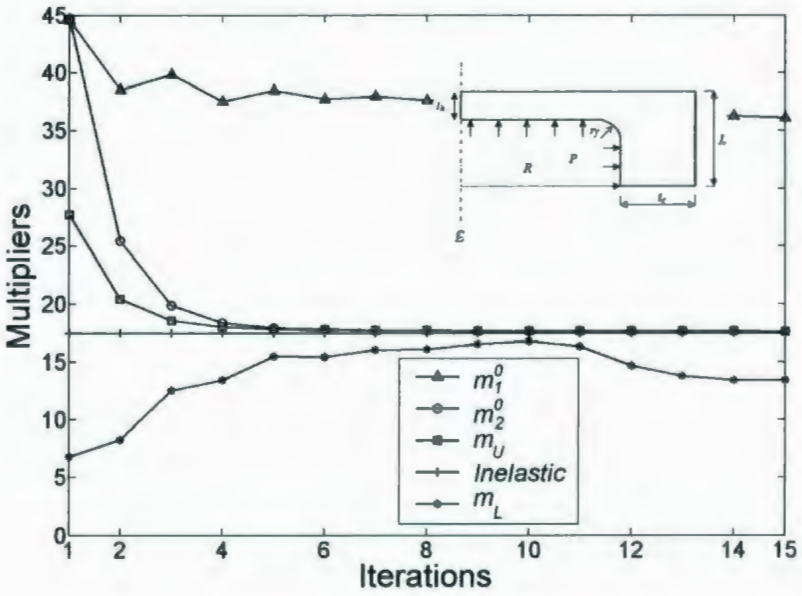

Figure 6.7: Variation of limit load multipliers with iterations, Flat thin head

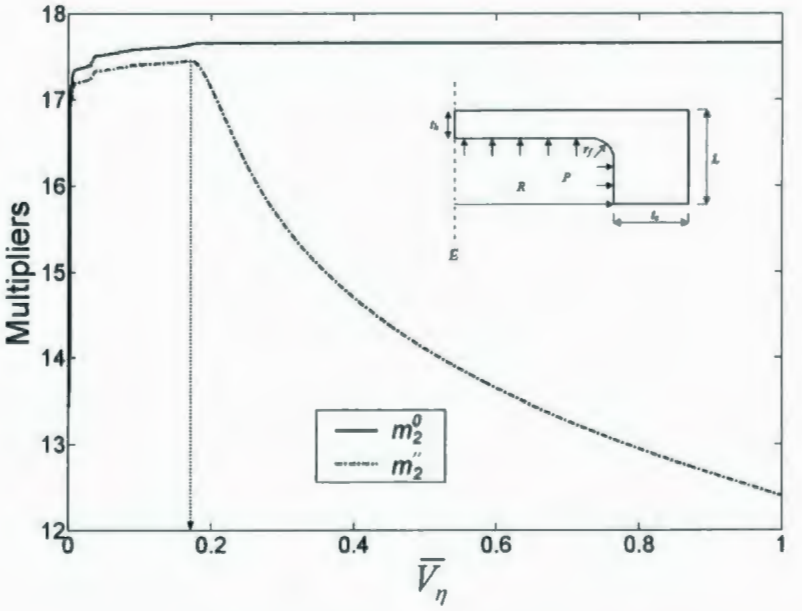

Figure 6.8: Variation of multipliers versus $\overline{V}_\eta$ (Iteration No. 15), Flat thin head

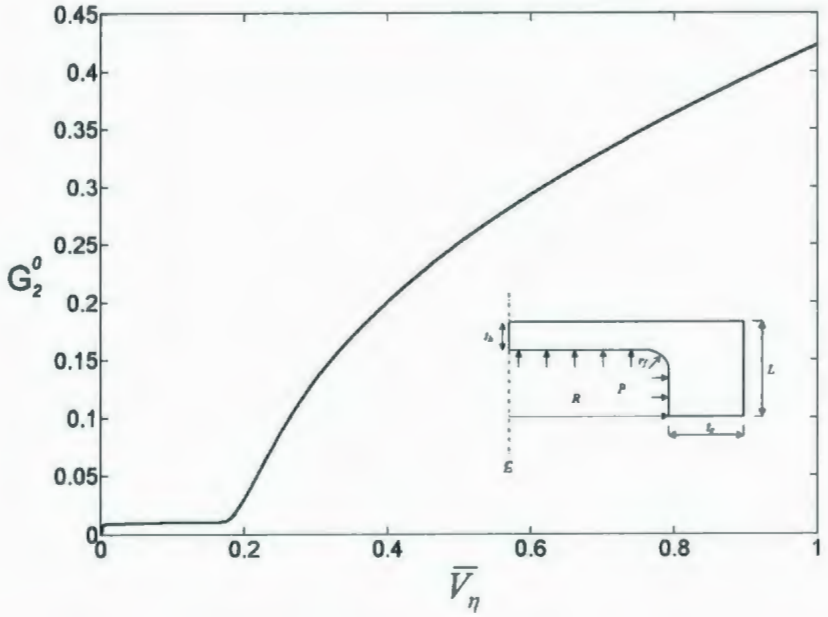

Figure 6.9: Variation of G_2^0 versus $\overline{V}_\eta$ (Iteration No. 15) - Flat Thin Head

6.3.3 Torispherical Head

With reference to Fig. 6.10, a torispherical head of thickness t=25.4 *mm*, average diameter D=7620 mm, normalized spherical cap radius R_s /D=0.8, normalized knuckle radius of R_k /D=0.12 and an internal pressure P=1 MPa is examined here. To avoid discontinuity effects at the boundaries, the length of the cylindrical part (H) is specified as $H = 6\sqrt{Dt/2}$ (this is sufficiently grater, 2.35 times more, than the decay length given in ASME Codes, 1998). The material properties are assumed as E=206.85 GPa; σ_y=206.85 MPa and ν =0.3. The component is modeled axisymmetrically with six elements across the thickness. The limit load multipliers versus iterations are presented in Fig. 6.11. The reference volume is $\overline{V}_R$ =0.28, where m_2'' reaches a maximum value, i. e., $m_2''(V_R)$=0.865 and $m_2^0(V_R)/m_2^0(V_T) \approx 1$ (Fig. 6.12). The variation of G_2^0 respect to $\overline{V}_R$ is shown in Fig. 6.13.

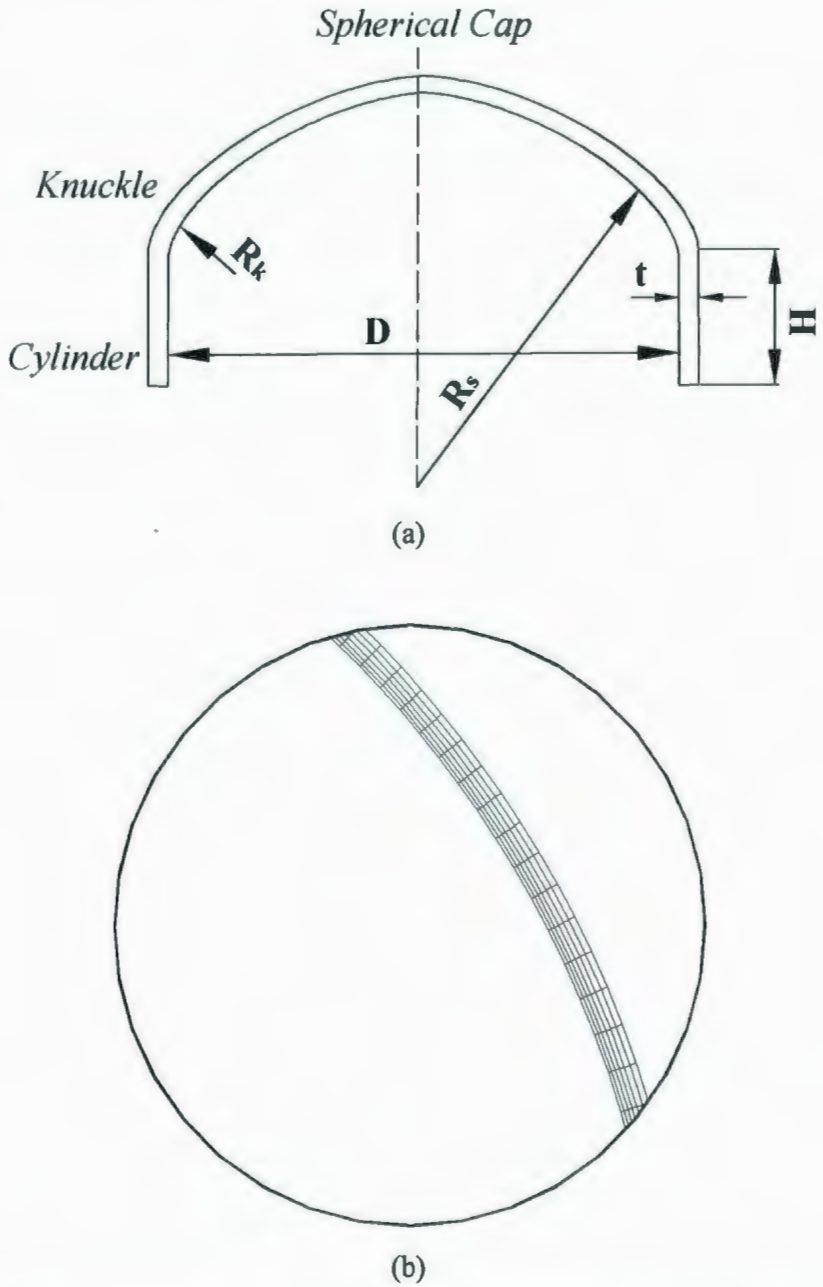

Figure 6.10: Torispherical head: (a) Geometry and dimensions, (b) Finite element mesh at Knuckle region

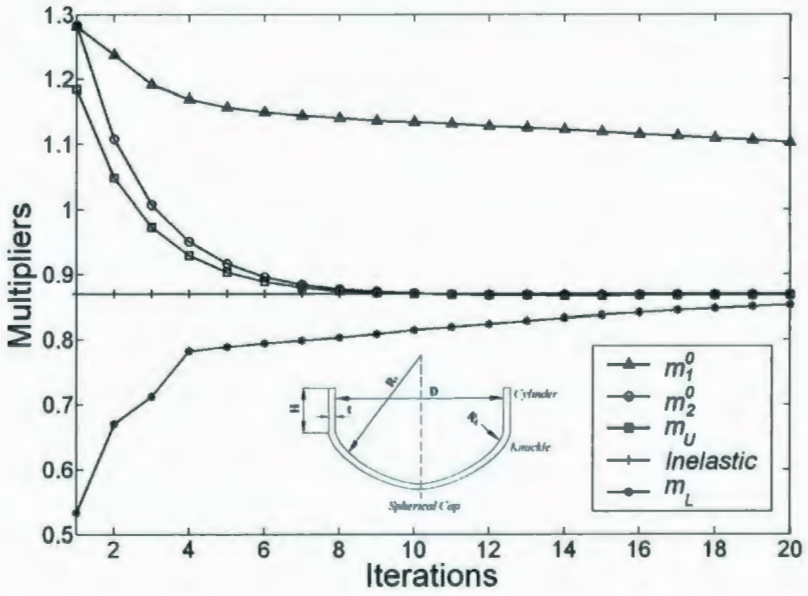

Figure 6.11: Variation of limit load multipliers with iterations, Torispherical head

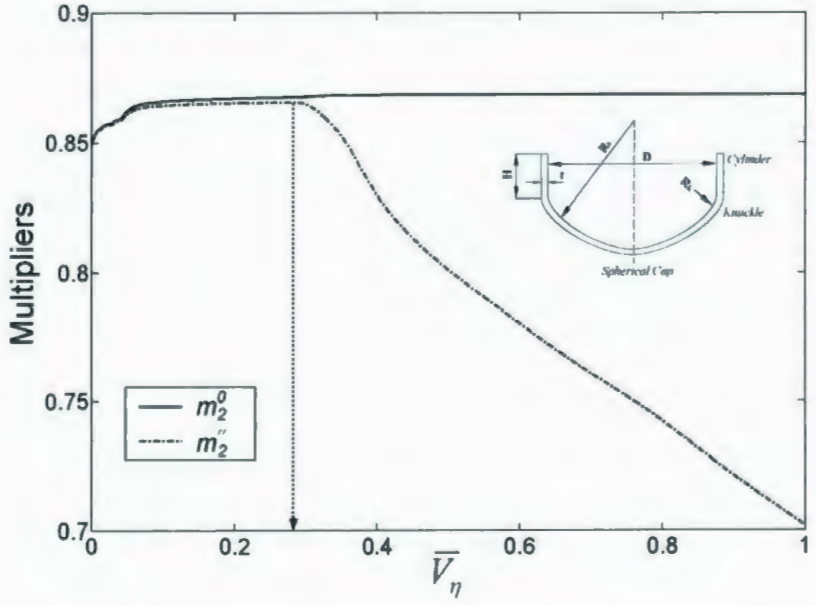

Figure 6.12: Variation of multipliers versus $\overline{V}_\eta$ (Iteration No. 20), Torispherical head

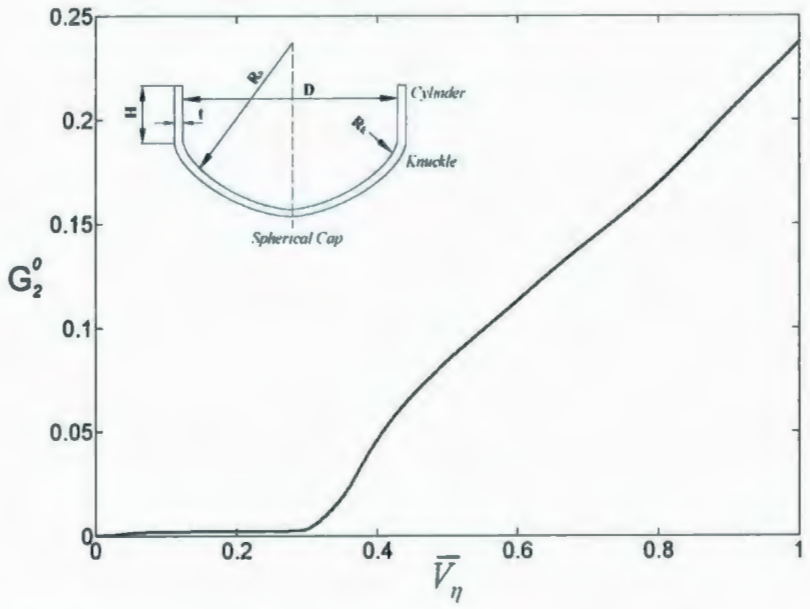

Figure 6.13: Variation of G_2^0 versus $\overline{V}_\eta$ (Iteration No. 20), Torispherical head

6.3.4 Plate with a Hole

A plate with a hole (Fig. 6.14) is modeled in plane stress condition with a uniform tensile stress of 100 MPa. The plate width is $2W$ =150 mm and the notch diameter is $2r$ =46 mm. The modulus of elasticity is 152.95 GPa, and the yield strength is 131.90 MPa. The variation of limit load multipliers respect to iterations is shown in Fig. 6.15. Similarly, the variation of the multipliers and G_2^0 with $\overline{V}_\eta$ at the converged 20th iteration are presented in Fig. 6.16 and Fig. 6.17, respectively. The reference volume is $\overline{V}_R$ =0.170, where m_2'' reaches a maximum value. The corresponding lower bound limit load, which is suggested for design, is $m_2''(V_R)$ =0.917.

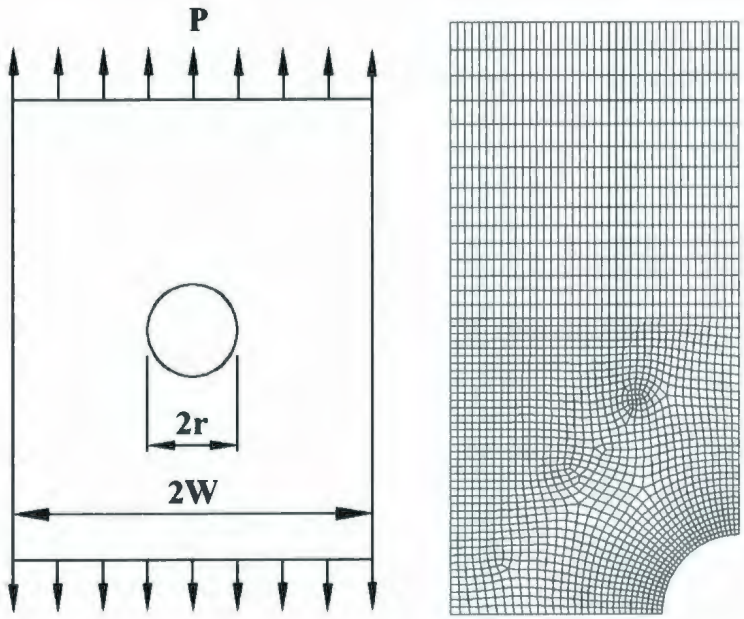

Figure 6.14: Plate with a hole: (a) Geometry and dimensions, (b) Finite element mesh

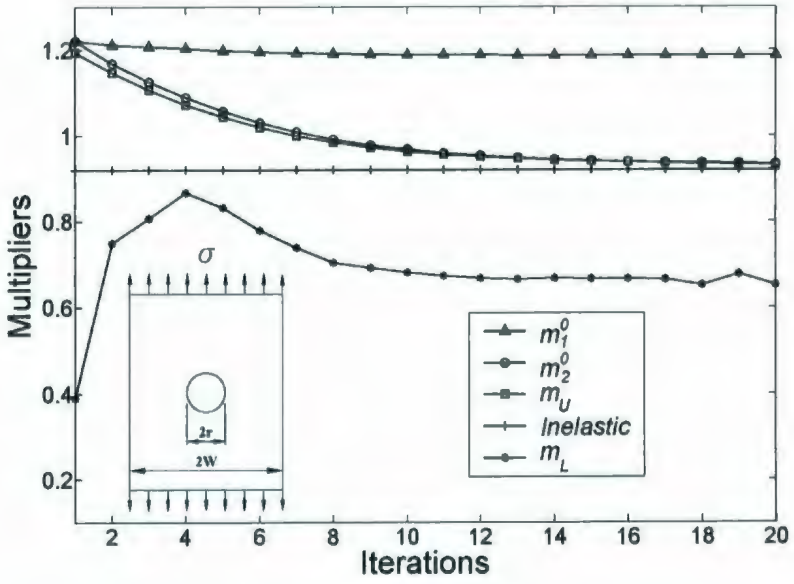

Figure 6.15: Variation of limit load multipliers with iterations, Plate with a hole

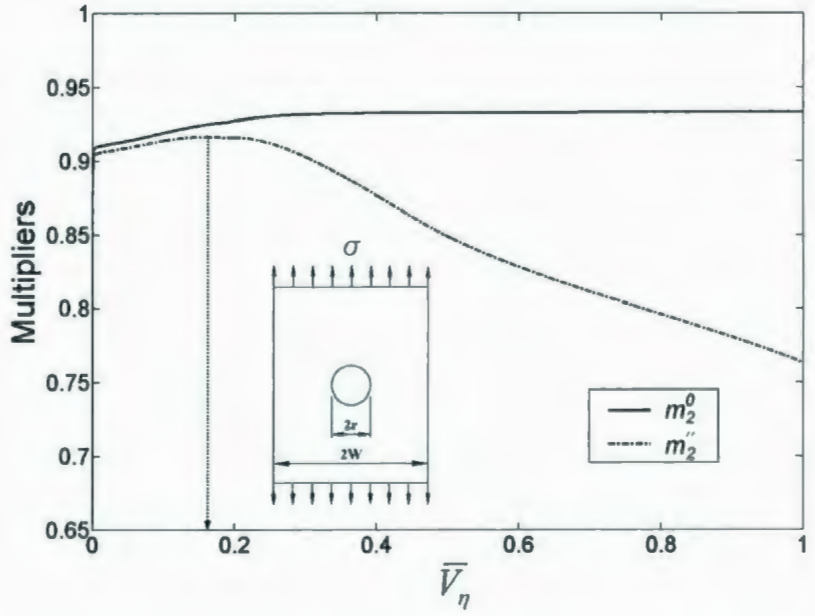

Figure 6.16: Variation of multipliers versus $\overline{V}_\eta$ (Iteration No. 20), Plate with a hole

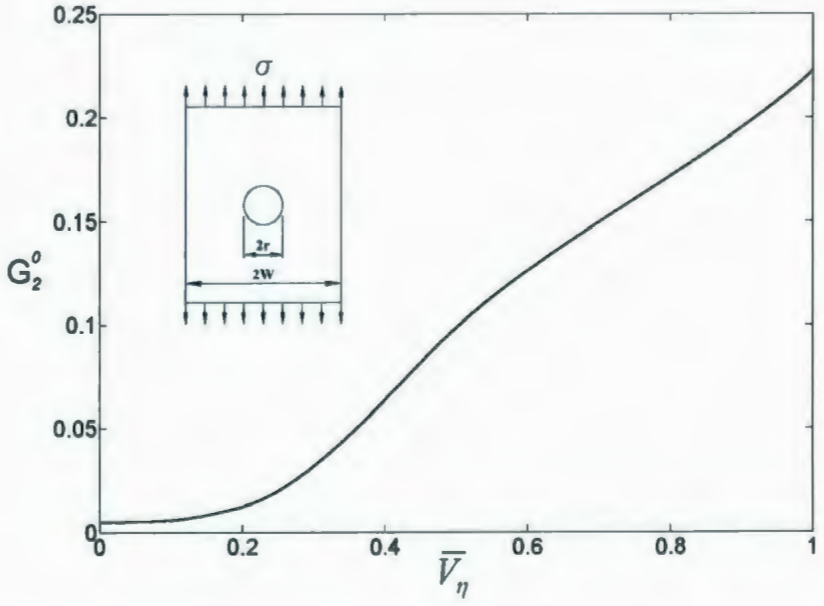

Figure 6.17: Variation of G_2^0 versus $\overline{V}_\eta$ (Iteration No. 20), Plate with a hole

6.3.5 Compact Tension (CT) Specimen

The compact tension specimen that was studied in Chapter 4 is discussed next, with the similar geometry and material properties. The variation of limit load multipliers and G_2^0 with respect to $\overline{V}_\eta$ at the converged 20th iteration are shown in Fig. 6.18 and Fig. 6.19, respectively. The maximum value for m_2'' (where $m_2''(V_R)$=0.818) is the value corresponding to the reference volume location ($\overline{V}_\eta$=0.079).

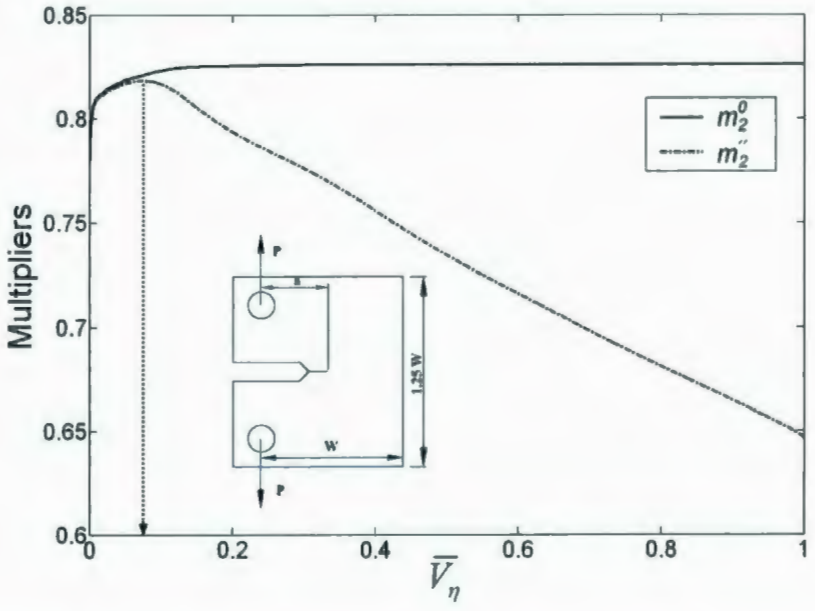

Figure 6.18: Variation of multipliers versus $\overline{V}_\eta$ (Iteration No. 20), Compact tension specimen

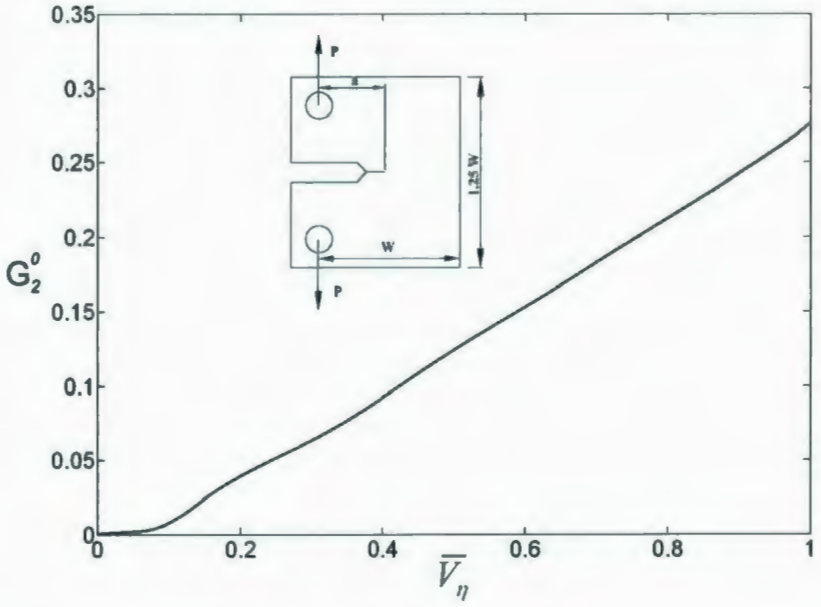

Figure 6.19: Variation of G_2^0 versus $\overline{V}_\eta$ (Iteration No. 20), Compact tension specimen

6.3.6 Plate with multiple cracks

A thin plate with multiple cracks is modeled next using the same geometry and material properties discussed in Chapter 4. The variation of the multipliers and parameter G_2^0 with $\overline{V}_\eta$ at converged 25th iteration are shown in Figs. 6.20 and 6.21, respectively. The maximum value of m_2'' occurs at $\overline{V}_R$=0.058, which is also the transition point between zones I and II (where $m_2''(V_R)$=1.341).

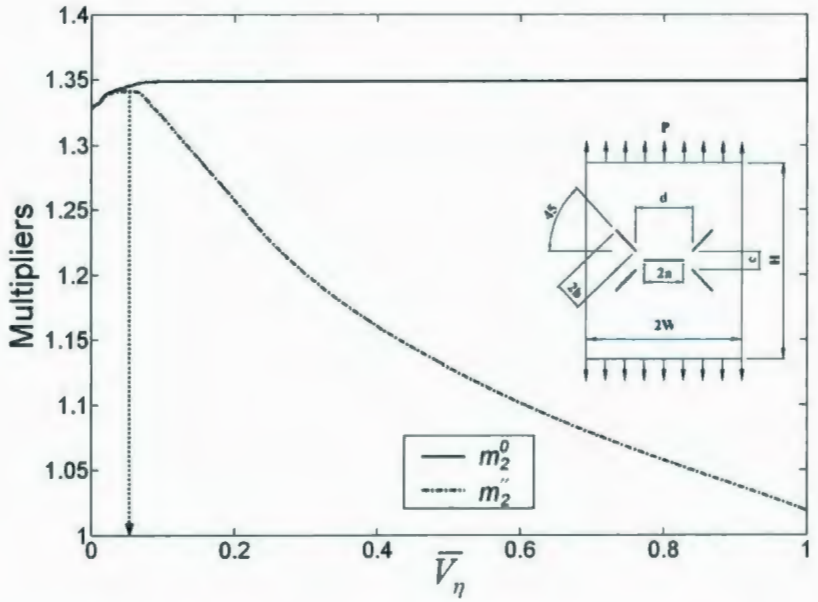

Figure 6.20: Variation of multipliers versus $\overline{V}_\eta$ (Iteration No. 25), Plate with multiple cracks

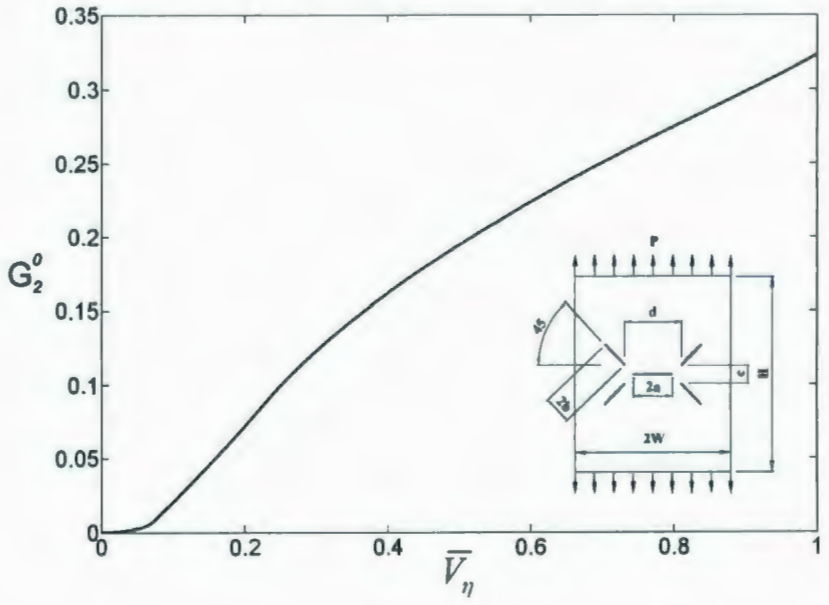

Figure 6.21: Variation of G_2^0 versus $\overline{V}_\eta$ (Iteration No. 25), Plate with multiple cracks

For better understanding of the reference volume concept, the extents of plasticity at limit state for some of the mechanical components are presented in Fig. 6.22. The shaded areas are reference volume regions that directly participate in plastic action.

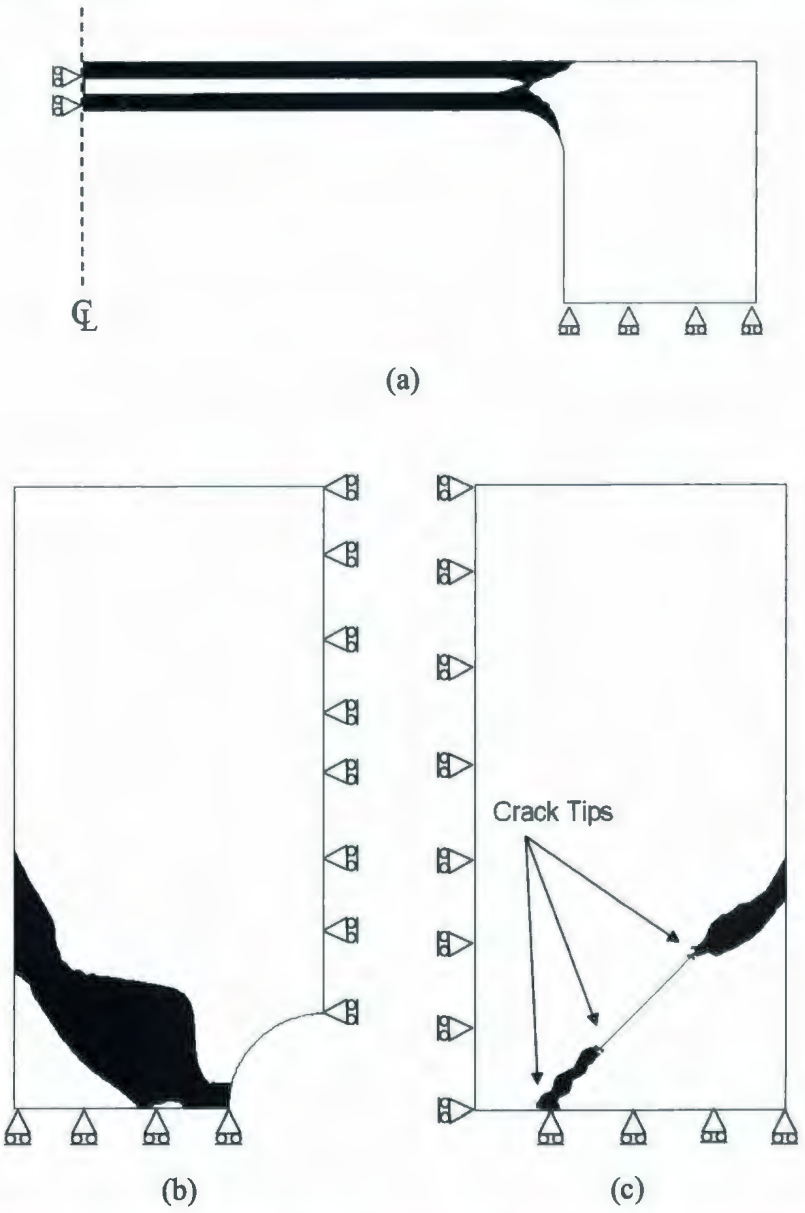

Figure 6.22: Plasticity spread at limit load: (a) Flat thin head, (b) Plate with a hole, (c) Plate with multiple cracks

The multiplier m_β, which is calculated from the entire stress distribution in a component, is determined by evaluating the reference parameter β_R. This can be done by rewriting Eq. (6.8) as

$$\beta_R = \left(\frac{m_2^0(\overline{V}_T)}{m_2''(\overline{V}_R)} - 1 \right) / G_2^0(\overline{V}_T) \tag{6.8}$$

The reference parameter β_R for all components considered in this study are presented in Table 6.1.

Table 6.1: Estimated value of β_R

	$m_2''(V_R)$	$m_2^0(V_T)$	$G_2^0(V_T)$	β_R
Thick cylinder(Iteration No. 5)	7.611	7.611	0.0	N/A
Flat thin head(Iteration No. 15)	17.450	17.653	0.423	0.027
Torispherical head(Iteration No. 20)	0.865	0.868	0.237	0.014
Plate with a hole(Iteration No. 20)	0.917	0.933	0.223	0.078
Compact tension specimen(Iteration No. 20)	0.818	0.826	0.278	0.035
Plate with multiple cracks(Iteration No. 25)	1.341	1.349	0.323	0.018

Table 6.2 is a comparison of different limit load multipliers for the various components analyzed. The estimated limit load multipliers using EMAP are at the last iteration (see Table 6.2) with the exception of the classical lower bound multiplier (m_L) that is estimated using the maximum value among all the iterations. For the flat thin head and plate with a hole, the classical lower bound multiplier (m_L) is estimated at the 10^{th} and 4^{th} iterations, respectively.

Table 6.2: Comparison of different limit load multipliers

	m_{NFEM}	$m_2''(V_R)$	$m_2^0(V_R)$	m_L
Thick cylinder	7.611	7.611	7.611	7.611
Flat thin head	17.501	17.450	17.589	16.735*
Torispherical head	0.867	0.865	0.867	0.848
Plate with a hole	0.928	0.917	0.930	0.867**
Compact tension specimen	0.821	0.818	0.822	0.781
Plate with multiple cracks	1.343	1.341	1.345	1.328

* The maximum value of m_L is at the 10^{th} iteration.

** The maximum value of m_L is at the 4^{th} iteration.

Table 6.3 is a comparison of relative computational times for various component analyses (all times are in seconds). In this Table the computational times using EMAP are given at the converged iteration, iteration at which the limit load multipliers become invariant for succeeding iterations. It can be seen that the present method represents savings in time for most cases. The main advantage of the present study is that it represents an independent verification method.

Table 6.3: Comparison of Computational Time (Seconds)

	Converged iteration (s)	**Inelastic FEA* (s)**
Thick cylinder	5 iterations: 46	92
Flat thin head	10 iterations: 83	78
Torispherical head	11 iterations: 30	86
Plate with a hole	18 iterations: 310	291
Compact tension specimen	17 iterations: 80	97
Plate with multiple cracks	16 iterations: 62	68

* Using automatic time stepping

6.4 CLOSURE

Local lower bound limit loads are determined for some practical components (including cracks and notches) by making use of the reference volume concept. For applications involving dead zones, the multiplier m_2^0 provides an acceptable estimation of limit load (lowest upper bound); however, for design purposes, in order to guarantee a safe margin of the limit load of the components and structures, use is made of the reference volume concept, leading to m_2'', which is the highest lower bound.

CHAPTER 7

REFERENCE TWO BAR METHOD

7.1 INTRODUCTION

Limit loads for mechanical components and structures are determined in this Chapter by invoking the concept of equivalence of "static indeterminacy" that relates a multidimensional component configuration to a "reference two-bar structure." Simple scaling relationships are developed that enable the rapid determination of limit loads. The reference two-bar structure method is applied to a number of component configurations with or without cracks.

7.2 THEORY

The concept of R-Node plays a key role in the understanding of the relationship between the concepts of reference stress, limit load and primary stress. There is explicit

recognition of load and deformation-controlled effects in the various pressure vessel codes. Load-controlled stresses are statically determinate in that they are induced in order to preserve equilibrium with externally applied forces and moments. Deformation-controlled stresses on the other hand are induced as a result of statically indeterminate actions. When widespread inelastic action (plasticity or creep) occurs leading to a limit state, the statically indeterminate stresses and strains undergo redistribution throughout the component except at the R-Nodes that are almost statically determinate.

7.2.1 Plastic Collapse of Components and Structures

The concept of R-Node underpins the theory behind the "reference two-bar structure". For a statically determinate component, the formation of a plastic hinge would result in a collapse. A typical statically indeterminate mechanical component or structure releases static indeterminacies through the sequential formation of plastic hinges (or plastic hinge contours) eventually resulting in a collapse mechanism. The number of plastic hinge locations that would form depends on the degree of static indeterminacies. For example, if a plastic collapse mechanism corresponding to two hinges develops for the beam structure (Fig. 7.1), then there would be a pair of R-Nodes peaks at the hinge locations since bending is dominant. If σ_{n1} and σ_{n2} are the elastic equivalent stresses at the R-Nodes peaks corresponding to the plastic hinge locations, then these can be represented by the two-bar model.

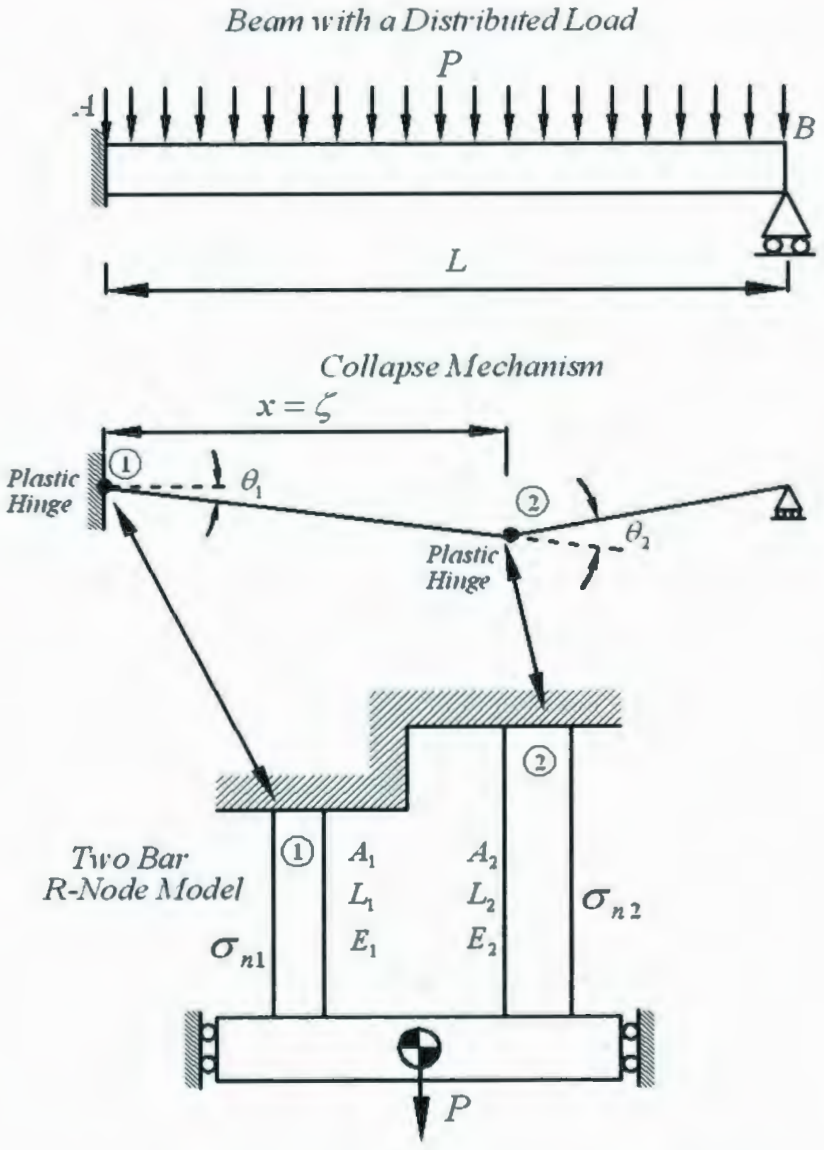

Figure 7.1: Collapse mechanism for a beam with a distributed load

General components (plates and shells) often generate more than two R-Nodes peaks. However, the various R-Node peaks can be expressed in terms of the basic reference two-bar structure as follows:

$$\sigma_{nj} = c_j\sigma_1 + d_j\sigma_2 \tag{7.1}$$

σ_1 and σ_2 are the stresses in bar 1 and bar 2, respectively; and c_j and d_j are coefficients. Now σ_{ref} for a R-Node multibar structure is given by

$$\sigma_{ref} = \frac{\sum_{j=1}^{N}\sigma_{nj}}{N} \tag{7.2}$$

where σ_{nj} are the R-Node peaks, and N is the total number of R-Node peaks. Therefore,

$$\sigma_{ref} = \frac{\sigma_1\left(\sum_{j=1}^{N}c_j\right) + \sigma_2\left(\sum_{j=1}^{N}d_j\right)}{N} \tag{7.3}$$

Essentially, σ_{ref} can be expressed in terms of the reference two-bar structure.

Finally, the limit load is given by

$$P_L = \left(\frac{\sigma_y}{\sigma_{ref}}\right)P \tag{7.4}$$

7.2.2 Relating the General Component to the Reference Two-Bar Structure

As discussed in Chapter 3, the m^0 and m_L limit load multipliers can be obtained using Eqs. (3.117) and (3.120), respectively. By assuming that $L_1 < L_2$ and $A_1 = A_2$, the m^0 limit load multiplier defined in Eq. (3.117) fro the two-bar model can be re-written as

$$m^0 = \frac{\sigma_y \sqrt{L_1 + L_2}}{\sigma_1 \sqrt{L_1 + \left(\frac{\sigma_2}{\sigma_1}\right)^2 L_2}} \tag{7.5}$$

Similarly,

$$\frac{\sigma_1}{\sigma_2} = \frac{L_2}{L_1} \tag{7.6}$$

Making use of Eqs. (3.120) and (7.5) the ratio of m^0 / m_L is given as

$$\frac{m^0}{m_L} = \frac{\sqrt{L_1 + L_2}}{\sqrt{L_1 + \left(\frac{\sigma_2}{\sigma_1}\right)^2 L_2}} \tag{7.7}$$

Making use of Eq. (7.6), the Eq. (7.7) can be rewritten as

$$\frac{m^0}{m_L} = \sqrt{\frac{1+\left(\frac{L_1}{L_2}\right)}{\left(\frac{L_1}{L_2}\right)+\left(\frac{L_1}{L_2}\right)^2}} \tag{7.8}$$

By assuming $\lambda = L_1 / L_2$, Eq. (7.8) is further simplified as

$$\frac{m^0}{m_L} = \frac{1}{\sqrt{\lambda}} \tag{7.9}$$

Clearly, $\lambda \leq 1$ for the range of components. Since from equilibrium consideration $P = \sigma_1 A_1 + \sigma_2 A_2$, where $\sigma_1 / \sigma_2 = 1/\lambda$ and $A_1 = A_2 = A_0$; we have

$$\frac{m^0}{m} = \frac{(L_1 + L_2)\sqrt{L_1 + L_2}}{2L_2\sqrt{L_1 + (\sigma_2 / \sigma_1)^2 L_2}} \tag{7.10}$$

Making use of Eq. (7.6), the Eq. (7.10) can be rewritten as

$$\frac{m^0}{m} = \frac{L_1 / L_2 + 1}{2}\sqrt{\frac{L_1 / L_2 + 1}{L_1 / L_2 + (L_1 / L_2)^2}} \tag{7.24}$$

By assuming $\lambda = L_1 / L_2$, Eq. (7.11) is further simplified as

$$\frac{m^0}{m} = \frac{\lambda + 1}{2\sqrt{\lambda}} \tag{7.12}$$

In the above equation, m^0 / m and m^0 / m_L are useful parameters for characterizing the state of static indeterminacy of a given component undergoing plastic flow. General components can be related to the reference two-bar structure

7.2.3 Constraint Trajectory

Limit loads of mechanical components and structures are determined herein by relating the inelastic parameter (m^0 / m, m^0 / m_L) of the general component to those of the "reference two-bar structure". The underlying concept that enables the relationship is the notion of statical indeterminacy equivalence. Figure 7.2 is a constraint map, which is a variation of m^0 / m verses m^0 / m_L. For a given component, m^0 and m_L can be calculated using Eqs. (3.76) and (3.80). The exact multiplier, *m*, for the component is not known a priori. However, for the reference two-bar structure, *m* can be defined. Both m^0 / m and m^0 / m_L are greater than one, except at the incipient limit load state for which $m^0 / m = m^0 / m_L = 1$. The EMAP trajectory is essentially a locus of m^0 / m versus m^0 / m_L from an initially elastic state through to the plastic collapse state.

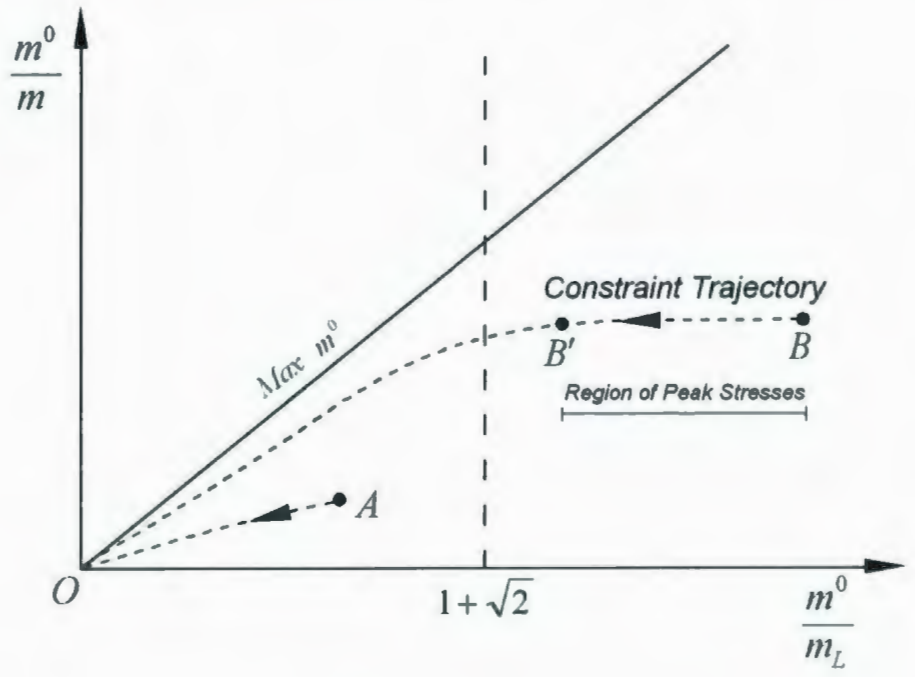

Figure 7.2: Constraint map

It is important to note that m^0 is a multiplier that is based on the overall "statically admissible" stress distribution; whereas m_L is dependent on the maximum stress in the component. Therefore, m_L is sensitive to the magnitude of peak stress whereas m^0 is almost invariant during the blunting of peak stresses.

7.2.4 Scaling Equations

Points such as *A* and *B* in Fig. 7.2 represent states of static indeterminacy. The component EMAP trajectory *AO* or *BB'O* (for components with peak stress) can be

readily generated if required. Equivalence of static indeterminacy of the multidimensional components and the "reference two bar structure" (Fig. 7.3) can be expressed as:

$$\frac{m^0_{Comp}}{m_{L,Comp}} = \frac{m^0_{Bar}}{m_{L,Bar}} = \frac{1}{\sqrt{\lambda}} \tag{7.13}$$

$$\frac{m^0_{Comp}}{m_{Comp}} = \frac{m^0_{Bar}}{m_{Bar}} = \frac{\lambda+1}{2\sqrt{\lambda}} \tag{7.14}$$

where λ is the parameter that represents the sate of static indeterminacy. Also, $\lambda = L_1/L_2 = \sigma_2/\sigma_1$.

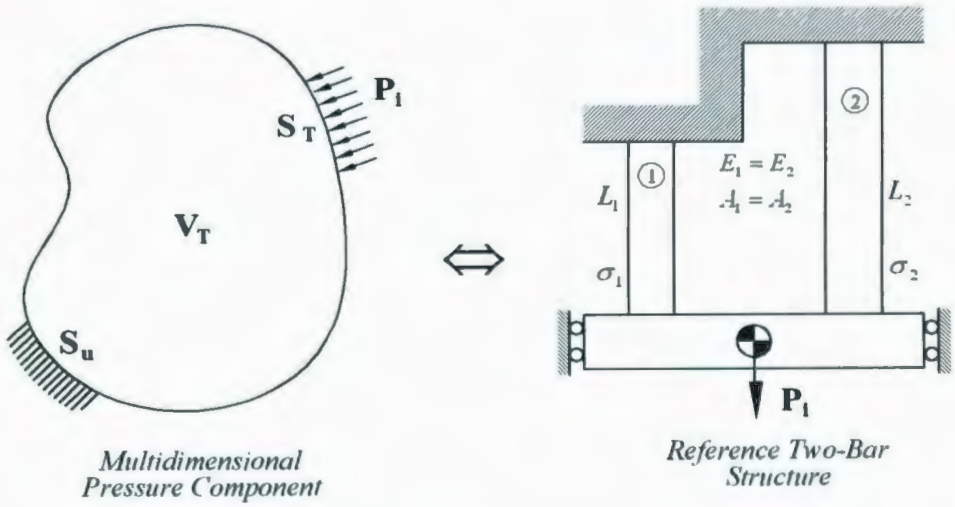

Figure 7.3: Reference two-bar structure

The EMAP trajectory for the reference two-bar structure depicts the redistribution of secondary stress, whereas an EMAP trajectory for a component depicts the

redistribution of secondary as well as peak stresses. For many components with notches and cracks, BB' is nearly horizontal. Therefore, m^0_{comp} is almost invariant while m_L increases as m^0 / m_L decreases.

7.2.5 Calculation Procedure

1. Single Linear Elastic Analysis

In order to evaluate the limit loads, the value of λ is determined using Eq. (7.13), on the basis of a linear elastic analysis of a given component as

$$\lambda = \left(\frac{m_{L,Comp}}{m^0_{Comp}} \right)^2 \tag{7.15}$$

Using Eq. (7.14), the limit load multiplier for a component can be estimated as

$$m_{Comp} = \frac{2\sqrt{\lambda}}{1+\lambda} (m^0_{Comp}) \tag{7.16}$$

With reference to Fig. 7.2, m^0_{comp} is specified as follows:

(1) For $1.0 \le m^0_{Comp} / m_{L,Comp} \le 1+\sqrt{2}$, m^0_{Comp} is the initial linear elastic value designated by point A. These values are within the m_α-triangle. Therefore, λ can be estimated using Eq. (7.15). Applying estimated λ into Eq. (7.16), limit load of the component can be estimated.

(2) For $m^0_{Comp} / m_{L,Comp} > 1+\sqrt{2}$, m^0_{Comp} is evaluated at the linear elastic value designated by point B'. The distance BB' is assumed to be the region of blunting of the peak stresses in a component. The procedure to locate point B' will be discussed later in this Chapter.

Therefore, λ corresponding to point B' can be calculated as follows:

$$\left(\frac{m^0_{Comp}}{m_{L,Comp}}\right)_{Point\,B'} = \frac{1}{\sqrt{\lambda}} \rightarrow \lambda = \left(\frac{m_{L,Comp}}{m^0_{Comp}}\right)^2_{Point\,B'}$$

By substituting λ into Eq. (7.16) the limit load multiplier can be estimated. Now the question is that how the point B' can be defined for a given component.

2. Two Iterations Method

The main idea behind the two-bar structure method is to equate the static indeterminacy of a given component to that of the reference two-bar structure. The static

indeterminacy in a component is due to the secondary stresses and peak stresses. As discussed in Chapter 3, the m_α limit load multiplier becomes imaginary when the ratio of $m^0/m_L \geq 1+\sqrt{2}$ due to the magnitude of peak stresses. Therefore, the procedure is discussed here to locate point B' that represents the location where the effect of peak stress is removed in a given component. The procedure is given below:

- The first analysis is carried out with homogeneous material properties, i. e. E_0,ν .

- The second linear elastic FEA is performed by systematically, but artificially, reducing the elastic moduli of the elements that exceed the reference stress, σ_{ref} .

$$(E_s)_j = \left[\frac{\sigma_{ref}}{(\sigma_{eq})_j}\right]^q E_0 \tag{7.17}$$

where, the subscript "*j*" is the element number, and q is assumed equal to 1. And reference stress is calculated as

$$\sigma_{ref} = \left[\frac{\int_{V_T} \sigma_{eq}^2 \, dV}{V_T}\right]_i^{1/2} \tag{7.18}$$

- The parameter m^0_{Comp} (m^0_1) and $m_{L,Comp}$ are calculated using Eqs. (3.76) and (3.80) respectively. Therefore, the ratio of $m^0_{Comp} / m_{L,Comp}$ at the second iteration represents points B' in constraint map.

3. Alternative Method for Components with Cracks

Figure 7.4 shows the stress distribution in the ligament ahead of crack, where the x-axis is the distance ahead of crack tip, and y-axis is the normalized stress distribution based on yield strength. As can be seen from this figure, the magnitude of peak stress ($\overline{\sigma}_F$) at the crack tip is considerably high; therefore, it is assumed that the peak stresses are very localized and that the following expression is valid:

$$\int_A \overline{\sigma}_F \, dA \approx 0 \tag{7.19}$$

where A is the area on which $\overline{\sigma}_F$ acts.

The shaded area in Fig. 7.4 represents the elastically based secondary stresses (Q) that are essentially self-equilibrating, and tend to redistribute around the redistribution node (R-Node). Therefore, theoretically it does not have any effect on the limit load of a component. As well, the primary stresses, which are "load-controlled" stresses do not redistribute under plastic deformation or inelastic action, as shown in Fig. 7.4.

The aim of this section is to introduce a simple procedure that considers the effect of peak stress in a given crack configuration.

For sake of the discussion, consider the stress distribution ahead of a crack shown in Fig. 7.5. By modifying the elastic modulus of regions around the crack tip (i.e., singular elements that surrounded the crack tip in a finite element discretization scheme), stress distributions can be plotted as shown in Fig. 7.5. In this figure, E_s is the modified value of elastic modulus around the crack tip. At a specific value of $E_s = E_s^*$, the stress distribution ahead of crack becomes almost horizontal; this means that the magnitude of stress gradient reaches a minimum, and the effect of peak stresses becomes small. Numerical simulation of different crack configurations (see the numerical examples section) shows that $E_s \approx E_0/3$ is a good choice for modifying the crack tip elements. This also can be explained as follows:

Consider a crack configuration (Fig. 7.6) for which the stresses at the crack tip can be expressed as

$$\begin{cases} \sigma_{xx} = \sigma_{yy} = \sigma_{\max} \\ \sigma_{zz} = \begin{cases} 0 & \textit{Plane Stress} \\ 2\nu\sigma_{\max} & \textit{Plane Strain} \end{cases} \end{cases} \tag{7.20}$$

where $\sigma_{\max} = \dfrac{K_I}{\sqrt{2\pi r}} = \dfrac{Y\sigma_n\sqrt{\pi a}}{\sqrt{2\pi r}}$

σ_n is remote field stress and Y is crack configuration factor.

The above stresses are the principal stresses at the crack tip. The von-Mises criterion can be written as

$$[(\sigma_1-\sigma_2)^2+(\sigma_2-\sigma_3)^2+(\sigma_3-\sigma_1)^2]=2\sigma_{eq}^2 \tag{7.21}$$

Substituting the stresses from Eq. (7.20) into (7.21), the following expression can be obtained

$$\sigma_{eq}=A\,\sigma_{\max}=\frac{AY\sigma_n\sqrt{\pi a}}{\sqrt{2\pi r}} \tag{7.22}$$

where A=1 for plane stress and A=(1-2ν) for plane strain conditions.

The average stress along the crack orientation in the singularity domain can be calculated as

$$\overline{\sigma}_{eq}=\frac{\int_0^{r_s}\sigma_{eq}}{r_s}=\frac{2AY\sigma_n\sqrt{\pi a}}{\sqrt{2\pi r_s}} \tag{7.23}$$

Referring to Fig. 7.6, at $r=r_s$ the equivalent stress is equal to the reference stress; thus,

$$\sigma_{ref} = \frac{AY\sigma_n\sqrt{\pi a}}{\sqrt{2\pi r_s}} \tag{7.24}$$

Making use of Eq. (7.17), the relationship between the modified elastic modulus (E_s) and initial modulus of elasticity (E_0) can be written as

$$\frac{E_s}{E_0} = \left(\frac{\sigma_{ref}}{\overline{\sigma}_{eq}}\right)^q \tag{7.25}$$

As discussed in Chapter 4, the parameter q can be within the range $1 \le q \le 2$. Applying the values q=1 and q=2, the E_S / E_0 will vary between 0.5 and 0.25, respectively. Based on numerous FEA on different crack configurations $E_s = E_0/3$ works out to be a good choice for modifying singular elements around a crack tip.

The modified elastic modulus of the singular elements around the crack tip can be obtained as $E_s = E_0/3$. A linear elastic FEA with $E_s / E_0 = 1/3$ for all adjacent elements around the crack tip and with $E_s = E_0$ for all other elements is carried out. The resulting parameters ($m^0/m, m^0/m_L$) are used to locate B'.

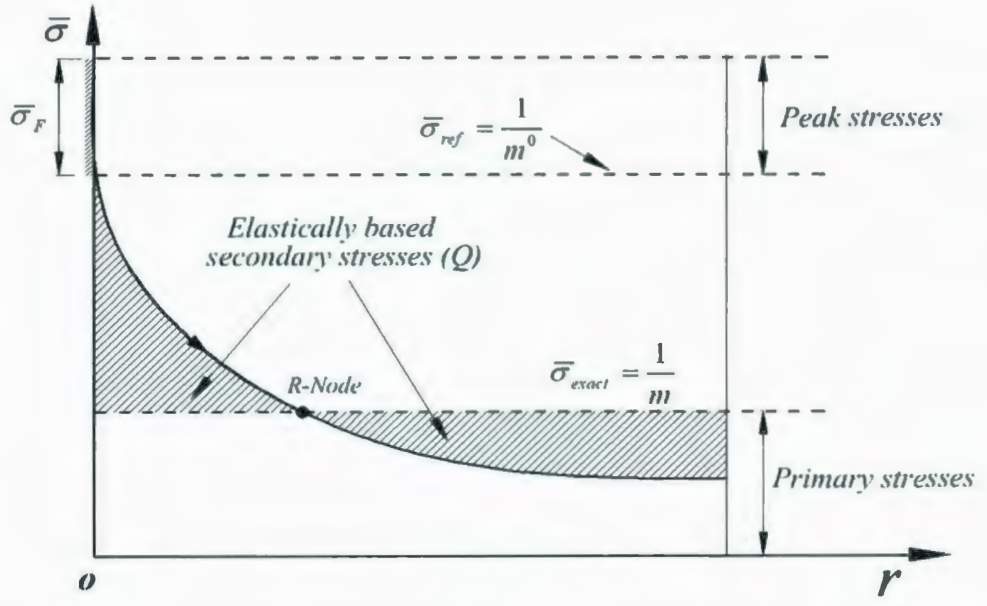

Figure 7.4: Stress distribution ahead of crack tip

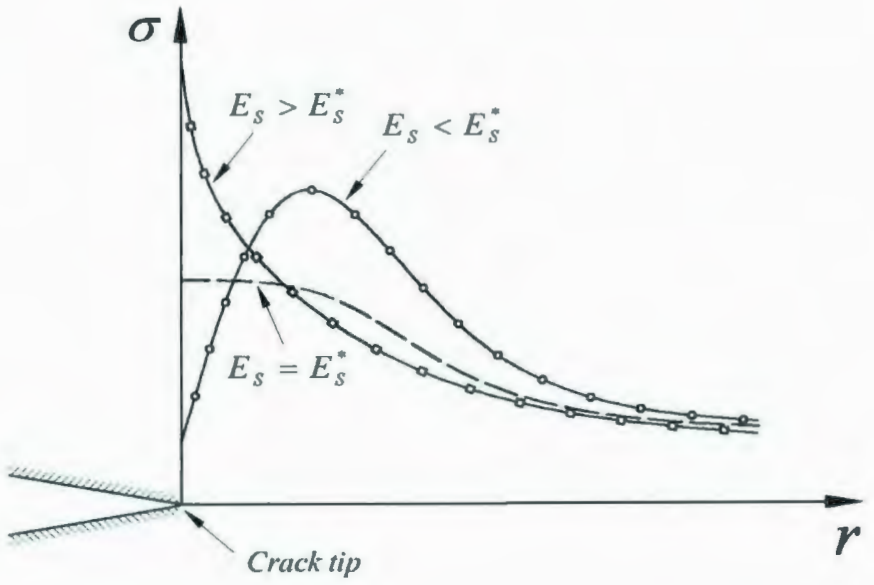

Figure 7.5: Stress distribution ahead of crack tip for different value of E_s

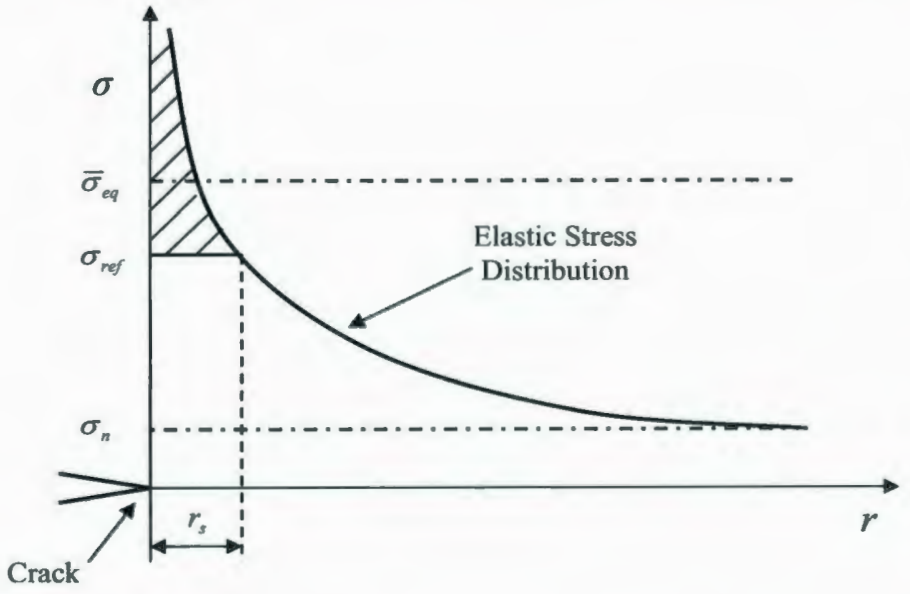

Figure 7.6: Average stress ahead of the crack tip

7.3 VERIFICATION

A simple beam subjected to both axial tensile force and bending moment is considered with original length of L=508 mm, height is D=25.4 mm, and width is B=25.4 mm. Two different models are developed to demonstrate the procedure. The first model is the basic beam (without notch) as shown in Fig.7.7 (a) and the second model is the beam with two sharp notches placed at the mid-section of the beam as shown in Fig. 7.7(b). The radius of each notch is r=1/80 of the original beam height.

The beams are modeled with the same material having modulus of elasticity E=206.85 GPa and yield strength σ_y=206.85 MPa. Both beams are subjected to axial

tensile force of P= 0.3 P_y and bending moment of M=0.1 M_y, where P_y ($=\sigma_y D B$) is axial force of the beam at yield and M_y ($=\sigma_y D^2 B/6$) is the bending moment of the beam at yield.

The basic beam (without notch) is analyzed using the reference two-bar structure method. An initial linear elastic FEA is performed. From the results of the initial elastic FEA, m^0_{Comp}=3.273 and $m_{L,Comp}$=2.508, using Eq. (3.76) and Eq. (3.80). Since $m^0_{Comp}/m_{L,Comp}$=1.3047 is less than $1+\sqrt{2}$, there is negligible peak stress in the component. Now the statically indeterminacy parameter λ=0.342, using Eq. (7.15), and the corresponding limit load multiplier m_{Comp}=3.1605, using Eq. (7.16), is evaluated.

The general solution for combined tension and bending is not known. The lower bound solution for plane stress is given by Miller (1988) as:

$$m_{Analytical} = \frac{\sigma_y (D-2r)^2}{|2M| + \sqrt{4M^2 + P^2 (D-2r)^2}} \tag{7.26}$$

where r is the notch radius (for simple beam without notch r=0).

Therefore, by applying Eq. (7.26) the limit load is calculated as $m_{Analytical}$=2.983.

The beam with two through thickness sharp notches is considered next as shown in Figure 7.7(b). The notches are located at the opposite sides of the beam. Similar material properties and loading are applied for this example. From the results of the initial linear elastic FEA, m^0_{Comp}=3.273 and $m_{L,Comp}$=1.180. Since $m^0_{Comp}/m_{L,Comp}$=2.773 is greater than $1+\sqrt{2}$ peak stress is present in the component. Then, another linear elastic FEA is performed by modifying the elastic modulus of the elements, using Eq. (7.17), stressed above σ_{ref}, using the elastic modulus adjustment parameter q=1.0. From the results of the second analysis, m^0_{Comp}=3.2690, $m_{L,Comp}$=1.7516 and corresponding λ= 0.287 is obtained. Now, the limit load multiplier is estimated as m_{Comp}=2.721. The constraint map for both components is presented in Fig. 7.8. The comparison of limit load for the two components shows that the primary stress is slightly overestimated (conservative for limit load design) for the notched beam. Therefore, the discussion is given in this section to explain this difference.

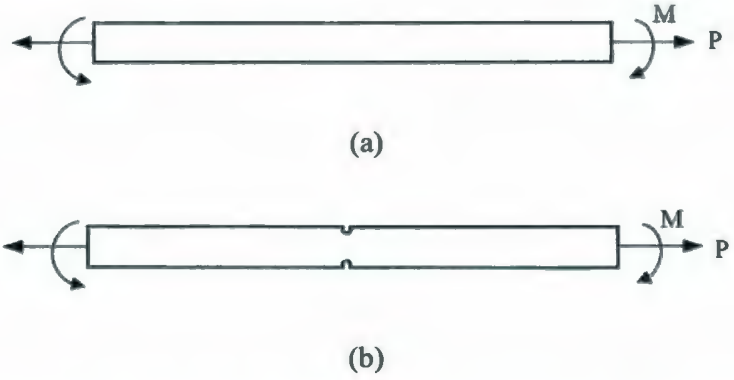

Figure 7.7: Beam under axial tensile force and bending moment: (a) simple beam without notch, (b) beam with two sharp notches

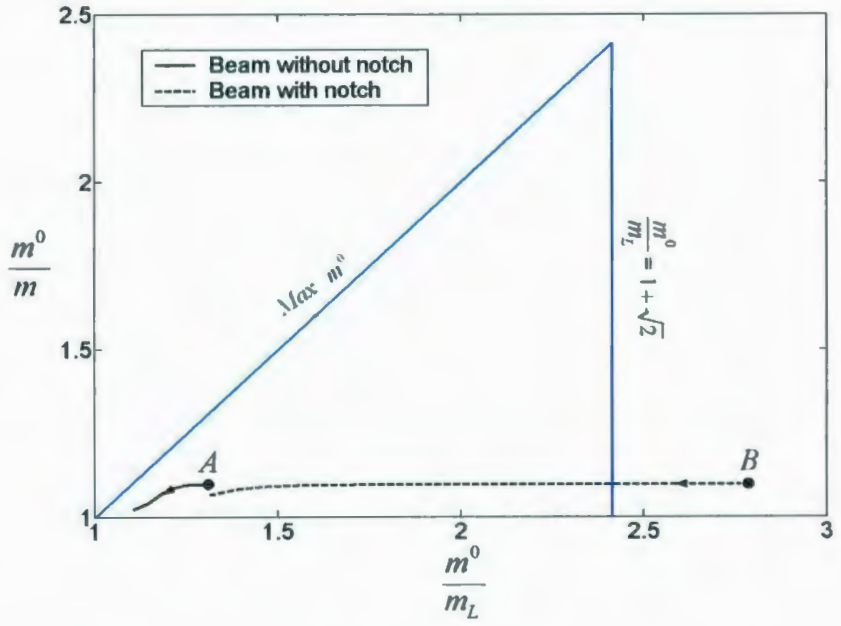

Figure 7.8: Constraint map for a beam with and without notch

Figure 7.9 represents the schematic elastic stress distribution resulting from two subsequent finite element iterations (first and second iteration) at the critical section of a given component or structure. The different categories of stresses are labeled in the figure in order to relate them with the finite element stress distributions (primary (*P*), secondary (*Q*) and peak (*F*) stresses).

The stress distribution at the critical section of a component after the initial linear elastic FEA is shown by the "solid-line" in Fig. 7.9, where σ_{max} represents the maximum stress in the component. The "dashed-line" represents the stress distribution resulting from the second linear elastic EMAP iteration.

The upper bound limit load multiplier (m^0) will remain almost unchanged when blunting of the peak (F) stresses. After the second linear elastic FEA, Q' is the amount of secondary stress estimated by the proposed method, which is problem-dependent. Therefore, the estimation of secondary stresses might be slightly underestimated or overestimated depending on the EMAP iteration as well as geometry, loading and boundary conditions of the given component or structure.

Figure 7.10 represents the actual stress distribution at the mid-section (notch) of the notched beam as shown in Fig. 7.7(b). The figure represents the stress distribution of two consecutive linear elastic FEA (the initial analysis and the subsequent EMAP iteration) results. The stress distribution at converged limit state is also plotted in the figure.

It can be observed from Fig. 7.10 that the actual stress distribution obtained from the linear elastic FEA is almost similar to the conceptual model as shown in Fig. 7.9. Once again it should be noted that the actual stress distribution resulting from the second EMAP iteration might be different depending on the geometry, loading, and boundary condition of the problem.

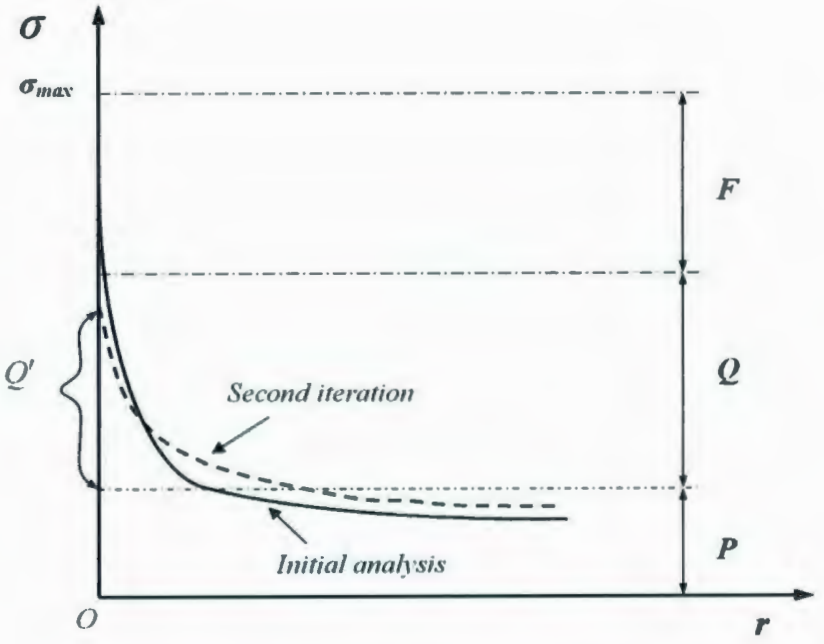

Figure 7.9: Stress distribution of linear elastic FEA

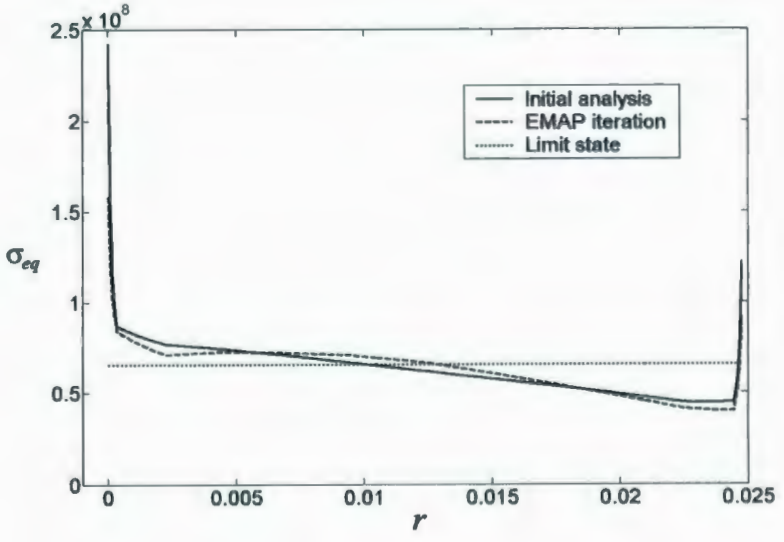

Figure 7.10: Actual stress distribution of notched beam

7.4 NUMERICAL EXAMPLES FOR COMPONENTS WITHOUT CRACK

7.4.1 Thick-Walled Cylinder

The thick walled cylinder with inside radius of R=130 mm and thickness t=50 *mm* is modeled. An internal pressure of 50 MPa is applied. The material is assumed to be elastic-perfectly plastic. The modulus of elasticity is specified as E=200 GPa and the yield strength is assumed to be σ_y =300 MPa. Linear elastic FEA of the cylinder yields a statically admissible stress distribution on the basis of which we have:

$$m^0_{Comp} = 2.294$$

$$m_{L,Comp} = 1.649$$

Therefore, $m^0_{Comp} / m_{L,Comp} = 1.391$, pointing to an insignificant notch effect.

From Eq. (7.15), the statically indeterminate parameter estimated as λ =0.516; therefore, using Eq. (7.16), the limit load multiplier of the component is estimated as

$$m_{Comp} = \frac{2\sqrt{\lambda}}{\lambda+1}(m^0_{Comp}) = 2.173$$

The value of m_{Comp} using the exact solution is equal to 2.254. As shown in Fig. 7.11, the initial point (point *A*) for this component is located inside the triangle, which means that peak stress in the component is very small.

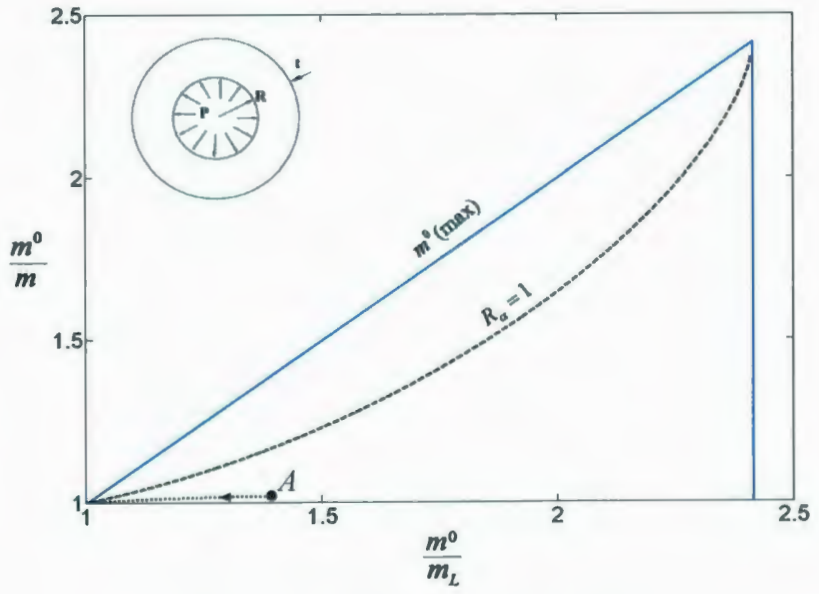

Figure 7.11: Constraint map for thick-walled cylinder

7.4.2 Torispherical Head

Linear elastic FEA of the torispherical head, the same dimension and material property has been used as in Chapter 6, leads to a statically admissible stress distribution, on the basis of which m^0_{Comp} =1.231 and $m^0_{Comp}/m_{L,Comp}$ =2.413. Since $m^0_{Comp}/m_{L,Comp} \le 1+\sqrt{2}$, the magnitude of peak stresses are negligible.

Using Eq. (7.15) λ=0.171. Therefore, from Eq. (7.16) the limit load multiplier is estimated as

$$m_{Comp} = \frac{2\sqrt{\lambda}}{\lambda+1}(m^0_{Comp}) = 0.870$$

The value of m_{NFEM} (inelastic FEA) =0.873. The constraint map for torispherical head is presented in Fig. 7.12.

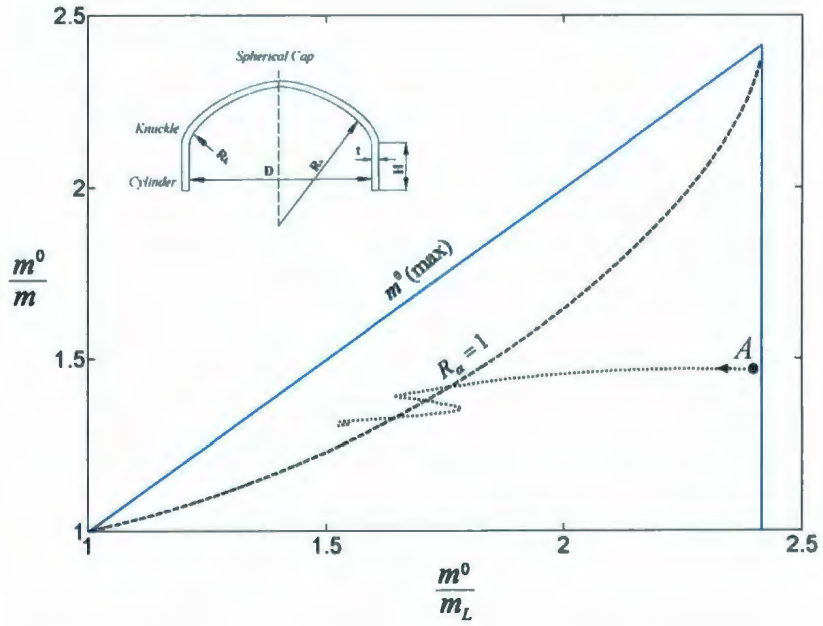

Figure 7.12: Component constraint map for torispherical head

7.4.3 Indeterminate Beam

An indeterminate beam is modeled in plane stress condition with a uniform tensile distributed load on top of the beam. The geometry and material properties are the same as the example in Chapter 4.

Linear elastic FEA of the plate with a hole leads to a statically admissible distributions for which m^0_{Comp}=15.686; $m_{L,Comp}$=2.864. Using Eq. (7.15) λ=0.033. Since $m^0_{Comp} / m_{L,Comp} > 1+\sqrt{2}$, peak stresses are present. With reference to Fig. 7.13, m^0_{comp} at B and B' are equal in magnitude. The point B is obtained from a linear elastic FEA whereas point B' is obtained by modifying the elastic modulus, using Eq. (7.17), of the elements that their stresses are exceeded the value of σ_{ref}. From the results of the second analysis, m^0_{comp}=15.137 and $m_{L,Comp}$=4.837 and corresponding constraint parameter λ=0.102 is obtained. Then, by applying value of λ at point B' into Eq. (7.16) the limit load multiplier can be estimated as

$$m_{Comp}=8.778$$

The value of analytical limit load multiplier from Mendelson (1968) is given as

$$m_{Analytical} = \frac{11.6587\sigma_y}{P}\left(\frac{W}{2L}\right)^2 \tag{7.27}$$

The results are summarized in Table 7.1.

Table 7.1: Constraint map parameters, Indeterminate beam

	m^0_{Comp}	$m_{L,Comp}$	$(m^0/m_L)_{Comp}$	m_{Comp}	$m_{Analytical}$
Point B	15.686	2.864	5.476	5.543	8.735
Point B'	15.137	4.837	3.129	8.778	

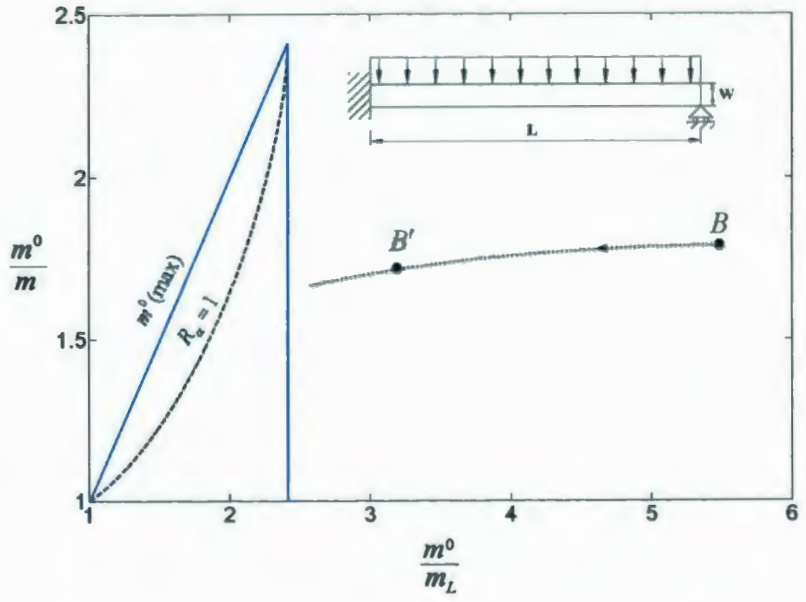

Figure 7.13: Component constraint map for indeterminate beam

7.3.4 Non Symmetric Rectangular Plate

The proposed method is applied to non-symmetric plate structure (Fig. 7.14) with complex boundary conditions under a lateral pressure. The dimensions of the plate are:

Length (L): 381 mm, Width (W): 254 mm, Thickness (t): 12.7 mm, E=206.85 GPa

σ_y=206.85 MPa, ν=0.3, P=6.895 MPa.

For the plate structure, statically admissible stress distributions based on linear elastic FEA leads to the following:

m^0_{Comp}=0.630, $m_{L,Comp}$ =0.072

Therefore, $m^0_{Comp} / m_{L,Comp}$ =8.75 for which λ =0.142.

Since $m^0_{Comp} / m_{L,Comp} > 1+\sqrt{2}$ peak stresses are present. The second elastic linear iteration is performed and the elastic modulus of the elements for which stresses exceed σ_{ref}, estimated from Eq. (7.18), are modified using Eq. (7.17). Then, the point B' represents the results obtained from second iteration. Therefore, the calculations are based on point B' where BB' is horizontal (Fig. 7.15).

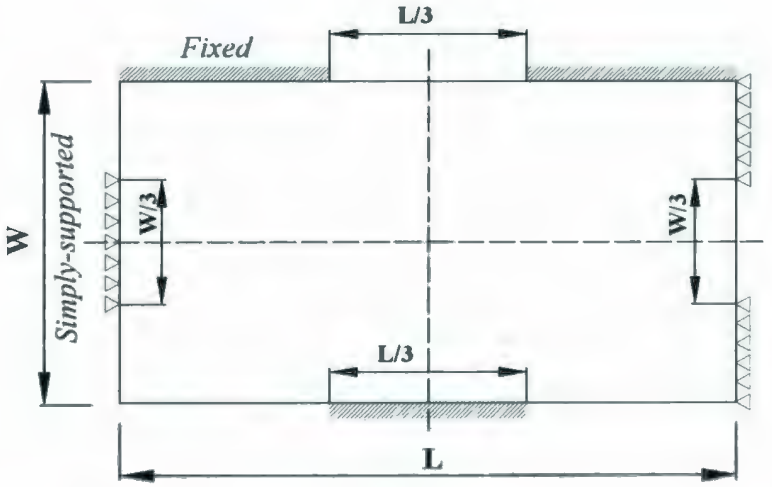

(a)

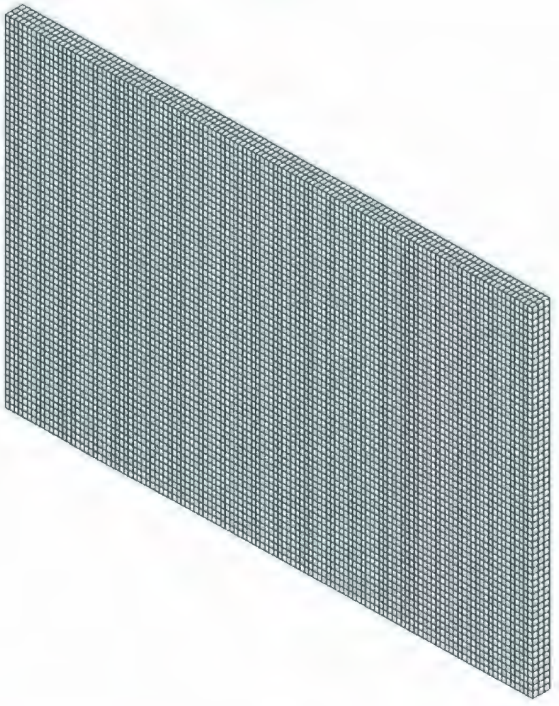

(b)

Figure 7.14: Non symmetric rectangular Plate: Geometry and dimensions,

(b) Finite element mesh

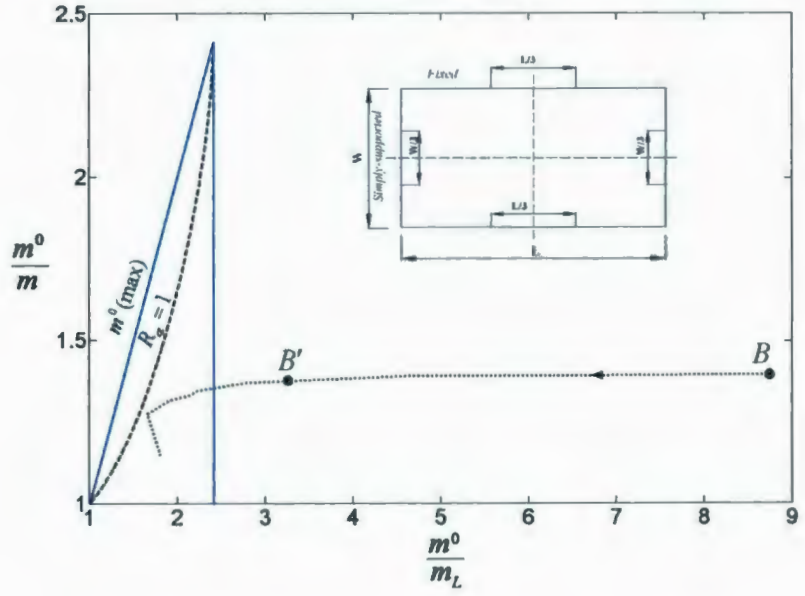

Figure 7.15: Constraint map for non symmetric plate

Using Eq. (7.16), m_{Comp}=0.449. The corresponding inelastic FEA result is m_{NFEM}=0.451 (see Table 7.2).

Table 7.2: Constraint map parameters, Non symmetric rectangular plate

	m^0_{Comp}	$m_{L,Comp}$	$(m^0/m_L)_{Comp}$	m_{Comp}	m_{NFEM}
Point B	0.630	0.072	8.750	0.142	0.451
Point B'	0.603	0.185	3.248	0.339	

Table 7.3 is a comparison of relative computational times for various component analyses (all the times are in seconds). It can be seen that the present method represents savings in time.

Table 7.3: Comparison of computational times

Components	Present study (s)	Inelastic FEA* (s)
Thick-Walled Cylinder (Plane strain)	48	176
Torispherical Head (Axisymmetric)	27	86
Indeterminate Beam	389	776
Non Symmetric Rectangular Plate (3D)	937	7820

* Using automatic time stepping

7.5 NUMERICAL EXAMPLES FOR COMPONENTS WITH CRACK(S)

7.5.1 Compact Tension (CT) Specimen

The compact tension specimen (which contains axial force and moment on the ligament ahead of the crack) is widely used in fracture toughness testing. A compact tension specimen with the similar geometry and material property as in Chapter 4 are studied in this section. Due to the symmetry in geometry and loading, a half of the plate is modeled in plane stress condition using ANSYS. The variation of lower bound and upper

bound limit load multipliers obtained from linear FEA for different values of elastic modulus reduction in the singular elements surrounding the crack tip is shown in Figs. 7.16 and 7.17, respectively. As it can be seen from Fig. 7.16, for $E_s / E_0 = 1/3$ the lower bound limit load m_L reaches its maximum value; however, referring to Fig. 7.17, m^0 limit load multiplier does not change much for $E_s / E_0 > 1/3$. At $E_s / E_0 = 1/3$ the stress gradient in the crack tip vicinity reaches to its lowest value, which results in a smaller value of maximum stress in the component. As shown in Fig. 7.18, this can be visualized by plotting stress distribution ahead of crack for different values of E_s / E_0.

Linear elastic FEA of the component gives m^0_{Comp} =1.4975; and $m_{L,Comp}$ =0.2631, which represents initial point B on the constraint map (Fig. 7.19). In order to blunt the peak stresses, the elastic modulus of the singular elements around the crack tip are modified by $E_s = E_0 / 3$; consequently, the limit load multipliers become m^0_{Comp} =1.4895 and $m_{L,Comp}$ =0.4328 (point B'). Therefore, the static indeterminacy parameter (λ) can be obtained at point B' using Eq. (7.15) as

$$\lambda = \left(\frac{m_{L,Comp}}{m^0_{Comp}} \right)^2 = 0.0844$$

Using Eq. (7.16) and based on the values at point B', the limit load can be estimated as

$$m_{Comp} = \frac{2\sqrt{\lambda}}{1+\lambda}(m^0_{Comp}) = 0.7982$$

Inelastic FEA result is obtained as m_{NFEM}=0.8210. The various parameters at points B and B' are summarized in Table 7.4. In this table, the parameters at point B' are based on both using alternative method for crack and two iterations methods. However, in constraint map shown in Fig. 7.19, point B' is located based on the alternative method for cracks.

Table 7.4: Constraint map parameters, Compact tension specimen (Plane stress)

	m^0_{Comp}	$m_{L,Comp}$	$(m^0/m_L)_{Comp}$	m_{Comp}	m_{NFEM}
Point B (Initial point)	1.4975	0.2631	5.6914	0.5105	
Point B' (Alternative method)	1.4895	0.4328	3.4418	0.7982	0.8210
Point B' (Two iterations method)	1.4627	0.4615	3.1697	0.8394	

In order to show the general applicability of the method, the compact tension specimen is modeled using a three-dimensional elements and in plane strain conditions. As presented in Figs. 7.20 and 7.21, modifying the singular elements around the crack tip leads to similar behavior (as in plane stress) for the three-dimensional model and plane strain.

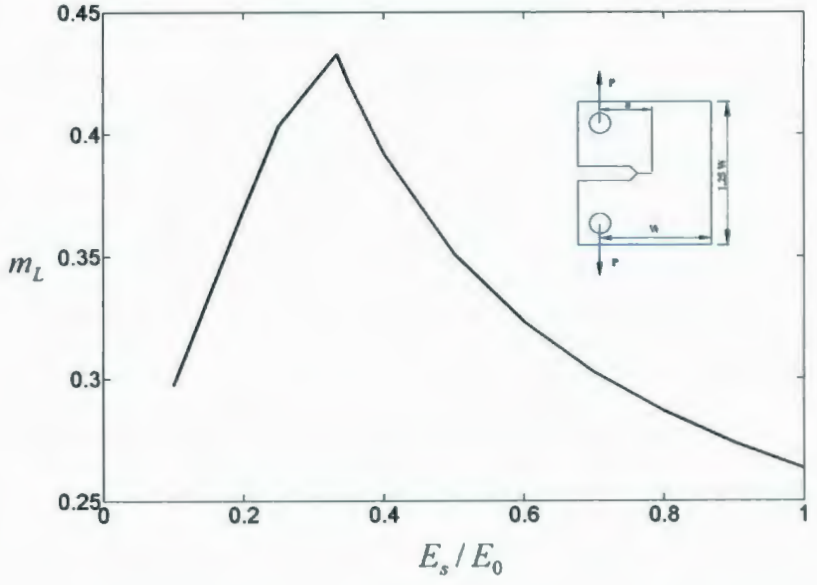

Figure 7.16: Variation of lower bound limit load multiplier with E_s/E_0: Plane stress

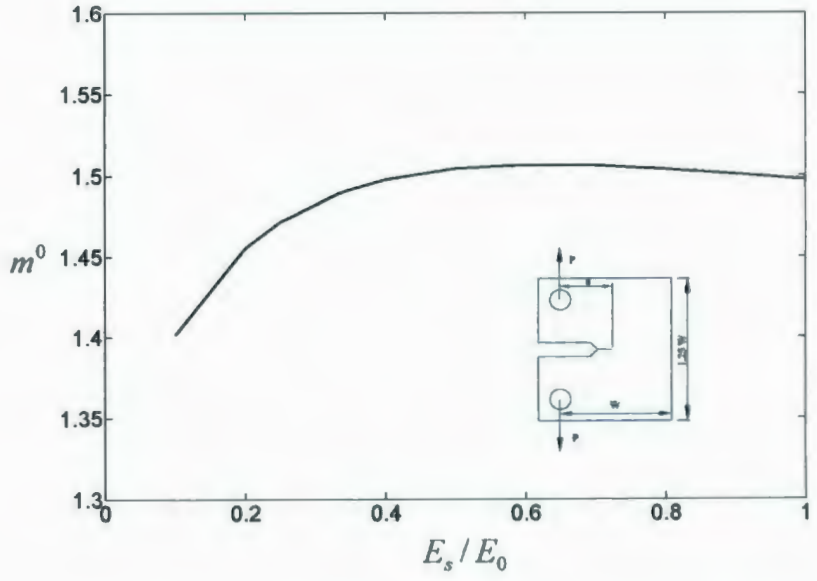

Figure 7.17: Variation of upper bound limit load multiplier with E_s/E_0: Plane stress

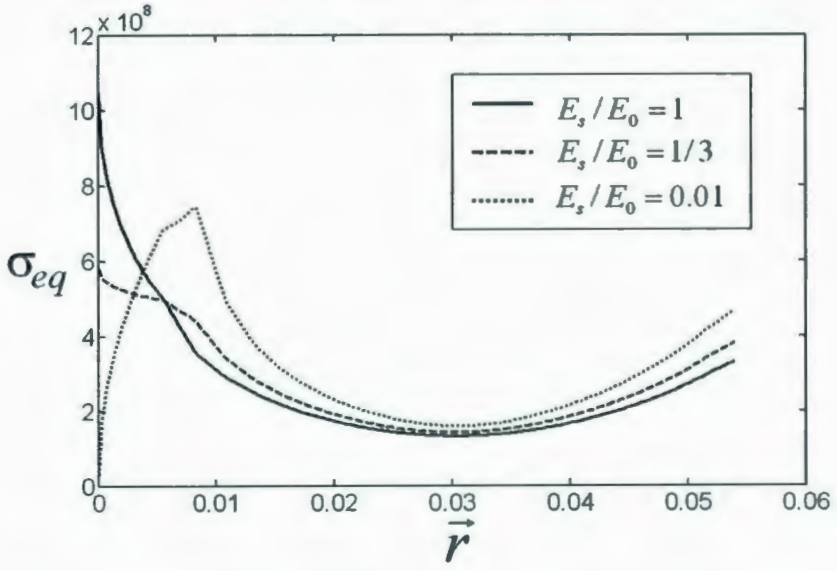

Figure 7.18: Stress distribution ahead of crack tip for different value of E_s/E_0: Plane stress

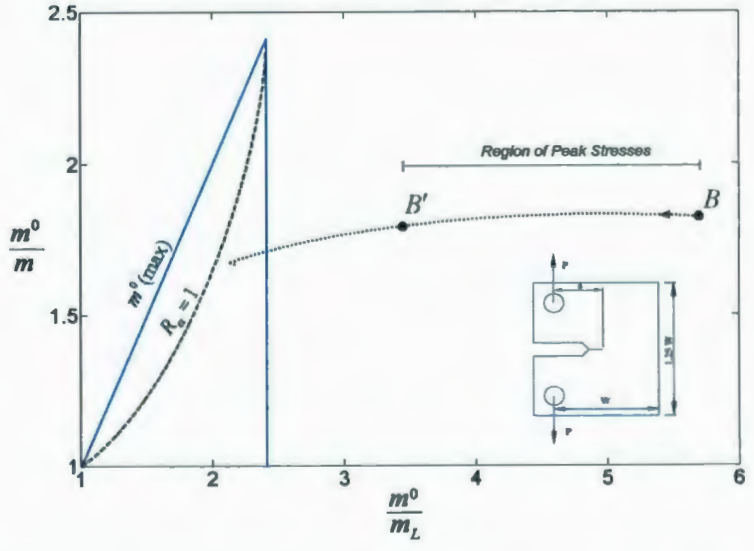

Figure 7.19: Constraint map for compact tension specimen: Plane stress

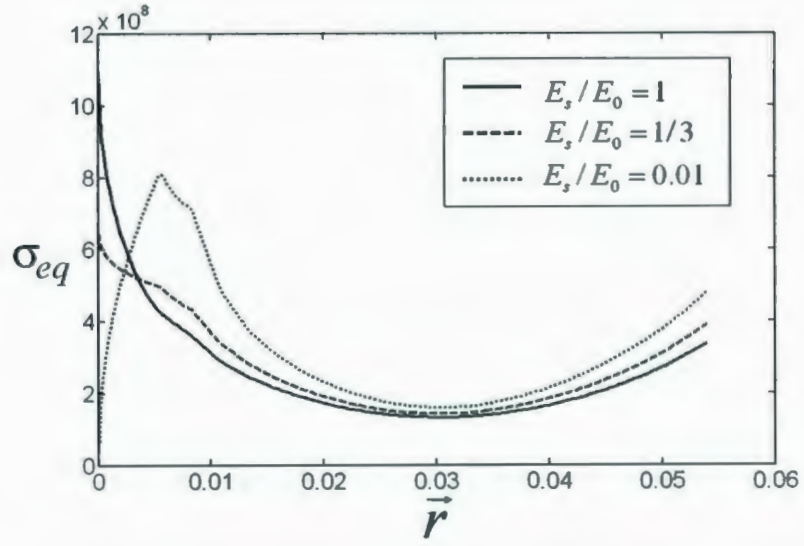

Figure 7.20: Stress distribution ahead of crack tip for different value of E_s/E_0:Three-dimensional model

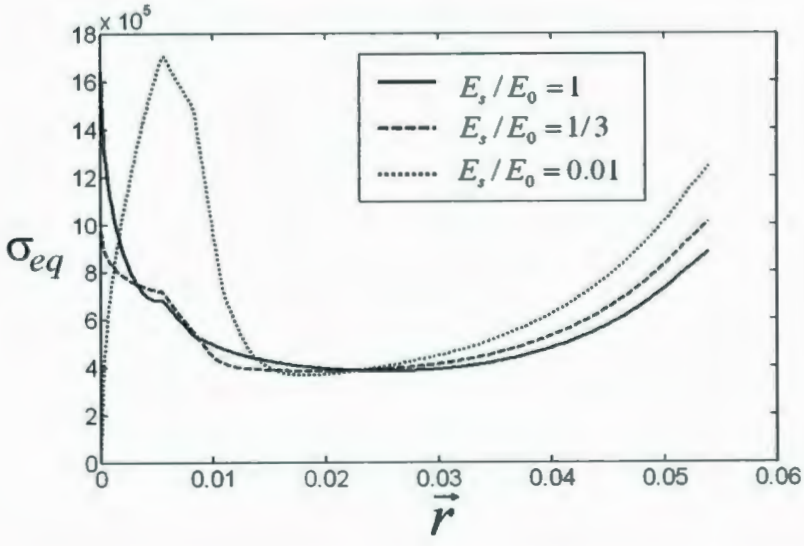

Figure 7.21: Stress distribution ahead of crack tip for different value of E_s/E_0: Plane strain

7.4.2 Middle Tension Panel

Consider a thin middle tension panel (Fig. 7.22) with width $2W$ = 250 mm, thickness t= 3 mm, length $2L$ = 600 mm and crack length $2a$=50 mm, subjected to a remote tensile stress, σ = 100 MPa. The material properties are the same as compact tension specimen. Only a quarter of the plate is modeled due to the symmetry.

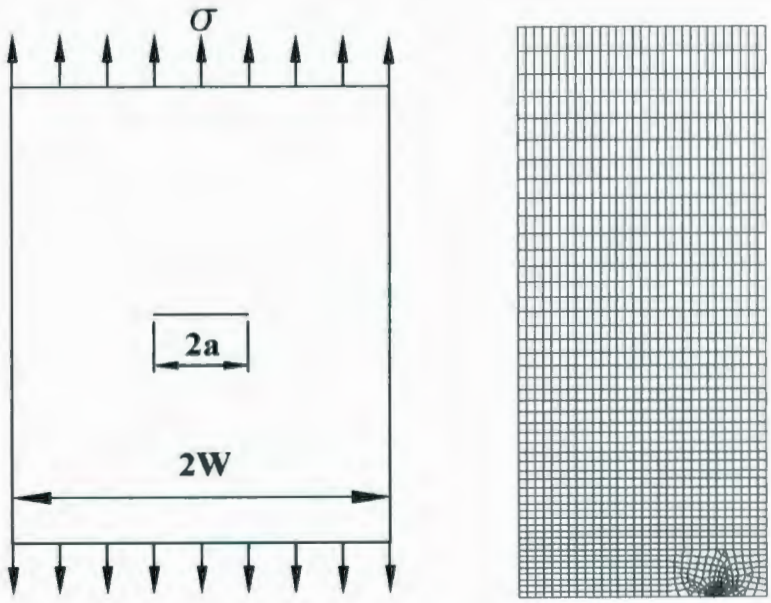

Figure 7.22: Middle tension panel: (a) Geometry and dimensions, (b) Finite element mesh

Modifying the elastic modulus of the singular elements around the crack tip by one third of initial elastic modulus value, the limit load multipliers are obtained as m^0_{Comp}=2.4630 and $m_{L,Comp}$ =1.1878, which represent point B' in constraint map shown in Fig. 7.23. Therefore, the static indeterminacy parameter at this point is calculated using Eq. (7.15) as λ=0.2326, and finally using Eq. (7.16) the limit load multiplier for middle tension panel is obtained as m_{Comp}=1.9274. The estimated parameters at initial point (point B) and point B'(using both the alternative method and two iterations method) in constraint map are given in Table 7.5.

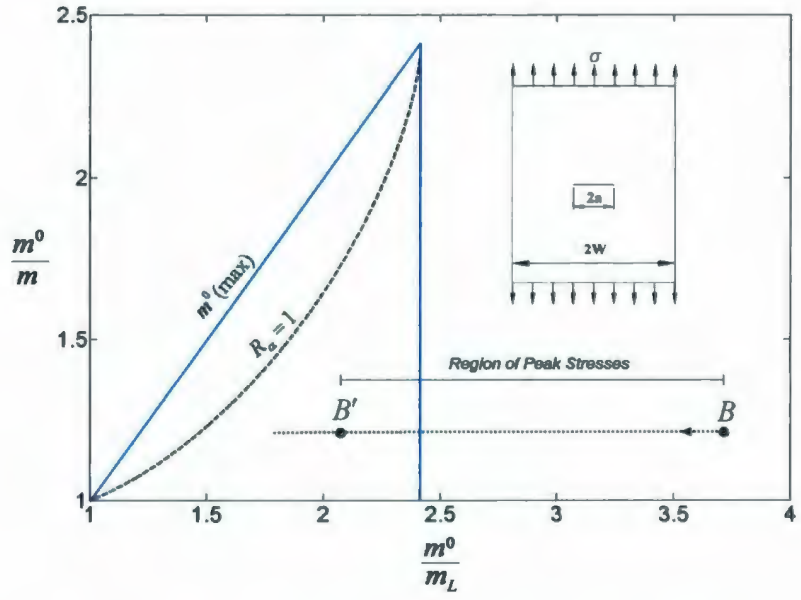

Figure 7.23: Constraint map for middle tension panel

Table 7.5: Constraint map parameters, Middle tension panel

	m^0_{Comp}	$m_{L,Comp}$	$(m^0/m_L)_{Comp}$	m_{Comp}	m_{NFEM}
Point B (Initial point)	2.4636	0.6638	3.7111	1.2378	
Point B' (Alternative method)	2.4630	1.1878	2.0735	1.9274	2.031
Point B' (Two iterations method)	2.2462	1.1826	1.8994	1.8519	

7.5.3 Plate with Multiple Cracks

The material properties and geometry are the same as the example in Chapter 4. Linear elastic FEA of leads to m^0_{Comp}=2.3378 and $m_{L,Comp}$=0.5170. Since $m^0_{Comp}/m_{L,Comp} > 1+\sqrt{2}$, peak stresses are present. With reference to Fig. 7.24, m^0_{comp} at B and B' are equal in magnitude. The point B is obtained from a linear elastic FEA considering homogenous material property in the component whereas point B' is obtained by modifying the elastic modulus of singular elements around the crack tips using $E_s = E_0/3$. Therefore, by estimating λ at point B' the limit load multiplier is estimated as m_{Comp} =1.2878, which is reasonably accurate when compared with the inelastic FEA (see Table 7.6).

Table 7.6: Constraint map parameters, Plate with multiple cracks

	m^0_{Comp}	$m_{L,Comp}$	$(m^0/m_L)_{Comp}$	m_{Comp}	m_{NFEM}
Point B (Initial point)	2.3378	0.5170	4.5218	0.9858	
Point B' (Alternative method)	2.3354	0.7021	3.3264	1.2878	1.3480
Point B' (Two iterations method)	2.3410	0.6314	3.7077	1.1772	

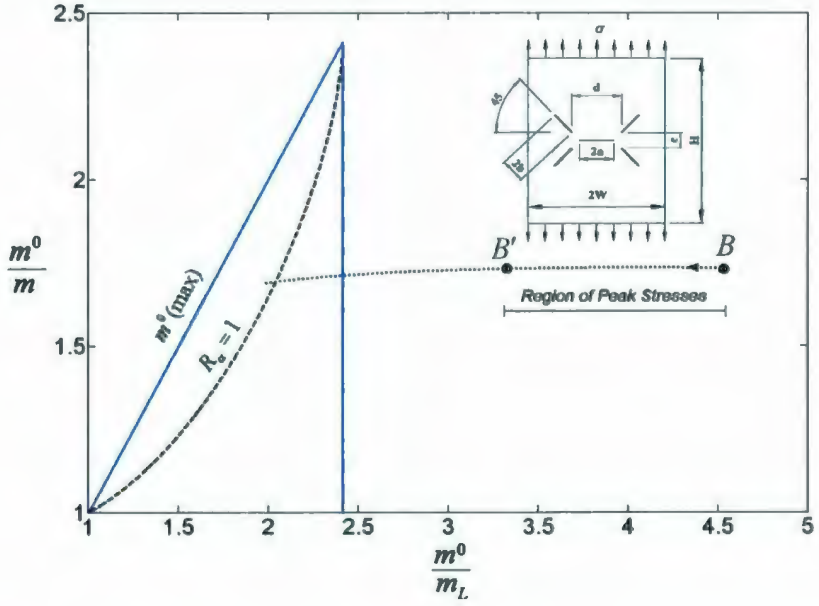

Figure 7.24: Constraint map for plate with multiple cracks

7.5.4 Pipe with an Extended Inner Axial Crack

With reference to Fig. 7.25, a pipe with an extended inner axial crack in of thickness t=10 mm, crack length a=2 mm, average radius R_m=25 mm and an internal pressure P=50 MPa is examined here. The material properties are: elastic modulus E= 206.85 GPa and yield strength σ_y = 250 MPa, with a Poisson's ratio of ν=0.3. Due to symmetry only half of the pipe is modeled in plane strain condition. After modifying the elastic modulus of singular elements around the crack tip by $E_s = E_0/3$, the upper bound and lower bound multipliers are estimated as m^0_{Comp}=2.3624 and $m_{L,Comp}$=1.0600 (point B' in Fig. 7.26). Using Eqs. (7.15) and (7.16) the limit load for a given component is obtained as m_{Comp}=1.7647. The estimated parameters using the reference two-bar structure are given in Table 7.7.

Table 7.7: Constraint map parameters, Pipe with an extended inner axial crack

	m^0_{Comp}	$m_{L,Comp}$	$(m^0/m_L)_{Comp}$	m_{Comp}	m_{NFEM}
Point B (Initial point)	2.3629	0.6037	3.9137	1.1335	
Point B' (Alternative method)	2.3624	1.0600	2.2287	1.7647	2.1150
Point B' (Two iterations method)	2.2155	1.0170	2.1784	1.6800	

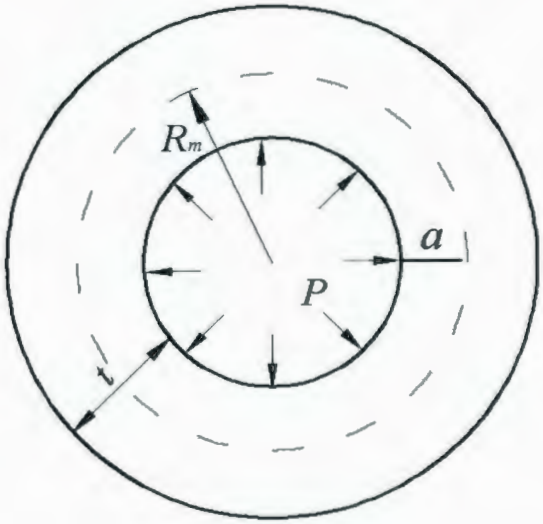

(a)

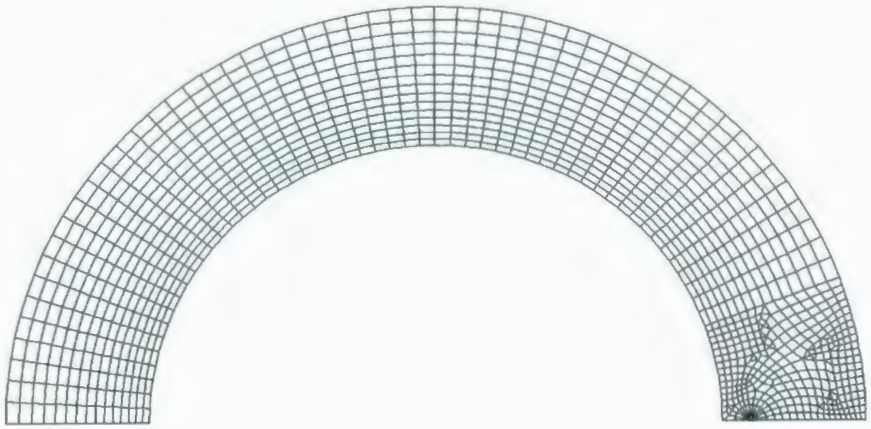

(b)

Figure 7.25: Pipe with an extended inner axial crack: (a) Geometry and dimensions, (b) Typical finite element mesh

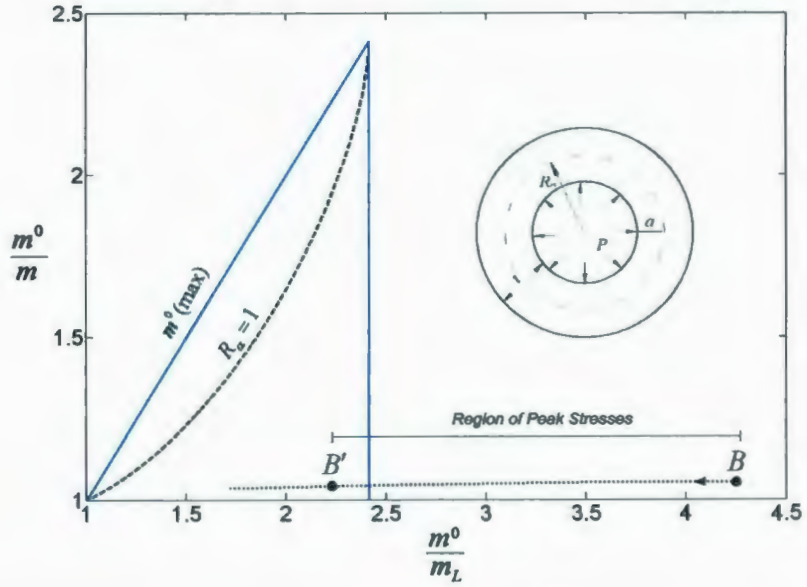

Figure 7.26: Constraint map for pipe with an extended inner axial crack

7.5.5 Single Edge Notched Bend

A single edge notched bend (Fig. 7.27) with a span of S=400 mm, a width W=100 mm, thickness t=3 mm and a crack length a=50 mm under load P=12 kN is modeled. The modulus of elasticity is specified as 211.85 GPa, with a Poisson's ratio of ν=0.3. The yield strength is assumed to be 488.43 MPa. Half of the specimen is analyzed due to symmetry. The estimated parameters at point B and B' in Fig. 7.28 are given in Table 7.8. The estimated limit load using reference two-bar method is m_{Comp}=0.8014, whereas the inelastic FEM is m_{NFEM}=0.8214.

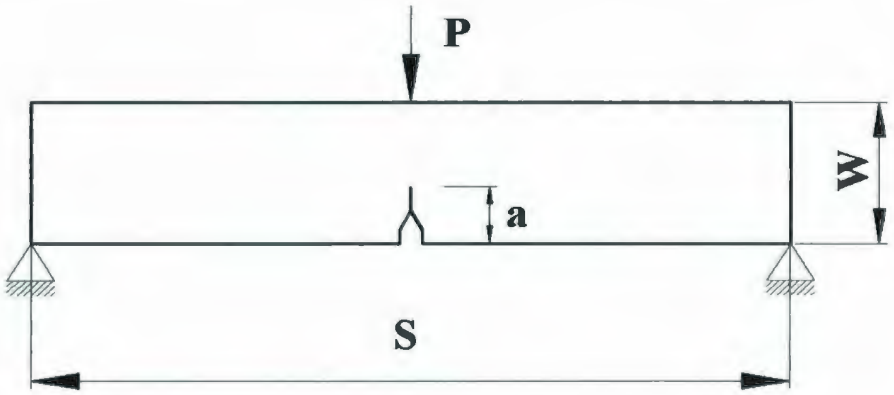

(a)

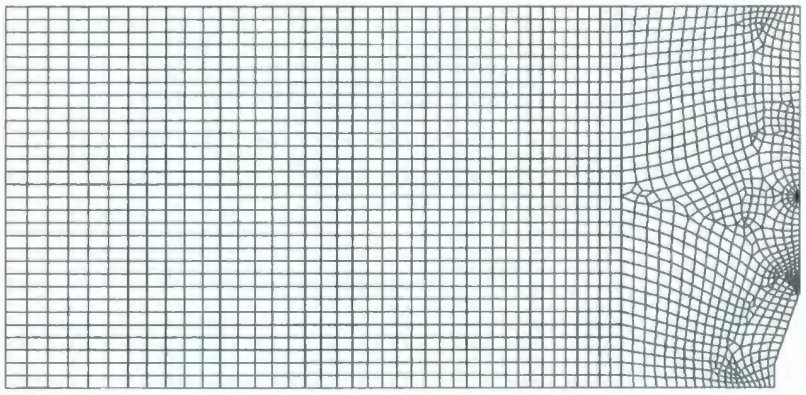

(b)

Figure 7.27: Single edge notched bend: (a) Geometry and dimensions, (b) Typical finite element mesh

Table 7.8: Constraint map parameters, Single edge notched bend

	m^0_{Comp}	$m_{L,Comp}$	$(m^0/m_L)_{Comp}$	m_{Comp}	m_{NFEM}
Point B (Initial point)	3.1052	0.2473	12.5572	0.4914	
Point B' (Alternative method)	3.0837	0.4077	7.5639	0.8014	0.8214
Point B' (Two iterations method)	2.9885	0.5092	5.8691	0.9896	

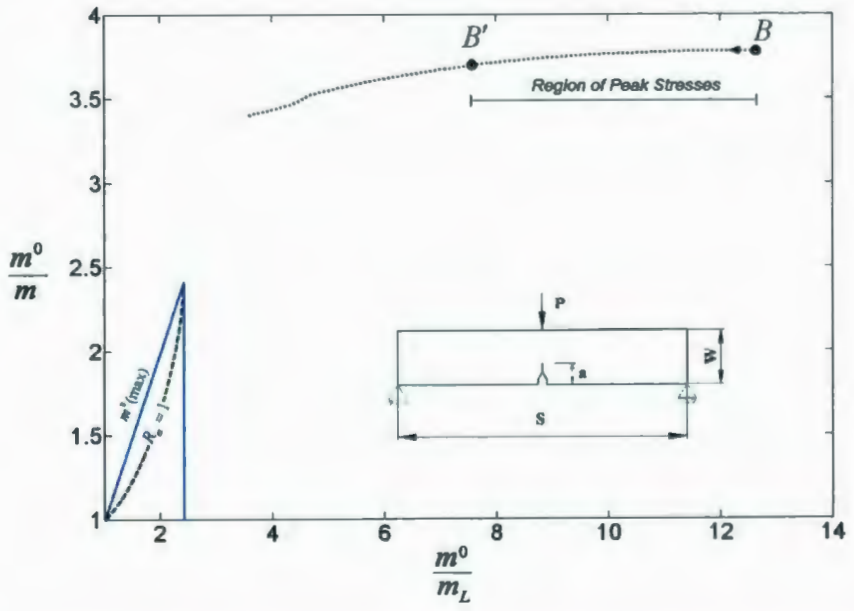

Figure 7.28: Constraint map for single edge notched bend specimen

7.6 FURTHER SIMPLIFICATIONS

As mentioned in this Chapter, when $m^0_{Comp} / m_{L,Comp} > 1+\sqrt{2}$ in the initial elastic solution the magnitude of the peak stresses are considerable. Limit load estimation based on the two-bar method requires that the magnitude of the peak stresses estimated to locate point B' in the constraint map; therefore, the two iterations method was proposed earlier in this Chapter. As mentioned before, $1+\sqrt{2}$ is the transition point that due to the magnitude of the peak stresses the m_α limit load multiplier becomes imaginary. As an approximate method, point B' can be assumed to be located at $1+\sqrt{2}$ along the x-axis in constraint map (see Fig. 7.29). The point B is obtained from a linear elastic FEA whereas point B' is intersection of the assumed horizontal EMAP trajectory with the $m^0 / m_L = 1+\sqrt{2}$ line on the constraint map. Thus, the parameter, λ, can be estimated as

$$\frac{m^0_{Comp}}{m_{L,Comp}} = \frac{1}{\sqrt{\lambda}} \rightarrow \lambda = \left(\frac{m_{L,Comp}}{m^0_{Comp}}\right)^2 = \left(\frac{1}{1+\sqrt{2}}\right)^2 = 0.171$$

Therefore, by applying value of λ at point B' (λ=0.171) into Eq. (7.16) the limit load multiplier can be estimated as

$$m_{Comp} = \frac{m^0_{Comp}}{1.415} \tag{7.28}$$

This method provides rapid estimation of limit load based on only one elastic solution. This simple method is useful for preliminary scoping and feasibility studies of a

given components against failure. Table 7.9 compares the estimated limit load multiplier using one linear elastic solution with inelastic FEA.

Table 7.9: Comparison of estimated limit load multiplier

Example	One elastic method	Inelastic FEA
Indeterminate beam (Fig. 4.3)	10.697	8.735
Non-symmetric rectangular plate (Fig. 7.14)	0.445	0.451
Compact tension specimen (Fig. 4.9)	1.058	0.8210
Middle tension panel (Fig. 7.22)	1.741	2.031
Plate with multiple cracks (Fig. 4.20)	1.652	1.3480

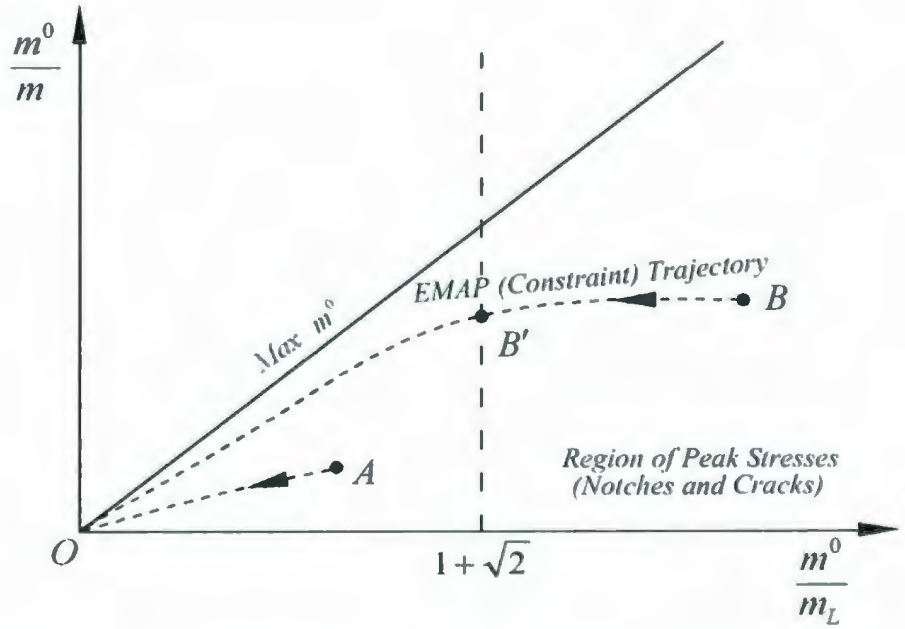

Figure 7.29: Constraint map by considering location of point B' at $1+\sqrt{2}$

7.7 CLOSURE

The concept of equivalence of "static indeterminacy" is invoked to relate multidimensional component configuration to a reference two bar structure in the context of limit load determination. On the basis of Mura's variational theorems, upper and lower bound multipliers are defined, and simple "scaling" relationships are developed. For the crack configuration, in order to eliminate the peak stress at the crack tip, the elastic modulus of the singular elements around the crack tip are modified as one third of original elastic modulus of the component. Several examples are worked out involving component or structure with/without crack(s), and the lower bound limit load estimates are shown to compare well with elastic-plastic FEA or available exact solutions.

CHAPTER 8

INTEGRITY ASSESSMENT PERSPECTIVES

8.1 INTRODUCTION

Cracks and flaws occur in many mechanical components and structures, and sometimes can lead to disastrous failures. The integrity assessment of components with defects is performed to ensure safety and prevent catastrophic failure. In integrity assessment of such components both limit analysis and estimation of fracture mechanics parameters are to be considered.

Based on the limit load estimation method proposed in this thesis, a robust method for estimating the inelastic fracture energy release rate in terms of reference stress and linear elastic fracture parameters for components or structures undergoing hardening material model, e.g., bilinear hardening and Ramberg-Osgood, is proposed. Integrity assessment of two dimensional crack such as in a compact tension specimen, and three-

dimensional configurations such as the axial semi-elliptical (inner) surface, are studied by this method and compared with inelastic finite element analysis. Also, a case study on integrity assessment of a pipe with an axial semi-elliptical crack under cyclic loading is studied.

8.2 EFFECT OF STRAIN HARDENING

In the development of the robust J design procedure, the material behavior is assumed to be elastic perfectly plastic (EPP). However, if the material behavior is elastic-plastic hardening then the approach needs to be modified.

Assuming a hardening material model:

$$\varepsilon = f(\sigma_0, \sigma) \tag{8.1}$$

where σ_0 is a reference value of stress that is usually taken as the yield strength, and σ is the applied stress.

By equating the strain energy densities shown in Fig. 8.1, the strain hardening curve can be represented by an equivalent elastic-perfectly plastic curve in which σ_y^* is the assumed yield strength, i.e., area A_1 should be equal to area A_2. Therefore, σ_y^* can be determined by following equation:

$$\int_{\sigma_0}^{\sigma_y^*}(\varepsilon-\frac{\sigma_0}{E_0})\,d\sigma=\int_{\sigma_y}^{\sigma_f}(\varepsilon-\varepsilon_y^*)\,d\sigma \tag{8.2}$$

where $(\sigma_y^*, \varepsilon_y^*)$ is equivalent yield strength point and $(\sigma,\ \varepsilon)$ is an arbitrary point on a hardening curve, and σ_f related stress to fracture strain, ε_f.

Different material models such as the bilinear hardening (BH) material and Ramberg-Osgood (RO) relationship, have been studied herein. Using the relationship between stress and strain ($\sigma = f(\varepsilon)$ or its inverse $\varepsilon = f^{-1}(\sigma)$), and Eq. (8.2), it is possible to obtain the equivalent yield strength to elastic-perfectly plastic material model.

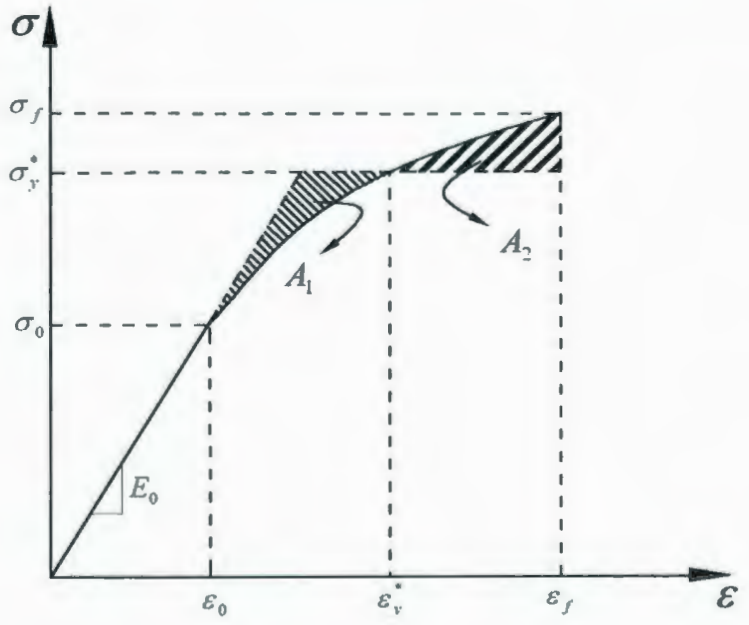

Figure 8.1: Illustrative determination of σ_y^*

8.2.1 Bilinear Hardening Material Model

In Fig. 8.2 the bilinear hardening material model is presented; for which the relationship between stress and strain can be written as:

$$\sigma = \sigma_y + E_P(\varepsilon - \sigma_y / E_0) \tag{8.3}$$

where $E_p = \dfrac{E_t E_0}{E_0 - E_t}$.

Making use of Eq. (8.2), the equivalent yield strength for bilinear hardening material can be obtained as

$$\sigma_y^* = \sigma_y + 0.5 E_p(\varepsilon_f - \sigma_y / E_0) \tag{8.4}$$

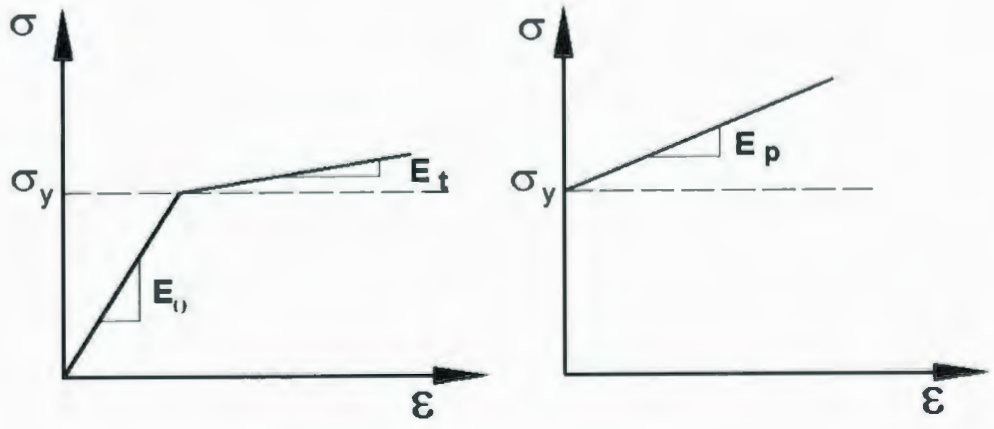

Figure 8.2: Bilinear hardening material model

8.2.2 Ramberg-Osgood Material Model

The Ramberg-Osgood material model can be written as

$$\varepsilon = \frac{\sigma}{E_0} + \frac{\alpha \sigma_0}{E_0}\left(\frac{\sigma}{\sigma_0}\right)^n \tag{8.5}$$

where α is dimensionless material constant, usually chosen to be equal to 3/7, and n is the strain hardening exponent.

Simplifying Eq. (8.2), we get an expression that leads to the equivalent yield strength, σ_y^*

$$a_1 \sigma_y^{*n+1} - a_2 \sigma_y^{*n} + a_3 \sigma_y^{*2} - a_4 \sigma_y^* + a_5 = 0 \tag{8.6}$$

where a_1, a_2, a_3, a_4 and a_5 are expressed in terms of material properties

$$a_1 = \frac{\alpha(n-1)}{(n+1)\sigma_0^{n+1}}$$

$$a_2 = \frac{\alpha \sigma_f}{\sigma_0^{n-1}}$$

$$a_3 = 0.5$$

$$a_4 = 0.5 + \sigma_f - \sigma_0$$

$$a_5 = (\frac{\alpha}{n+1} - 0.5)\sigma_0^2 + \frac{\sigma_f^2}{2} + \frac{\alpha}{(n+1)\sigma_0^{n-1}}\sigma_f^{n+1}$$

Usually, the value of fracture strain, ε_f, is available as a material parameter; therefore, in order to calculate σ_f the following equation needs to be solved

$$\sigma_f^n + \frac{\sigma_0^{n-1}}{\alpha}\sigma_f - \frac{E_0\,\sigma_0^{n-1}\varepsilon_f}{\alpha} = 0 \tag{8.7}$$

8.3 NUMERICAL EXAMPLES

Fracture integrity assessment of several cracks configurations are studied in this section. In order to simulate infinite stress field in the crack vicinity, singular elements have been used in the FEA simulation.

The J-integral estimation technique that is discussed by Seshadri and Wu (2001) is compared with the estimated J-integral based on the R6 method (2004) and inelastic FEA by applying the virtual crack extension method (VCEM) for different material models. The VCEM procedure, incorporated in the ANSYS finite element program (2001), has

been used to evaluate J-integrals. This evaluation is supported by a macro program, using the ANSYS Parametric Design Language (APDL). This program can be conveniently used as part of a post-processing program and uses stress and displacement data from a linear elastic fracture mechanics analysis to calculate the J-integral values. This procedure was carried out for three separate contours around the crack tip, which are shown in Fig. 8.3. Contours 1 and 3 encircle the crack with regular shape, whereas contour 2 has irregular shape. All contour integrals generally showed good path independence, as illustrated in Table 8.1 where the J-values are normalized with respect to the value for elastic energy release rate obtained from stress intensity factor, using Eq. (2.27). Consequently, the values for contour 1 were used throughout this study. It can be seen that the agreement between the two approaches is good.

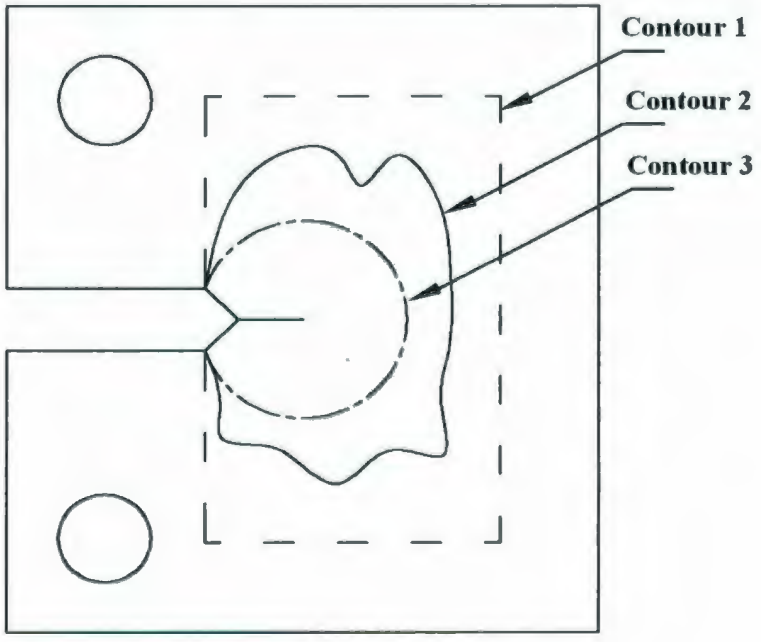

Figure 8.3: J-integral contour paths

Table 8.1: Normalized J-integrals for typical contour paths

Contour	1	2	3
Normalized *J*	0.998	0.988	0.993

Using the method proposed in this Chapter, the inelastic release rate (J) is estimated using the expressions given in R6 routine (Rev. 4, 2001) and by Seshadri and Wu (2001). Making use of Eq. (2.20), the Eq. (2.26) given in R6 (2001) can be expressed as:

$$\frac{J_{e/p}}{J_e} = \frac{1+0.5(L_r)^2}{[0.3+0.7e^{-0.6L_r^6}]^2} \tag{8.8}$$

The following relationship is valid for linear elastic analysis

$$\frac{P}{P_L} = \frac{\sigma_{ref}}{\sigma_y} = \frac{\varepsilon_{ref}}{\varepsilon_y} = \sqrt{\frac{J_e(\varepsilon_{ref})}{J_e(\varepsilon_y)}} \tag{8.9}$$

Therefore, applying Eq. (8.9) into Eq. (2.35), the proposed method by Seshadri and Wu (2001) for evaluating the elastic-plastic J-integral can be rewritten in terms of J_e at a given load,

$$\frac{J_{e/p}}{J_e} = \begin{cases} 1 & 0 \le L_r \le 0.5 \\ 2L_r & 0.5 < L_r < 1 \end{cases} \tag{8.10}$$

8.3.1 Compact Tension Specimen

The J-integral estimates using different methods for EPP materials is presented in Fig. 8.4. If the material model is considered as BH with E_t=0.1 E_0 and the limiting strain of 0.01, then the equivalent yield strength using Eq. (8.4) is σ_y^*=353 MPa. The variation of J, using Eqs. (8.8), (8.10) and inelastic FEA with respect to L_r making use of the new value of yield strength is plotted in Fig. 8.5.

Consider next a compact tension specimen with RO material model (σ_0=250 MPa, n=5, E_0=211 GPa, and ε_f=0.01), for which the stress-strain curve is presented in Fig. 8.6. Using Eq. (8.7), the equivalent yield strength is σ_y^*=369 MPa. The design curve with the new yield strength is presented in Fig. 8.7, where in the nonlinear FEA, the RO material model is implemented in the FEA program.

As it can be seen from Fig. 8.5 and Fig. 8.7, the equivalent yield strength method gives good estimates of J when compared to inelastic FEA using the strain hardening stress-strain curve.

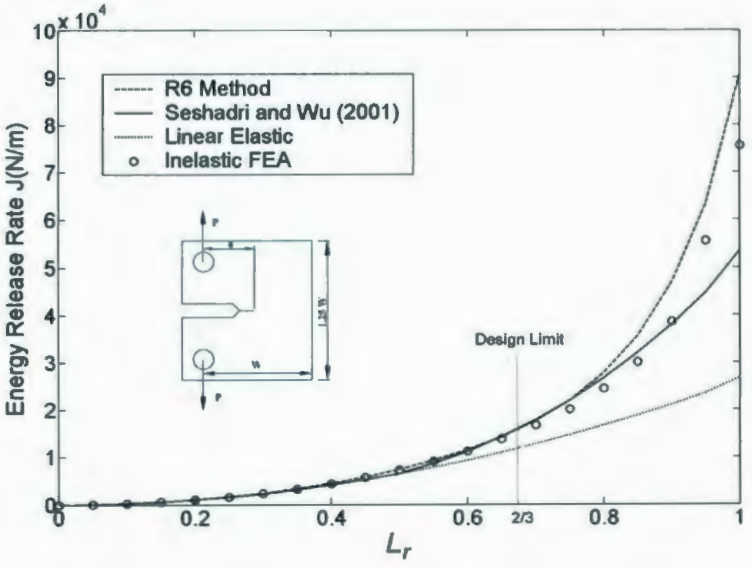

Figure 8.4: Compact tension specimen (J versus L_r), Elastic-perfectly plastic material model

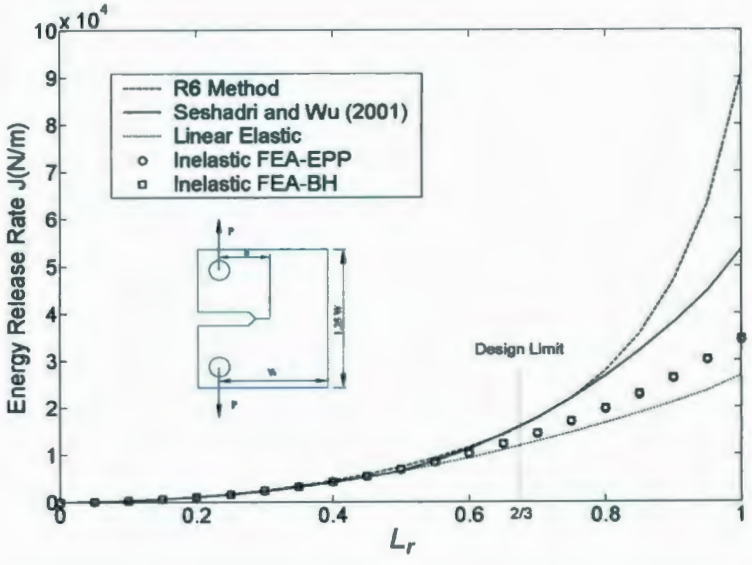

Figure 8.5: Compact tension specimen (J versus L_r) , Bilinear hardening material model

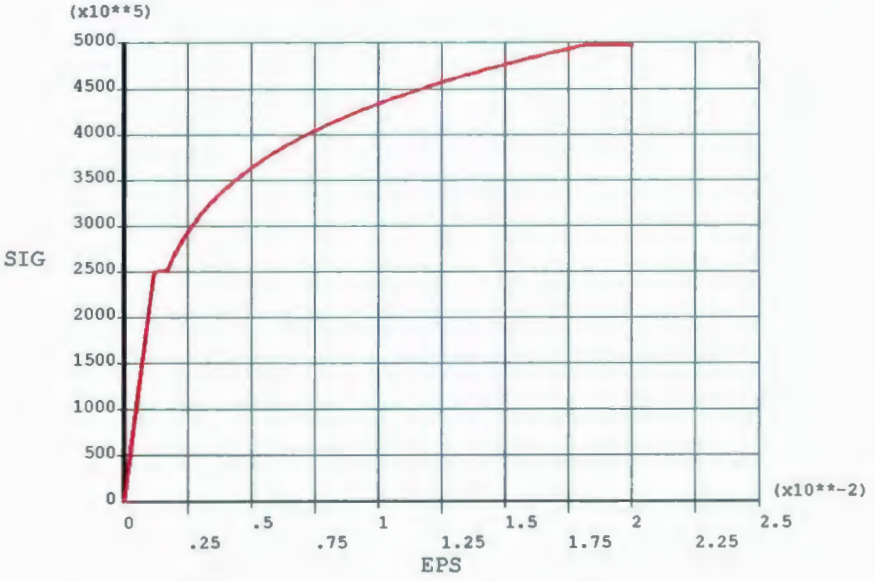

Figure 8.6: Ramberg-Osgood stress-strain curve

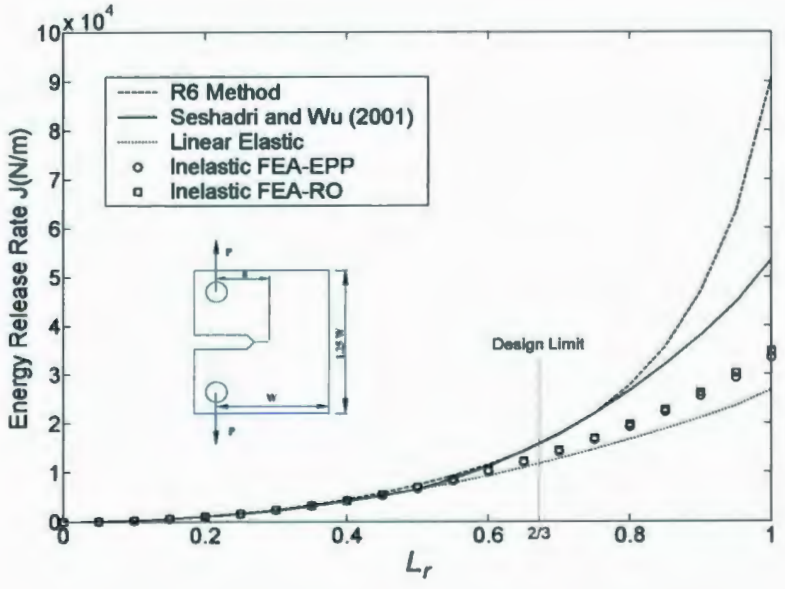

Figure 8.7: Compact tension specimen (J versus L_r), Ramberg-Osgood material model

8.3.2 Axial Semi-Elliptical (Inner) Surface Cracks (3D)

An axial semi-elliptical (inner) surface crack under internal pressure is modeled with the same dimension and material property as in Chapter 4. In some cases where the FEA J-integral estimation is not available the CDF curve can be plotted in terms of normalized nonlinear J-integral on the basis of elastic J-integral at limit load (see Fig. 2.12). The J-integral estimation by different methods for the axial semi-elliptical (inner) surface crack under internal pressure is presented in Fig. 8.8.

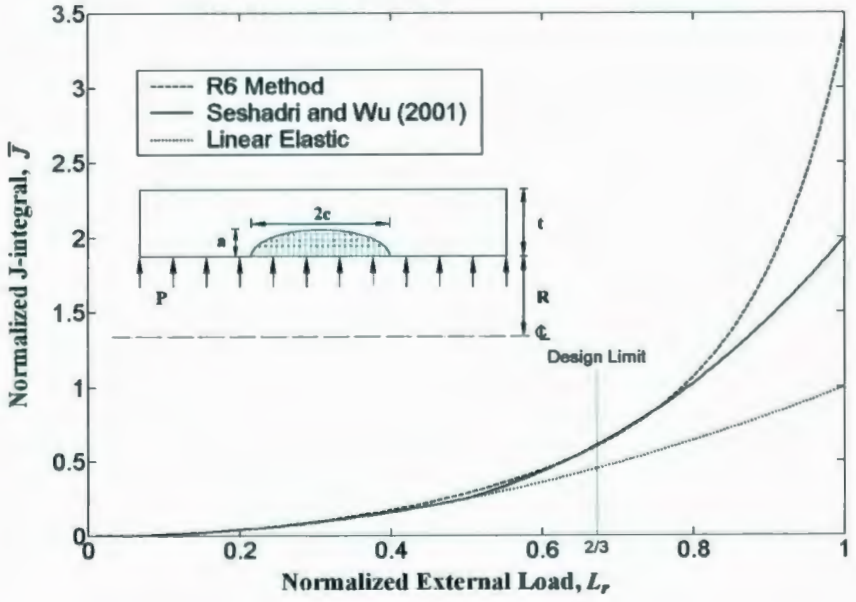

Figure 8.8: Axial semi-elliptical (inner) surface cracked (J versus L_r), Elastic-perfectly plastic material model

8.4 APPLICATION

In this section, the applicability of the methods proposed in this thesis for integrity assessment of typical situation in related industries is examined. The example is hypothetical, but it has some similarities to the condition experienced by the actual component.

Problem statement: The management of a power station wants to assess the integrity of the pipes to ensure that they are capable of carrying a higher load and thereby avoiding unnecessary replacement of the piping system. Several axial part-through wall cracks have been detected during ultrasound test (In this section, only the assessment of a typical pipe geometry is studied).

Material Properties: The pipe is made from BS 4360 Grade 50D steel, the chemical composition and mechanical material properties are summarized in Table 8.2. It is assumed that the stress strain curve follows the Ramberg-Osgood material model, Eq. (8.5), with E=200 GPa, $\sigma_0 = \sigma_y$, n=4.5 and α =5.016. The crack propagation rate is given as:

$$\frac{da}{dN} = 0.39\,\Delta J^{1.64}$$

where da/dN is in mm/cycle and ΔJ is in MN/m.

Table 8.2: Chemical composition and mechanical properties

(Aboutorabi and Cowling, 1986)

Chemical composition (Wt%)								
C	Si	Mn	P	S	Cr	Mo	Cu	Nb
0.17	0.29	1.30	0.010	0.008	0.09	0.01	0.11	0.045

Mechanical properties				
Yield strength (σ_y)	Ultimate strength (σ_U)	Elastic Modulus (E)	Fracture toughness (K_{IC})	Poisson's ratio (ν)
MPa	MPa	GPa	MP√m	
360	558	200	40	0.3

Geometry Description: The most critical crack among the detected cracks is considered for integrity assessment. Because of the large pipe diameter, it is assumed that the crack acts as a surface crack in a thick plate subjected to a tensile stress that is equal to circumferential stress induced in the pipe due to the internal pressure. With refererence to Fig. 8.9, the dimensions for the plate and the crack (the crack is semi-elliptical shape) are summarized in Table 8.3.

Table 8.3: Crack geometry and dimensions

Wall thickness	Crack initial length in radial direction	Crack initial length in longitudinal direction	Inner radius
t=71.5 mm	a_0=0.25 t	c_0=3 a_0	R_i=10 t

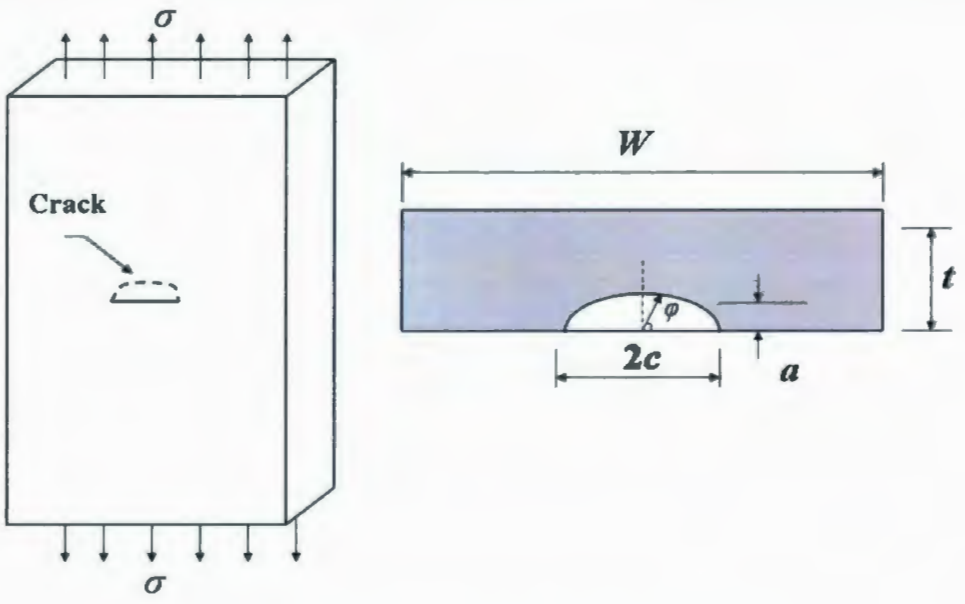

Figure 8.9: Semi-elliptical surface cracked specimen

Loading Condition: For the new loading condition (i.e., fifteen percent more power required), the pipe is subjected to the internal pressure that indicate a circumferential stress of σ_θ=140 MPa that fluctuates between the maximum value and zero at a frequency of 5 times a day.

Methodology: The first step for integrity assessment of the pipe is to determinate the equivalent yield strength (flow stress) using the procedure proposed in this Chapter. It is assumed that the fracture stress is equal to the ultimate strength ($\sigma_f = \sigma_U$). Thus, using Eq. (8.6), the equivalent yield strength is given as:

$$\sigma_y^* = 460.57 \text{ MPa}$$

Reference stress solution

The reference stress solution is given in API (2000) as

$$\sigma_{ref} = \frac{\sigma}{1-F} \tag{8.10}$$

where

$$F = \frac{a/t}{1+t/c} \qquad for\ W \geq (c+t)$$

$$F = (a/t)(c/W) \quad for\ W < (c+t)$$

Stress Intensity Factor

From API (2000), the stress intensity factor can be calculated as:

$$K_I = M_m \sigma \sqrt{\pi \frac{a}{Q}}$$

where

$$Q = 1.0 + 1.464\left(\frac{a}{2c}\right)^{1.65} \qquad for\ a/c \leq 1.0$$

$$Q = 1.0 + 1.464\left(\frac{c}{a}\right)^{1.65} \quad for\ a/c > 1.0$$

$$M = M_s\left[M_1 + M_2\left(\frac{a}{t}\right)^2 + M_3\left(\frac{a}{t}\right)^4\right] g\, f_\varphi\, f_w$$

$$M_s = 1.0$$

$$f_w = \left\{\sec\left(\frac{\pi c}{2c}\sqrt{\frac{a}{t}}\right)\right\}^{0.5}$$

For $a/c \le 1.0$

$$M_1 = 1.13 - 0.09(a/c)$$

$$M_2 = \frac{0.89}{0.2 + a/c} - 0.54$$

$$M_3 = 0.5 - \frac{1}{0.65 + a/c} + 14(1 - a/c)^{24}$$

$$g = 1 + \left[0.1 + 0.35(a/t)^2\right](1 - \sin\varphi)^2$$

$$f_\phi = \left[\sin^2\varphi + (a/c)^2\cos^2\varphi\right]^{1/4}$$

For $a/c > 1.0$

$$M_1 = (a/c)^{0.5}\left[1 + 0.04(c/a)\right]$$

$$M_2 = 0.2(c/a)^4$$

$$M_3 = -0.11(c/a)^4$$

$$g = 1 + \left[0.1 + 0.35(c/a)(a/t)^2\right](1 - \sin\varphi)^2$$

$$f_\phi = \left[\cos^2\varphi + (c/a)^2 \sin^2\varphi\right]^{1/4}$$

Inelastic Energy Release Rate (J)

For cyclic loading, the J-integral estimation proposed by Seshadri and Wu (2001) in Eq. (8.10) can be modified in terms of ΔJ as:

$$\Delta J_{e/p} = \begin{cases} \dfrac{Y^2 \pi a}{E'} \Delta\sigma_{ref}^2 & 0 \le \dfrac{\Delta\sigma_{ref}}{\sigma_y} \le 0.5 \\ \dfrac{2Y^2 \pi a}{\sigma_y E'} \Delta\sigma_{ref}^3 & 0.5 < \dfrac{\Delta\sigma_{ref}}{\sigma_y} < 1 \end{cases} \tag{8.11}$$

where $\Delta\sigma_{ref} = \sigma_{ref}^{\max} - \sigma_{ref}^{\min}$.

The parameter crack configuration factor, Y, can be obtained using following equation

$$Y = \frac{K_I}{\sigma_{ref}\sqrt{\pi a}} \tag{8.12}$$

Critical Crack length

The critical crack length at which the pipe will break is to be estimated in the next step. This can be done in an iterative manner as shown in Fig. 8.10. Using Eq. (2.45), the calculation ceases when $\Delta J_{e/p} = J_{IC}$. The corresponding crack length is considered as the critical crack length. The critical energy release rate, J_{IC}, can be estimated using Eq. (2.47) (assuming Poisson's ratio equal to ν=0.3):

$$J_{IC} = \frac{K_{IC}^2}{E/(1-\nu^2)} = 7.280\times10^3\ [Pa.m]$$

Since the crack propagates in the radial direction as well as the longitudinal direction the critical crack length in both directions is determined. The variation of normalized elastic-plastic J-integral ($J_{e/p}/J_{IC}$) with a/t and c/t at locations φ=0 and φ=π/2 is presented in Fig. 8.11. The critical crack lengths (a_{cr} and c_{cr}) are labeled in this figure as a_{cr}/t =0.506 and c_{cr}/t =1.006 in the depth and length direction, respectively.

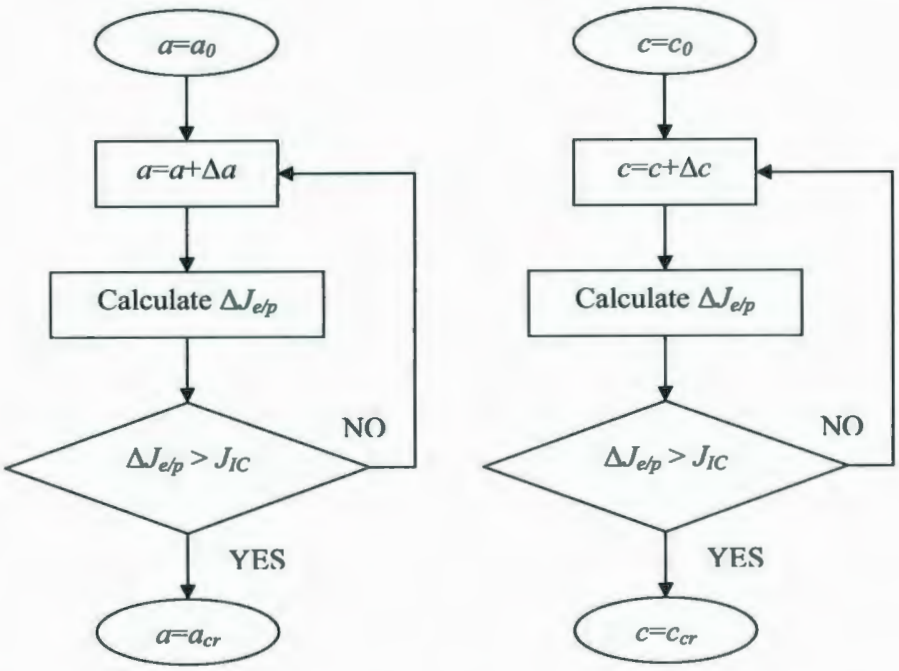

(a) (b)

Figure 8.10: Flow chart of estimating the critical crack length: (a) Depth direction (a_{cr}), (b) Length direction (c_{cr})

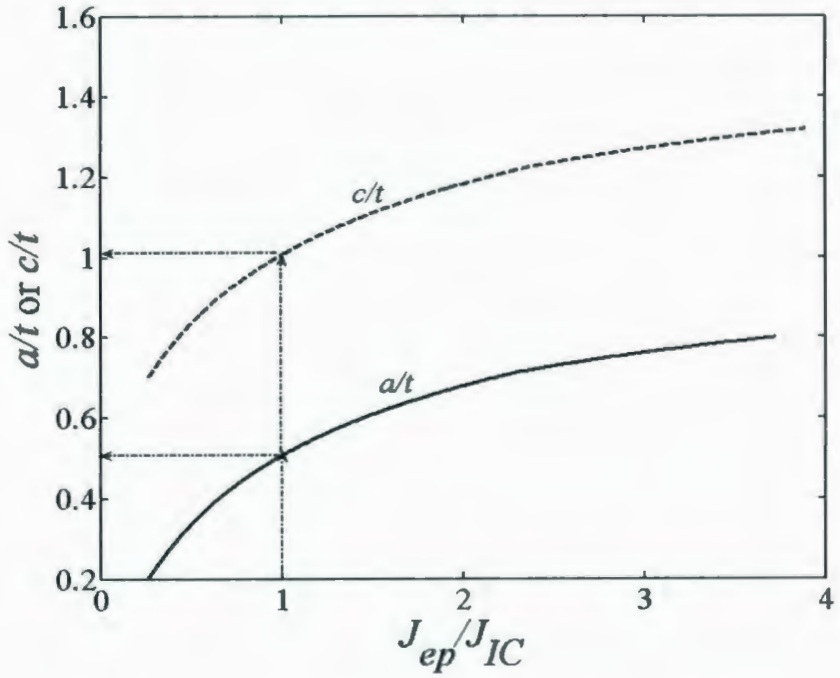

Figure 8.11: Variation of $J_{e/p}/J_{IC}$ with a/t for φ=0 and φ=π/2

Fatigue Propagation Life

The fatigue propagation life (N_p) of the pipe can be estimated by using the procedure presented in Fig. 8.12. Referring to the flow chart in Fig. 8.12, the procedure is terminated when the crack length reaches the critical crack length. Figure 8.13 shows the crack growth rate at the deepest point (φ=π/2) and at the inner surface (φ=π/2).

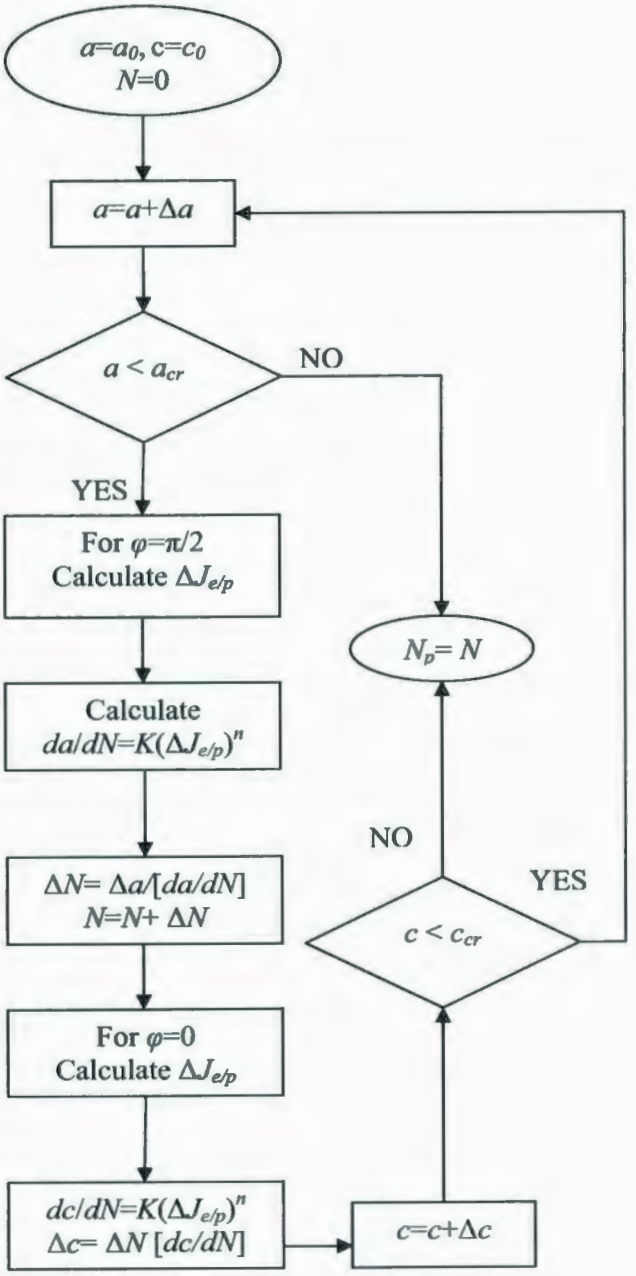

Figure 8.12: Flow chart of estimating the fatigue crack propagation life (N_p)

It can be seen from Fig. 8.13, when $a=a_{cr}$ the fatigue crack propagation life is obtained as N_p=21555 cycles; whereas, for $c=c_{cr}$ the pipe fatigue life is N_p=21460 cycles. Therefore, the final fatigue life is estimated when $a=a_{cr}$ (N_p=21555 cycles as 5 cycles per day or 11.81 years). The predicted fatigue propagation life is compared with the experimental work reported by Aboutorabi and Cowling (1986).

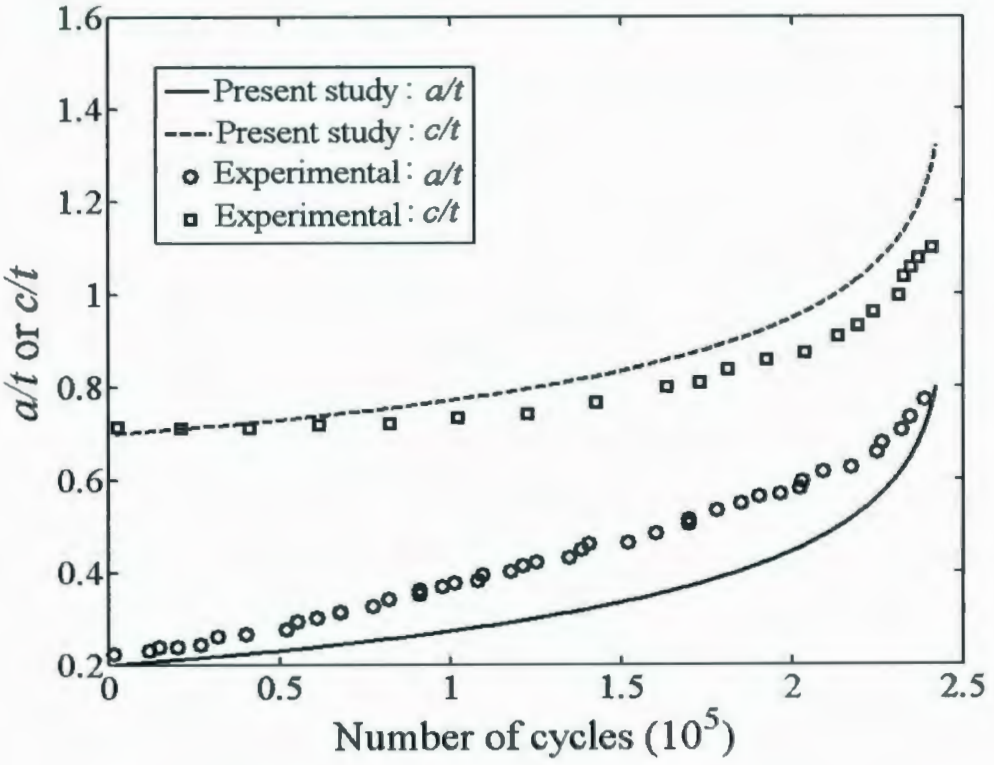

Figure 8.13: Crack growth through the thickness and on the surface

8.5 CLOSURE

The robust method discussed in this Chapter demonstrates a simple and systematic approach for performing the integrity assessments of structure and component with strain hardening material. The proposed method comes in handy for practicing engineers involved in routine design and analysis since the method does not require high cost, time and computer memory, it also is a way for quick and conservative design assessments.

CHAPTER 9

CONCLUSION AND RECOMMENDATION

9.1 CONCLUSION

Inelastic finite element methods are widely used for level 3 integrity assessment of component or structure. However, accurate results are dependent on the specification of adequate mesh density and an assurance of numerically stable solutions. Independent verification methods that are alternatives to inelastic finite element methods are often required for engineering designs. In this thesis, the proposed procedures and methods, based on elastic solution provide rapid and stable solutions for a relatively lower cost.

As a result, developing reasonably accurate methods based on linear elastic analysis would be useful for:

- Preliminary scoping and feasibility studies

- Identification of critical locations in complex components or structures

- New independent methods for verification of inelastic analysis

- Fitness-for-service evaluations

The main contributions in this thesis can be described as follows:

1. A criterion for establishing the degree of convergence of EMAP, and a simple procedure for achieving improved convergence, is developed based on the use of the variable constraint method. Using the variable q concept there is no need to classify the components and structures as previously reported by Seshadri and Mangalaramanan (1997). The parameter q in the general EMAP equation, Eq. (4.1), plays an important role in the convergence and numerical stability of the results during successive linear elastic iterations. Lower values of q provide more stable conditions but result in slow convergence (i.e., requires a larger number of iterations). In contrast, the higher values of q result in a relatively fast convergence but unstable results during the successive iterations.

2. Due to the expected local plastic collapse in components or structure containing defects, the reference volume concept is applied to identify the kinematically active and dead zones in a component. Using the reference volume method, the components or structures can be divided into two main regions at the limit load

state; i.e, reference volume and dead zone. Having the knowledge of the reference volume and dead, the optimum condition (minimum weight design) can be achieved for a given component and structure at limit load state. The reference volume method is shown to give a more accurate prediction of the local limit load.

3. The multiplier m_β, which relies on the entire statically admissible stress distribution rather than the maximum stress, depends on the estimation of the reference parameter, β_R. Based on the reference volume concept, a systematic procedure is developed for estimating β_R, and consequently the corresponding lower bound limit load multiplier, m_β, is obtained. This method estimates a lower bound limit load which is very close to the inelastic limit load.

4. The concept of equivalence of "static indeterminacy" is used to estimate the limit loads for mechanical components and structures. This method relates a multidimensional component configuration to a "reference two-bar structure." Simple scaling relationships are developed that enable the rapid determination of limit load multipliers. The two-bar method provides very rapid estimation of limit load using linear elastic finite element results. The method is shown to be applicable to variety of pressurized component including components with cracks and notched and component with complicated geometry.

5. Limit load multipliers are mostly based on elastic-perfectly plastic models; however, hardening material models are being used to simulate the real behavior

of components. Based on same limit load estimation method proposed in this thesis, a simple procedure for estimating the fracture energy release rate in terms of the reference stress and elastic fracture parameters for components or structures for bilinear hardening and Ramberg-Osgood models, is proposed. The procedure converts a hardening material model to an equivalent elastic–perfectly plastic model.

9.2 RECOMMENDATIONS

Some suggestions for future work can be summarized as follows:

1. The variable q scheme has been developed to improved convergence of EMAP. This method is based on the specification of elastic modulus for two successive iterations; however, the effects of Poisson's ratio need to be studied when using EMAP.

2. Inelastic finite element analysis (FEA) is widely used to estimate the limit loads in a component or structure. However, it can be sometimes diverge from the exact limit load. This can occur when appropriate finite element discretization is not used or other numerical difficulties occur during the iterative solution procedure. The "parameter G" introduced in this thesis, which is indicative of the deviation of any statically admissible stress distributions from the limit state, can be used as a convergence parameter for inelastic FEA. The lower the converged value of G, the

better is the estimate of the limit load, i.e., G=0 would correspond to the converged solution

3. The stress classification concept is widely used in the design of pressure vessels and piping. This means that different types of stress. i.e. primary, secondary and peak stresses require different stress limits as provided by the ASME boiler and pressure vessel codes and standards. The concept of constraint map is introduced in this thesis to provide a robust and effective insight into the study of the stress classification in the components and structures.

4. Integrity assessment of the components and structures made of bilinear hardening and Ramberg-Osgood material models has been studied in this thesis. Also, explicit expressions for converting these two material models to an equivalent elastic-perfectly plastic have been derived. The procedure can be applied to other material models, i.e., power hardening model.

REFERENCES

1. Aboutorabi, A. A., and Cowling, M. J., 1986, "Determination of Stress Intensity Factors for Surface Cracks using Fatigue Crack Growth Data," Int. J. of Fracture, Vol. 31, pp. 67-79.

2. Adibi-Asl, R., Seshadri, R., 2006 "Modulus Adjustment Procedures (EMAP) in Metal Forming Analysis," Transactions of the Canadian Society for Mechanical Engineering, Vol. 30, pp. 239-161.

3. Adibi-Asl, R., Fanous, Ihab F. Z., and Seshadri. R., 2006 "Elastic Modulus Adjustment Procedures-Improved Convergence Schemes," Int. J. of Pressure Vessels and Piping, Vol. 83, pp.154-160.

4. Ainsworth, R. A., 1984, "The Assessment of Defects in Structures of Strain Hardening Materials," Engineering. Fracture Mechanics, Vol. 19, 633-642.

5. Ainsworth, R. A., Bannister, A. C., and Zerbst, U., 2001, "An Overview of the European Flaw Assessment Procedure SINTAP and Its Validation," Int. Journal of Pressure Vessels and Piping, Vol. 77, pp. 869 - 876.

6. Amestoy, M., Bui, H. D., and Labbens, R., 1981, "On the Definition of Local path Independent Integrals on Three-Dimensional Crack problems," Mechanics research communications, Vol. 8, pp. 231-236.

7. Anderson, T. L., 2005, *Fracture Mechanics: Fundamentals and Application*, CRC Press.

8. Anon., 1999, "SINTAP: Structural Integrity Assessment Procedure," Final Revision, EU-Project BE 95-1462, Brite Euram Programme, Brussels, Belgium.

9. ANSYS, 2001, Version 7.1 Online User Guide, SAS IP Inc., Houston, PA.

10. API, 2000, "Recommended Practice for Fitness-For-service," API 579, American Petroleum Institute, Washington DC.

11. ASME, 1998, Boiler and pressure vessel code section III. New York: American Society for Mechanical Engineers.

12. ASME, 1998, Boiler and pressure vessel code section VIII. New York: American Society for Mechanical Engineers.

13. Barbero, E. J., and Reddy, J.N. ,1992, "The Jacobian Derivative Method for Three-dimensional Fracture Mechanics," Communications in Applied Numerical Methods Vol. 6, pp. 507- 518

14. Begley, J. A., and Landes, J. D., 1972, "The J-integral as a Fracture Criterion," In Fracture Toughness, ASTM STP 514, pp. 1-23 and 24-39 (American Society for Testing and Materials, Philadelphia, Pennsylvania).

15. Biron A., and Hodge P. G., 1967, "Limit Analysis of Rotationally Symmetric Shells under Central Boss Loadings by a Numerical Method," J. Appl. Mech., Vol. 34, pp. 644-650.

16. Bloom, J. M., 1980, "Prediction of Ductile Tearing Using a Proposed Strain Hardening Failure Assessment Diagram," Int. J. Fract, Vol. 16, pp. R73-R77.

17. Bochenek, B., Kordas, Z., and Zyczkowski, M., 1983, "Optimal Plastic Design of a Cross-Section under Torsion with Small Bending," J. Struct. Mech. 11, 383–400.

18. Bold, P. E., Brown, M. W., and Allen, R. J., 1992, "A Review of Fatigue Crack Growth in Steels under Mixed Mode I and II Loading," Fatigue and Fracture of Engng. Mater. Struct., Vol. 15, 965-977.

19. Boyle, J. T., Hamilton, R., Shi, J., and Mackenzie, D., 1997, "A Simple Method for Calculating Limit Loads for Axisymmetrivc Thin Shells," ASME J. Pressure Vessel Technology, Vol. 119, pp. 236– 242.

20. BSI, 1999, "Guide on Methods for Assessing the Acceptability of Flaws in Structures", BS 7910, British Institute.

21. Calladine, C. R, 2000, *Plasticity for Engineers*, Horwood Publishing, Chichester, UK.

22. Calladine, C. R., and Drucker, D. C., 1962, "Nesting Surfaces for Constant Rate of Energy Dissipation in Creep;" Q. Appl. Math., Vol. 20, pp. 79-84.

23. Capsoni, A., and Corradi, L., 1997, "A Finite Element Formulation of the Rigid-Plastic Limit Analysis Problem," International Journal for Numerical Methods in Engineering, Vol. 40, pp. 2063-2086.

24. CEN, prEN 13445-3: Part 3. Unfired Pressure Vessels. European Committee for Standardisation (CEN), 1999.

25. Charnes, A., and Greenberg, H. J, 1951, "Plastic Collapse and Linear Programming," Bull. Am. Math. Soc., Vol. 57.

26. Charnes, A., Lemke, C. E., and Zienkiewicz, O. C., 1959, "Virtual Work, Linear Programming and Plastic Limit Analysis" Proceedings of the Royal Society of London. Series A, Mathematical and Physical Sciences, Vol. 251, No. 1264, pp. 110-116.

27. Coffin L. F., 1969, "Manual on Low Fatigue Testing," ASTM STP 465, Introduction.

28. Commissariat a 1'Energy Atomique (CEA), 1999, "A16: Guide for Defect Assessment and Leak Before Break Analysis," draft.

29. Cyras, A.A., 1983, "Mathematical Models for the Analysis and Optimization of Elastoplastic Structures," Chichester: Ellis Horwood Lim.

30. Davis, R. O., and Selvadurai, A. P., 2002, *Plasticity and Geomechanics*, Cambridge University Press.

31. Dems, K., and Mróz, Z., 1978, "Multiparameter Structural Shape Optimization by the Finite Element Method," Int. J. for Numerical Methods in Engineering , Vol. 13, pp. 247 – 263.

32. Dinno, K. S., and Gill, S. S., 1974, "A Method for Calculating the Lower Bound Limit Pressure for Thick Shells of Revolution with Specific Reference to Cylindrical Vessels with Torispherical ends," IJMS 16, 6, 515-427.

33. Dittmann, K. J., 1991 "Ein Beitrag zur Festigkeitsberechnung und Lebensdauervohersage für Bauteile aus Stahl unter Mehrachsiger Synchroner Beanspruchung," PhD Thesis, TU Berlin.

34. Dorn, W. S., and Greenberg, H. S., 1997, "Linear Programming and Plastic Limit Analysis of Structures," Quart. Appl. Math., Vol. 15, 155-167.

35. Dowling, A. R., and Townley, C. H. A., 1975 "The Effect of Defects on Structural Failure: A Two-Criteria Approach," Int J Pre Ves and Piping, Vol. 3, pp. 77-107.

36. Drucker, D. C., and Shield, R. T., 1957, "Design for Minimum Weight", in Proc. 9th Intern. Congr. Appl, Mech., Brussels, Vol. 5, pp. 212-222.

37. Egner, W. 2000 "Optimal Plastic Shape Design of Heads of Plane Tension Members with Skew Bearing Surfaces," Eng. Optim., Vol. 32, 463–483.

38. Egner, W., Kordas, Z., and Zyczkowski, M., 1994, "Optimal Plastic Shape Design via the Boundary Perturbation Method" Struct. Optim., Vol. 8, 145–155.

39. Fanous, Ihab F. Z., Adibi-Asl, R., and Seshadri, R., 2005 "Limit Load Analysis of Pipe Bend Using the R-Node Method," J. of Pressure Vessel Technology, Vol. 127, pp. 487-494.

40. Foulkes, J., 1955, "Linear Programming and Structural Design," Proceeding of the Second Symposium in Linear Programming, Vol. 1, 177-184.

41. Gdoutos,E. E., 1990, *Fracture Mechanics Criteria and Applications*, Kluwer Academic Publishers, Boston and London.

42. Gill, P. E., Murray, W., and Wright, M. H., 1991, "Numerical Linear Algebra and Optimization" Volume 1, Addison-Wesley, Redwood City, CA.

43. Gopinathan, V., 1982, *Plasticity Theory and its Application in Metal Forming*, NewYork, John Wiley.

44. Gerdeen, J. C., 1979, "A Critical Evaluation of Plastic Behavior Data and a United Definition of Plastic Loads for Pressure Components," Welding Research Council Bulletin, Vol. 254.

45. Hamilton, R., Boyle, J., T., Shi, J., and Mackenzie, D., 1996, "A Simple Upper-Bound Method for Calculating Approximate Shakedown Loads," ASME J. Pressure Vessel Technology, Vol. 120, pp. 195-199.

46. Hardy, S. J., Gowhari-Anaraki, A. R., and Pipelzadeh M. K., 2001, "Upper and Lower Bound Limit and Shakedown Loads for Hollow Tubes with Axisymmetric Internal Projections under Axial Loading", J. Strain Analysis, Vol. 36, pp. 595–604.

47. Harrison, R. R., Loosemore, K., Milne, I., and Dowling A. R., 1976,"Assessment of the Integrity of Structures Containing Defects," Report R/H.R6, Central Electricity Generating Board (CEGB).

48. Harrison, R. P., and Milne, I., 1981, "Assessment of Defects: The C.E.G.B. Approach" Philosophical Transactions of Royal Society of London, Vol. 299, pp. 145-153.

49. Hodge, P. G., 1964, "Yield-point Load Determination by Non-linear Programming", 11th ICAM, 554-561.

50. Hodge, P. G., Belytschko, T., "Numerical Methods for the Limit Analysis of Plates", J. Appl. Mech., Vol. 35, pp. 769-801.

51. Iida, S. and Kabayashi, A. S., 1969, "Crack Propagation Rate in 7075-T6 Plates under Cyclic Tensile and Transverse Shear Loading," Trans. ASME, J. Basic Engng, Vol. 91, 764-769.

52. Janković, M., 2001, "The Application of some Approximate Solutions of Stress and Strain Concentration for Life Estimation in the low Cycle Fatigue Region," The Scientific J. FACTA UNIVERSITATIS.

53. Jones, G. L., and Dhalla, A. K., 1981, "Classification of Clamp Induced Stresses in Thin Walled Pipe," ASME PVP, Vol. 81, pp. 17–23.

54. Kachanov, L. M., 1971, *Foundations of the Theory of Plasticity*, North-Holland, Amsterdam.

55. Kikuchi, K., and Miyamoto, H., 1982, "On the Three-Dimensional J integrals," Bull. Frac. Mech. Lab., Science University of Tokyo, Vol. 1, pp. 46-73.

56. Kim, Y. J., Shim, D. J., Huh, N.S., and Kim Y. J. , 2002 "Plastic Limit Pressures for Cracked Pipes using Finite Element Limit Analyses," Int. J. of Pressure Vessels and Piping, Vol. 79 , pp. 321-330

57. Kirkwood, M. G., and Moffat, D. G., 1994, "Plastic Loads for Piping Branch Junctions Subjected to Combined Pressure and In-Plane Moment Loads," Part E, J. Process Mech. Engng., Proc Inst Mech Engrs ImechE , Vol. 208, pp. 31–43.

58. Kobayashi, H., Nakamura, H., Kasai, K. I., Saito, M., Funada, T., Shibata, K., and Iida, K., 1990, "Construction of a Fatigue-Crack-Growth Database for Nuclear-Component Ferritic Steels in Japan and Its Statistical Analysis," Int. J. of Pressure Vessels and Piping. Vol. 44, pp. 67-83.

59. Koopman , D. C . A . and Lance , R . H, 1965, "On Linear Programming and Plastic Limit Analysis," J. Mech. Phys. Solids, Vol. 13, pp. 77-87.

60. Kraus H., 1980, *Creep Analysis*, John Wiley & Sons.

61. Kumar, V., German, M. D., and Shih, C. F., 1981, "An Engineering Approach for Elastic-Plastic Fracture Analysis," EPRI NP-1931, Topical Report, General Electric Company, Schenectady, NY.

62. Lamba, H. S., 1975, "The. J-Integral. Applied to Cyclic. Loading" Engng. Fracture Mechanics, Vol. 7, pp. 693-703.

63. Lee, S. L., Mura, T., and Kao, J. S., 1967, "A Variational Method for the Limit Analysis of Anisotropic Plates," Q. of Applied Mathematics, Vol. 14, pp. 323-330.

64. Li, H., and Mackenzie, D., 2005 "Characterising Gross Plastic Deformation in Design by Analysis", Int. J. Pressure Vessels Piping, Vol. 82 , pp. 777-786.

65. Lyamin, A.V., Sloan, and S.W., 2002a, "Upper Bound Limit Analysis using Linear Finite Elements and Non-linear Programming," Int. J. Numer. Anal. Meth. Geomech., Vol. 26, 181–216.

66. Lyamin, A.V., and Sloan, S.W., 2002b "Lower Bound Limit Analysis using Non-linear Programming," Int. J. Numer. Meth. Engng., Vol. 55, 573–611.

67. Mackenzie, D., and Boyle, J. T., 1993, "A Method of Estimating Limit Loads Using Elastic Analysis, I: Simple Examples," Int. J. Pressure Vessels Piping, Vol. 53, pp. 77–85.

68. Mackenzie, D., Boyle, J. T., and Hamilton, R., 2000, "The Elastic Compensation Method for Limit and Shakedown Analysis: A Review," J. Strain Analysis, Vol. 35, pp. 171–188.

69. Mackenzie, D., Shi J, and Boyle, J. T., 1994, "Finite Element Modeling for Limit Analysis using the Elastic Compensation Method," Comp. Struct., Vol. 51, pp. 403-410.

70. Mangalaramanan, S. P., and Seshadri, R., 1997, "Minimum Weight Design of Pressure Components Using R-Nodes," ASME J. Pressure Vessel Technology, Vol. 119, pp. 224– 231.

71. Manson, S. S., 1965, "Fatigue: A Complexe Subject-Some Simple Approximations," Experimental Mechanics, pp. 193-226.

72. Marriott, D. L., 1988, ''Evaluation of Deformation or Load Control of Stress under Inelastic Conditions using Elastic Finite Element Stress Analysis,'' ASME-PVP Conference. Pittsburgh, Vol. 136, pp. 3–9.

73. Mendelson, A., 1968, *Plasticity*: *Theory and Application*, Macmillan Co., New York.

74. Miller, A. G., 1988 "Review of Limit Loads of Structures Containing Defects," Int. J. Pressure Vessels and Piping, Vol. 32, 97–327.

75. Milne, I., Ritchie, R.O., and Karihaloo, B., 2003, "Comprehensive Structural Integrity: 10 - Volume set," Elsevier 2003, United Kingdom.

76. Moffat, D. G., Hsieh, M. F., and Lynch, M., 2001, "An Assessment of ASME III and CEN TC54 Methods of Determining Plastic and Limit Loads for Pressure System Components", J. Strain Analysis, Vol. 36, pp. 301–312.

77. Mohamed, A. I., Bayoumi, L. S., Megahed, M. M., and Younan, M. Y. A., 1999, "Applications of Iterative Elastic Techniques for Elastic-Plastic Analysis of Pressure Vessels," ASME J. Pressure Vessel Technology, Vol. 121, pp. 24-29.

78. Molski, K., and Glinka, G. , 1981 "A Method of Elastic-Plastic Stress and Strain Calculation at a Notch Root," Materials Science and Engineering, vol. 50, pp. 93-100.

79. Mura, T., Kao, J. S., and Lee, S. L., 1964, "Limit Analysis of Circular Orthotropic Plates," Journal of the Engineering Mechanics Division, ASCE, Vol. 90, pp. 375-395.

80. Mura, T., and Lee, S. L., 1963, "Application of Variational Principles to Limit Analysis," Quarterly of Applied Mathematics, Vol. 21, pp. 243–248.

81. Mura, T., Rimawi, W. H., and Lee, S. L., 1965, "Extended Theorems of Limit Analysis," Q. of Applied Mathematics, Vol. 23, pp. 171–179.

82. Narasimhan, R., and Rosakis, A. J., 1988, "Three-Dimensional Effects Near a Crack Tip in a Ductile Three Point Bend Specimen. Part I: Numerical Analysis," J. of Applied Mechanics, Vol. 57, pp. 607–617.

83. Nadarajah, C., Mackenzie, D., and Boyle, J. T., 1996, "Limit and Shakedown Analysis of Nozzle/Cylinder Intersections under Internal Pressure and In-Plane Moment Loading," Int. J. Pressure Vessels Piping, Vol. 68, pp. 261–272.

84. Neuber, H., 1961, "Theory of Stress Concentration for Shear Strained Prismatic Bodies with Arbitrary Non-linear Stress-strain Law," ASME. J. of Appl. Mech. Vol. 26, pp. 544-550.

85. Newman, Jr., J. C., and, Raju, I. S., 1980 "Stress Intensity Factors for Internal Surface Cracks in Cylindrical Pressure Vessel," ASME J. Pressure Vessel Technology, Vol. 102, pp. 342–346

86. Pan, L., and Seshadri, R., 2002, "Limit Analysis for Anisotropic Solids using Variational Principle and Repeated Elastic Finite Element Analyses," ASME- PVP-Vol. 442, pp. 149–155.

87. Pan, L., and Seshadri, R., 2002, "Limit Loads for Layered Structures Using Extended Variational Principles and Repeated Elastic Finite Element Analysis," ASME J. Pressure Vessel Technology, Vol. 124, pp. 425-432.

88. Pan, L., and Seshadri, R., 2001, "Limit Load Estimation using Plastic Flow Parameter in Repeated Elastic Finite Element Analysis," ASME J. Pressure Vessel Technology, Vol. 124, pp. 433-439.

89. Paris, P. C., 1963, "The Fracture Mechanics Approach to Fatigue," In Proceedings of 10th Sagamore Conference, (Syracuse University Press, Syracuse, New York).

90. Plancq, D., and Berton, M. N., 1998, "Limit Analysis Based on Elastic Compensation Method of Branch Pipe Tee Connection under Internal Pressure and Out-Of-Plane Moment Loading," Int. J. Pressure Vessels Piping, Vol. 75, pp. 819–825.

91. Ponter, A. R. S., and Leckie, F. A., 1970, "Application of Energy Theorems to Bodies which Creep in the Plastic Range", J. of Applied Mechanics, Vol. 37, pp. 753-758.

92. Ponter, A. R. S., Fuschi, P., and Engelhardt, M., 2000, "Limit Analysis for a General Class of Yield Conditions," Eur. J. Mech. A/Solids, Vol. 19, pp. 401–421.

93. Ponter, A. R. S, and Carter, K. F., 1997, "Limit State Solution upon Linear Elastic Solutions with a Spatially Varying Elastic Modulus," Computer Methods in Applied Mechanics and Engineering, Vol. 140, pp. 237-258.

94. Ponter, A. R. S., and Chen, H., 2001, "A Programming Method for Limit Load and Shakedown Analysis of Structures," ASME PVP, Vol. 430, pp. 155–160.

95. R6, "Assessment of Integrity of Structures Containing Defects", Revision 4, British Energy; 2001.

96. Reinhardt, W. D., and Mangalaramanan, S. P., 2001, "Efficient Tubesheet Design Using Repeated Elastic Limit Analysis," ASME J. Pressure Vessel Technology, Vol. 123, pp. 197– 202.

97. Reinhardt, W. D., and Seshadri, R., 2003, "Limit Load Bounds for the m_α Multipliers," ASME J. Pressure Vessel Technology, Vol. 125, pp. 11– 18.

98. Rice, J. R., 1968, "A Path Independent Integral and the Approximate Analysis of strain Concentration by Notches and cracks," ASME Journal of Applied Mechanics, Vol. 35, pp. 379-286.

99. Robertson, A., Li, H., and Mackenzie, D., 2005, "Plastic Collapse of Pipe Bends under Combined Internal Pressure and In-plane Bending," Int. J Pressure Vessel and Piping Vol. 82, pp. 407–16.

100. Sacchi G, and Save M., 1968, "On the Evaluation of the Limit Load for Rigid-Perfectly Plastic Continua," Meccanica, Vol. 3, pp. 199-206.

101. Save, M. and Prager W. 1985, "Structural Optimization, Vol. 1, Optimality Criteria", New York, Plenum Press.

102. Saxena, A., 1998, *Non-linear Fracture Mechanics,* CRC Press.

103. Seshadri, R., 1991, "The Generalized Local Stress Strain GLOSS Analysis—Theory and Applications," ASME J. Pressure Vessel Technology, Vol. 113, pp. 219– 227.

104. Seshadri, R., 1994, "Residual Stress Estimation and Shakedown Evaluation using GLOSS Analysis," ASME J. Pressure Vessel Technology, Vol. 116, pp. 290–294.

105. Seshadri, R., 1998, "Simplified Methods in Plasticity, Creep and Fracture - Some Recent Developments," Trans. of the Canadian Society for Mechanical Engineering," Vol. 22, pp. 419 – 433.

106. Seshadri, R., and Babu, S., 2000, "Extended GLOSS Method for Determining Inelastic Effects in Mechanical Components and Structures: Isotropic Materials," ASME J. Pressure Vessel Technology, Vol. 122, pp. 413– 420.

107. Seshadri, R., and Fernando, C. P. D., 1992, "Limit Loads of Mechanical Components and Structures using the GLOSS R-Node Method," ASME J. Pressure Vessel Technology, Vol. 114, pp. 201–208.

108. Seshadri, R., and Indermohan, H., 2004, "Lower Bound Limit Load Determination: The m_β-multiplier Method," ASME J. Pressure Vessel Technology, Vol. 126, pp. 237– 240.

109. Seshadri, R., and Kizhatil. R. K., 1993, "Notch Root Inelastic Strain Estimates using GLOSS Analysis," Advances in Multiaxial Fatigue, ASTM STP 1191. D. L. Mc-Dowell and R. Ellis, Eds., American Society for Testing and Materials. Philadelphia pp. 397-411.

110. Seshadri, R., and Kizhatil, R. K., 1995, "Robust Approximation Methods for Estimating Inelastic Fracture Parameters," ASME J. Pressure Vessel Technology, Vol. 117, pp. 115– 123.

111. Seshadri, R., and Mangalaramanan, S. P., 1997, "Lower Bound Limit Load Using Variational Concepts: The m_α -Method," Int. J. Pressure Vessels Piping, Vol. 71, pp. 93-106.

112. Seshadri, R., and Marriot, D. L., 1993, "On Relating the Reference Stress, Limit Load, and the ASME Stress Classification Concepts," Int. J Pressure Vessel and Piping Vol. 56, pp. 382–408.

113. Seshadri, R., and Wu, S., 2001, "Robust Estimation of Inelastic Fracture Energy Release Rate (*J*): a Design Approach", ASME J. Pressure Vessel Technology, Vol. 123, pp. 241-219.

114. Shih, C. F., and Hutchison, J. W., 1976, "Fully Plastic Solutions and Large Scale Yielding Estimates for Plane Stress Crack Problems," ASME J. Engineering Materials and Technology, Vol. 98, pp. 289-295.

115. Sim, R. G., 1968, "Creep of structures", PhD dissertation, University of Cambridge

116. Socie, D. F., Hua, C. T., and Worthem, D. W., 1987, "Mixed mode small crack growth. Fatigue and Fracture of Engng Mater. Struct., Vol. 10, 1-16.

117. Szczepinski, W. and Szlagowski, J., 1990, Plastic design of complex shape structures, Warszawa : PWN; Chichester [England] : E. Horwood.

118. Tanaka, K., 1974 "Fatigue Crack Propagation from a Crack Inclined to the Cyclic Tensile Axis," Engng. Fracture Mechanics" Vol. 6, 493-507.

119. Theocaris, P. S., Kardomateas, G. A. and Andrianopoulos, N. P. 1982, "Experimental Study of the T-criterion in Ductile Fracture," Engng. Fracture Mechanics, Vol. 17, 439-447.

120. Topper, T. H. and Gowda, C. V. B. G., 1970, "Local Stress-Strain Approach to Fatigue Analysis and Design," In ASME Design Engineering Conference, Chicago, Illinois, paper 70- DE-24.

121. Townley, C. H. A., Findlay, G. E., Goodman A.M., and Stanley, P., 1971, "Elastic–Plastic Computations as a Basis for Design Charts for Torispherical Pressure Vessel Ends", Proc I Mech E, Vol. 185, pp. 869–877.

122. Webster, G. A., and Ainsworth, R. A., 1994, *High Temperature Component Life Assessment*, London,. Chapman and Hall.

123. Wu, S., and Seshadri, R., 1996, "A Simplified Three-Dimensional Model for Analyzing Pressure Components With Defects," ASME-PVP Conference, Vol. 324, pp. 35–46.

124. Yang, P., Liu, Y., Ohtake, Y., Yuan, H., and Cen, Z., 2005, "Limit Analysis Based on a Modified Elastic Compensation Method for Nozzle-to-Cylinder Junctions," Int. J. Pressure Vessels Piping, Vol. 82, pp. 770–776.

125. Zavelani, A., 1973, "A Compact Linear Programming Procedure for Optimal Design in Plane Stress" J. of Structural Mechanics. Vol. 2, pp. 301-324.

126. Zerbst, U., Ainsworth, R. A., and Schwalbe, K. H., 2001, "Basic Principles of Analytical Flaw Assessment Methods," Int. J. Pressure Vessels Piping, Vol. 77, pp. 855 - 867.

127. Zouain, N., Herskovits, J., Borges, L.A., and Feijóo, R.A., 1993, "An Iterative Algorithm for Limit Analysis with Nonlinear Yield Functions," Int. J. Solids Struct. 30, 1397–1417.

128. Zyczkowski, M., 1981, *Combined loadings in the theory of plasticity*, Polish-Scientific Publ.

PUBLICATIONS

1. R. Adibi-Asl, and R. Seshadri, 2007, "Simplified Limit Load Estimation of Components with Cracks using the Reference Two-Bar Structure," ASME Journal of Pressure Vessel Technology (In press).

2. R. Adibi-Asl, and R. Seshadri, 2007, "Limit Load Analysis of Cracked Components using the Reference Volume Method," ASME Journal of Pressure Vessel Technology, pp. 391-399, No. 3, Vol.129.

3. R. Seshadri, and R. Adibi-Asl, 2007, "Limit Loads of Pressure Components using the Reference Two-Bar Structure," ASME Journal of Pressure Vessel Technology, pp. 280-286, No. 2, Vol.129.

4. R. Adibi-Asl, and R. Seshadri, 2007, "Local Limit Load Analysis using the M-Beta Method," ASME Journal of Pressure Vessel Technology, pp. 296-305, No. 2, Vol.129.

5. R. Adibi-Asl, and R. Seshadri, 2006, "Modulus Adjustment Procedures (EMAP) in Metal Forming Analysis," CSME Transactions, pp. 239-260, No. 2, Vol. 30.

6. R. Adibi-Asl, Ihab F. Z. Fanous, and R. Seshadri, 2006, "Elastic Modulus Adjustment Procedures-Improved Convergence Schemes," Int. Journal of Pressure Vessels and Piping, pp. 154-160, No. 2, Vol. 83.

7. Ihab F. Z. Fanous, R. Adibi-Asl, and R. Seshadri, 2005, "Limit Load Analysis of Pipe bend Using the R-Node Method," ASME J Pressure Vessel Technology, pp. 443-448, No. 4, Vol. 127.

APPENDIX A

ANSYS INPUT FILE

An ANSYS macro is written to implement the elastic modulus adjustment procedure (EMAP). The results of stresses and volumes for all the elements at each subsequent iteration are stored in a file named as "main.dat". The parameters are stored in this file will be used as an input file for the MATLAB script in Appendix B to calculate the limit load multipliers, reference volumes and other parameters discussed in this thesis.

```
!********** PARAMETERS **************
ALLSEL,ALL

Ex=200e9   ! Modulus of Elasticity
Nu=0.3     ! Poisson's Ratio

multipro,'start',2
*cset,1,3,itter,'No. OF ITTERATION',10
*cset,4,6,'criter','ELEMENT MODIFICATION CRITERION',0.000001
*cset,61,62,'Input the parameters'
*cset,63,64,'or use default'
multipro,'end'

multipro,'start',2
*cset,1,3,Full,'Full Region',1
*cset,4,6,Partial,'Partial Region',0
*cset,61,62,'Input the parameters'
*cset,63,64,'or use default'
multipro,'end'

*IF,Full,EQ,0,THEN
multipro,'start',8
*cset,1,3,AREA1,,1
*cset,4,6,AREA2,,2
*cset,7,9,AREA3,,3
*cset,10,12,AREA4,,4
*cset,13,15,AREA5,,5
```

```
*cset,16,18,AREA6,,6
*cset,19,21,AREA7,,7
*cset,22,24,AREA8,,8
*cset,61,62,'CHOOSE THE AREAS FOR MODIFICATION'
*cset,63,64,'PUT AREA NUMBER'
multipro,'end'
*ENDIF

!************************************
!******** PRE PROCESSING ************
!************************************
/prep7

*IF,Full,EQ,0,THEN
ASEL,S, , ,     AREA1      ! Choosing the proper area
ASEL,A, , ,     AREA2
ASEL,A, , ,     AREA3
ASEL,A, , ,     AREA4
ASEL,A, , ,     AREA5
ASEL,A, , ,     AREA6
ASEL,A, , ,     AREA7
ASEL,A, , ,     AREA8
ESLA,S,1
*ENDIF

*get,nelem,elem,,COUNT,    ! Count No. of ELEMENT
*GET, EMIN, ELEM,  0, NUM, MIN
*GET, EMAX, ELEM,  0, NUM, MAX

EPRE=EMIN-1
  *do,k,1,nelem                ! Assign each element MP
  *GET, EPRO, ELEM,EPRE, NXTH
      mp,EX,EPRO,Ex
      mp,NUXY,EPRO,nu
      *if,miu,GT,0,THEN
      mp,MU,EPRO,miu
      *endif
      *if,density,GT,0,THEN
      MP,dens,EPRO,density
      *endif
     mpchg,EPRO,EPRO     !CHANGE MP COMMAND
     EPRE=EPRO
   *enddo
    ALLSEL,ALL
finish

*get,nnode,node,,COUNT,  ! No. of nodes


!************ ARRAYS ***************

 *dim,seqmxt,,itter
 *dim,itt,,itter
```

```
*dim,Emt,,nelem      ! Em (Modification Modules) at each element
*dim,Nut,,nelem      ! Nu at each element


*DIM,StsTable,ARRAY,nelem,itter,1, , ,
*DIM,StnTable,ARRAY,nelem,itter,1, , ,
*DIM,VolTable,ARRAY,nelem,itter,1, , ,
*DIM,S1Table,ARRAY,nelem,itter,1, , ,
*DIM,S2Table,ARRAY,nelem,itter,1, , ,
*DIM,S3Table,ARRAY,nelem,itter,1, , ,

!*********************************************
*IF,Full,EQ,0,THEN
ASEL,S, , ,      AREA1      ! Choosing the proper area
ASEL,A, , ,      AREA2
ASEL,A, , ,      AREA3
ASEL,A, , ,      AREA4
ASEL,A, , ,      AREA5
ASEL,A, , ,      AREA6
ASEL,A, , ,      AREA7
ASEL,A, , ,      AREA8
ESLA,S,1
*ENDIF

    *do,i,1,nelem
        Emt(i)=Ex
        Nut(i)=Nu
     *enddo
ALLSEL,ALL
finish

*VFILL, StsTable, Ramp, 1,0
!@@@@@@@@@@@@@@@@@@@@@@@@@@@@@@@@@@@@
 *Do,j,1,itter
!@@@@@@@@@@@@@@@@@@@@@@@@@@@@@@@@@@@@

!************************************
!******** PRE PROCESSING ************
!************************************

/prep7
*IF,Full,EQ,0,THEN
ASEL,S, , ,      AREA1      ! Choosing the proper area
ASEL,A, , ,      AREA2
ASEL,A, , ,      AREA3
ASEL,A, , ,      AREA4
ASEL,A, , ,      AREA5
ASEL,A, , ,      AREA6
ASEL,A, , ,      AREA7
ASEL,A, , ,      AREA8
ESLA,S,1
*ENDIF
```

```
*MSG, UI,j
Iteration = %G

   EPRE=EMIN-1
  *do,i,1,nelem                    ! Assign each elemnt MP
  *GET, EPRO, ELEM,EPRE, NXTH
        mp,EX,EPRO,Emt(i)      !CHANGING MP(EX)
        mp,NUXY,EPRO,Nut(i)

        EPRE=EPRO
         *enddo
ALLSEL,ALL
finish
!************************************
!******** SOLUTION *****************
!************************************
/solu
solve
finish
!************************************
!******** POST PROCESSING *********
!************************************
/post1
*IF,Full,EQ,0,THEN
ASEL,S, , ,      AREA1      ! Choosing the proper area
ASEL,A, , ,      AREA2
ASEL,A, , ,      AREA3
ASEL,A, , ,      AREA4
ASEL,A, , ,      AREA5
ASEL,A, , ,      AREA6
ASEL,A, , ,      AREA7
ASEL,A, , ,      AREA8
ESLA,S,1
*ENDIF


*MSG, UI,j
Iteration = %G


ETABLE,seqvt,S,EQV
ETABLE,eeqvt,EPTO,EQV
ETABLE,volt ,VOLU,
ETABLE,s1t,S,1
ETABLE,s2t,S,2
ETABLE,s3t,S,3


PLETAB,SEQVt,AVG          ! Based on Max. Elemental


*get,seqmx,plnsol,,max      ! seqmx=Maximum Eq. Stress
seqmxt(j)=seqmx
```

```
 EPRE=EMIN-1
*do,i,1,nelem

*GET, EPRO, ELEM,EPRE, NXTH
 esel,s,elem,,EPRO,EPRO


      *get,seqel,elem,EPRO,etab,seqvt
      *get,eeqel,elem,EPRO,etab,eeqvt
      *get,volel,elem,EPRO,etab,volt
      *get,s1,elem,EPRO,etab,s1t
      *get,s2,elem,EPRO,etab,s2t
      *get,s3,elem,EPRO,etab,s3t

StsTable(i,j)=seqel
StnTable(i,j)=eeqel
VolTable(i,j)=volel
S1Table(i,j)=s1
S2Table(i,j)=s2
S3Table(i,j)=s3

       EPRE=EPRO
       allsel,all
     *enddo


!***** Arbitrary Stress **************


z1=0
z2=0


    *do,m,1,nelem
ztemp1=(StsTable(m,j)*StsTable(m,j)*VolTable(m,j))
ztemp2=VolTable(m,j)

z1=z1+ztemp1
z2=z2+ztemp2
     *enddo

sarbit=SQRT(z1/z2)

!****************************************
i=0
!****************************************
nu=0.49


    *do,i,1,nelem
        ratio=(StsTable(i,j)/sarbit)
      *IF,ratio,LT,criter,THEN
      Emt(i)=1*Ex
        q=(log((1+ratio**2)/2))/(log(ratio))
```

```
                    *else
            *if,ratio,GE,1,THEN
                q=(log((1+ratio**2)/2))/(log(ratio))

  Emt(i)=(sarbit/StsTable(i,j))**q*Emt(i)   ! Modification Modulus

                Nut(i)=nu
                 *endif
            *if,ratio,LT,1,THEN
                q=(log((1+ratio**2)/2))/(log(ratio))

  Emt(i)=(sarbit/StsTable(i,j))**q*Emt(i)   ! Modification Modulus

                Nut(i)=nu
             *endif
        *endif
      *enddo
!*****************************************
finish
       ALLSEL,ALL

itt(j)=j

!@@@@@@@@@@@@@@@@@@@@@@@@@@@@@@@@@@@@@@
*ENDDO
!@@@@@@@@@@@@@@@@@@@@@@@@@@@@@@@@@@@@@@


*CFOPEN,main,dat,
 *do,j,1,itter
  *do,i,1,nelem
  cont=i
seq=StsTable(i,j)
eeq=StnTable(i,j)
vol=VolTable(i,j)
s1=S1Table(i,j)
s2=S2Table(i,j)
s3=S3Table(i,j)

  *VWRITE,cont,seq,eeq,vol,s1,s2,s3
 ((F10.1,x),(F24.3,x),(F24.18,x),(F24.18,x),3(F20.3,x))
 *enddo
 *enddo
*cfclos
```

APPENDIX B

MATLAB CODE

The MATLAB code is written to calculate the different parameter such as limit load multipliers, reference volume and etc. Different plots generated in this thesis are generated using the following code. This code requires an input file named as "main.dat" that is the output of the linear elastic FEA from Appendix A.

```
%************************************************************

clear


set(0,'DefaultAxesFontSize',30)
set(0,'DefaultLineLineWidth',2.3)
set(0,'DefaultLineMarkerSize',11)
set(0,'DefaultAxesGridLineStyle','--')
set(0,'DefaultAxesLineWidth',2)

tiltles=32;
labels=42;
lines=3;
divition=30;
legen=32;

itter=10;          % No. of iterations
sy=250e6  ;        % Yield Stress
NFEM=0.7415;  % Inelastic FEA limit load multiplier (for comparison)
%************************************************************

path(path,'D:/workplane/')    % Destination of the main file

fid = fopen('main.dat','r');
a = fscanf(fid,'%g %g',[7 inf]);
a = a';
fclose(fid);

cont=a(:,1);
```

```
seq=a(:,2);
eeq=a(:,3);
vol=a(:,4);
s1=a(:,5);
s2=a(:,6);
s3=a(:,7);

m1=length(cont);

n=m1/itter;
%************************************************************
            %@ CONVERTING TO ITTERATIONS @%
k=0;
for j = 1:itter;

  for i = 1:n;
      k=k+1;
      seqtot(i,j)=seq(k);
      eeqtot(i,j)=eeq(k);
      voltot(i,j)=vol(k);
   end;
end;
          %@ SORTING BASED ON MAX. STRESSES @%
k=0;
 for k = 1:itter;
  for i = 1:n;
     for j=i+1:n;
      if seqtot(i,k)<seqtot(j,k); % ##########

         temp=seqtot(i,k);
         seqtot(i,k)=seqtot(j,k);
         seqtot(j,k)=temp;

         temp=eeqtot(i,k);
         eeqtot(i,k)=eeqtot(j,k);
         eeqtot(j,k)=temp;

         temp=voltot(i,k);
         voltot(i,k)=voltot(j,k);
         voltot(j,k)=temp;

      end;
     end;
   end;
end;
%************************************************************

for j = 1:itter
  mnfem(j)=NFEM;
  itteration(j)=j;
end

          % #### UPPER BOUND ####
```

```
% CLASSICAL UPPER BOUND

for j = 1:itter;
   tempA1=0;
   tempA2=0;


   for i = 1:n;

   tempB1=(eeqtot(i,j)*voltot(i,j));
   tempB2=(seqtot(i,j)*eeqtot(i,j)*voltot(i,j));

   tempA1=tempA1+tempB1;
   tempA2=tempA2+tempB2;


   end;
   mu(j)=sy*(tempA1/tempA2);
end;

% M01 UPPER BOUND

for j = 1:itter
   tempA1=0;
   tempA2=0;

   for i = 1:n;

   tempB1=(voltot(i,j));
   tempB2=(seqtot(i,j)*seqtot(i,j)*voltot(i,j));

   tempA1=tempA1+tempB1;
   tempA2=tempA2+tempB2;
   end;
   m01(j)=sy*sqrt(tempA1/tempA2);
   Vtot=tempA1;
end;

% M02 UPPER BOUND

for j = 1:itter
   tempA1=0;
   tempA2=0;

   for i = 1:n;

   tempB1=(voltot(i,j)*eeqtot(i,j)/seqtot(i,j));
   tempB2=(seqtot(i,j)*eeqtot(i,j)*voltot(i,j));

   tempA1=tempA1+tempB1;
   tempA2=tempA2+tempB2;
   end;
   m02(j)=sy*sqrt(tempA1/tempA2);
end;
```

```
        % #### LOWER BOUND ####
% CLASSICAL LOWER BOUND

for j = 1:itter;
   smax=max(seqtot(:,j));
   mL(j)=sy/smax;
end;

% M-ALFA LOWER BOUND
k=0;
for j = 1:itter;

     Rx=m02(j)/mL(j);

     if Rx < (1+sqrt(2));
        k=k+1
      tempB1=2*Rx^2+sqrt(Rx*(Rx-1)^2*(1+sqrt(2)-Rx)*(Rx-1+sqrt(2)));
      tempB2=(Rx^2+2-sqrt(5))*(Rx^2+2+sqrt(5));
      ma(k)=2*m02(k)*(tempB1/tempB2);
      itterationp(k)=j;
     end;

 end;

%  MBETA LOWER BOUND
beta=0.1
for j = 1:itter
   tempA1=0;
   tempA2=0;

   for i = 1:n;

   tempB1=((m02(j)*seqtot(i,j)/sy)^2-1)^2*voltot(i,j);
   tempB2=voltot(i,j);

   tempA1=tempA1+tempB1;
   tempA2=tempA2+tempB2;
   end;
   mb(j)=m02(j)/(1+(beta)*sqrt(tempA1/tempA2));
   G02(j)=0.5*sqrt(tempA1/tempA2);
end;

%  MPP LOWER BOUND

for j = 1:itter
   tempA1=0;
   tempA2=0;

   for i = 1:n;

   tempB1=((m02(j)*seqtot(i,j)/sy)^2-1)^2*voltot(i,j);
   tempB2=voltot(i,j);
```

```
   tempA1=tempA1+tempB1;
   tempA2=tempA2+tempB2;
   end;
   mpp(j)=m02(j)/(1+sqrt(tempA1/tempA2));
end;
%*************************************************************

 %%%%%%%%%%%%     PLOTTING    %%%%%%%%%%%%
         %@   MULTIPLIERS-ITTERATIONS   @%
lines1=2.8;
    figure;
  plot(itteration,m01,'-^k','linewidth',lines1)
hold on
  plot(itteration,m02,'-ok','linewidth',lines1)
hold on
  plot(itteration,mu,'-sk','linewidth',lines1)
hold on
  plot(itteration,mnfem,'+-K','linewidth',lines1)
  hold on
 plot(itteration,mpp,'--sr','linewidth',lines1)
 hold on
  plot(itterationp,ma,'--ok','linewidth',lines1)
hold on
 plot(itteration,mb,'--ok','linewidth',lines1)
hold on
  plot(itteration,mL,'--sk','linewidth',lines1)


    xlabel('Iterations','FontSize',labels)
    ylabel('Multipliers','FontSize',labels)


    hold off

%*************************************************************

                    %@   G-ITTERATIONS   @%

 for j = 1:itter
   tempA1=0;
   tempA2=0;

   for i = 1:n;

   tempB1=((mu(j)*seqtot(i,j)/sy)^2-1)^2*voltot(i,j);
   tempB2=voltot(i,j);

   tempA1=tempA1+tempB1;
   tempA2=tempA2+tempB2;
   end;
    Gu(j)=0.5*sqrt(tempA1/tempA2);
end;

 for j = 1:itter
```

```
   tempA1p=0;
   tempA2p=0;

   for i = 1:n;

   tempB1p=((m02(j)*seqtot(i,j)/sy)^2-1)^2*voltot(i,j);
   tempB2p=voltot(i,j);

   tempA1p=tempA1p+tempB1p;
   tempA2p=tempA2p+tempB2p;
   end;
    G02(j)=0.5*sqrt(tempA1p/tempA2p);
end;

    figure;
     plot(itteration,Gu,'-ok','linewidth',lines)
         hold on
     plot(itteration,G02,'-sk','linewidth',lines)

    xlabel('Iterations','FontSize',labels)
    ylabel('G_{u}','G_{2}','FontSize',labels)

         hold off

%*************************************************************

              %****** m-Beta *****
b1=0.5;
b2=1;
b3=1.55;
b4=2;
b5=2.5;

for j=1:itter

   mbeta1(j)=m02(j)/(1+b1*G02(j));
   mbeta2(j)=m02(j)/(1+b2*G02(j));

   mbeta3(j)=m02(j)/(1+b3*G02(j));

   mbeta4(j)=m02(j)/(1+b4*G02(j));
   mbeta5(j)=m02(j)/(1+b5*G02(j));

end

         figure;
         plot(itteration,mbeta1,'-k','linewidth',lines)
         hold on
         plot(itteration,mbeta2,'-k','linewidth',lines)
         hold on
         plot(itteration,mbeta3,'-k','linewidth',lines)
         hold on
         plot(itteration,mbeta4,'-k','linewidth',lines)
         hold on
```

```
        plot(itteration,mbeta5,'-k','linewidth',lines)
        hold on
        plot(itteration,mnfem,'-.k','linewidth',lines)


    h=legend('\beta=??','\beta=1','\beta^{\fontsize{22} R}=1.73','\beta=??','\beta=??',0)
    set(h,'FontAngle','it','FontSize',legen);
    xlabel('Iterations','FontSize',labels)
    ylabel('m_{\beta}','FontSize',labels)
    grid on
        hold off


%*************************************************************

    %@ REFERENCE VOLUME @%

      % METHOD II %
   tempA0p1=0 ;
   tempA1p1=0 ;
   tempA2p1=0 ;
   tempA3p1=0 ;
   tempA0p2=0 ;
   tempA1p2=0 ;
   tempA2p2=0 ;
   tempA3p2=0 ;
   tempA0p3=0 ;
   tempA1p3=0 ;
   tempA2p3=0 ;
   tempA3p3=0 ;
   tempA0p4=0 ;
   tempA1p4=0 ;
   tempA2p4=0 ;
   tempA3p4=0 ;
   tempA0p5=0 ;
   tempA1p5=0 ;
   tempA2p5=0 ;
   tempA3p5=0 ;


    for i=1:n;
      % 1-iteration
       tempA0p1= tempA0p1+voltot(i,1);
       tempB1p1=(voltot(i,1)*eeqtot(i,1)/seqtot(i,1));
       tempB2p1=(seqtot(i,1)*eeqtot(i,1)*voltot(i,1));


       tempA1p1=tempA1p1+tempB1p1;
        tempA2p1=tempA2p1+tempB2p1;


   V1(i)=tempA0p1/Vtot;
   m02r1(i)=sy*sqrt(tempA1p1/tempA2p1);
```

```
tempB3p1=((m02r1(i)*seqtot(i,1)/sy)^2-1)^2*voltot(i,1);
tempA3p1=tempA3p1+tempB3p1;
G02r1(i)=0.5/sqrt(tempA3p1/Vtot);

    % 2-iteration
     tempA0p2= tempA0p2+voltot(i,2);
     tempB1p2=(voltot(i,2)*eeqtot(i,2)/seqtot(i,2));
     tempB2p2=(seqtot(i,2)*eeqtot(i,2)*voltot(i,2));

     tempA1p2=tempA1p2+tempB1p2;
      tempA2p2=tempA2p2+tempB2p2;
V2(i)=tempA0p2/Vtot;
m02r2(i)=sy*sqrt(tempA1p2/tempA2p2);

tempB3p2=((m02r2(i)*seqtot(i,2)/sy)^2-1)^2*voltot(i,2);
tempA3p2=tempA3p2+tempB3p2;
G02r2(i)=0.5*sqrt(tempA3p2/Vtot);

   % 3-iteration
     tempA0p3= tempA0p3+voltot(i,3);
     tempB1p3=(voltot(i,3)*eeqtot(i,3)/seqtot(i,3));
     tempB2p3=(seqtot(i,3)*eeqtot(i,3)*voltot(i,3));

     tempA1p3=tempA1p3+tempB1p3;
      tempA2p3=tempA2p3+tempB2p3;


V3(i)=tempA0p3/Vtot;
m02r3(i)=sy*sqrt(tempA1p3/tempA2p3);

tempB3p3=((m02r3(i)*seqtot(i,3)/sy)^2-1)^2*voltot(i,3);
tempA3p3=tempA3p3+tempB3p3;
G02r3(i)=0.5*sqrt(tempA3p3/Vtot);

   % 4-iteration
   itter4=4;
     tempA0p4= tempA0p4+voltot(i,itter4);
     tempB1p4=(voltot(i,itter4)*eeqtot(i,itter4)/seqtot(i,itter4));
     tempB2p4=(seqtot(i,itter4)*eeqtot(i,itter4)*voltot(i,itter4));

     tempA1p4=tempA1p4+tempB1p4;
      tempA2p4=tempA2p4+tempB2p4;


V4(i)=tempA0p4/Vtot;
m02r4(i)=sy*sqrt(tempA1p4/tempA2p4);

tempB3p4=((m02r4(i)*seqtot(i,itter4)/sy)^2-1)^2*voltot(i,itter4);
tempA3p4=tempA3p4+tempB3p4;
G02r4(i)=0.5*sqrt(tempA3p4/Vtot);

   % last-iteration
   itter5=itter;
```

```
        tempA0p5= tempA0p5+voltot(i,itter5);
        tempB1p5=(voltot(i,itter5)*eeqtot(i,itter5)/seqtot(i,itter5));
        tempB2p5=(seqtot(i,itter5)*eeqtot(i,itter5)*voltot(i,itter5));

        tempA1p5=tempA1p5+tempB1p5;
         tempA2p5=tempA2p5+tempB2p5;


      V5(i)=tempA0p5/Vtot;
      m02r5(i)=sy*sqrt(tempA1p5/tempA2p5);

      tempB3p5=((m02r5(i)*seqtot(i,itter5)/sy)^2-1)^2*voltot(i,itter5);
      tempA3p5=tempA3p5+tempB3p5;
      G02r5(i)=0.5*sqrt(tempA3p5/Vtot);

     end;

     V1=V1';
     m02r1=m02r1';
     G02r1=G02r1';
     V2=V2';
     m02r2=m02r2';
     G02r2=G02r2';
     V3=V3';
     m02r3=m02r3';
     G02r3=G02r3';
     V4=V4';
     m02r4=m02r4';
     G02r4=G02r4';
     V5=V5';
     m02r5=m02r5';
     G02r5=G02r5';

      figure;


lines=1.5;
  plot(V1,m02r1,'-k','linewidth',lines)
hold on

lines=3;
 plot(V2,m02r2,'--k','linewidth',lines)
hold on
 plot(V3,m02r3,':k','linewidth',lines)
hold on
 plot(V4,m02r4,'-k','linewidth',lines)
hold on
 plot(V5,m02r5,'-.k','linewidth',lines)
hold on

    h=legend('i=1','i=2','i=3','i=4','i=5',0)   ;
   set(h,'FontAngle','it','FontSize',legen);
   xlabel('V_{\eta}','FontSize',labels);
    ylabel('m^{0}_{2}','FontSize',labels);
```

```
   grid on

%*********************************************************

                %%% METHOD II %%%


        Vratio=[0.99 0.95 0.9 0.8 0.7 0.6 0.3 0.1 0.05 0.01];
        Vratio=Vratio';
  nelem=n
for i = 1:nelem
   if V1(i)>=Vratio(1);
      p1=i;
      break
   end
end

for i = 1:nelem
      if V2(i)>=Vratio(1);
      p2=i;
      break
   end
end

for i = 1:nelem
      if V3(i)>=Vratio(1);
      p3=i;
      break
   end
end
for i = 1:nelem
       if V4(i)>=Vratio(1);
      p4=i;
   end
end
for i = 1:nelem
       if V5(i)>=Vratio(1);
      p5=i;
   end
end
  %q

 for i = 1:nelem
   if V1(i)>=Vratio(2);
      q1=i;
      break
   end
end
for i = 1:nelem
      if V2(i)>=Vratio(2);
      q2=i;
```

```
      break
   end
end
for i = 1:nelem
      if V3(i)>=Vratio(2);
      q3=i;
      break
   end
end
for i = 1:nelem
      if V4(i)>=Vratio(2);
      q4=i;
      break
   end
end
for i = 1:nelem
      if V5(i)>=Vratio(2);
      q5=i;
      break
   end
end
  %r
for i = 1:nelem
   if V1(i)>=Vratio(3);
      r1=i;
      break
   end
end
for i = 1:nelem
      if V2(i)>=Vratio(3);
      r2=i;
      break
   end
end
for i = 1:nelem
      if V3(i)>=Vratio(3);
      r3=i;
      break
   end
end
for i = 1:nelem
      if V4(i)>=Vratio(3);
      r4=i;
      break
   end
end
for i = 1:nelem
      if V5(i)>=Vratio(3);
      r5=i;
      break
   end
end
   %s*****
for i = 1:nelem
```

```
   if V1(i)>=Vratio(4);
      s1=i;
      break
   end
end
for i = 1:nelem
      if V2(i)>=Vratio(4);
      s2=i;
      break
   end
end
for i = 1:nelem
      if V3(i)>=Vratio(4);
      s3=i;
      break
   end
end
for i = 1:nelem
      if V4(i)>=Vratio(4);
      s4=i;
      break
   end
end
for i = 1:nelem
      if V5(i)>=Vratio(4);
      s5=i;
      break
   end
end
   %t
for i = 1:nelem
      if V1(i)>=Vratio(5);
      t1=i;
      break
   end
end
for i = 1:nelem
      if V2(i)>=Vratio(5);
      t2=i;
      break
   end
end
for i = 1:nelem
      if V3(i)>=Vratio(5);
      t3=i;
      break
   end
end
for i = 1:nelem
       if V4(i)>=Vratio(5);
      t4=i;
      break
   end
end
```

```
for i = 1:nelem
      if V5(i)>=Vratio(5);
      t5=i;
      break
   end
end
   %u
for i = 1:nelem
      if V1(i)>=Vratio(6);
      u1=i;
      break
   end
end
for i = 1:nelem
      if V2(i)>=Vratio(6);
      u2=i;
      break
   end
end
for i = 1:nelem
      if V3(i)>=Vratio(6);
      u3=i;
      break
   end
end
for i = 1:nelem
      if V4(i)>=Vratio(6);
      u4=i;
      break
   end
end
for i = 1:nelem
      if V5(i)>=Vratio(6);
      u5=i;
      break
   end
end
   %v
for i = 1:nelem
      if V1(i)>=Vratio(7);
      v1=i;
      break
   end
end
for i = 1:nelem
      if V2(i)>=Vratio(7);
      v2=i;
      break
   end
end
for i = 1:nelem
      if V3(i)>=Vratio(7);
      v3=i;
      break
```

```
    end
end
for i = 1:nelem
    if V4(i)>=Vratio(7);
    v4=i;
    break
    end
end
for i = 1:nelem
    if V5(i)>=Vratio(7);
    v5=i;
    break
    end
end
    %w
for i = 1:nelem
    if V1(i)>=Vratio(8);
    w1=i;
    break
    end
end
for i = 1:nelem
    if V2(i)>=Vratio(8);
    w2=i;
    break
    end
end
for i = 1:nelem
    if V3(i)>=Vratio(8);
    w3=i;
    break
    end
end
for i = 1:nelem
    if V4(i)>=Vratio(8);
    w4=i;
    break
    end
end
for i = 1:nelem
    if V5(i)>=Vratio(8);
    w5=i;
    break
    end
end
    %x
for i = 1:nelem
    if V1(i)>=Vratio(9);
    x1=i;
    break
    end
end
for i = 1:nelem
    if V2(i)>=Vratio(9);
```

```
      x2=i;
      break
   end
end
for i = 1:nelem
      if V3(i)>=Vratio(9);
      x3=i;
      break
   end
end
for i = 1:nelem
      if V4(i)>=Vratio(9);
      x4=i;
      break
   end
end
 for i = 1:nelem
      if V5(i)>=Vratio(9);
      x5=i;
      break
   end
end

   %y
for i = 1:nelem
      if V1(i)>=Vratio(10);
      y1=i;
      break
   end
end
for i = 1:nelem
      if V2(i)>=Vratio(10);
      y2=i;
      break
   end
end
for i = 1:nelem
      if V3(i)>=Vratio(10);
      y3=i;
      break
   end
end
for i = 1:nelem
      if V4(i)>=Vratio(10);
      y4=i;
      break
   end
end
 for i = 1:nelem
      if V5(i)>=Vratio(10);
      y5=i;
      break
   end
end
```

```
%************************************************************
      %  M02(ETA)-ITERATION

eta1=[m02r1(p1) m02r2(p2) m02r3(p3) m02r4(p4) m02r5(p5)];
eta2=[m02r1(q1) m02r2(q2) m02r3(q3) m02r4(q4) m02r5(q5)];
eta3=[m02r1(r1) m02r2(r2) m02r3(r3) m02r4(r4) m02r5(r5)];
eta4=[m02r1(s1) m02r2(s2) m02r3(s3) m02r4(s4) m02r5(s5)];
eta5=[m02r1(t1) m02r2(t2) m02r3(t3) m02r4(t4) m02r5(t5)];
eta6=[m02r1(u1) m02r2(u2) m02r3(u3) m02r4(u4) m02r5(u5)];
eta7=[m02r1(v1) m02r2(v2) m02r3(v3) m02r4(v4) m02r5(v5)];
eta8=[m02r1(w1) m02r2(w2) m02r3(w3) m02r4(w4) m02r5(w5)];
eta9=[m02r1(x1) m02r2(x2) m02r3(x3) m02r4(x4) m02r5(x5)];
eta10=[m02r1(y1) m02r2(y2) m02r3(y3) m02r4(y4) m02r5(y5)];
itterp=[1 2 3 4 5];

figure;
 plot(itterp,eta1,'-k','linewidth',lines)
hold on
 plot(itterp,eta2,'-k','linewidth',lines)
hold on
 plot(itterp,eta3,'-k','linewidth',lines)
hold on
 plot(itterp,eta4,'-k','linewidth',lines)
hold on
 plot(itterp,eta5,'-k','linewidth',lines)
hold on
 plot(itterp,eta6,'-k','linewidth',lines)
hold on
 plot(itterp,eta7,'-k','linewidth',lines)
hold on
 plot(itterp,eta8,'-k','linewidth',lines)
hold on
 plot(itterp,eta9,'-k','linewidth',lines)
hold on
 plot(itterp,eta10,'-k','linewidth',lines)
hold off


    set(gca,'XLim',[1 5])
   set(gca,'XTick',[1 2 3 4 5])
  xlabel('Iterations','FontSize',labels)
   ylabel('m^{0}_{2}','FontSize',labels)
   grid on

    %  G-value
etap1=[G02r1(p1) G02r2(p2) G02r3(p3) G02r4(p4) G02r5(p5)];
etap2=[G02r1(q1) G02r2(q2) G02r3(q3) G02r4(q4) G02r5(q5)];
etap3=[G02r1(r1) G02r2(r2) G02r3(r3) G02r4(r4) G02r5(r5)];
etap4=[G02r1(s1) G02r2(s2) G02r3(s3) G02r4(s4) G02r5(s5)];
etap5=[G02r1(t1) G02r2(t2) G02r3(t3) G02r4(t4) G02r5(t5)];
etap6=[G02r1(u1) G02r2(u2) G02r3(u3) G02r4(u4) G02r5(u5)];
etap7=[G02r1(v1) G02r2(v2) G02r3(v3) G02r4(v4) G02r5(v5)];
```

```
etap8=[G02r1(w1) G02r2(w2) G02r3(w3) G02r4(w4) G02r5(w5)];
etap9=[G02r1(x1) G02r2(x2) G02r3(x3) G02r4(x4) G02r5(x5)];
etap10=[G02r1(y1) G02r2(y2) G02r3(y3) G02r4(y4) G02r5(y5)];

      %  G02(ETA)-ITERATION
figure;

 plot(itterp,etap1,'-k','linewidth',lines)
hold on
 plot(itterp,etap2,'-k','linewidth',lines)
hold on
 plot(itterp,etap3,'-k','linewidth',lines)
hold on
 plot(itterp,etap4,'-k','linewidth',lines)
hold on
 plot(itterp,etap5,'-k','linewidth',lines)
hold on
 plot(itterp,etap6,'-k','linewidth',lines)
hold on
 plot(itterp,etap7,'-k','linewidth',lines)
hold on
 plot(itterp,etap8,'-k','linewidth',lines)
hold on
 plot(itterp,etap9,'-k','linewidth',lines)
hold on
 plot(itterp,etap10,'-k','linewidth',lines)
hold off

    set(gca,'XTick',[1 2 3 4 5])
   xlabel('Iterations','FontSize',labels)
    ylabel('G_{2}','FontSize',labels)


%*********************************************************

        %@ M-BETA & REFERENCE METHOD

     tempA0=0 ;
     tempA1=0 ;
     tempA2=0 ;
     tempAp1=0 ;
     tempAp2=0 ;


    for i=1:n;
          % Last iteratiion
           tempA0= tempA0+voltot(i,itter);

           tempB1=(voltot(i,itter)*eeqtot(i,itter)/seqtot(i,itter));
           tempB2=(seqtot(i,itter)*eeqtot(i,itter)*voltot(i,itter));

           tempC1=(voltot(i,itter));
           tempC2=(seqtot(i,itter)*seqtot(i,itter)*voltot(i,itter));
```

```
        tempA1=tempA1+tempB1;
        tempA2=tempA2+tempB2;

        tempAp1=tempAp1+tempC1;
        tempAp2=tempAp2+tempC2;


   Veta(i)=tempA0/Vtot;
   m02eta(i)=sy*sqrt(tempA1/tempA2);
   m01eta(i)=sy*sqrt(tempAp1/tempAp2);

   tempA3=0 ;
    for m=1:l;
     tempB3=((m02eta(i)*seqtot(m,itter)/sy)^2-1)^2*voltot(m,itter);
     tempA3=tempA3+tempB3;
     G02etatemp=0.5*sqrt(tempA3/Vtot);
    end;

    G02eta(i)=G02etatemp;
    mppeta(i)=m02eta(i)/(1+G02eta(i));

    % mL (classical lower bound) %

    mLeta(i)=sy/seqtot(1,itter);
end;

  Veta=Veta';
  m02eta=m02eta';
  G02eta=G02eta';
  mppeta=mppeta';
  %m01eta=m01eta';

  % MULTIPLIERS-ETA (LAST ITERATION)
figure;
plot(Veta,m02eta,'-k','linewidth',lines)
hold on
plot(Veta,mppeta,'-.k','linewidth',lines)
hold on
plot(Veta,m01eta,':r','linewidth',lines)
hold on
plot(Veta,mLeta,':r','linewidth',lines)

 xlabel('V_{\fontsize{35}\eta}','FontSize',labels)
 ylabel('Multipliers','FontSize',labels)

  % MULTIPLIERS-ETA (LAST ITERATION)

 figure;
 plot(Veta,G02eta,'-k','linewidth',lines)

set(gca,'XLim',[0 1])
xlabel('V_{\fontsize{35}\eta}','FontSize',labels)
ylabel('G','FontSize',labels)
```

```
    grid on

    hold off
%*************************************************************

          %@ M-ALFA CURVE @%

  for j=1:itter;
   r01x(j)=m01(j)/mL(j);
   r01y(j)=m01(j)/mnfem(j);
  end  ;


   % R-alfa components

P=13333;
E0=30e6;
zmin=0.0001;
zmax=1;
zdelta=(zmax-zmin)/1000;
z = zmin:zdelta:zmax;
m=length(z);

x=zmin-zdelta;

k=0;


   for i=1:m;

      x=x+zdelta;


sig1p(i)=(E0./(E0+E0*x))*P;
sig2p(i)=(E0*x./(E0+E0*x))*P;

mexact=2*sy/P;
mexactt(i)=mexact;
if (sig1p(i)>=sig2p(i));
   sigmax=sig1p(i);
else
   sigmax=sig2p(i);
end;

mlp(i)=sy./sigmax;
m0p(i)=(sy*sqrt(x+1))./sqrt(x.*(sig1p(i).^2)+sig2p(i).^2);


Rxp(i)=m0p(i)./mlp(i);
Ryp(i)=m0p(i)/mexact;


A1=sqrt((Rxp(i).*(Rxp(i)-1).^2).*(1+sqrt(2)-Rxp(i)).*(Rxp(i)-1+sqrt(2)));
A2=(Rxp(i).^2+2-sqrt(5)).*(Rxp(i).^2+2+sqrt(5)) ;
```

```
if  ((Rxp(i)) <= (1+sqrt(2)));
   k=k+1;

   Rxpp(k)=Rxp(i);
y0(k)=1.15  *(0.5*(A2./(2*Rxpp(k).^2+A1)));
y1(k)=1  *(0.5*(A2./(2*Rxpp(k).^2+A1)));
y2(k)=0.9*(0.5*(A2./(2*Rxpp(k).^2+A1)));
y3(k)=0.8*(0.5*(A2./(2*Rxpp(k).^2+A1)));

y4(k)=0.7  *(0.5*(A2./(2*Rxpp(k).^2+A1)));
y5(k)=0.6  *(0.5*(A2./(2*Rxpp(k).^2+A1)));
y6(k)=0.5  *(0.5*(A2./(2*Rxpp(k).^2+A1)));

end

   end


        figure;
        plot(r01x,r01y,'-ok','linewidth',lines)

        xmax=1+sqrt(2);

    set(gca,'YLim',[1 2.5])
    xlabel('m0/mL','FontSize',labels)
    ylabel('m0/m','FontSize',labels)

hold on;
% General m-alfa curves
%plot(Rxpp,y0,':k','linewidth',lines)
hold on
plot(Rxpp,y1,'--k','linewidth',lines)
hold on
%plot(Rxpp,y2,':k','linewidth',lines)
hold on
%plot(Rxpp,y3,':k','linewidth',lines)
hold on
%plot(Rxpp,y4,':k','linewidth',lines)
hold on
%plot(Rxpp,y5,':k','linewidth',lines)
hold on
%plot(Rxpp,y6,':k','linewidth',lines)
hold on

    hold on
X1=[1 1+sqrt(2)];
Y1=[1 1+sqrt(2)];
line(X1,Y1);

hold on

X2=[1+sqrt(2) 1+sqrt(2)];
```

```
Y2=[1 1+sqrt(2)];
line(X2,Y2);

%************************************************************
        %@ Reverse sorting method

            iteration=1

    % m02 (m02 new) %

    tempA0=0 ;
    tempA1=0 ;
    tempA2=0 ;
    tempAp1=0 ;
    tempAp2=0 ;


   for i=1:n;
        % Last iteratiion
         tempA0= tempA0+voltot(i,iteration);

         tempB1=(voltot(i,iteration)*eeqtot(i,iteration)/seqtot(i,iteration));
         tempB2=(seqtot(i,iteration)*eeqtot(i,iteration)*voltot(i,iteration));

         tempC1=(voltot(i,iteration));
         tempC2=(seqtot(i,iteration)*seqtot(i,iteration)*voltot(i,iteration));


          tempA1=tempA1+tempB1;
          tempA2=tempA2+tempB2;

          tempAp1=tempAp1+tempC1;
          tempAp2=tempAp2+tempC2;


     Veta1(i)=tempA0/Vtot;
     m02eta1(i)=sy*sqrt(tempA1/tempA2);

      %% G(VR) and m"
            tempA3=0 ;
      for m=1:i;
        tempB3=((m02eta1(i)*seqtot(m,iteration)/sy)^2-1)^2*voltot(m,iteration);
        tempA3=tempA3+tempB3;
        G02etatemp=0.5*sqrt(tempA3/Vtot);
     end;

      G02eta1(i)=G02etatemp;
      mppeta1(i)=m02eta1(i)/(1+G02eta(i));

  end;

    Veta1=Veta1';
    m02eta1=m02eta1';
    G02eta1=G02eta1';
```

```
    mppeta1=mppeta1';


    % mL (classical lower bound) %
    tempA0=0 ;
    q=n+1

   for i=1:n;
     tempA0= tempA0+voltot(q-i,iteration);
     Veta2(i)=tempA0/Vtot;
      mLeta2(i)=sy/seqtot(q-i,iteration);
      mNFEM(i)=NFEM;
  end;

    Veta2=Veta2';

    % MULTIPLIERS-ETA
figure;
  plot(Veta1,m02eta1,'-k','linewidth',lines)
hold on
  plot(Veta2,mLeta2,'-r','linewidth',lines)
hold on
  plot(Veta2,mNFEM,'-.b','linewidth',lines)

   set(gca,'XLim',[0 1])
   xlabel('V_{\fontsize{35}\eta}','FontSize',labels)
   ylabel('Multipliers','FontSize',labels)
   grid on

        % G-ETA
figure;
  plot(Veta1,G02eta1,'-k','linewidth',lines)

   set(gca,'XLim',[0 1])
   xlabel('V_{\fontsize{35}\eta}','FontSize',labels)
   ylabel('G','FontSize',labels)
   grid on

figure;
   mstar=[8.3106 7.1948 7.5624 7.6092 7.6109];
   mexact=[NFEM NFEM NFEM NFEM NFEM];
   zeta=[1 2 3 4 5];
plot(zeta,mstar,'-ok','linewidth',lines)
hold on
plot(zeta,mexact,'-.b','linewidth',lines)


%************************************************************
```